ROADMAP • OPEN ACCESS

Roadmap on energy harvesting materials

To cite this article: Vincenzo Pecunia *et al* 2023 *J. Phys. Mater.* **6** 042501

View the article online for updates and enhancements.

Journal of Physics: Materials

ROADMAP

Roadmap on energy harvesting materials

Vincenzo Pecunia[1,*] , S Ravi P Silva[2,*] , Jamie D Phillips[3] , Elisa Artegiani[4] , Alessandro Romeo[4] , Hongjae Shim[5], Jongsung Park[6], Jin Hyeok Kim[7], Jae Sung Yun[2], Gregory C Welch[8] , Bryon W Larson[9], Myles Creran[10], Audrey Laventure[10] , Kezia Sasitharan[11], Natalie Flores-Diaz[11], Marina Freitag[11], Jie Xu[12] , Thomas M Brown[12] , Benxuan Li[13,14], Yiwen Wang[15], Zhe Li[15], Bo Hou[16] , Behrang H Hamadani[17], Emmanuel Defay[18], Veronika Kovacova[18], Sebastjan Glinsek[18], Sohini Kar-Narayan[19,*], Yang Bai[20], Da Bin Kim[21] , Yong Soo Cho[21], Agnė Žukauskaitė[22,78] , Stephan Barth[22] , Feng Ru Fan[23], Wenzhuo Wu[24], Pedro Costa[25,26], Javier del Campo[27,28], Senentxu Lanceros-Mendez[25,26,27,28], Hamideh Khanbareh[29], Zhong Lin Wang[30], Xiong Pu[31], Caofeng Pan[31], Renyun Zhang[32], Jing Xu[33], Xun Zhao[33], Yihao Zhou[33], Guorui Chen[33], Trinny Tat[33], Il Woo Ock[33], Jun Chen[33], Sontyana Adonijah Graham[34], Jae Su Yu[34], Ling-Zhi Huang[35], Dan-Dan Li[35], Ming-Guo Ma[35], Jikui Luo[36] , Feng Jiang[37], Pooi See Lee[37], Bhaskar Dudem[2] , Venkateswaran Vivekananthan[2,79] , Mercouri G Kanatzidis[38], Hongyao Xie[38], Xiao-Lei Shi[39], Zhi-Gang Chen[39], Alexander Riss[40], Michael Parzer[40], Fabian Garmroudi[40], Ernst Bauer[40], Duncan Zavanelli[41], Madison K Brod[41], Muath Al Malki[41], G Jeffrey Snyder[41], Kirill Kovnir[42,43], Susan M Kauzlarich[44], Ctirad Uher[45], Jinle Lan[46], Yuan-Hua Lin[47], Luis Fonseca[48] , Alex Morata[49] , Marisol Martin-Gonzalez[50] , Giovanni Pennelli[51] , David Berthebaud[52], Takao Mori[53,54], Robert J Quinn[55] , Jan-Willem G Bos[55] , Christophe Candolfi[56], Patrick Gougeon[57], Philippe Gall[57], Bertrand Lenoir[56], Deepak Venkateshvaran[58] , Bernd Kaestner[59] , Yunshan Zhao[60], Gang Zhang[61], Yoshiyuki Nonoguchi[62], Bob C Schroeder[63], Emiliano Bilotti[80], Akanksha K Menon[65], Jeffrey J Urban[66], Oliver Fenwick[64] , Ceyla Asker[64], A Alec Talin[67], Thomas D Anthopoulos[68], Tommaso Losi[69], Fabrizio Viola[69], Mario Caironi[69], Dimitra G Georgiadou[70] , Li Ding[71], Lian-Mao Peng[71], Zhenxing Wang[72], Muh-Dey Wei[73], Renato Negra[73], Max C Lemme[72,74], Mahmoud Wagih[70,75] , Steve Beeby[70] , Taofeeq Ibn-Mohammed[76], K B Mustapha[77] and A P Joshi[76]

1 School of Sustainable Energy Engineering, Simon Fraser University, Surrey V3T 0N1 BC, Canada
2 Advanced Technology Institute, Department of Electrical and Electronic Engineering, University of Surrey, Guildford, Surrey, GU2 7XH, United Kingdom
3 Department of Electrical and Computer Engineering, University of Delaware, Newark, DE 19716, United States of America
4 LAPS- Laboratory for Photovoltaics and Solid-State Physics, Department of Computer Science, University of Verona, Ca' Vignal 1, Strada Le Grazie 15, 37134 Verona, Italy
5 Australian Centre for Advanced Photovoltaics (ACAP), School of Photovoltaic and Renewable Energy Engineering, University of New South Wales, Sydney, NSW 2052, Australia
6 Department of Energy Engineering, Future Convergence Technology Research Institute, Gyeongsang National University, Jinju, Gyeongnam 52828, Republic of Korea
7 Optoelectronics Convergence Research Center and Department of Materials Science and Engineering, Chonnam National University, Gwangju, 61186, Republic of Korea
8 Department of Chemistry, University of Calgary, Calgary, AB, T2N 4K9, Canada
9 National Renewable Energy Laboratory, Golden, CO 80401, United States of America
10 Département de chimie, Université de Montréal, Montréal, QC H2V 0B3, Canada
11 School of Natural and Environmental Sciences, Bedson Building, Newcastle University, NE1 7RU Newcastle upon Tyne, United Kingdom
12 CHOSE (Centre for Hybrid and Organic Solar Energy), Department of Electronic Engineering, University of Rome Tor Vergata, Via del Politecnico 1, 00133 Rome, Italy
13 International Collaborative Laboratory of 2D Materials for Optoelectronics Science and Technology of Ministry of Education, Institute of Microscale Optoelectronics, Shenzhen University, Shenzhen 518060, People's Republic of China
14 Electrical Engineering Division, Engineering Department, University of Cambridge, 9 J J Thomson Avenue, Cambridge CB3 0FA, United Kingdom
15 School of Engineering and Materials Science, Queen Mary University of London, London E1 4NS, United Kingdom
16 School of Physics and Astronomy, Cardiff University, Cardiff CF24 3AA, United Kingdom
17 National Institute of Standards and Technology, Gaithersburg, MD 20899, United States of America
18 Materials Research and Technology Department, Luxembourg Institute of Science and Technology (LIST), 41 Rue du Brill, Belvaux L-4422, Luxembourg
19 Department of Materials Science and Metallurgy, University of Cambridge, 27 Charles Babbage Road, Cambridge CB3 0FS, United Kingdom

[20] Microelectronics Research Unit, Faculty of Information Technology and Electrical Engineering, University of Oulu, FI-90570 Oulu, Finland

[21] Department of Materials Science and Engineering, Yonsei University, Seoul 03722, Republic of Korea

[22] Fraunhofer Institute for Organic Electronics, Electron Beam and Plasma Technology FEP, 01277 Dresden, Germany

[23] State Key Laboratory of Physical Chemistry of Solid Surfaces, College of Chemistry and Chemical Engineering, Innovation Laboratory for Sciences and Technologies of Energy Materials of Fujian Province (IKKEM), Xiamen University, Xiamen 361005, People's Republic of China

[24] School of Industrial Engineering, Purdue University, West Lafayette, IN 47907, United States of America

[25] Physics Centre of Minho and Porto Universities (CF-UM-UP), University of Minho, 4710-053 Braga, Portugal

[26] LaPMET-Laboratory of Physics for Materials and Emergent Technologies, University of Minho, 4710-057 Braga, Portugal

[27] BCMaterials, Basque Center for Materials, Applications and Nanostructures, UPV/EHU Science Park, 48940 Leioa, Spain

[28] OIKERBASQUE, Basque Foundation for Science, 48009 Bilbao, Spain

[29] Department of Mechanical Engineering, University of Bath, Claverton Down, Bath BA2 7AY, United Kingdom

[30] School of Materials Science and Engineering, Georgia Institute of Technology, Atlanta, GA 30332-0245, United States of America

[31] CAS Center for Excellence in Nanoscience, Beijing Key Laboratory of Micro-nano Energy and Sensor, Beijing Institute of Nanoenergy and Nanosystems, Chinese Academy of Sciences, Beijing 101400, People's Republic of China

[32] Department of Natural Sciences, Mid Sweden University, Holmgatan 10 SE 851 70 Sundsvall, Sweden

[33] Department of Bioengineering, University of California, Los Angeles, Los Angeles, CA 90095, United States of America

[34] Department of Electronics and Information Convergence Engineering, Kyung Hee University, 1732 Deogyeong-daero, Giheung-gu, Yongin-Si, Gyeonggi-do 17104, Republic of Korea

[35] Research Center of Biomass Clean Utilization, College of Materials Science and Technology, Beijing Forestry University, Beijing 100083, People's Republic of China

[36] College of Information Science and Electronic Engineering, Zhejiang University, Hangzhou 310027, People's Republic of China

[37] School of Materials Science and Engineering, Nanyang Technological University, 50 Nanyang Avenue, Singapore 639798, Singapore

[38] Department of Chemistry, Northwestern University, Evanston, IL 60208, United States of America

[39] School of Chemistry and Physics, Queensland University of Technology, Brisbane, QLD 4000, Australia

[40] Institute of Solid-State Physics, TU Wien, A-1040 Wien, Austria

[41] Department of Materials Science and Engineering, Northwestern University, Evanston, IL 60208, United States of America

[42] Department of Chemistry, Iowa State University, Ames, IA 50011, United States of America

[43] US DOE Ames National Laboratory, Ames, IA 50011, United States of America

[44] Department of Chemistry, University of California, Davis, CA 95616, United States of America

[45] Department of Physics, University of Michigan, Ann Arbor, Michigan 48109, United States of America

[46] State Key Laboratory of Organic-Inorganic Composites, College of Materials Science and Engineering, Beijing University of Chemical Technology, North Third Ring Road 15, Chaoyang District, Beijing 100029, People's Republic of China

[47] State Key Laboratory of New Ceramics and Fine Processing, School of Materials Science and Engineering, Tsinghua University, Shuangqing Road 30, Haidian District, Beijing 100084, People's Republic of China

[48] Instituto de Microelectrónica de Barcelona (IMB-CNM, CSIC), C/Til·lers s/n (Campus UAB), Bellaterra, Barcelona, Spain

[49] Catalonia Institute for Energy Research (IREC), Jardins de Les Dones de Negre 1, 08930, Sant Adrià de Besòs, Barcelona, Spain

[50] Instituto de Micro y Nanotecnología (IMN-CNM-CSIC), C/Isaac Newton 8, PTM, E-28760 Tres Cantos, Spain

[51] Dipartimento di Ingegneria dell'Informazione, Università di Pisa, Via G. Caruso, I-56122 Pisa, Italy

[52] CNRS-Saint Gobain-NIMS, IRL 3629, LINK, National Institute for Materials Science (NIMS), 1–1 Namiki, Tsukuba 305–0044, Japan

[53] National Institute for Materials Science (NIMS), WPI International Center for Materials Nanoarchitectonics (WPI-MANA), 1-1 Namiki, Tsukuba 305-0044, Japan

[54] Graduate School of Pure and Applied Sciences, University of Tsukuba, Tennoudai 1-1-1, Tsukuba 305-8671, Japan

[55] Institute of Chemical Sciences and Centre for Advanced Energy Storage and Recovery, School of Engineering and Physical Sciences, Heriot-Watt University, Edinburgh EH14 4AS, United Kingdom

[56] Institut Jean Lamour, UMR 7198 CNRS—Université de Lorraine, 2 allée André Guinier-Campus ARTEM, BP 50840, 54011 Nancy Cedex, France

[57] Institut des Sciences Chimiques de Rennes, UMR 6226 CNRS—Université de Rennes 1—INSA de Rennes, 11 allée de Beaulieu, CS 50837, F-35708 Rennes Cedex, France

[58] Cavendish Laboratory, University of Cambridge, JJ Thomson Avenue, Cambridge CB3 0HE, United Kingdom

[59] Physikalisch-Technische Bundesanstalt (PTB), Abbestrasse 2-12, Berlin, 10587, Germany

[60] NNU-SULI Thermal Energy Research Center (NSTER) and Center for Quantum Transport and Thermal Energy Science (CQTES), School of Physics and Technology, Nanjing Normal University, Nanjing 210023, People's Republic of China

[61] Institute of High Performance Computing, A*STAR, Singapore 138632, Singapore

[62] Faculty of Materials Science and Engineering, Kyoto Institute of Technology, Kyoto 606-8585, Japan

[63] Department of Chemistry, University College London, 20 Gordon Street, London WC1H 0AJ, United Kingdom

[64] School of Engineering and Materials Science, Queen Mary University of London, Mile End Road, London E1 4NS, United Kingdom

[65] George W. Woodruff School of Mechanical Engineering, Georgia Institute of Technology, Atlanta, GA 30332, United States of America

[66] The Molecular Foundry, Lawrence Berkeley National Laboratory, Berkeley, CA 94720, United States of America

[67] Sandia National Laboratories, Livermore, CA 94551, United States of America

[68] King Abdullah University of Science and Technology (KAUST), KAUST Solar Center (KSC), Thuwal 23955-6900, Saudi Arabia

[69] Center for Nano Science and Technology@PoliMi, Istituto Italiano di Tecnologia, Via Pascoli 70/3, 20133 Milano, Italy

[70] Electronics and Computer Science, University of Southampton, Highfield Campus, Southampton SO17 1BJ, United Kingdom

[71] Key Laboratory for the Physics and Chemistry of Nanodevices and Center for Carbon-based Electronics, School of Electronics, Peking University, Beijing 100871, People's Republic of China

[72] AMO GmbH, Otto-Blumenthal-Str. 25, 52074 Aachen, Germany

[73] Chair of High Frequency Electronics, RWTH Aachen University, Kopernikusstr. 16, 52074 Aachen, Germany

74 Chair of Electronic Devices, RWTH Aachen University, Otto-Blumenthal-Str. 2, 52074 Aachen, Germany
75 James Watt School of Engineering, University of Glasgow, Glasgow G12 8QQ, United Kingdom
76 Warwick Manufacturing Group (WMG), The University of Warwick, Coventry CV4 7AL, United Kingdom
77 Departments of Mechanical, Materials and Manufacturing Engineering, University of Nottingham (Malaysia Campus), Semenyih 43500 Selangor, Malaysia
78 Institute of Solid State Electronics, Technische Universität Dresden, 01062 Dresden, Germany
79 Department of Electronics and Communication Engineering, Koneru Lakshmaiah Education Foundation, Andhra Pradesh 522302, India
80 Department of Aeronautics, Imperial College London, Exhibition Road, London SW7 2AZ, United Kingdom
*   Authors to whom any correspondence should be addressed

E-mail: vincenzo_pecunia@sfu.ca, sk568@cam.ac.uk and s.silva@surrey.ac.uk

Abstract

Ambient energy harvesting has great potential to contribute to sustainable development and address growing environmental challenges. Converting waste energy from energy-intensive processes and systems (e.g. combustion engines and furnaces) is crucial to reducing their environmental impact and achieving net-zero emissions. Compact energy harvesters will also be key to powering the exponentially growing smart devices ecosystem that is part of the Internet of Things, thus enabling futuristic applications that can improve our quality of life (e.g. smart homes, smart cities, smart manufacturing, and smart healthcare). To achieve these goals, innovative materials are needed to efficiently convert ambient energy into electricity through various physical mechanisms, such as the photovoltaic effect, thermoelectricity, piezoelectricity, triboelectricity, and radiofrequency wireless power transfer. By bringing together the perspectives of experts in various types of energy harvesting materials, this Roadmap provides extensive insights into recent advances and present challenges in the field. Additionally, the Roadmap analyses the key performance metrics of these technologies in relation to their ultimate energy conversion limits. Building on these insights, the Roadmap outlines promising directions for future research to fully harness the potential of energy harvesting materials for green energy anytime, anywhere.

Contents

1. Introduction

Vincenzo Pecunia[1] *and S Ravi P Silva*[2]
[1] School of Sustainable Energy Engineering, Simon Fraser University, Surrey V3T 0N1, BC, Canada
[2] Advanced Technology Institute, Department of Electrical and Electronic Engineering, University of Surrey, Guildford, Surrey GU2 7XH, United Kingdom

In the face of the rising global energy demand and the existential challenge posed by climate change, it is more urgent than ever to generate green energy in order to preserve our planet and sustain human development. Alongside the need for renewable energy technologies for the conversion of primary green energy into electricity in large-scale installations (e.g. solar, wind, and wave farms), reducing our carbon footprint also requires harnessing the vast energy reservoir all around us in the form of ambient light, mechanical vibrations, thermal gradients, and radiofrequency electromagnetic waves [1]. Harvesting this energy via compact harvesters paves the way not only for more efficient use of our energy sources (for instance, consider the recycling of waste heat from an oven or industrial machinery) but also for sustainably powering technologies with considerable potential to enhance our quality of life without increasing our carbon footprint [2, 3]. Prominently, compact energy harvesters are key to enabling the Internet of Things (IoT), which aims to make our everyday objects and environments 'smart' via its ecosystem of interconnected smart sensors, thereby allowing for better functionality of technology and its optimum use (for instance, leading to smart homes, smart cities, smart manufacturing, precision agriculture, smart logistics, and smart healthcare) [4]. Importantly, the IoT device ecosystem will comprise several trillions of sensors in the near future [5]. This would make it unfeasible and unsustainable to exclusively rely on batteries as their power source—due to their environmental impacts as well as the challenge and cost of replacing hundreds of millions of batteries globally every day. However, compact energy harvesters could overcome this challenge by allowing IoT devices to operate continuously and in an eco-friendly manner throughout their lifetime [6, 7]. The burgeoning of wearable electronics, with its vast potential for health and wellness applications [8], is another related domain that would greatly benefit from compact energy harvesters—given that, in addition to being surrounded by ambient energy, the human body itself is a source of waste energy in the form of body heat and motion.

Energy harvesting is critically dependent on the availability of suitable materials (and devices thereof) to convert ambient energy into usable electric energy. Therefore, research in materials and devices for energy harvesting is key to providing energy harvesting technologies that can meet the needs of real-world applications. Such research requires a broad, cross-cutting effort, ranging from the discovery of new materials to the study of their energy harvesting properties, the engineering of their compositions, microstructure, and processing, and their integration into devices and systems. Given the diverse forms of ambient energy, materials are being developed to convert such energy through various physical mechanisms, the most prominent of which are the photovoltaic effect, piezoelectricity, triboelectricity, thermoelectricity, and radiofrequency power transfer (figure 1). The rapid rise in the number of publications in this field (figure 2) demonstrates its growing importance and the breadth of the community that has joined this research effort.

While the vision of 'green energy anytime, anywhere' may still be some way into the future, energy harvesting technologies already offer numerous opportunities. For instance, photovoltaic harvesters have already been commercialized to power various smart sensors, while triboelectric, thermoelectric, piezoelectric, and radiofrequency energy harvesters have already been demonstrated to be capable of powering wearable devices [9–12].

Although the various energy harvesting technologies rely on considerably different classes of materials and devices, they all share the same overarching goals and challenges—which will continue to drive future research pursuits in this area—as discussed below.

Efficiency

A major challenge faced by all energy harvesting technologies is the limited power density available from ambient energy sources, which makes it essential to develop energy harvesting materials and devices that can efficiently convert such energy. Current energy harvesting technologies typically deliver electric power densities well below the mW cm^{-2} when harvesting ambient energy. This can be limiting for energy-intensive applications that do not allow aggressive duty cycling (i.e. a system operation pattern with long intervals in sleep mode, during which the harvested energy can be stored, alternating with short intervals in active mode, during which the stored energy is consumed) [2, 7]. Additionally, many emerging applications require compact energy harvesters with feature sizes in the millimetre-to-centimetre range. Therefore, boosting power conversion efficiencies is a vital goal of energy harvesting research. The success of

Figure 1. Prominent energy harvesting technologies covered in this Roadmap (RF: radiofrequency). Reproduced from [7] under the terms of a CC BY 4.0 open-access license.

Figure 2. Publications per year for the various energy harvesting technologies covered in this Roadmap. This data was obtained from the Web of Science by searching the phrases 'indoor photovoltaics', 'piezoelectric harvesting', 'triboelectric harvesting', 'thermoelectric harvesting', and 'RF harvesting' (PV: photovoltaics; RF: radiofrequency).

this endeavour critically depends not only on characterizing and gaining insight into the fundamental properties of energy harvesting materials, but also on the discovery of new materials and the engineering of their device architectures to reduce loss mechanisms.

Manufacturability

Real-world applications critically require the development of energy harvesting technologies that can be manufactured at scale. Therefore, a priority is to develop energy harvesting materials that can be produced with simple methods, involving low capital cost and low material and energy consumption.

Environmental Sustainability

While energy harvesters inherently have no carbon emissions during operation, they will fully realize their purpose of providing green energy if they have minimal environmental impacts throughout their lifecycle. Therefore, a priority is to develop energy harvesting technologies that rely on Earth-abundant, non-toxic source materials and can be processed with low energy consumption. Additionally, it is important to consider the fate of these materials and devices at their end of life. Therefore, a key priority is to pursue energy harvesting materials and devices that lend themselves to be easily recycled from cradle to grave [13]. Moreover, for applications that involve a short life cycle, energy harvesters that are biodegradable would be highly desirable.

Cost

For any energy harvesting technology to have a practical impact, it is necessary that its cost is sufficiently low to enable widespread deployment. In contrast to large-scale installations for the conversion of primary green energy into electricity (e.g. solar and wind farms), the crucial cost-related objective for ambient energy harvesters is not necessarily to minimize the cost per Watt. Indeed, the paramount aim is to ensure that ambient energy harvesters have a cost that is a manageable fraction of the system cost, while also being capable of supplying an energy output adequate for the application at hand. Cost is obviously a challenging metric to evaluate at the early stage of a technology, given that learning curves typically result in substantial cost reductions over time. Nonetheless, it is important to keep cost considerations in context as energy harvesting technologies are being developed, prioritizing solutions that rely on Earth-abundant materials and low-energy manufacturing processes.

Form Factors

For energy harvesters to be deployed ubiquitously, it is essential to develop them in flexible form factors so as to seamlessly place them on all kinds of objects and surfaces. Therefore, a research direction of paramount importance is to develop energy harvesting materials and devices capable of high power conversion efficiencies while being mechanically flexible or stretchable and optimized for small areas. The ubiquity and functionality of this novel system will act as an overlay to future wearables.

This Roadmap provides extensive insights into the status and prospects of the various energy harvesting technologies being researched to address the aforementioned challenges. It does so by covering the various classes of materials being developed for photovoltaic (section 2), piezoelectric (section 3), triboelectric (section 4), thermoelectric (section 5), and radiofrequency (section 6) energy harvesting. In particular, this Roadmap highlights the key trends in materials properties and device performance underlying these prominent energy harvesting technologies, also discussing the open challenges and the potential strategies to overcome them. Finally, a perspective is presented on the key sustainability challenges that need to be tackled in energy harvesting materials research (section 7). Based on these insights, it is envisaged that this Roadmap will catalyse further advances in energy harvesting materials and devices, bringing us closer to realizing the vision of 'green energy anywhere, anytime'.

2. Materials for indoor photovoltaics

2.1. Introduction to indoor photovoltaics

Vincenzo Pecunia[1] and S Ravi P Silva[2]
[1] School of Sustainable Energy Engineering, Simon Fraser University, Surrey V3T 0N1, BC, Canada
[2] Advanced Technology Institute, Department of Electrical and Electronic Engineering, University of Surrey, Guildford, Surrey GU2 7XH, United Kingdom

Photovoltaic devices enable the direct conversion of light into electricity: the energy harvested from the light impinging on the photoactive material of choice (*absorber*) excites the charges within the material; the resultant mobile charges are transported to and collected at two opposite electrodes, thereby delivering an electric current and voltage (figure 3(a)) that can be used for doing work. The ubiquity of light makes photovoltaics a highly attractive energy harvesting technology due to their wide deployability [7]. Moreover, the wave nature of light—with its very short wavelength in comparison to the thickness of the material layers typically found in photovoltaic devices—ensures that much energy density can be transported even in the case of non-line-of-sight situations without a physical medium being present. Additionally, based on typical ambient illumination levels, the power density that photovoltaics can supply is at the high end of all the energy harvesting technologies (section 1), with the intermittency of its underlying energy transmission being generally manageable due to the predictability of its temporal patterns. By virtue of all these factors, photovoltaics occupies a prominent role both in indoor energy harvesting and for large-scale outdoor deployment, with its significance and impact being expected to grow dramatically in the future as the current materials challenges are addressed [14].

The use of photovoltaics for the conversion of terrestrial outdoor solar light into electricity—through arrays of solar panels deployed on rooftops or in large-scale solar farms (*outdoor solar photovoltaics*)—is undoubtedly dominant and justifiably so due to the high energy density (in the range of 10–100 mW cm^{-2}) of outdoor terrestrial solar illumination. Harvesting outdoor solar light also applies to building-integrated photovoltaics, which involves solar panels embedded into the building envelope (e.g. as part of façades, roofs, and windows). Alongside solar photovoltaics, recent years have witnessed the rapid rise of indoor photovoltaics, which involves the conversion of ambient *indoor* light into electricity. This trend parallels the strong demand for energy technologies that could sustainably power the exponentially growing ecosystem of IoT smart sensors—expected to grow to several trillion units in the near future—that are an essential constituent of the IoT. Indeed, most IoT applications rely on smart devices placed indoors (e.g. for smart homes, smart buildings, and smart manufacturing). From an energy harvesting perspective, indoor photovoltaics presents a more stringent scenario, given the considerably lower power density found in the ambient indoor light (in the range of 70–350 μW cm^{-2}) supplied by fluorescent and white light-emitting diode lighting. Therefore, developing photovoltaic technologies that can function at such low illumination levels is critical to sustainably powering the vast IoT smart sensor ecosystem. The significance and potential of indoor photovoltaics are also confirmed by the growth of its market size, which is projected to reach 1 billion dollars within the next few years, meanwhile having a compound annual growth rate (CAGR) of 70% and hence being the fastest-growing segment within the entire photovoltaic market (by contrast, solar and building-integrated photovoltaics are growing with a CAGR of 7.4% and 16%, respectively) [15].

The performance of an indoor photovoltaic cell can be quantified in terms of its indoor power conversion efficiency (PCE(i)), which expresses the ratio between the maximum electric power generated by the cell, $P_{el,max}$, and the optical power reaching the cell from the indoor light source, $P_{opt,S_n(\lambda)}$, where $S_n(\lambda)$ is the spectral irradiance at the surface of the photovoltaic cell:

$$\text{PCE(i)}_{S_n(\lambda)} = P_{el,max}/P_{opt,S_n(\lambda)}. \qquad (1)$$

Note that, due to the current lack of a standard spectrum for the assessment of PCE(i), a given indoor photovoltaic cell may present differing PCE(i) values depending on the light source considered—with the relative efficiency variations depending on the level of spectral match between the absorber and the illuminant as well as the irradiance of the latter. Additionally, note that the acronym PCE(i) is adopted herein to refer to the power conversion efficiency of indoor photovoltaic cells to prevent confusion with the power conversion efficiency of outdoor terrestrial solar cells (commonly indicated as PCE). Indeed, while conceptually analogous, the two metrics are not directly comparable due to the different luminous sources relevant to the two scenarios.

In addition to their much lower irradiance levels compared to outdoor terrestrial solar light, typical artificial indoor light sources (i.e. fluorescent and white-light-emitting-diode lighting) are characterized by a

Figure 3. (a) Sketch of the operation of a photovoltaic device: photons (each having an energy equal to $h\nu$) are dissipated in the absorber and are thus converted into mobile charges, i.e. electrons (denoted by a solid black circle) and holes (denoted by an empty circle), whose transport to and collection at the electrodes result in an electric current and voltage. The icon representing a light-emitting-diode bulb is re-used with permission from Flaticon.com. (b) Normalized emission spectra of the Sun and fluorescent and white-light-emitting-diode lamps. FL: fluorescent lighting. WLED: white-light-emitting-diode lighting. AM 1.5G: reference Air Mass 1.5 Gobal spectrum of sunlight.

Figure 4. (a) PCE(i) of the champion devices of various indoor photovoltaic technologies for an illuminance of or close to 1000 lx. We calculated the radiative limit (denoted by the green trace) for single-layer device structures based on the white-light-emitting-diode spectrum shown in figure 3(b), while the data points are derived from [17–24]. (b) Relative PCE(i) deficit with respect to the PCE(i) in the radiative limit, PCE(i)$_{RL}$, for the various technologies presented in (a). PVSK: halide perovskites; Pb-Free PVSK: lead-free halide perovskites; DSSC: dye-sensitized solar cells; OPV: organic photovoltaics; QD: quantum dots.

rather distinct spectral content, as their emission spectra exclusively cover the visible range (by contrast, approximately half of the terrestrial solar light falls in the near-infrared spectral region) (figure 3(b)). This aspect is particularly consequential because it impacts the conditions that an absorber should meet to deliver optimum photovoltaic efficiency. As shown in figure 4(a), in the radiative limit and for typical indoor light sources (i.e. fluorescent and white-light-emitting-diode lamps), the optimum bandgap for an absorber to deliver high-efficiency indoor photovoltaics amounts to 1.8–2.0 eV (by contrast, outdoor terrestrial solar photovoltaics requires a bandgap of $\cong$1.1–1.5 eV for optimum performance) [7]. Moreover, the narrower spectral range of indoor light sources compared to the solar spectrum (figure 3(b)) enables maximum theoretical efficiencies (in the radiative limit) of up to $\cong$60% for single-junction devices (by contrast, the corresponding limit for outdoor terrestrial solar photovoltaics amounts to 33.7%) [7]. This implies that indoor photovoltaics could theoretically deliver power densities of up to $\cong$40–200 μW cm^{-2} (for typical indoor illumination levels of 70–350 μW cm^{-2}).

While crystalline silicon (c-Si) is the dominant semiconductor technology for terrestrial solar photovoltaics, the PCE(i) values of commercial c-Si solar cells are rather low (up to $\cong 12\%$) because of their low shunt resistance and comparatively narrow bandgap of c-Si (1.12 eV) [16]. In fact, hydrogenated amorphous silicon (a-Si:H) cells have long been the commercially dominant technology for indoor photovoltaics [12]: not only do they deliver PCE(i) values of 4%–9% [16] in commercial devices due to the wider bandgap of a-Si:H ($\cong 1.6$–1.8 eV), but they also allow simpler manufacturing and mechanical flexibility, thereby enabling significant cost reductions and straightforward integration of indoor photovoltaics in a wide range of objects and environments. Notwithstanding the commercial dominance of a-Si:H in the indoor photovoltaics arena, commercial a-Si:H cells are characterized by a particularly large efficiency deficit with respect to the ultimate efficiency potential of indoor photovoltaics (i.e. the radiative-limit efficiency $PCE(i)_{RL}$), which can be traced to a significant extent to the inherent optoelectronic and materials properties of a-Si:H. Consequently, a grand challenge in indoor photovoltaics research is to develop absorbers and device architectures that are capable not only of reliably surpassing the commercial state of the art (essentially, the 10% PCE(i) threshold) but that can also approach the ultimate PCE(i) limit of 60%. This endeavour is all the more worthwhile because its success would enhance the reach and impact of indoor photovoltaics as a leading energy harvesting technology: it would enable indoor photovoltaics to extend the operational lifetime of battery-less smart devices, enhance their miniaturization, and deliver sufficient power for smart devices capable of more complex, multifunctional, and energy-intensive computing.

The ambition to realize indoor photovoltaics with efficiencies approaching the radiative limit has prompted the exploration of new materials and new device architectures, as well as the revisitation of conventional photovoltaic technologies in the context of indoor light harvesting. In regard to emerging technologies, remarkable progress has been achieved with organic (section 2.5), dye-sensitized (section 2.6), and perovskite (section 2.7) cells, all delivering PCE(i) values in the range of 30%–40% in champion devices (figure 4(a)). Meanwhile, alternative families of absorbers—e.g. kesterites (section 2.4), lead-free perovskite derivatives (section 2.8), and non-toxic quantum-dot semiconductors (section 2.9)—have been pursued to address the toxicity or material scarcity issues faced by some of the emerging technologies. Moreover, the re-energized exploration of silicon-based absorbers and the optimization of III–V technologies (section 2.2) for indoor photovoltaics have delivered significant progress, with efficiencies in the 30%–40% being achieved in some cases (figure 4(a)). Concurrently, CdTe has also shown promising indoor photovoltaic performance (section 2.3) (figure 4(a)).

Despite these considerable research achievements, the ultimate radiative efficiency limit of 60% is far from being reached, as also revealed by the plot in figure 4(b), which presents the relative PCE(i) deficit of the various photovoltaic technologies with respect to the PCE(i) in the radiative limit, $PCE(i)_{RL}$. This plot highlights a particularly large relative efficiency deficit of 40%–70% for nearly all technologies, which therefore prompts the pursuit of new materials and device architectures to advance the state of the art—e.g. compositional engineering and defect passivation strategies to reduce recombination losses, as well as device engineering to enhance the shunt resistance. Additionally, even when a smaller deficit is achieved (as in the perovskite case), figure 4(a) highlights that bandgap optimization remains crucial for the 60% efficiency limit to be approached, which points to the need to focus on materials technologies that allow bandgap tuning toward the $\cong 1.9$ eV optimum.

Furthermore, the lack of a standard indoor light spectrum (e.g. see figure 3(b)) has made the characterization of the efficiency of indoor photovoltaics prone to ambiguities (see equation (1)), thereby giving rise to the need to establish solid characterization protocols for the field to advance further, as discussed in section 2.10.

Apart from performance considerations, the future progress of indoor photovoltaics will also considerably depend on the use of technologies that are based on eco-friendly, Earth-abundant materials and straightforward manufacturing processes. Toxicity issues are particularly significant because indoor photovoltaics are intended to be deployed in everyday objects and environments. Hence, it is crucial to avoid that the end-users could be exposed to toxic materials accidentally released from indoor photovoltaic cell. Therefore, materials engineering and materials discovery toward eco-friendly, Earth-abundant, and easy-to-make indoor photovoltaics are key to ensuring its sustainability [7].

The following contributions (sections 2.2–2.10) discuss the specifics of these grand challenges in the context of various indoor photovoltaic technologies, also identifying potential avenues to overcome these challenges. By presenting a comprehensive roadmap of indoor photovoltaic materials, we envisage that the insights provided herein and in the rest of this section could catalyse further advances in the field toward the realization of the full potential of indoor photovoltaics as a green energy harvesting technology.

2.2. III–V compound semiconductors for indoor photovoltaics

Jamie D Phillips
Department of Electrical and Computer Engineering, University of Delaware, Newark, DE 19716, United States of America
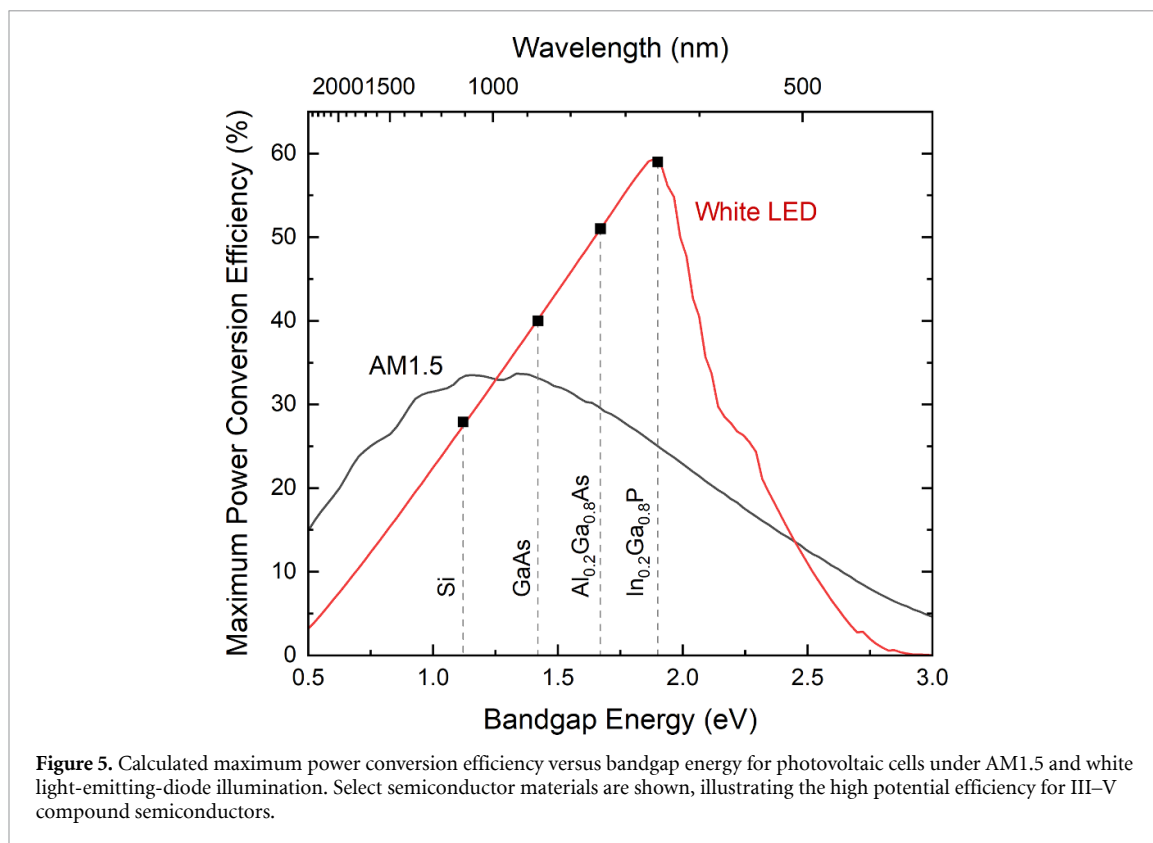
Status

Photovoltaic energy harvesting from indoor lighting sources presents unique challenges and constraints in comparison to conventional solar photovoltaics, where the differing cost and performance tradeoffs lend themselves to consider III–V compound semiconductor devices. The narrowband spectrum of indoor lighting sources, irradiance levels that are orders of magnitude lower than typical sunlight conditions, and desire for direct integration of power systems on devices place emphasis on high cell performance and integration capabilities. Compound semiconductors based on III–V materials provide a range of available bandgap energies that span the desired window in the visible spectrum for indoor lighting (see figure 5), while also demonstrating very high optical absorption coefficients and carrier transport properties that can achieve high power conversion efficiency at low irradiance conditions. The optimal bandgap energy of approximately 2 eV for photovoltaics operating under high-efficiency indoor lighting are well matched to mature III–V materials including AlGaAs and InGaP, with a theoretical power conversion efficiency of around 50% and higher [16] at typical indoor irradiance conditions (500 lx). Experimentally, power conversion efficiencies of >20% have been reported for AlGaAs [25] and >30% for InGaP [20], dramatically outperforming prior commercial indoor photovoltaic devices based on amorphous silicon (<10%). The high performance of III–V devices and opportunities for further improvements in efficiency (see figure 5) are linked to the outstanding fundamental electronic and optical material properties and the ability to 'bandgap engineer' sophisticated device structures. The superior power conversion efficiency offered by III–V photovoltaics provides unique opportunities for miniaturized self-powered systems, where unlike solar photovoltaics, power density is more important than cost per unit area. Indoor photovoltaics based on III–V compounds are likely to play a major role in self-powered devices for the IoT through continued advances to improve power conversion efficiency and to develop architectures for direct system integration.

Current and future challenges

Primary research challenges for realizing the potential of III–V indoor photovoltaics can be categorized as issues related to cell performance, cost feasibility, and system integration. While high power conversion efficiency has already been realized for AlGaAs and InGaP devices, performance is still only about half of the theoretical limit for indoor lighting conditions. Continued optimization of device structures for the indoor lighting spectrum and irradiance levels would be expected to result in substantial gains in efficiency. Device structure optimization parameters to pursue include epitaxial structure thickness, bandgap, and doping concentration of emitter, base, window, and barrier layers [26]. Reduction of dark current is a primary limitation for low irradiance conditions, which is dominated in III–V devices by non-radiative surface/sidewall perimeter recombination [27]. Further reductions in dark current will require approaches to passivate recombination centres or to isolate minority carriers from these interfaces. Cost feasibility is a pervasive challenge for III–V devices due to the higher cost of substrate materials and epitaxial growth processes in comparison to silicon microelectronics. However, the high performance offered by III–V photovoltaics make them preferable for applications where power density is at a premium provided that the cost of the energy harvesting device is a manageable fraction of the overall system cost. Cost-effective approaches to realize III–V photovoltaics are a current research challenge, which includes strategies for large scale production to leverage economies of scale. The adoption of III–V photovoltaics will depend on the ability for direct system integration to provide an effective power unit. Target applications will likely be miniaturized self-powered systems where the overall efficiency of the power unit require optimization and co-design of the photovoltaic device, power management circuitry, and any energy storage devices. At the photovoltaic device level, there are research challenges to consider the development of appropriate multi-junction devices and series-connected modules on a chip for efficient voltage up-conversion [28].

Advances in science and technology to meet challenges

A primary thrust for improving the efficiency of III–V indoor photovoltaics should explore means of reducing non-radiative surface/sidewall recombination. Example techniques may include continued exploration of chemical surface treatments and surface passivation layers. High-quality epitaxial regrowth of wide-bandgap III–V materials on exposed interfaces may offer dramatic improvements in interface quality. There have been several techniques that have been proposed to develop cost-effective III–V photovoltaics (primarily for solar energy conversion) including epitaxial liftoff [29], hydride vapour phase epitaxy (HVPE)

Figure 5. Calculated maximum power conversion efficiency versus bandgap energy for photovoltaic cells under AM1.5 and white light-emitting-diode illumination. Select semiconductor materials are shown, illustrating the high potential efficiency for III–V compound semiconductors.

[30], and roll-to-roll printing [31]. The epitaxial liftoff approach offers a method for substrate reuse, eliminating the major cost of substrates as a part of the overall cell cost. Techniques such as HVPE can reduce the cost of epitaxial growth through efficient use of precursor materials. Large scale production such as roll-to-roll printing offer a means to achieve low cost at high volume. Technology advances will be needed to enable III–V device integration with systems ranging from the macroscale to the microscale. Larger scale devices and systems (approximately 1 cm and larger) will require development of suitable packaging technologies to interface with systems. An attractive advantage of III–V devices is the ability to use thin device layers via wafer liftoff, where mechanically flexible photovoltaic devices [29] may be used to accommodate a wide range of system form factors. Smaller scale systems at the millimetre size and below will rely on continued advances in heterogeneous integration with silicon microelectronics. This is a technology area that is rich for development, where there is a desire to leverage both the high-performance of III–V materials and sophistication of silicon microelectronics for applications including photonic integrated circuits, microelectromechanical systems, high-frequency electronics, and energy conversion systems such as described in this work. Heterogeneous integration strategies include epitaxial liftoff and cold welding, direct wafer bonding, micro-transfer printing, and selective epitaxy of III–V materials on silicon.

Concluding remarks

The outstanding optical and electronic properties of III–V compound semiconductors offer the highest power conversion efficiency for indoor photovoltaics, with continued room for performance improvement through optimization of device structures and material interfaces. The adoption of III–V photovoltaics will depend on the cost practicality of these devices for a given system application. The most likely applications to incorporate III–V indoor photovoltaics will be systems where size, weight, and power are at a premium. Furthermore, the continued trajectory of advanced self-powered microscale systems may be enabled by the high power density provided by III–V photovoltaics.

2.3. CdTe solar cells for indoor applications

Elisa Artegiani and Alessandro Romeo
LAPS- Laboratory for Photovoltaics and Solid-State Physics, Department of Computer Science, University of Verona, Ca' Vignal 1, Strada Le Grazie 15, 37134, Verona, Italy

Status

CdTe thin film based solar cell technology has achieved, so far, the largest deployment on large scale manufacturing among thin film technologies. These have a very good advantage for product-integrated photovoltaics that is the capability to be deposited on every type of substrate, from glass to metal and they can become extremely lightweight and flexible when deposited on flexible substrates [32].

In year 2021 almost 80% of the thin film solar cell market was CdTe based with an overall production of 6.1 GWp [33]. CdTe photovoltaic devices have achieved an efficiency of 22.1% on a small area for outdoor solar photovoltaics [34] but most important, unlike other technologies, the efficiency of the solar modules in production is not far from the record values: 18.7%. The main reason for this achievement is due to the intrinsic properties of the CdTe absorber, which has a very simple phase diagram. The required stoichiometry (tendentially 50–50 for Cd and Te) is easily obtained also at relatively low temperatures (below 400 °C) and with no issues of unexpected and uncontrolled secondary phases [34].

CdTe is a direct band gap semiconductor with a value of 1.45 eV which is very near to the Shockley–Queisser optimum for outdoor solar photovoltaics, it also has a high absorption coefficient that allows to collect the photons with thicknesses down to 2 μm [34]. Furthermore, CdTe can be successfully deposited with a large variety of different deposition methods, the most important are: thermal evaporation [35], close space sublimation [36], electrodeposition [37], vapour transport deposition [38].

In low light conditions, the spectrum changes with a wavelength shift towards the blue region, so the light power is concentrated in the 300–500 nm range. In this case, CdTe, which is mainly operating in the visible part of the spectrum, is much better performing, as also shown by different independent analysis. The highest indoor photovoltaic efficiency obtained from CdTe devices to date is 17.1% under white light-emitting-diode illumination.

Current and future challenges

CdTe thin film solar cells are typically fabricated in superstrate configuration, on a transparent conductive oxide coated soda lime glass.

Historically the cell is based on a CdS buffer layer for the separation of the charges. CdS is a semiconductor with a band gap of 2.4 eV and needs to be very thin in order to reduce the parasitic absorption in the 400 nm range. However, in recent times the structure of the solar cell has been radically changed with the introduction of a graded band gap. In this case CdTe compound forms a junction with a $CdSe_xTe_{1-x}$ mixed compound (with a band gap of 1.4 eV). In this configuration CdS is no longer necessary and a high resistance layer (HRT) is interposed between the $CdSe_xTe_{1-x}$ film and the front contact.

This is particularly important for indoor application because it increases the spectral response in the spectral region of indoor lights, as shown in figure 6.

CdTe solar cells are most successfully fabricated by physical vapour deposition processes, such as vapour transport deposition/ close space sublimation that are based on the sublimation of the CdTe in an inert gas atmosphere at a substrate temperature of about 500 °C, as well as thermal evaporation where CdTe is deposited in vacuum at a substrate temperature in the range of 300 °C–350 °C.

The device made in our laboratories consists of a commercial SnO_2/SnO_2:F (TO/FTO) coated soda lime glass (TEC12), so in our case the HRT layer is TO, while also $Mg_xZn_{1-x}O$ can be used [21]. CdSe and CdTe are deposited by thermal evaporation, the typical standard $CdCl_2$ treatment for CdTe recrystallization, CdSe–CdTe mixing and $CdSe_xTe_{1-x}$/CdTe junction promotion is provided by drop casting of methanol solution.

With a similar process, CdS was used as buffer layer, we have previously demonstrated flexible CdTe devices on either polyimide or ultra-thin glass [32]. This is a very important feature for consumer electronics and so for indoor applications since it allows to adapt to different products, and it does not increase the weight of the final device.

CdTe solar cells have a demonstrated superior performance under low light irradiance where the reduction of open circuit voltage is restrained. With a very simple 1-diode model the ideality factor reduces

Figure 6. External quantum efficiency: CdS/CdTe vs. CdSe$_x$Te$_{1-x}$/CdTe.

Figure 7. Efficiency of CdTe solar cells in respect to irradiation power and spectrum. LED: light-emitting diode.
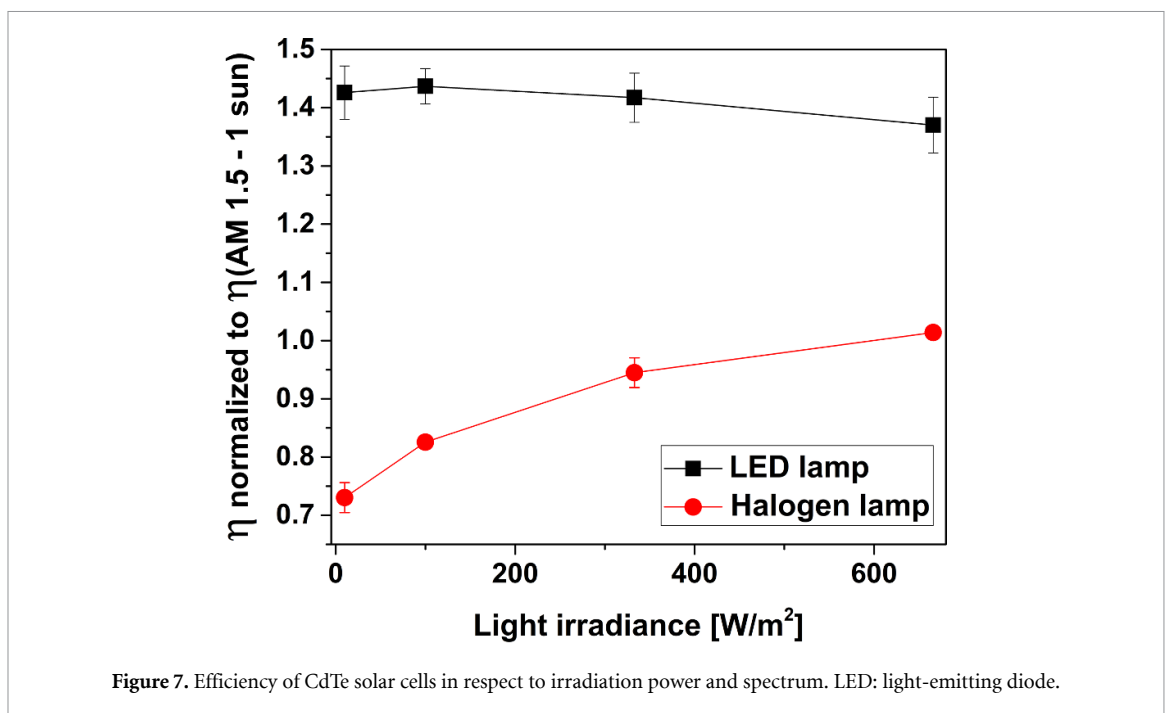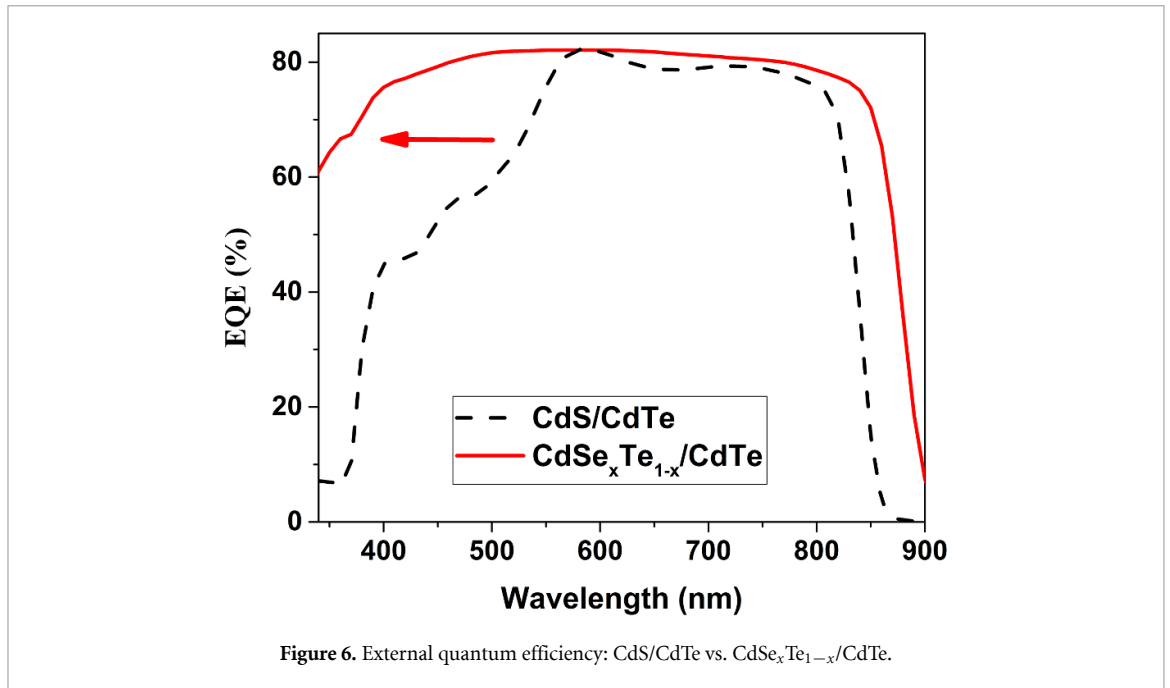
towards one suggesting a change in transport mechanism corresponding to a more ideal junction [39]. This effect has been registered also in our samples.

Advances in science and technology to meet challenges

In figure 7 we compare the efficiencies of the cells measured under halogen and light-emitting-diode illumination, with different light irradiances. These values are normalized to the efficiency measured in standard conditions (AM 1.5–1 sun).

Under low light irradiance, the efficiency is only slightly reduced in the case of halogen lamp, while it even increases when illuminated by a light-emitting diode. In both cases, this is due to a modest reduction in open circuit voltage along with an improvement in fill factor.

The increase of efficiency for the light-emitting-diode case is due to the irradiation spectrum of this light which is exactly concentrated in the same range of the CdTe response (see figure 6). This, considering the transition to light-emitting-diode lighting, further favours CdTe technology for indoor applications.

One very important limitation for CdTe technology to indoor application is the national and international regulations that consumer electronics are subjected to. These set a maximum concentration of chemical elements that are considered dangerous to humans. Despite that CdTe is not registered as carcinogenic due to its impressive stability (decomposition occurs with temperatures above 1100 °C and dissolution in water does not occur), it is subjected to RoHS (Restriction of Hazardous Substances Directive) in the European Union (similar directives are extended to other countries). According to RoHS , the maximum permitted concentrations in non-exempt products are 0.1% or 1000 ppm (except for cadmium, which is limited to 0.01% or 100 ppm) by weight. The restrictions are attributed to a so-called *homogeneous* material in the product, this applies to each part that can be separated mechanically. In the latest design of CdTe solar cells where CdS is removed, cadmium, which is a heavy metal, is present only in the absorber. Considering the different densities of CdTe (5.85 g cm^{-3}) and of soda lime glass (2.8 g cm^{-3}) as well as considering the thickness of the two encapsulating glasses ($\geqslant 3$ mm) we can roughly estimate a required CdTe thickness of less than 0.8 μm. Our standard CdTe thickness is about 4.5 μm, about 5 times above the limit. However, we have demonstrated that is possible to fabricate CdTe devices with 0.7 μm with still an overall conversion efficiency of 8% [40].

Concluding remarks

CdTe has shown to be a very good candidate for product-integrated photovoltaics due to its robustness, reliability, high efficiency, and its suitability to be deposited on flexible devices.

Moreover, it has shown a remarkable behaviour for low light irradiation as demonstrated by different reports and papers also mentioned in this section. Furthermore, we have proved that with the new CdSe$_x$Te$_{1-x}$/CdTe configuration the device is very well performing under low light, and it is particularly suitable for light-emitting-diode indoor irradiation.

The main limitation to its application on devices is the ROHS directive which allows only 0.01% of Cd weight compared to the complete photovoltaic device. This however can be overcome if the solar cell is made with ultra-thin CdTe, below 0.8 μm. This configuration has been already demonstrated also at our laboratory. Efficiencies could become quite interesting if a back reflecting mirror would be applied on the back contact.

Acknowledgments

2.4. Kesterites for indoor photovoltaics

Hongjae Shim[1], Jongsung Park[2], Jin Hyeok Kim[3] and Jae Sung Yun[4]
[1] Australian Centre for Advanced Photovoltaics (ACAP), School of Photovoltaic and Renewable Energy Engineering, University of New South Wales, Sydney, NSW 2052, Australia
[2] Department of Energy Engineering, Future Convergence Technology Research Institute, Gyeongsang National University, Jinju, Gyeongnam 52828, Republic of Korea
[3] Optoelectronics Convergence Research Center, and Department of Materials Science and Engineering, Chonnam National University, Gwangju 61186, Republic of Korea
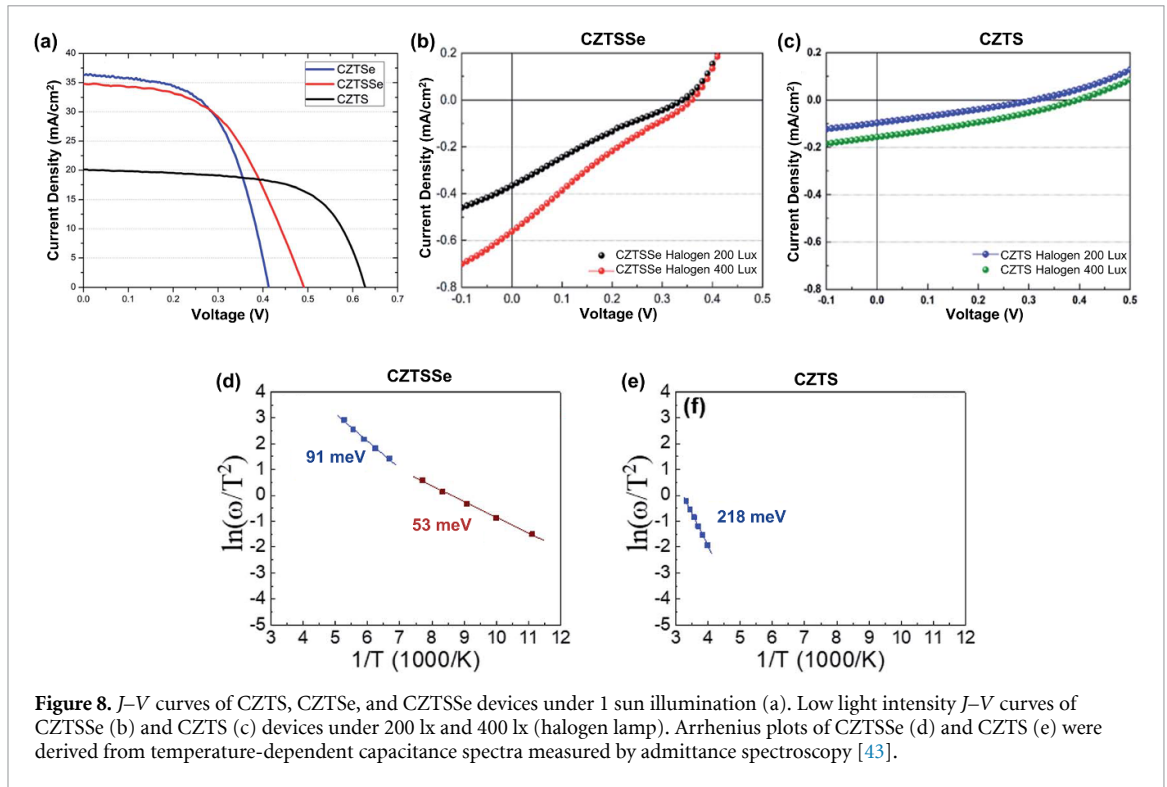[4] Advanced Technology Institute, Department of Electrical and Electronic Engineering, University of Surrey, Guildford, Surrey GU2 7XH, United Kingdom

Status
Kesterite $Cu_2ZnSn(S,Se)_4$ (CZTSSe) absorbers have incontrovertible advantages for indoor photovoltaics due to their non-toxicity, high stability, high absorption coefficient (10^4 cm^{-1}), and direct bandgap. Their bandgap tuneability (from 1.0 to 1.94 eV) by adjusting the [S]/[S +Se] ratio and substituting their constituents (Cu and Sn with Ag and Ge, respectively) allows the deposition of kesterites with optimum bandgap for indoor photovoltaics (1.9–2.0 eV) [41]. Furthermore, the possibility of depositing kesterite absorbers on flexible substrates facilitates their integration into diverse shapes and dimensions, as needed for IoT devices. In fact, related $Cu(In,Ga)(S,Se)_2$ (CIGS) chalcopyrite absorbers also have the same advantages; however, their rare constituents (In, Ga) may hinder the mass production of indoor energy harvesters. Therefore, kesterite absorbers can be a promising solution for indoor applications. However, their indoor photovoltaic performance requires further improvement, given that their highest reported efficiency to date is 8.8% under visible light-emitting-diode illumination with an irradiance of 18.5 mW cm^{-2} [42–44].

Current and future challenges
The advantages of kesterites have expanded their potential for both outdoor and indoor applications. However, these assets may only be exploited if the efficiencies reach levels attractive for commercialization (15%). In this regard, enormous works, including optimization of their elemental compositions, interface engineering, heterojunction optimization and treatment, and defect engineering have been conducted. Despite the diverse approaches to improving device performance, the evolution of their outdoor efficiency has stagnated at around 13% for a decade. The considerably high density of intrinsic defects (e.g. Cu_{Zn} and Zn_{Cu} antisites) and defect clusters (e.g. $[Cu_{Zn} + Zn_{Cu}]$), originating from compatible ionic radii of Cu and Zn, have been widely reported [44]. The charged point defects and defect clusters in bulk and near the interface of the p-type absorber layer and n-type buffer layer have been suspected to reduce V_{OC}, thus limiting the device performance. Considering the vulnerability of indoor photovoltaic devices caused by charge carrier traps under weak light, the role of defects and defect clusters that can induce trap levels would become more significant. Furthermore, CZTSSe-based devices with a high composition of Se possess the highest outdoor performance whilst increasing S incorporation generally deteriorates the device performance by forming Sn-related defects. A higher Se composition results in the reduction of bandgap around 1.1 eV, which is far away from the optimum bandgap range for indoor photovoltaics (1.8 eV to 2.0 eV); hence, it is not preferable for the performance of indoor kesterites. Park *et al* [43] compared the indoor device performance of CZTS-, CZTSe-, and CZTSSe-based solar cells (figures 8(b) and (c)), whose outdoor performances were compatible (figure 8(a)). This study demonstrated reduced efficiency in the CZTS devices due to a severe V_{OC} drop under weak light (figure 8(c)). The deeper defect level at 218 meV in the CZTS device compared to those (at 53 and 91 meV) in the CZTSSe counterpart was regarded as responsible for the lower device performance (figure 8(e)). A higher sulphur ratio is needed to widen the bandgap of CZTS absorbers for indoor photovoltaics. Hence, investigating the role of defects in kesterite films and developing proper defect engineering methods seem to be the key priorities for kesterite indoor photovoltaics.

Figure 8. *J–V* curves of CZTS, CZTSe, and CZTSSe devices under 1 sun illumination (a). Low light intensity *J–V* curves of CZTSSe (b) and CZTS (c) devices under 200 lx and 400 lx (halogen lamp). Arrhenius plots of CZTSSe (d) and CZTS (e) were derived from temperature-dependent capacitance spectra measured by admittance spectroscopy [43].

Advances in science and technology to meet challenges

One powerful approach to alleviate the dysfunctionalities of the antisite defects and defect clusters in kesterites for indoor applications is substituting Cu ions with cations such as Ag and Ge. Park *et al* [41] demonstrated that the antisite defects related to Cu, Zn, and Sn were effectively suppressed by the cations, achieving enhanced device performance at low light illuminations. Under 1 sun illumination, the performance enhancement by incorporation of both Ag and Ge was comparable (from 7.5 to 9.04 and 9.05%, respectively). Nevertheless, at low-intensity light conditions, the CZTSSe device with Ag incorporation exhibited higher performance than that with Ge incorporation. While the Ag device had a higher defect density ($\sim 2 \times 10^{17}$ cm^{-3} eV^{-1}) than the Ge device, its lower defect energy level (86 meV) was found to be beneficial under low light illumination. Therefore, the superior performance of the Ag device in weak light despite high defect density can be interpreted based on its lower defect energy level. This work gives an insight into the necessity of different approaches to defect engineering for kesterite indoor photovoltaics compared to outdoor photovoltaics, opening possibilities for high-performance indoor photovoltaics based on kesterites with wider bandgaps. Also, improved efficiency in CZTS solar cells was achieved by inserting a passivation layer (Al$_2$O$_3$) between the kesterite absorber and Cd-free buffer layer was reported by Cui *et al* [45]. The passivation reduced the local potential fluctuation of band edges and resulted in the widening of bandgap and enhancement of V$_{OC}$ (see figure 9(a)). For further efficient absorption of indoor light entering from all directions for more homogenous intensities, dedicated device engineering efforts are also required. For instance, Deng *et al* [42] designed robust bifacial CZTSSe-based photovoltaics with outdoor efficiency of over 9% and indoor efficiency of 8.8%, which could harvest energy from light absorbed via both the front and back surfaces, using flexible Mo-foil substrates (see figure 9(b)).

Figure 9. (a) (Top) Diagram illustrating the band gap fluctuation in CZTS with and without Al$_2$O$_3$ treatment and (bottom) surface modification mechanism in CZTS subjected to ALD-Al$_2$O$_3$ treatment [45]. (b) Device structure of bifacial CZTSSe photovoltaic cells on a flexible substrate [42]. Roadmap for efficient and eco-friendly kesterite photovoltaics for indoor applications.

Concluding remarks

Among various candidates for indoor photovoltaic absorbers, kesterites can be promising due to their non-toxicity, high stability, high absorption coefficient, and direct and tuneable bandgap. In figure 9(c), we illustrate a schematic of the roadmap for efficient and eco-friendly kesterites for indoor applications. Firstly, the right bandgap composition has to be set with appropriate defect engineering to mitigate the defect density as well as the defect level positions. Also, the Cd buffer layer must be replaced with other materials to realize fully eco-friendly photovoltaics. Finally, novel device engineering (for instance, a device architecture with kesterite absorbers coated on both sides of a flexible substrate) will lead kesterites to be competitive in the future indoor photovoltaics market.

Acknowledgments

2.5. Organic photovoltaics for indoor-light-to-electricity conversion

Gregory C Welch[1], Bryon W Larson[2], Myles Creran[3] and Audrey Laventure[3]
[1] Department of Chemistry, University of Calgary, Calgary, AB, T2N 4K9, Canada
[2] National Renewable Energy Laboratory, Golden, CO 80401, United States of America
[3] Département de chimie, Université de Montréal, Montréal, QC, H2V 0B3, Canada

Status
Organic photovoltaics are a widely investigated clean energy (light-to-electricity) conversion technology in academia [46–48]. Recently, the technology has been commercialized with various products available to the general public. Key advantages compared to traditional silicon-based photovoltaics include solution processability of the photoactive layer and charge transport interlayers components, which enables ultra-low-cost manufacturing via coating and printing techniques, a high degree of module flexibility/conformability and form factors (i.e. shapes and sizes), and tunable light harvesting properties. Limitations include the power conversion efficiency and operational lifetimes, both inhibiting widespread utilization.

Owing to the high molar absorptivity of organic molecules in the visible region of the electromagnetic spectrum (i.e. white light) and the exciton-based processes involved in organic photovoltaics, they have been predicted to be capable of converting indoor light into useable electricity [12, 49, 50]. Indeed, the global indoor light harvesting market is expected to grow from \$140 M in 2017 to >\$1 B (USD) by 2023, with a projected demand for such devices by then exceeding 60 million per year. While the output power is by default low (microwatts per cm^2) such devices are suitable for low-power, wireless electronic sensors for the IoT. Potential application has been recently demonstrated with an organic photovoltaic device reaching 25% efficiency under 1000 lx (i.e. a standard light-emitting-diode bulb) [51].

The organic semiconductors (p- and n-types, π-conjugated compounds) that comprise the photoactive layers of organic photovoltaics are ideally suited for utility in harvesting light from artificial sources including light-emitting diodes and incandescent bulbs. Fine control of the chemical structure of these compounds allows for tailoring of optoelectronic properties. Design rules related to the p- and n-type organic semiconductors are now well established and optical absorption of photoactive blends can be matched to specific light emission and energy levels optimized to minimize energy loss and maximize operating voltages [52]. In addition, such materials can be (1) prepared via atom-economical synthetic procedures rendering them low-cost and accessible and (2) be processed into photoactive films from halogen-free solvents using roll-to-roll compatible coating methods facilitating a transition from laboratory-to-fabrication, as shown in figure 10(b) [53].

Current and future challenges
Materials design
Most reports on indoor organic photovoltaics have simply used known materials developed for outdoor (1 sun, i.e. 100 mW cm^{-2}) environments. Thus, there is a great opportunity to develop new custom-made photoactive materials with matched optical absorption to the emission from specific light sources (approximately 400–700 nm). In the design of such organic semiconductor materials, minimizing energy loss and maximizing operating voltages is far more important than reaching higher and higher power conversion efficiencies, as the intended use is to run low-power devices. Materials should adopt a facile synthesis and be processible from halogen-free solvents, and thus be compatible with large area roll-to-roll coating. In this case, classic organic semiconductors that have fallen out of favour such as P3HT and PCDTBT may find new life owing to a low-cost synthesis and strong absorption of indoor lighting.

Accurate photovoltaic measurements
Standardization of organic photovoltaics characterization is easier when the reference spectrum is always our Sun (outdoor photovoltaics). The task of standardizing non-solar light conversion is a challenge that must be overcome so that reliable power output specifications to design IoT or sensors around are known. Translational equations are used by institutions like NREL, EST-JRC, and AIST to interpret device output under a given reference condition [54]. When the reference condition is not the Sun (the case for the majority of intended uses for indoor organic photovoltaics), existing translational equations are invalid. Since new translational methodologies do not exist yet for indoor photovoltaics standards, substantial uncertainty exists in reported indoor power conversion efficiencies to date, especially when lux meters, as opposed to spectral radiometric equipment, are used to establish incident power. One major current challenge is that the traceable reference cells that are used to measure indoor light power, were calibrated against 1 sun when certified, and therefore do not apply to the indoor spectrum.
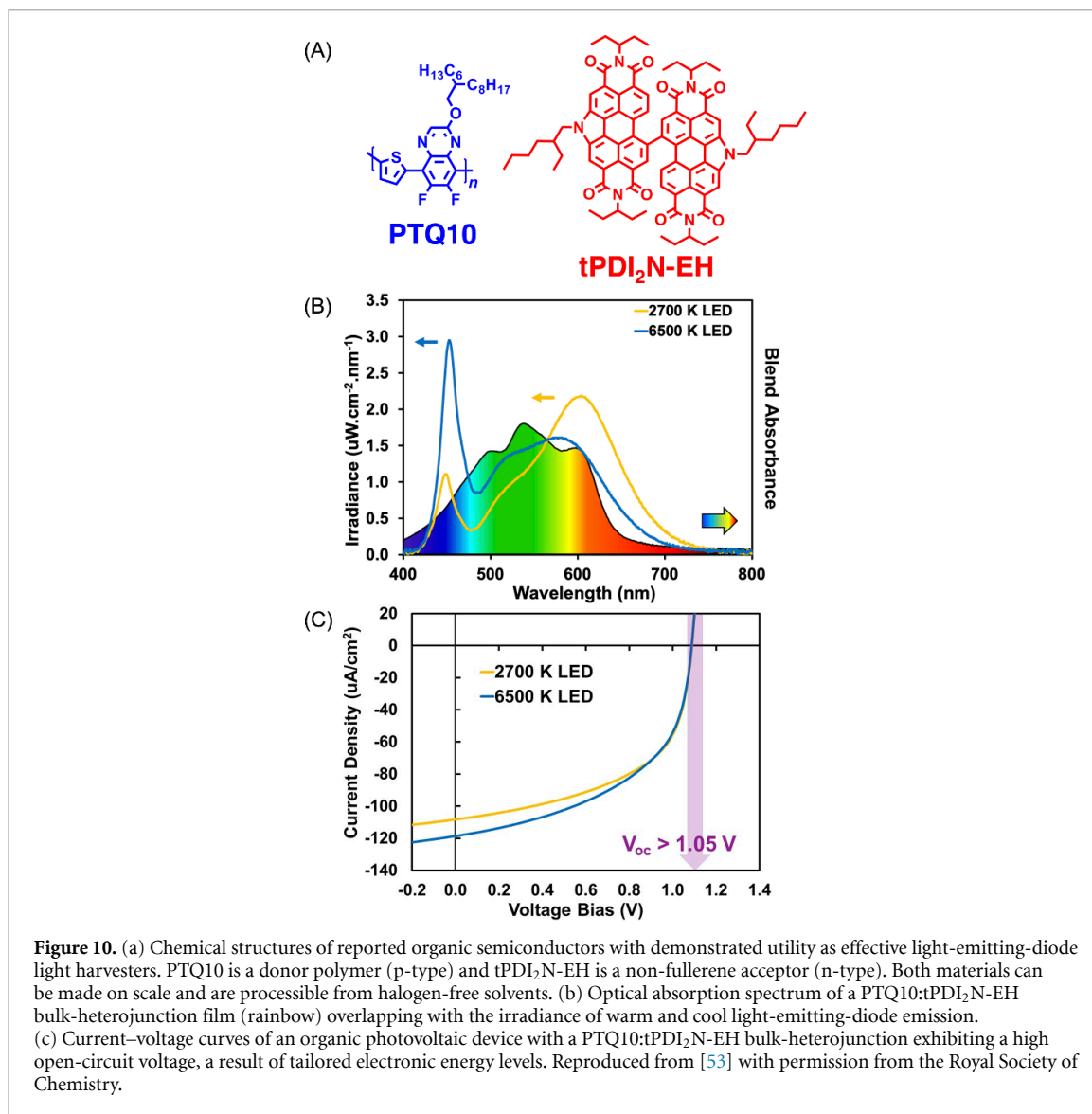
Figure 10. (a) Chemical structures of reported organic semiconductors with demonstrated utility as effective light-emitting-diode light harvesters. PTQ10 is a donor polymer (p-type) and tPDI$_2$N-EH is a non-fullerene acceptor (n-type). Both materials can be made on scale and are processible from halogen-free solvents. (b) Optical absorption spectrum of a PTQ10:tPDI$_2$N-EH bulk-heterojunction film (rainbow) overlapping with the irradiance of warm and cool light-emitting-diode emission. (c) Current–voltage curves of an organic photovoltaic device with a PTQ10:tPDI$_2$N-EH bulk-heterojunction exhibiting a high open-circuit voltage, a result of tailored electronic energy levels. Reproduced from [53] with permission from the Royal Society of Chemistry.

Device engineering

Given the different environmental operating constraints of indoor *vs.* outdoor light harvesting, indoor organic photovoltaics requires new design criteria (in many ways relaxed relative to outdoor organic photovoltaics) for device stack materials that are tailored specifically for indoor conditions. Indeed, metal-oxide ultraviolet-light soaking does not happen inside, reinforcing the need to use different charge transport layer materials.

Advances in science and technology to meet challenges

Matching the indoor light emission wavelength range to the absorbance spectrum of the photoactive layer of an indoor organic photovoltaic device can be achieved by a rational design and/or blending of the p- and n-type organic π-conjugated compounds. To meet this challenge faster, the conventional experimental trial-and-error approach would benefit from pairing up with computational simulations and predictions. Feedback loops could also be developed where the results of molecular design and/or processing conditions act as inputs, while output designs and conditions are suggested via artificial intelligence tools. Once the formulation of the photoactive layer is selected, another major challenge lies in its processing, especially since processing
can dramatically affect the resulting microstructure of the film, and thus, its absorption profile. It needs to be compatible with industrially relevant coating techniques, such as blade- and slot-die coating (cf figure 11) and be conducted in ambient conditions (no spin-coating nor glove-box processing). Photoactive layer formulations that present a performance that is thickness independent also need to be targeted.

Figure 11. Required transition for the application of organic photovoltaics in indoor light recycling. (a) Common lab-scale organic photovoltaic devices made via spin-coating. (b) Affordable roll-coaters for research and development. (c) Organic photovoltaic module (5 cell) made via roll-coating using halogen-free solvents with current photoactive and interlayer materials. Photos original from Welch lab.

A way to ensure a proper comparison of device performance is to move away from power conversion efficiency and instead compare W m^{-2} values produced directly against appropriate reference incident total irradiance spectra. The latter will require the most effort to produce, since many indoor reference spectra, in W m^{-2}, will need to be collected, but afterwards new reference cells can be certified against these spectra and then the traditional translational equation methodologies can be applied.

Alternatives to charge transport layers requiring post-processing high temperature annealing and ultraviolet-light activation or soaking are required for indoor organic photovoltaics prepared on flexible (mostly polymer-based) substrates and operating with indoor light. Such charge extracting interfaces design is a paramount to ensure operational lifetime in a context where the absence of ultraviolet light, humidity and temperature swings in indoor conditions impact far less the photoactive layers than under 1 sun conditions. Formulations that can be coated using roll-to-roll compatible techniques without requiring a high temperature annealing, like SnO$_2$ nanoparticles, need to be further developed. Module fabrication (different form factors) and circuit integration would greatly benefit from electrical engineering inputs, where connection of devices (series or parallel) can tune the module power delivery.

Concluding remarks

Overall, organic photovoltaics for indoor light conversion to electricity presents several challenges for the scientific community that are yet to be tackled. Seizing this opportunity to develop the next generation of indoor organic photovoltaics calls for interdisciplinary research efforts, leading to advances within the materials chemistry, device engineering and metrology landscapes. Moreover, three key concepts need to be

kept in mind during this endeavour towards a lab-to-fab transition for indoor organic photovoltaics: scalability, sustainability, and standardization. Scalability and sustainability concern the photoactive layer and charge transport interlayer compounds synthesis and their thin-film coating processes. Standardization concerns the device performance evaluation. These key concepts stand as *sine qua non* conditions to ensure a perennial technology transfer from research and development to a widespread adoption of indoor organic photovoltaics as power sources for wireless, low-voltage devices.

Acknowledgments

2.6. Dye-sensitized photovoltaics for indoor applications

Kezia Sasitharan, Natalie Flores-Diaz and Marina Freitag
School of Natural and Environmental Sciences, Bedson Building, Newcastle University, NE1 7RU Newcastle upon Tyne, United Kingdom

Status

Dye-sensitized solar cells comprise a mesoporous semiconducting layer (usually TiO_2) functioning as a working electrode, to which sensitizer molecules are adsorbed. The counter electrode faces the sensitizer, with a redox mediator between the counter electrode and working electrode. Upon light absorption, photo-induced electron transfer occurs from the sensitizer to the TiO_2. The redox mediator enables regeneration of the dye, facilitating the transfer of positive charges from the working electrode to the counter electrode, as demonstrated in figure 12. Dye-sensitized solar cells primarily absorb in the visible region (from 400 to 650 nm) and outperform GaAs solar cells under diffuse light conditions, while also being inexpensive and environment friendly [12].

Even under ambient light illumination, dye-sensitized solar cells can maintain a high photovoltage. This is attributed to the tuneable energy levels in Cu(II/I) electrolyte systems and reduced recombination along with fast charge separation processes in organic dyes. Molecular engineering of the dyes, and their combination (co-sensitizers) for improved matching of their absorbance with the emission of the artificial light sources (as shown in figure 13) has significantly pushed the efficiency of dye-sensitized solar cells for indoor photovoltaics. A power conversion efficiency of 28.9% was observed under a 1000 lx fluorescent light tube using $[Cu(tmby)_2]^{2+/1+}$ redox coupled with TiO_2 films co-sensitized with the dye D35 and XY1 [55]. The continued development of panchromatic rigid-structure dyes, alternative hole transport materials and design flexibility has enabled improved power conversion efficiencies, currently reaching 13% under AM1.5G conditions and 34% under indoor light [23].

In recent years, dye-sensitized solar cells have shown remarkable progress in harvesting energy from artificial light sources, making them a suitable option for various low power devices used indoors. In 2020, dye-sensitized solar cells were successfully tested to power battery-free IoT devices capable of machine learning under ambient light conditions [56].

Current and future challenges

The conversion of ambient light into usable energy paves the way for the widespread implementation of self-powered wireless devices [57]. To attain their full potential for indoor photovoltaics, dye-sensitized solar cells must achieve power conversion efficiencies closer to the maximum theoretical value of 52% [58]. Their integration as a sustainable power source for sensors and wireless electronics will lead to self-powered monitoring systems, data collection, and wireless communication, thereby saving energy in buildings, industries, and households [59]. Indoor dye-sensitized solar cells with co-sensitized systems can achieve high power conversion efficiencies employing dyes absorbing at 550–600 nm and a co-sensitizer absorbing in the blue region of the visible spectra, offering an excellent match to the ambient light spectra. This approach also reduces electron recombination rates from the conduction band of the TiO_2 to the redox mediator. Interfacial engineering and redox mediators with high redox potentials are required to further reduce electron recombination and maintain high photovoltage. The commercialization of dye-sensitized solar cells is hindered by the inability to develop solid-state devices on a large scale. Solid-amorphous copper-based hole-transport materials showed significant output power densities at 1000 lx, and scalable deposition methods are being developed [60].

Advances in science and technology to meet challenges

To advance the field of dye-sensitized solar cells for ambient applications, it will be necessary to simultaneously improve dye-sensitized solar cells and IoT devices with innovative hardware and software, combining chemistry, engineering, and computer science. By developing new materials, it is possible to increase the V_{oc} above 1.0 V at 1000 lx. For instance, novel preparation methods and surface treatments for semiconductors with higher conduction band energies than TiO_2 (such as Zn_2SnO_4, $SrTiO_3$, and $BaTiO_3$) should be investigated to increase dye loading and decrease interfacial electron recombination.

Since recombination processes cause most performance losses in dye-sensitized solar cells, research should focus on developing a fundamental understanding of the interaction between dyes and charge transport materials and their impact on photovoltaic processes. This will enable the development of alternative charge carrier materials with improved charge transport, reduced recombination losses, and enhanced long-term stability. Furthermore, liquid electrolytes should be replaced with solid-state charge transport materials to reduce leakage, solvent evaporation, dye photodegradation, dye desorption, and

Figure 12. Working principle of a dye-sensitized solar cell with a co-sensitized system and a redox mediator Ox/Red.

Figure 13. Normalized emission spectra of warm white compact fluorescent and light-emitting-diode bulbs, and of the AM1.5G solar spectrum with absorption overlay of prominent indoor dyes: L1, XY1 and MS5. LED: light-emitting diode. CFL: compact fluorescent lamp.

counter electrode corrosion. Novel architecture designs are needed to allow backside illumination and incorporate carbon-based composites at the counter electrodes, enabling solid-state monolithic devices [58].

Future research will focus on efficient converters with low power fluctuations and energy buffers to maintain a constant voltage throughout the operation/sleep cycles of indoor electronic devices. Due to the scarcity of battery recycling facilities and materials, supercapacitor research must be addressed. Coupling

supercapacitors or novel energy storage devices to dye-sensitized solar cells will enable constant power delivery when the indoor light is unavailable [59].

Concluding remarks

Self-powered and 'smart' IoT devices and networks can now be powered by ambient light harvesters, a previously untapped energy source. Indoor dye-sensitized photovoltaics with nontoxic materials and high efficiency will play an important role in IoT sustainability.

Considering that indoor environments are more stable in terms of temperature, humidity, and light, designing materials with higher performance properties is plausible. New electronic configurations custom designed for various IoT applications must be developed to provide constant voltage and power. With these further developments in both material design and device architecture, the power conversion efficiencies of dye-sensitized solar cells under indoor light can be pushed closer to the theoretical limit to generate a new era of autonomous, smart and self-powered devices.

The progress of these systems can depend on the following factors:

- Upscaling dye-sensitized solar cells to minimodules delivering 3–5 V to fulfil IoT requirements.
- Advances in the stability and efficiency of commercially available indoor photovoltaics.
- Novel energy storage devices, particularly non-conventional storage approaches.
- New methods to improve the energy of CPUs/MCUs, wireless communication devices and sensors.
- Computing algorithms and topologies enabling self-powered IoT devices with environmental- and self-awareness.

Highly efficient ambient dye-sensitized solar cells are ultimately intended to assist us in maximizing the benefits of interconnected IoTs and wireless device innovations while reducing their own environmental and energy impacts [60].

Acknowledgments

2.7. Lead-halide perovskites for indoor photovoltaics

Jie Xu and Thomas M Brown
CHOSE (Centre for Hybrid and Organic Solar Energy), Department of Electronic Engineering, University of Rome Tor Vergata, Via del Politecnico 1, 00133 Rome, Italy

Status
Recent and ever-increasing published literature has shown that perovskite solar cells are clearly one of the best candidates for indoor photovoltaics owing to their exceptional power conversion efficiency under low light conditions in the visible range, i.e. those emitted by white light sources such as light-emitting diodes and compact fluorescent lamps used for indoor illumination. The earliest demonstrations of the indoor photovoltaic performance of perovskite solar cells can be traced to Chen *et al* for the PEDOT:PSS/PCBM p–i–n architecture in 2015 [61], and Di Giacomo *et al* [62] for the classical TiO_2 and Spiro-OMeTAD architecture. In both of these works, power conversion efficiencies as high as 24% at 200 lx and 27% at 1000 lx were obtained, which are substantially higher than those ever achieved at standard test conditions (see figure 14(a)). In 2017, Lucarelli *et al* reported the first flexible perovskite solar cells fabricated on PET substrates delivering a power conversion efficiency of 11%–12% in the 200–400 lx range under white light-emitting-diode illumination [63]. After only a few years, efficiencies of indoor perovskite solar cells (i-PSCs) have continued to soar, reaching current records in rigid cells of 34.8% at 200 lx, the most common range found in homes [22], and 40.2% at the higher 1000 lx found less often, in environments like supermarkets [64], and 30.7% (212 lx), 31.9% (1062 lx) in flexible PEN cells [65], and 20.6% (200 lx) in ultrathin flexible glass [66]. Notably, these record efficiencies of i-PSCs have surpassed their competitors, both commercial such as a-Si as well as new generation photovoltaics such as dye-sensitized solar cells and organic photovoltaics, as shown in figure 14(b) [22]. The continuing improvement in efficiency, together with corresponding step forwards in module performance and stability that is required in the future, as well as overcoming environmental/toxicity concerns of perovskite semiconductors, can open up huge markets for this technology. In fact, the fields of low-power (20–50 μW average power consumption) IoT devices and wireless sensor networks are becoming more and more prevalent in our daily lives, with more than tens of billions of IoT devices predicted to be deployed by 2025. Indoor photovoltaics can become a key enabling technology to power these indoor microelectronic devices (for example, sensors, watches, and calculators) [67].

Current and future challenges
Stability
Perovskite solar cells have achieved impressive efficiencies in a short period of time. Indoor stability remains an aspect of concern, although they operate in a milder environment compared to outdoors. Many of IoT devices need to last only a few years rather than more than 25 years under the much more taxing conditions under the sun, outdoors. Thus, systematic studies of degradation under indoor illumination as well as developing device and encapsulation materials that can match commercial lifetime requirements should be carried out.

Large-area fabrication
Scaling up the manufacturing processes is key for commercialization. Previous studies have shown that i-PSCs are more sensitive to trap-state density and recombination currents [62, 63], due to the lower incident optical power of indoor lights compared to sunlight, resulting in a higher ratio of recombining electrons to photo-generated electrons. Preparation of high-quality transport and perovskite films (figure 14(a)) over large areas as well as maintaining high shunt resistances in contacting series-connected cells in monolithic modules is crucial for device performance. Ideal geometries for modules will also differ depending on illumination conditions.

Manufacturing costs
Reducing manufacturing costs is an important factor for successful commercialization. Achieving comparable market price with its competitors, currently a-Si photovoltaics, as well as by other means such as conventional batteries, is required as well as reducing as much as possible the cost of its integration with the product.

Possible toxicity concerns
The operating environment of indoor photovoltaics consists in most places of spaces where there is human activity, such as the living room, office, and shops. Therefore, the possible toxicity of lead-halide perovskite
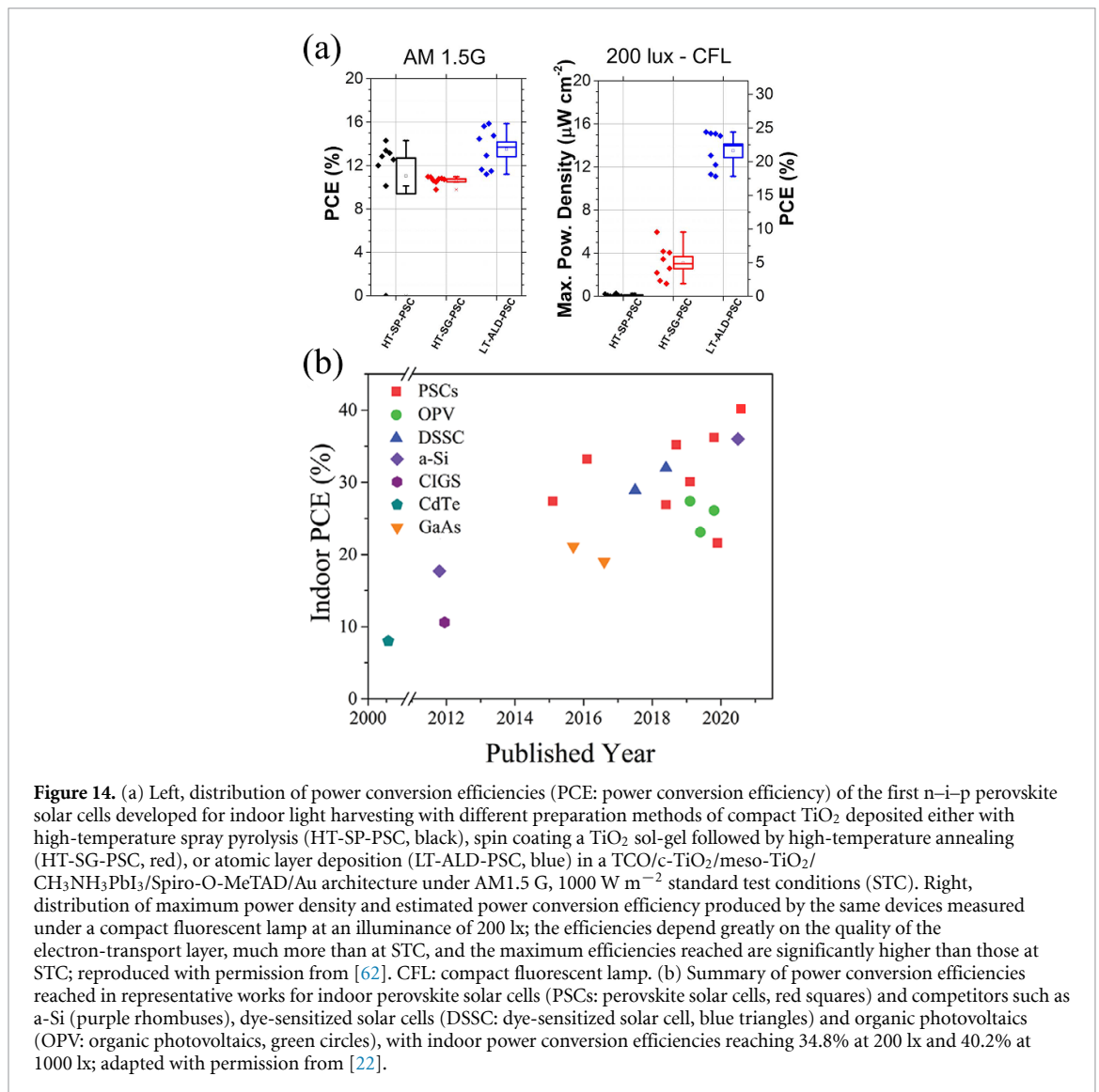
Figure 14. (a) Left, distribution of power conversion efficiencies (PCE: power conversion efficiency) of the first n–i–p perovskite solar cells developed for indoor light harvesting with different preparation methods of compact TiO₂ deposited either with high-temperature spray pyrolysis (HT-SP-PSC, black), spin coating a TiO₂ sol-gel followed by high-temperature annealing (HT-SG-PSC, red), or atomic layer deposition (LT-ALD-PSC, blue) in a TCO/c-TiO₂/meso-TiO₂/ CH₃NH₃PbI₃/Spiro-O-MeTAD/Au architecture under AM1.5 G, 1000 W m^{-2} standard test conditions (STC). Right, distribution of maximum power density and estimated power conversion efficiency produced by the same devices measured under a compact fluorescent lamp at an illuminance of 200 lx; the efficiencies depend greatly on the quality of the electron-transport layer, much more than at STC, and the maximum efficiencies reached are significantly higher than those at STC; reproduced with permission from [62]. CFL: compact fluorescent lamp. (b) Summary of power conversion efficiencies reached in representative works for indoor perovskite solar cells (PSCs: perovskite solar cells, red squares) and competitors such as a-Si (purple rhombuses), dye-sensitized solar cells (DSSC: dye-sensitized solar cell, blue triangles) and organic photovoltaics (OPV: organic photovoltaics, green circles), with indoor power conversion efficiencies reaching 34.8% at 200 lx and 40.2% at 1000 lx; adapted with permission from [22].

inevitably becomes an important question to answer even if the quantity of lead is minuscule in such devices. On the one hand this is a regulatory issue, on the other a technical one which can be tackled with formulation of new materials (e.g. lead-free alternatives) or proper encapsulation and sealing.

Standardization protocols
As an emerging technology, indoor photovoltaics does not yet have a generally accepted standard measurement protocol similar to established photovoltaic technologies for power generation outdoors. Moreover, there is only one standard light source outdoors (i.e. the Sun), while artificial light sources are continuously updated in pursuit of higher efficiency and longer lifetimes. Establishment of measurement protocols will greatly help the field.

Advances in science and technology to meet challenges
Continuing to improve efficiency towards its theoretical limit of 56% under light-emitting-diode illumination [68], can be achieved by band gap (the optimal one is around 1.9 eV, higher than that at STC) and defect-passivation engineering [22, 67, 69] both in the perovskite layer as well as the transport layers and its interfaces [62–64]. Stability needs to be tackled by new material and device architectures (intrinsic) as well as encapsulation (extrinsic) to avoid permeation of moisture and oxygen. For the former, reducing defect formation through grain boundary and interface passivation and replacing amounts of small molecular ions with inorganic ones can increase stability as well as synthesizing perovskite absorbers with more stable two-dimensional/three-dimensional structures. Cheng *et al* tailored a CH₃NH₃PbI₂₋ₓBrClₓ perovskite absorber with bandgap of 1.8 eV for indoor light harvesting, achieving a power conversion efficiency of
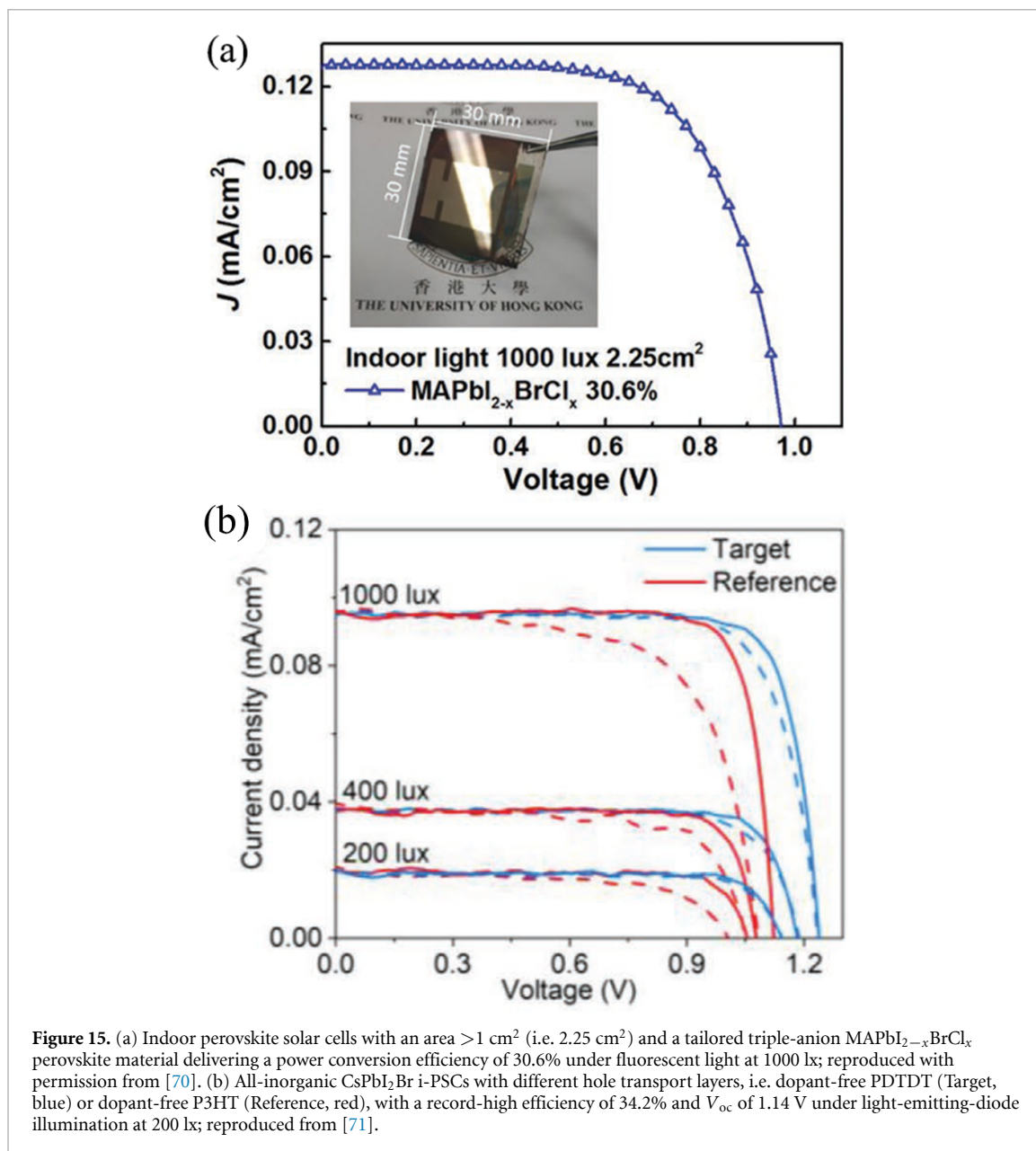
Figure 15. (a) Indoor perovskite solar cells with an area >1 cm^2 (i.e. 2.25 cm^2) and a tailored triple-anion MAPbI$_{2-x}$BrCl$_x$ perovskite material delivering a power conversion efficiency of 30.6% under fluorescent light at 1000 lx; reproduced with permission from [70]. (b) All-inorganic CsPbI$_2$Br i-PSCs with different hole transport layers, i.e. dopant-free PDTDT (Target, blue) or dopant-free P3HT (Reference, red), with a record-high efficiency of 34.2% and V_{oc} of 1.14 V under light-emitting-diode illumination at 200 lx; reproduced from [71].

36.2% on 0.1 cm^2 and 30.6% on an appreciable active area of 2.25 cm^2 under fluorescent light at 1000 lx (see figure 15(a)). Furthermore, halide segregation suppressed by chloride introduction led to excellent long-term stability, sustaining over 95% of original efficiency for 0.1 cm^2 encapsulated cells under 2000 h of continuous light soaking [70]. However, this work does not report performance in the more common 200–500 lx range found in home and offices. All-inorganic i-PSCs have recently attracted much attention due to improved thermal stability. Guo *et al* recently reported a CsPbI$_2$Br all-inorganic i-PSC with a power conversion efficiency of 34.2% and a V_{oc} of 1.14 V under light-emitting-diode illumination at 200 lx and superior thermal stability (see figure 15(b)) [71]. Commonly used approaches for encapsulation include curable adhesive and glass–glass laminated encapsulation using a variety of different adhesives [72]. Glass is an excellent permeation barrier, thus should also be considered as a possible substrate together with plastic ones even for flexible devices [66]. Encapsulation can become a solution also for the possible toxicity issue via lead sequestration engineering. Researchers have initially explored materials including epoxy resin, hydroxyapatite, and sulfonic acid-based resins to supress leakage of internal lead [73]. Research on lead free perovskites for i-PSCs is described in section 2.8. To reduce manufacturing costs, it is necessary to develop new cost-effective constituent materials and fabrication technologies that enable very uniform films over large areas as well as low costs, such as slot-die coating.

Concluding remarks

The huge market for IoT devices worth tens of billions in the future brings unprecedented opportunities for indoor photovoltaics. i-PSCs have numerous advantages for integration with indoor IoT electronic devices, such as being mechanical flexible, light weight, and low cost. Simultaneously, i-PSCs have surpassed their counterparts and achieved outstanding indoor efficiency of over 34% at 200 lx and 40% at 1000 lx, becoming one of the prominent leaders for potential commercialization. However, the above-mentioned achievements were obtained under laboratory conditions. Many challenges such as stability, maintaining performance over large sizes, possible toxicity, reducing manufacturing and integration costs must be addressed in the future to promote the commercialization of i-PSCs. The path to commercialization for indoor products compared to outdoor installations may be more evident not only because of the outstanding performance but also of the more lenient environment for stability. This review has aimed to propose some guidelines and ideas to overcome these challenges. Furthermore, the outstanding performance under low intensity light can be appealing not only for photovoltaics but also for imaging/vision devices of the future.

Acknowledgments

2.8. Lead-free halide perovskites and derivatives for indoor photovoltaics

Vincenzo Pecunia
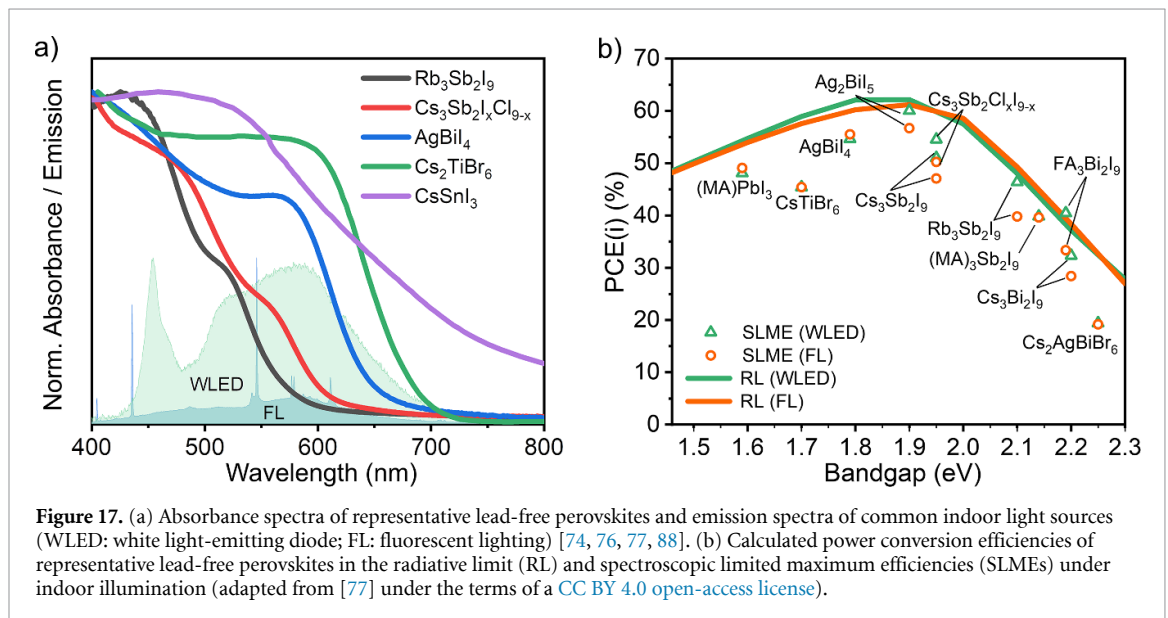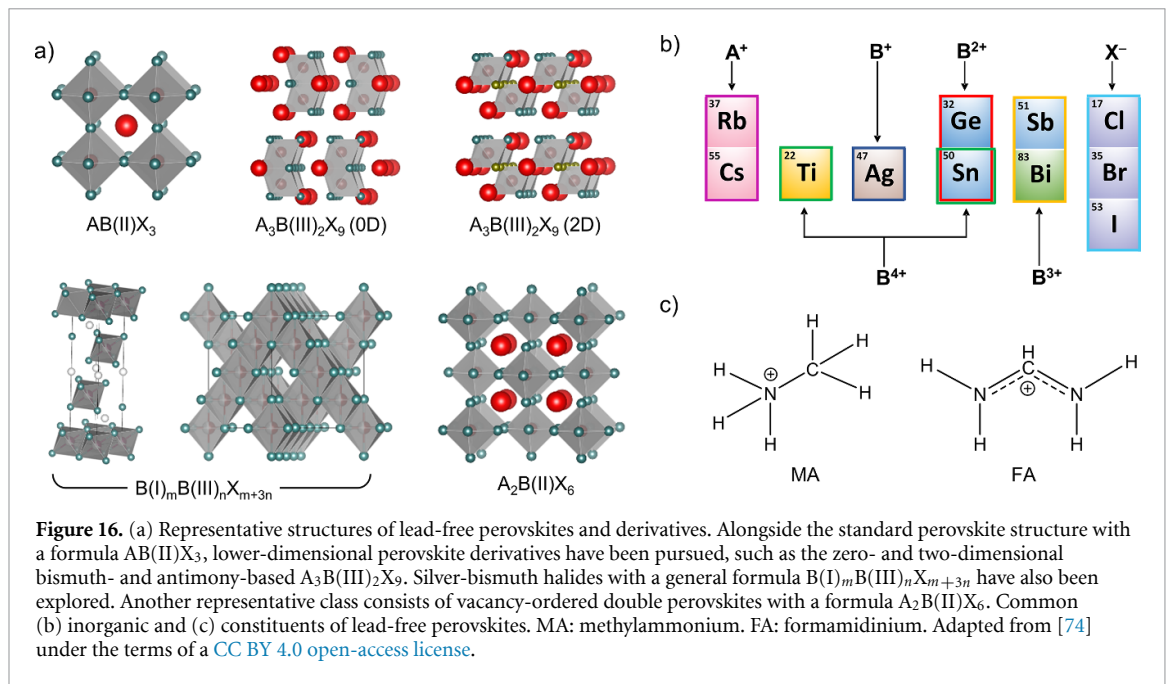School of Sustainable Energy Engineering, Simon Fraser University, Surrey V3T 0N1, BC, Canada

Status

Lead-free halide perovskites and derivatives (*lead-free perovskites* for short in the following) are a broad class of metal-halide-based compounds (figure 16) [74]. They may present the ABX_3 perovskite structure (with A^+ being a monovalent cation, B^{2+} a divalent metal/metalloid anion, and X^- a halide anion) featuring a three-dimensional network of corner-sharing $[BX_6]^{4-}$ octahedra. Derivatives of this structure may involve metal-halide octahedra arranged in different corner-sharing or edge-sharing structural motifs, which can be either three-dimensional (e.g. as in compounds with a formula $B(I)_m B(III)_n X_{m+3n}$, where B^+ and B^{3+} are monovalent and trivalent metals, respectively, and X^- is a halide anion) or lower-dimensional (e.g. as in zero- and two-dimensional $A_3B_2X_9$ compounds, with A^+ being a monovalent cation, B^{3+} a trivalent metal, and X^- a halide anion) (figure 16). A common feature of all of these compounds is their being based on metals/metalloids alternative to lead—for instance, tin, germanium, antimony, bismuth, and silver.

The development of lead-free perovskites, which has taken place primarily during the past 5 years, has been driven by the strong interest in realizing eco-friendly alternatives to lead-based halide perovskites, which manifest highly favourable optoelectronic properties but are burdened by the severe toxicity of lead. Originally, aiming to replicate the promising performance of lead-halide perovskites in solar photovoltaics, the development of lead-free perovskites exclusively targeted their use in solar cells [74]. Departing from this narrow view, the Author and his team began investigating in early 2019 the indoor photovoltaic performance of two-dimensional lead-free perovskites comprising planes of corner-sharing metal-halide octahedra [75], which deliver superior optoelectronic properties compared to their zero-dimensional counterparts [76] (figure 16(a)). Alongside the understanding that the typical placement of indoor photovoltaics in proximity to the end-users makes it beneficial to resort to lead-free, eco-friendly materials [7], this investigation was motivated by the realization that the wide bandgaps of many such compounds would lead to a favourable spectral match with indoor light sources (figure 17(a)). This effort resulted in the first-ever demonstration of the capabilities and potential of lead-free-perovskite indoor photovoltaics [77]. Despite this being the first demonstration, indoor power conversion efficiencies (PCE(i)s) approaching 5% (i.e. within the same range of mainstream, commercial a-Si:H indoor photovoltaics) were already obtained with $Cs_3Sb_2Cl_xI_{9-x}$, which also delivered device stability of more than 5 months [77]. Building on this breakthrough, a subsequent study adopted a triple-cation variant of $Cs_3Sb_2Cl_xI_{9-x}$ (by mixing Cs^+ with methylammonium and formamidinium cations; see figure 16(c)) to achieve a PCE(i) of 6.37% [78].

Alongside the discovery of the indoor photovoltaic capabilities of lead-free perovskites, the Author and his team also demonstrated, for the first time, mm-scale lead-free-perovskite indoor photovoltaics powering printed-transistor electronics, pointing to the opportunity of realizing solution-processed, wirelessly powered smart devices [2, 77]. Additionally, the analysis of the ultimate indoor photovoltaic performance of a wide range of lead-free perovskites pointed to other compounds with considerable indoor photovoltaic potential [77] (e.g. Ag-Bi-I compounds [79] and $Rb_3Sb_2I_9$ [80]). Fulfilling this prediction, $AgBiI_4$-based indoor photovoltaics with an efficiency of up to 5.2% was subsequently demonstrated [81]. Most recently, emerging Cu-Ag-Bi-I-based absorbers with near optimum bandgap for indoor photovoltaics have been shown to deliver PCE(i) values of up to 9.53% [82–84], thereby highlighting the considerable indoor photovoltaic potential of copper-silver pnictohalides [79]. Furthermore, a hybrid absorber combining $Cs_3Sb_2I_9$ and an organic molecule, ITIC, was reported to deliver PCE(i) values of up to 9.2% [85]. However, note that this result does not strictly fall within the lead-free-perovskite indoor photovoltaics domain, given that the resultant PCE(i) crucially builds on the optoelectronic properties of ITIC. In fact, ITIC has already delivered PCE(i) values of $\cong 18\%$ in organic indoor photovoltaics [86]; hence, the use of ITIC-$Cs_3Sb_2I_9$ essentially taps from the capabilities of organic indoor photovoltaics without impacting the intrinsic capabilities of lead-free-perovskite indoor photovoltaics, while delivering a considerable efficiency drop compared to fully organic ITIC-based indoor photovoltaics [86]. Finally, the investigation of tin-based-perovskite indoor photovoltaics has resulted in considerably higher PCE(i) values (up to 17.6% with $FA_{0.75}MA_{0.25}SnBrI_2$), given their higher photovoltaic capabilities already demonstrated in solar photovoltaics research, although burdened by considerable instability (e.g. undergoing a 40% efficiency drop after 400 min) [18, 87].

Figure 16. (a) Representative structures of lead-free perovskites and derivatives. Alongside the standard perovskite structure with a formula $AB(II)X_3$, lower-dimensional perovskite derivatives have been pursued, such as the zero- and two-dimensional bismuth- and antimony-based $A_3B(III)_2X_9$. Silver-bismuth halides with a general formula $B(I)_mB(III)_nX_{m+3n}$ have also been explored. Another representative class consists of vacancy-ordered double perovskites with a formula $A_2B(II)X_6$. Common (b) inorganic and (c) constituents of lead-free perovskites. MA: methylammonium. FA: formamidinium. Adapted from [74] under the terms of a CC BY 4.0 open-access license.

Figure 17. (a) Absorbance spectra of representative lead-free perovskites and emission spectra of common indoor light sources (WLED: white light-emitting diode; FL: fluorescent lighting) [74, 76, 77, 88]. (b) Calculated power conversion efficiencies of representative lead-free perovskites in the radiative limit (RL) and spectroscopic limited maximum efficiencies (SLMEs) under indoor illumination (adapted from [77] under the terms of a CC BY 4.0 open-access license).

Current and future challenges

The success of lead-free-perovskite indoor photovoltaics will depend on their ability to reliably deliver efficiencies well above mainstream a-Si:H, while allowing scalable manufacturing at a fraction of the cost and with lower environmental impacts, as detailed in the following.

Efficiency

Calculations have revealed that many lead-free perovskites could ultimately achieve PCE(i) values of up to $\cong 60\%$ (figure 17(b)) [77]. Therefore, a major challenge is to bridge the gap between current device efficiencies and this theoretical limit by developing suitable materials-, processing-, and device-based strategies. While tin-based perovskites have thus far delivered the highest PCE(i) values to date, importantly, their bandgaps are far from the optimum for indoor photovoltaics (i.e. 1.9 eV). By contrast, while antimony- and bismuth-based compounds have considerable potential for indoor photovoltaics due to their bandgaps

being close to the optimum, in the forms explored to date, these absorbers are characterized by non-ideal microstructures and comparatively low mobility-lifetime products, which reduces their charge collection efficiency. Additionally, the limited understanding of their electronic defects and interfacial properties prevents the rational development of suitable passivation treatments and the identification of charge transport layers for efficient charge extraction. Finally, while the PCE(i) of lead-free-perovskite indoor photovoltaics has been typically reported at illumination levels of 1000 lx, real-world applications involve illuminances down to 50 lx, which makes it critical to develop lead-free perovskite layers with particularly low bulk and interfacial defect concentrations.

Stability
Tin-based perovskites proper (i.e. $ASnX_3$ compounds, with $A+$ being a monovalent cation and X^- a halide anion) suffer from severe instability in air due to the oxidation of Sn^{2+} into Sn^{4+}. Despite recent advances, this still represents a key challenge to their adoption in real-world applications. By contrast, antimony- and bismuth-based compounds have generally demonstrated a much better stability profile; however, their behaviour under real-world operating conditions has not been assessed to date.

Upscaling
The lead-free-perovskite indoor photovoltaics demonstrated to date had active areas in the mm^2 range; additionally, they were processed by spin-coating, which does not lend itself to large-scale manufacturing. Therefore, an important challenge is to achieve high photovoltaic performance over large areas and with acceptable uniformity and yield via scalable manufacturing methods.

Cost
The solution-processability of many lead-free perovskites points to their potential to deliver indoor photovoltaics at a lower cost than current commercial technology. However, it will be critical to pursue high-throughput manufacturing methods to achieve this objective.

Environmental impacts
While their lead-free nature gives them a significant edge compared to their lead-based counterparts in terms of eco-friendliness, a detailed understanding of their potential sustainability hotspots and toxicity profiles is still lacking.

Advances in science and technology to meet challenges
The full realization of the potential of lead-free-perovskite indoor photovoltaics requires advances in materials and process engineering as well as in characterization and physical insight.

Materials and process engineering
The promising performance of tin-based perovskites prompts the development of compounds of this class with bandgaps $\cong$1.9 eV, alongside the investigation of processing protocols and additives that could fully inhibit the oxidation of Sn^{+2} in these materials. In regard to antimony- and bismuth-based perovskites, a key priority is to develop strategies for the control of the crystallization process to achieve compact films with grain size greater than 1 μm and favourable crystalline orientation. Moreover, it is essential to develop processing protocols for the passivation of bulk and interfacial defects in these materials to extend their carrier lifetimes well above the 10 ns range. Beyond the compounds developed to date, progress in lead-free-perovskite indoor photovoltaics would also benefit from the investigation of alternative lead-free compositions with high stability and defect tolerance, while delivering bandgaps of around 1.9 eV. Regardless of the absorber composition, the realization of high-performance lead-free-perovskite indoor photovoltaics suitable for real-world applications will also require the development of charge transport layers with adequate energy level alignment for efficient charge extraction, as well as the adoption of large-area deposition methods compatible with roll-to-roll processing.

Characterization and physical insight
Pursuing the systematic characterization and understanding of the oxidation mechanisms—at all stages of device fabrication and under real-world operating conditions—will be crucial for the advancement of indoor photovoltaics based on tin-based perovskites. Moreover, progress in bismuth- and antimony-based indoor photovoltaics will require the identification of the bulk defect levels currently limiting the carrier lifetimes in antimony- and bismuth-based perovskites, as well as the characterization of charge transport in these materials and the quantification of its limiting factors and the impact of anisotropy. Furthermore, the investigation of excitonic effects in these materials is essential to quantify their impact on the

photogeneration efficiency under photogeneration rates in the range relevant to indoor photovoltaics operation.

Concluding remarks

While still in its infancy, research in lead-free-perovskite indoor photovoltaics has already demonstrated efficiencies competitive or well above commercial indoor photovoltaics, highlighting the potential of this family of materials. Moreover, their superior eco-friendliness compared to their lead-based counterparts makes them particularly attractive for indoor photovoltaics, given the tighter constraints in terms of material toxicity that hold for technologies to be deployed in consumer products. In fact, the ultimate performance limits of lead-free-perovskite indoor photovoltaics (up to 60% for certain compositions) are far from being reached, which highlights a considerable opportunity for future improvements. To fully realize their potential for indoor photovoltaics, it will be necessary to engineer these materials and their processing for optimum absorption, superior microstructure, and low defect density over large areas, but also to pursue the systematic characterization and understanding of their fundamental optoelectronic properties and degradation mechanisms. Once these challenges are overcome, it is foreseeable that lead-free perovskites will play an important role as an easy-to-make, low-cost indoor photovoltaic technology with a promising sustainability profile.

Acknowledgments

2.9. Quantum-dot absorbers for indoor photovoltaics

Benxuan Li[1,2], Yiwen Wang[3], Zhe Li[3] and Bo Hou[4]

[1] International Collaborative Laboratory of 2D Materials for Optoelectronics Science and Technology of Ministry of Education, Institute of Microscale Optoelectronics, Shenzhen University, Shenzhen 518060, People's Republic of China

[2] Electrical Engineering Division, Engineering Department, University of Cambridge, 9 J J Thomson Avenue, Cambridge CB3 0FA, United Kingdom

[3] School of Engineering and Materials Science, Queen Mary University of London, London E1 4NS, United Kingdom

[4] School of Physics and Astronomy, Cardiff University, Cardiff CF24 3AA, United Kingdom

Status

Based on the detailed balance limit applied to artificial indoor lighting spectra, the optimal bandgap for indoor photovoltaics is 1.9 eV [12, 16]. (Figure 18 presents indoor lighting sources and AM 1.5 solar spectra). Therefore, new technologies based on absorbers with tunable bandgap, such as perovskites and quantum dots, have been developed for indoor photovoltaics [17, 58, 89]. Amongst these, quantum dots are theoretically the most promising absorber materials because they could potentially overcome the Shockley–Queisser limit in indoor photovoltaics owing to the unique quantum confinement effect and multiple exciton generation [90]. To date, lead-chalcogenide and lead-halide-perovskite quantum dots are the mainstream absorbers in quantum-dot-based solar cells, whereas quantum-dot-based indoor photovoltaics are still in an emerging state. As shown in figure 18, several types of quantum dots cover desirable absorption ranges for photovoltaics, and some have shown satisfying efficiency in quantum-dot-based indoor photovoltaics[17]. Meanwhile, the manufacturing cost of quantum-dot-based photovoltaic technologies is becoming competitive due to the mass production of quantum-dot-based high-definition televisions, in which solution-processed quantum dots are deposited via spin-coating, spray-coating, and blade-coating. However, the quantum-dot absorbers in most reported high-performance quantum-dot-based indoor photovoltaics comprise heavy metals such as lead and cadmium [91]. Recently, heavy-metal-free quantum dots have achieved more than 15% efficiency in quantum-dot-sensitised solar cells [92], but high quantum-dot loading and novel redox system remain a barrier for indoor photovoltaics.

Current and future challenges

Currently, quantum-dot-based solar cells are mainly in two categories: lead chalcogenides (PbX, X = S, Se) and lead halide perovskites. The large Bohr exciton radii in PbX quantum dots are suitable for indoor photovoltaics, rendering efficient light absorption and charge transport. Besides size-dependent photophysical properties, lead-halide-perovskite quantum dots feature more defect tolerance than PbX quantum dots, resulting in less energy loss such as photovoltage deficiency in devices. Although heavy metal Pb is dominant in both PbX and lead-halide-perovskite quantum dots due to the essential role of its $6s^2$ orbitals, enabling direct bandgap transition and stable crystal dimension, the technology is now moving towards eco-friendly quantum-dot materials such as $AgBiS_2$, CuInZnSSe, Sn-based-perovskite and InP nanocrystals (figure 18). Very recently, CuInZnSSe quantum dots employed as organic replacements in dye-sensitised solar cells have shown very promising performance (solar power conversion efficiency > 15%) [92]. However, quantum-dot-sensitised solar cells still suffer from device instability deriving from the liquid electrolyte, poor interdot carrier mobility due to capped long ligands, and high quantum-dot loading and corrosion of quantum dots by the electrolyte. Moreover, there is no report to date on indoor photovoltaics using eco-friendly quantum dots[93].

Several issues remain in developing quantum-dot indoor photovoltaics. (i) Long-chain organic ligands are adopted to provide quantum dots with good dispersion and stability. However, long-chain ligands prevent sufficient interdot charge transport, and improper removal of the long ligands can generate surface defects, phase transition, and degradation of quantum dots. The conventional layer-by-layer process is time-consuming and material-costly, which is unsuitable for large-scale manufacturing. Besides, high-quality quantum-dot deposition cannot be guaranteed in quantum-dot-sensitised solar cells by chemical bath deposition or successive ionic layer adsorption and reaction. (ii) The Schottky junction and the depleted heterojunction structure have several issues: relatively low charge collection efficiency, Fermi-level pinning effect, energy level tuning and insufficient charge carrier extraction. (iii) Quantum-dot-based indoor cells may undergo different open-circuit voltage loss and degradation mechanisms compared to reported conditions under AM 1.5 irradiation. Due to the significant overlap of indoor photovoltaics with human life, the source of heavy metals (Pb, Cd) and nanoparticles (quantum dots) present a particular risk to the built environment and the human body [94].
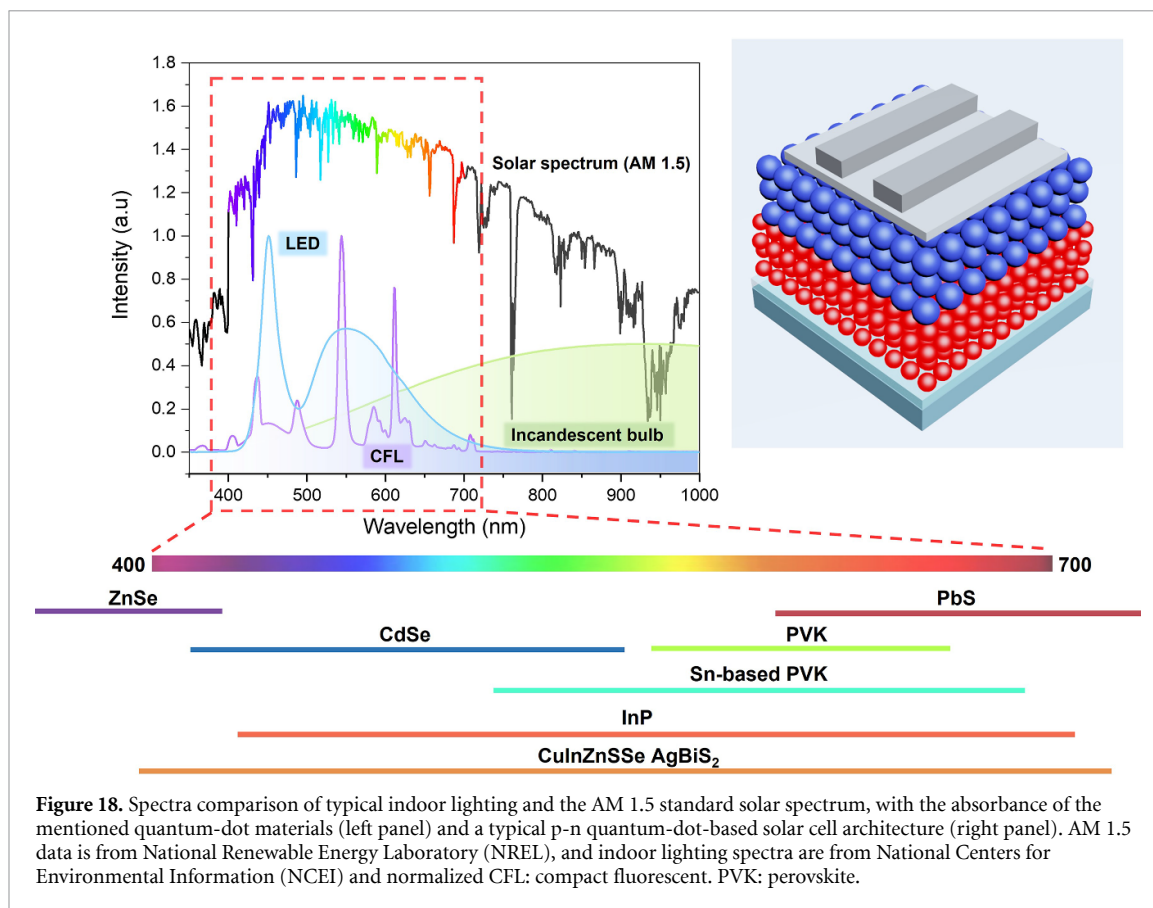
Figure 18. Spectra comparison of typical indoor lighting and the AM 1.5 standard solar spectrum, with the absorbance of the mentioned quantum-dot materials (left panel) and a typical p-n quantum-dot-based solar cell architecture (right panel). AM 1.5 data is from National Renewable Energy Laboratory (NREL), and indoor lighting spectra are from National Centers for Environmental Information (NCEI) and normalized CFL: compact fluorescent. PVK: perovskite.

Advances in science and technology to meet challenges

Advances in surface modification and synthesis routes have opened the door to more stable quantum dots. Apart from short ligands such as organic thiols and amines, inorganic halides are introduced for both PbX and perovskite quantum dots, passivating the trap sites and improving the device performance. In addition, the solution-phase ligand exchange strategy can substitute for layer-by-layer and the solid-state ligand exchange method. In this way, large-scale of quantum-dot-based indoor photovoltaics fabrication becomes feasible using prepared quantum-dot-based inks to form a controllable absorber layer. In addition, capping-ligand-induced self-assembly and quantum-dot secondary deposition have been developed to increase the quantum-dot loading in quantum-dot-sensitised solar cells and thus realize desirable device performance. Furthermore, inkjet printing, spray coating, blade coating, and slot-die coating are widely used methods for manufacturing quantum-dot-based optoelectronic devices, which is also practical for quantum-dot-based indoor photovoltaics.

Using homo- and heterojunction quantum-dot-based composite architectures can increase carrier diffusion length of quantum dots and active layer thickness, thus enhancing indoor device performance. Using size-dependent quantum confinement, the different bandgaps of halide-perovskite and PbX quantum dots can be used as front and back cells to form tandem indoor photovoltaics. Electron-transport layers and hole-transport layers also play a critical role in achieving good device performance, so elaborate interface engineering should be adopted between the quantum-dot absorber and the electron- and hole-transport layers. For instance, $CsPbI_3$ quantum dots can be coupled with transition-metal-oxide electron-transport layers (TiO_2 or SnO_2) and organic hole-transport layers (Spiro-OMeTAD, PTB7 or PTAA) to form a P–i–N device configuration. Device stability can be improved by passivation on the quantum-dot layers and device encapsulation that hinders the penetration of oxygen and moisture. However, comprehensive stability research of quantum-dot-based indoor photovoltaics is required to assess their tolerance to stressors such as moisture, heat, and light soaking. For instance, photoelectrons will not be fully generated to fill trap states under dim indoor lighting compared to AM 1.5 conditions, which may accelerate device degradation. Regarding quantum-dot-sensitised solar cells, an interesting alternative could be all-solid-state devices where conventional liquid polysulfide redox could be substituted. Since indoor photovoltaics target indoor and portable applications, ecotoxicity is an essential consideration [94]. Thus, eco-friendly quantum dots based on materials such as $AgBiS_2$, CuInZnSe, Sn- and Ge-based halide perovskites are more desirable than their heavy metal-based counterparts.

Concluding remarks

The emerging quantum-dot synthesis, engineering and cell fabrication technologies have demonstrated enormous potential for developing indoor photovoltaics. Recently, our group reported the first PbS-quantum-dot-based indoor photovoltaics device, exhibiting a promising power conversion efficiency of 19.5% under fluorescent illumination but lagging behind the expected maximum indoor power conversion efficiency (52 %) [17]. Several challenges remain before the final commercialization of quantum-dot-based indoor photovoltaics. From a device perspective, more studies are required on a homo- or heterojunction and band-aligned tandem configuration. From a materials perspective, it is necessary to develop a more efficient ligand exchange approach for quantum-dot film fabrication and proper interface engineering to maintain low trap states between layers. Moreover, comprehensive ecotoxicity studies are required to understand the leaching pathways for quantum dots [94]. With rapid advances in materials (metal chalcogenides, halides, phosphides, and nitrides) and devices (tandem, quantum-dot-sensitised solar cells), it is envisaged that quantum-dot-based indoor photovoltaics will soon realize their full potential for commercialization.

Acknowledgments

2.10. Accurate characterization of indoor photovoltaic performance

Behrang H Hamadani

National Institute of Standards and Technology, Gaithersburg, MD 20899, United States of America

Status

It is well understood that the standard reporting condition (SRC, air mass (AM) 1.5 global/25 °C/ 1000 W m^{-2}) for measurement of photovoltaic solar cells is not relevant for the ambient characterization of indoor photovoltaics [16, 95, 96]. Both the spectrum and the total irradiance of many artificial indoor light sources are significantly different from the AM 1.5 spectral irradiance. Unfortunately, no international standards or broadly adopted guidelines exist to clearly outline the measurement procedure to characterize and report the electrical performance of indoor photovoltaics. Hence, problems begin to arise when various laboratories report or compare the performance parameters of their indoor photovoltaics under common light sources such as fluorescent or white-light-emitting-diode lighting. Currently, most laboratories report the performance parameters of their indoor photovoltaics under a light source that has been measured with a lux meter, with the light intensity reported in the illuminance unit, lx (lm/m^2). Typically, 1000 lx or fractions of it are considered appropriate for the characterization of indoor photovoltaics. However, it has been clearly demonstrated that illuminance is not an appropriate quantity for measuring and comparing the performance of indoor photovoltaics so long as the precise reference spectrum remains undefined [97]. In some cases, an 18% discrepancy in the short circuit current (I_{sc}) may be reported under nominally similar lighting types at the same lux value, i.e. 1000 lx. It turns out the spectral distribution of the light source must also be considered. Adopting standards that clearly define the spectral irradiance profile of a given light source would help researchers conduct more accurate electrical measurements, even if lux continues to be used for measuring the light intensity. However, a more accurate method would involve extending the traditional reference-cell based method to the characterization of indoor photovoltaics under indoor lighting conditions. In short, reducing measurement uncertainties under well-defined reporting conditions (RC) would help advance the growing field of indoor photovoltaics and allow materials and device architects to better focus their efforts in developing high-efficiency devices, fine-tuned to specific ambient lighting profiles.

Current and future challenges

When it comes to accurate electrical characterization of photovoltaic devices, the biggest challenge is related to the accurate (low uncertainty) measurement of the irradiance of the light source used to perform the current vs. voltage (I–V) measurement. In an ideal world, all researchers would use the same exact light source with the same spectral and angular distribution. In this case, the intensity of the illumination incident on the cell could be measured and adjusted with a calibrated lux meter, spectroradiometer, reference solar cell or a similar equipment without any concerns or errors. However, indoor light sources or even solar simulators come in all sorts of spectral variations. Therefore, inter-comparison among different labs would be difficult unless everyone agreed on using one or a multitude of reference spectra for reporting results, much like we currently do with the AM 1.5G or AM 0 spectra, as codified in ASTM or International Electrotechnical Commission standards [98]. For the characterization of indoor photovoltaics, a reference spectrum has not yet been broadly adopted, although some steps towards that goal have been taken recently [99]. The challenge is that even if one agrees for their device to be traceable to a certain reference spectrum, achieving that exact illumination condition inside the laboratory is often unrealistic because spectral irradiance of artificial light sources vary significantly among manufacturers. Therefore, a universal protocol must be developed to allow each researcher to measure and adjust their light intensity such that everyone exposes their test specimen to the same exact *effective* irradiance when measuring I–V curves no matter the source of the illumination. For air mass 1.5 measurements, it is now universally accepted that the lowest uncertainty method to achieve traceability to this reference condition is accomplished through the use of a reference solar cell that has been calibrated by a primary national metrology institute or a secondary ISO-certified lab under a specific RC. There are currently efforts under way at some metrology institutes to extend this method to the characterization of indoor photovoltaics, but to do that, one or more appropriate reference spectra has to be adopted through international standard organizations.

Advances in science and technology to meet challenges

Efforts are currently under way to meet the challenges discussed above. Recently, the standard SEMI PV80-0218 [99], Specification of Indoor Lighting Simulator Requirements for Emerging Photovoltaic was
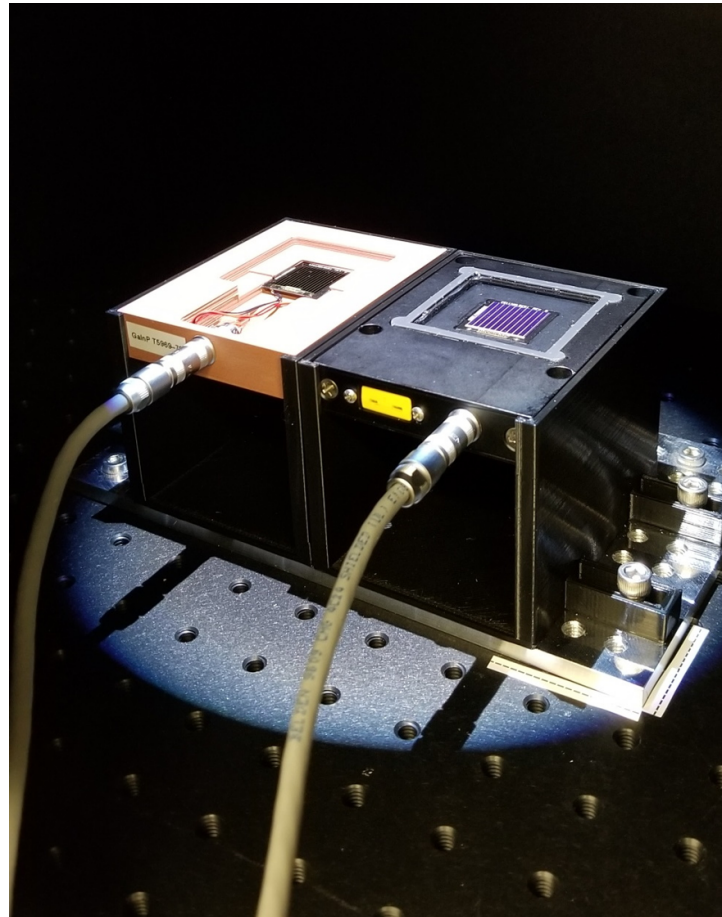
Figure 19. For current vs. voltage measurements of indoor photovoltaics, a calibrated reference cell (right) is placed next to the indoor photovoltaic cell (left) and used to measure and adjust the effective irradiance of the incident light-emitting-diode illumination. The objective is to measure and report the electrical performance parameters of indoor photovoltaics under a pre-defined reporting condition.

published, which clearly defined the normalized spectral distribution of five light sources adopted for the characterization of indoor photovoltaics from the International Commission of Illumination. These sources include illuminant A, which is a standard incandescent light bulb, and illuminant TL 84, which is a tri-band fluorescent lamp. Although the actual test method as described in this standard is still based on lux meter measurements, the methodology outlined will help reduce discrepancies between measurements. A more accurate method, however, is based on the use of a reference solar cell that has been specifically calibrated under a RC defined by one of the light sources in PV80-0218 or newly designated light sources. Such a calibrated reference solar cell can now be obtained from the National Institute of Standards and Technology in the USA. NIST uses the absolute irradiance spectral responsivity method to calibrate an appropriate reference solar cell (see figure 19) under any adopted reference spectrum, including three unique NIST-proposed reference spectra based on white light-emitting diodes of different correlated colour temperatures [97]. The chosen reference spectra are in absolute spectral irradiance (units: W m^{-2} nm^{-1}) and they are designed such that they correspond to a total illuminance of 1000 lx. Because the integrated irradiance value incident on the cell is known for a given RC, the power conversion efficiency can be easily computed, a task that is hard to achieve with low uncertainty if one only used lux to quantify the incident light intensity.

The complete procedure on how to use a calibrated reference cell to perform accurate *I–V* measurements traceable to a given RC has been published and is conceptually very similar to how we do *I–V* measurements under the SRC [97, 100]. The flowcharts in figure 20 outline the steps needed for accomplishing a traceable indoor photovoltaics measurement metrology. We believe that relative expanded uncertainties ($K = 2$) of

Figure 20. Under this proposed approach, standard organizations such as the ASTM would draft the necessary new standards for defining reporting conditions for indoor photovoltaics and the metrology institutes would calibrate reference cells under the published RCs. The testing labs or individual researchers will then use their in-house indoor photovoltaics simulators and the reference cells to carry out traceable *I–V* measurements. IPV: indoor photovoltaics.

2 % or lower are easily achievable with this technique for electrical performance measurements of indoor photovoltaics.

Concluding remarks

In conclusion, significant effort is under way to establish and formulate a well-defined metrology for electrical performance characterization of indoor photovoltaics. Given the significant market penetration and growth of indoor photovoltaics in recent years for energy harvesting under a variety of lighting conditions [12], it is imperative that *accurate* and *traceable* measurement procedures are followed when evaluating and reporting the performance parameters of these devices. Recent interlab-comparisons [101] have helped to better define and formulate the outline of this task but more inter-lab measurements among metrology institutes are needed to accelerate the progress towards standardization of indoor photovoltaics measurements.

Acknowledgments

3. Materials for piezoelectric energy harvesting

3.1. Introduction to piezoelectric energy harvesting—lead-based oxide perovskites

Emmanuel Defay, Veronika Kovacova and Sebastjan Glinsek
Materials Research and Technology Department, Luxembourg Institute of Science and Technology (LIST),
41 Rue du Brill, Belvaux L-4422, Luxembourg

Status
A piezoelectric energy harvester is a device that can absorb elastic work (W_{elast}) and convert this mechanical energy into electric energy. If we consider a one-dimensional model and a piezoelectric material with E_D its Young's modulus at constant charge (the largest one) and S_{max} the maximum strain it can withstand, the maximum W_{elas} stored in this piezoelectric material is $W_{elas,max} = \frac{1}{2}E_D S_{max}^2$. This work is then converted in electric work W_{elec} via the piezoelectric effect. The electromechanical coupling k enables quantifying $W_{elec} = k^2 W_{elas}$. Consequently, the maximum electric work—per unit volume—that a piezoelectric material can deliver is

$$W_{elec.max} = \frac{1}{2}k^2 E_D S_{max}^2. \tag{2}$$

This simple equation stands whatever the design, the structure, or the material. It corresponds to the energy enabled by one stroke. Table 1 depicts a broad picture of nowadays' state-of-the-art regarding an upper bound of the electric energy that can be generated by prototypical piezoelectric materials that are estimated from this one-dimensional model. Here we considered the best configuration possible regarding the coupling coefficient, which means the compression mode, enabling the use of k_{33}, which is generally the largest one. It is, however, difficult to use such coefficient in practice because bulk ceramics, the best piezoelectrics, are stiff materials and we generally prefer using softer structures such as membranes or cantilevers, better adapted to collect vibrations in the low frequency spectrum. This in turn considerably decreases the effective coupling coefficient. It is nonetheless interesting to contemplate the upper bound of piezoelectrics because it reveals their real potential at maximum. The three main things revealed by table 1 are: (1) the range of maximum energy harvester performances of typical piezoelectric materials encompasses three orders of magnitude, (2) the best possible material is a lead-based single crystal perovskite material that combines large strain and large electromechanical coupling and (3) lead zirconate titanate (PZT) films can withstand larger strain than bulk, which infers higher harvesting potential. In fact, lead-based oxide perovskite materials remain the best piezoelectric materials despite tremendous efforts to find lead-free alternatives with the same properties.

Current and future challenges
In realistic devices, Table 1's ranking is different because of practical limitations. Indeed, P(VDF-TrFE), AlN and PZT films-based energy harvesters are well represented in the literature because these materials are better suited to standard devices such as cantilevers [102–105]. The main issue in using the best materials could be phrased as a mismatch in mechanical impedance. Bulk piezoceramics are stiff and brittle. Therefore, finding harvesting conditions enabling a perfect impedance matching is scarce. Compliant structures are much better adapted to large strain and resonant conditions. This infers that piezo materials must be deposited or transferred on these well-adapted structures. This has been the case for a few decades with PZT buzzers or PZT/steel bilayers [106], associating an excellent piezo with a substrate able to withstand large strain. This leads to unprecedented harvested power per unit area beyond 1 mW cm^{-2} in resonant structures, as shown in figure 21 [104]. Doing the same with single crystals or lead-free piezoelectrics remains a big challenge, though our one-dimensional model reveals the potential of these materials.

To go further, as suggested by our previous figure of 1 mW cm^{-2}, we have to consider figures-of-merit that are based on practical devices that are most of the time related to vibrations in order to harvest more energy. A good description of these devices is provided by the following equation of the power density P_H (in W cm^{-2}) of a cantilever that reads [104]

$$P_H = \frac{e_{31,eff}^2}{2\varepsilon}\pi f S^2 V \tag{3}$$

$e_{31,eff}$ is the transverse effective piezoelectric coefficient, ε the dielectric constant, f the vibration frequency, S the longitudinal strain in the piezoelectric layer and V the volume of active piezoelectric material. Here the electric field is along the transverse direction (direction 3). This figure of merit is very similar to equation (2) because $e_{31,eff}^2/\varepsilon = k^2 E_D$. Equation (3) enables focusing (1) on materials properties that are practical to

Table 1. State of the art energy-harvesting characteristics of the main piezoelectric materials.

Material	Young's modulus E_D (GPa)	Max. strain S_{max} (%)	Coupling coefficient k^2_{max}	Electric Work $W_{elec,max}$ (mJ cm^{-3})
Pb(Mg,Nb)O$_3$-PbTiO$_3$ single crystal [107]	18	1.7	0.81	2110
Pb(Zr,Ti)O$_3$ films [108, 109]	80	0.5	0.5	500
(K,Na)NbO$_3$ bulk [102, 110]	70	0.46	0.40	296
Pb(Zr,Ti)O$_3$ 5H bulk [103]	50	0.175	0.56	43
P(VDF-TrFE) [104]	4	1.44	0.04	16.6
AlN [105]	300	0.028	0.07	0.82
Sc-doped AlN	200	0.028	0.12	0.94
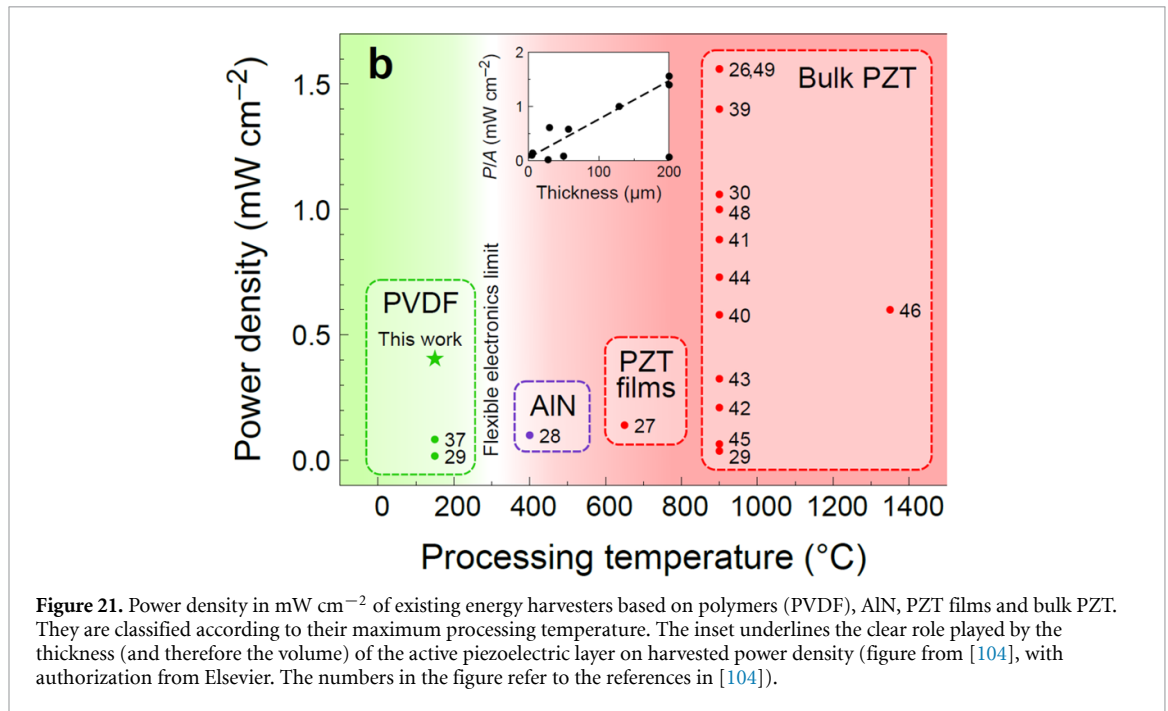
Figure 21. Power density in mW cm^{-2} of existing energy harvesters based on polymers (PVDF), AlN, PZT films and bulk PZT. They are classified according to their maximum processing temperature. The inset underlines the clear role played by the thickness (and therefore the volume) of the active piezoelectric layer on harvested power density (figure from [104], with authorization from Elsevier. The numbers in the figure refer to the references in [104]).

measure, namely $e^2_{31,eff}$ and ε and (2) on the extrinsic parameters, namely the frequency, the imposed strain and the volume of the active material.

Our ideal energy harvester therefore contains a substantial volume (large V) of a piezoelectric material with high piezoelectric properties (high $e_{31,eff}$), low dielectric constant (low ε) and is able to withstand large strain (large S). Note that we could also use a pure longitudinal configuration, such as compression-extension, that would enable using e_{33} instead of e_{31} in equation (3). Strain would then be along direction 3.

Advances in science and technology to meet challenges

Let us note that frequency cannot really be a parameter because mechanical and vibration energies in the environment lie in the low frequency range, typically below 100 Hz.

Here are the main ideas to carry on improving piezo-based energy harvesters.

Higher $e_{31,eff}$ and lower ε

As suggested in table 1, the best piezoelectric materials are based on lead and have perfect crystallographic structure. As mentioned, relying only on bulk ceramics is not an option because they are not well adapted to large strain. We need to consider films, and ideally epitaxial/highly oriented ones. Crystalline orientation plays also a paramount role in increasing $e_{31,eff}$, 100 being the most desired orientation in PZT layers. Improving piezo coefficients generally also increases ε. However, a proper stress management in the layer enables inducing a powerful imprint in the material, which in turn decreases ε.

Larger volume

The inset in figure 21 clearly shows that the power density per unit area is proportional to the thickness of piezoelectric material. This essentially disqualifies very thin films for energy harvesting, as long as one

considers 1 mW cm^{-2} as the power density target. Large thickness values for a piezoelectric material lead to high voltages, which is not easy to take full advantage of. Therefore, multilayers with intercalated electrodes fabricated via screen printing and aerosol jet have to be considered.

Larger strain

As seen in equations (2) and (3), strain has a positive quadratic effect on harvested energy. This is why, despite a low coupling factor, P(VDF-TrFE) can make energy harvesters with power density close to 1 mW cm^{-2}. One field of investigation to increase strain is to mix lead-based piezoelectrics with polymers and make composites. Another interesting approach consists in preparing a structure able to optimize the strain all along the piezoelectric material. It is referred to as compliant mechanism [111]. Finally, using substrates compatible with large strains, such as polymers, is a very interesting approach. Piezoelectrics are generally prepared on stiff and brittle substrates able to withstand very high temperatures, typically beyond 900 °C (see figure 21). Therefore, transferring top-quality piezoelectric layers on compliant substrates is a fundamental approach. An alternative way is to crystallize the piezoelectric layers directly on polymers by using innovative chemistry, laser or photonic annealing.

Concluding remarks

The simple figures of merit proposed herein enable figuring out the four parameters to improve in piezoelectric energy harvesters, and more specifically lead-based piezoelectric materials. These four parameters are the piezoelectric coefficients (notably, the transverse one, which matters the most in vibrating energy harvesters), the dielectric constant (the only one to decrease in order to improve electromechanical coupling), the volume of piezoelectric material, and finally the maximum strain that the piezoelectric material can withstand. Harvested energy as large as 2 J cm^{-3} per stroke can be predicted if all these parameters could be optimized.

Acknowledgments

3.2. Lead-free oxide perovskites for piezoelectric energy harvesting

Yang Bai

Microelectronics Research Unit, Faculty of Information Technology and Electrical Engineering, University of Oulu, FI-90570 Oulu, Finland

Status

Initial studies of lead-free oxide perovskites for piezoelectricity date to the early 2000s and intensive research in the recent two decades has been triggered by the European Union's legislation (EU-Directive 2002/95/EC) on the restriction of hazardous substances (widely known as the RoHS) [112]. In the case of piezoelectrics, the hazardous element refers to lead in the dominant PZT ($Pb(Zr,Ti)O_3$) family, where over 60 wt.% of lead is present in a compound. Oxide perovskites possess overwhelmingly higher performance among all piezoelectrics, due to which most research efforts have been put on searching for high-performance lead-free piezoelectrics from oxide perovskites. Looking at some key individual parameters such as piezoelectric charge coefficient (d) and electromechanical coupling factor (k), lead-free oxide perovskites are nowadays considered comparable to the PZT family if carefully designed in composition, microstructure, fabrication and post-processing [113].

For the time being, piezoelectric components account for only far below 1% of the entire market influenced by the RoHS regulations. However, considering the rapid development of piezoelectric energy harvesters and their potential applications in the ubiquitous IoT industry, sustainable and environmentally friendly piezoelectrics will weigh considerably more. This offers lead-free piezoelectrics an opportunity to flourish. Although there are many good lead-free piezoelectrics developed in laboratories, since they are not fully commercialized as is the PZT family, researchers such as device and system engineers at later stages in the value chain of piezoelectric energy harvesting have few options to choose from. It is admitted that design of energy harvesting systems is strongly case-by-case from materials to devices and systems [114]. Without a large selection pool of lead-free piezoelectrics, energy harvesting technologies built on top can hardly advance.

Current and future challenges

Most of the state of the art still envisage conventional actuators, sensors and transducers as applications of lead-free piezoelectrics. However, the design and engineering of piezoelectric performance for energy harvesting set distinguishing criteria. In line with lead-based counterparts, the piezoelectric energy harvesting figure of merit, *FOM*, defines the capability of kinetic-electric energy conversion working at off-resonance while k and quality factor (Q) determine the energy conversion efficiency at the resonance.

Ideally, *FOM* needs to be maximized, which brings the first issue. $FOM = d^2/\varepsilon$ where ε is the material's permittivity. However, in well-sintered piezoelectric ceramics and well-grown single crystals, not only d and ε evolve proportionally in the same direction but for lead-free piezoelectrics large d is achieved at a higher cost of ε compared to the case of lead-based counterparts. This significantly degrades the *FOM* values of lead-free piezoelectrics. Meanwhile, k and Q change in opposite directions and thus $k \cdot Q$ must be optimized. It is widely agreed that piezoelectric single crystals exhibit the best electromechanical properties, therefore, figure 22 summarizes and compares lead-based and lead-free single crystals in terms of *FOM* and k by taking the 33-mode as an example.

It is obvious that the champion lead-free oxide perovskites can only reach approximately 50% of the performance provided by lead-based counterparts, despite comparable k values. The situation is similar for ceramics with the best-performing lead-free $(Ba,Ca)(Zr,Ti)O_3$ (BCZT) showing only 70 %–80 % of the *FOM* and k values of the lead-based Sm-doped $Pb(Mg_{1/3}Nb_{2/3})O_3$-$PbTiO_3$ [113, 116]. These facts bring the crucial challenge of top performances for lead-free oxide perovskites which is urgently needed to be addressed especially for energy harvesting due to the crude requirement of output capabilities and efficiencies originated from the piezoelectric components. To the state of the art, comprehensive engineering of *FOM*, k and Q with energy harvesting as the target application is insufficient.

Advances in science and technology to meet challenges

Tremendous efforts are needed to keep improving the champion performance of lead-free oxide perovskites. This has always been the mutual aim in the lead-free piezoelectric community but considerably more attention should be paid to energy-harvesting-related material properties as discussed above. The key to this still lies in finding the most appropriate environmentally friendly A- and B-site cations that give the largest possible lattice distortion as well as proper morphotropic phase boundary. Rödel *et al* [117] have instructed what elements can be truly regarded as environmentally friendly. Apart from lead, elements such as antimony, which has been frequently adopted as a dopant in lead-free compositions, also need to be avoided.

Figure 22. Selection of top-performing lead-based and lead-free piezoelectric single crystals in terms of energy harvesting-related parameters (data extracted from [113, 115]). PMN-PT: $Pb(Mg_{1/3}Nb_{2/3})-PbTiO_3$.
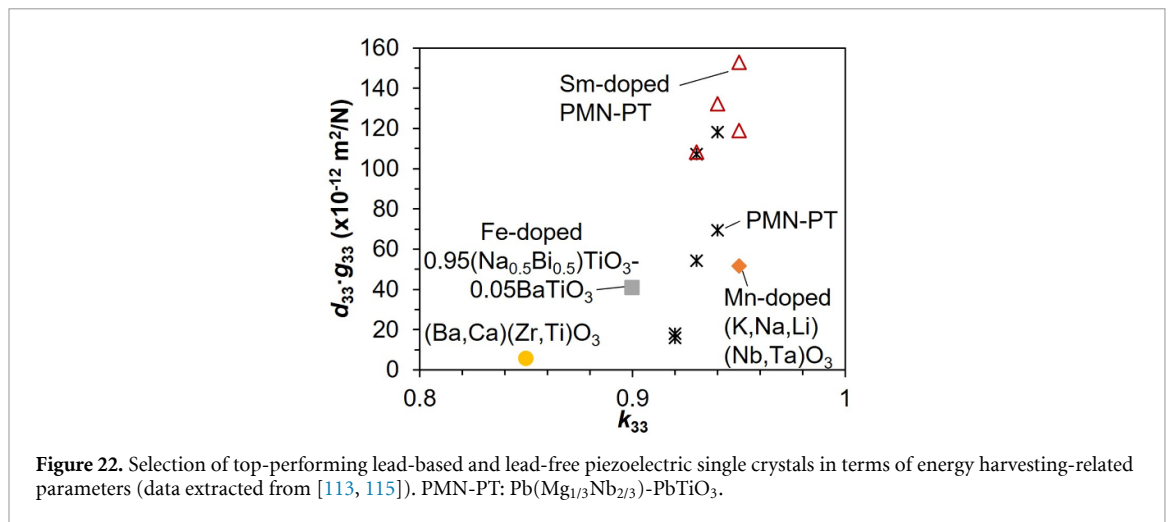
This leaves even a smaller room to optimize the compositions and thus the morphotropic phase boundary. Zheng *et al* [113] has provided a systematic review of how to design a proper morphotropic phase boundary for lead-free piezoelectrics.

Compositional optimization via experimental works is tedious and resource/time consuming. In the meantime, the use of density functional theory, multiscale modelling and machine learning to predict properties of oxide perovskite structures is rising [118]. Computation drastically increases the pace and effectiveness of material screening, discovery and development. These methods should be extended to the prediction of piezoelectric properties. The complexity of piezoelectric behaviours sensitively influenced by grains and boundary conditions is an essential issue to be addressed in simulation models before the adoption of computational methods in practical design and search of new lead-free piezoelectrics.

Application of lead-free piezoelectrics in energy harvesting is not only defined by top performance of the material family. Trade-offs between cost of raw materials and processing, working temperature range, and dynamic behaviours in the kinetic working conditions, also needs to be balanced. There are three promising compositions, BCZT-based, KNN ($(K,Na)NbO_3$)-based and NBT ($(Na,Bi)TiO_3$)-based. BCZT-based ceramics enjoy comparable *FOM* values to those of the PZT family, and even better $k \cdot Q$ values [113, 119]. PZT-based ceramics are the benchmark for lead-free piezoelectrics due to the seemingly best balance between cost and performance. The cost of BCZT is estimated to be similar to PZT [117] and for this reason, BCZT-based piezoelectrics are the most competitive lead-free candidates for energy harvesting at close to room temperature (Curie temperature < 100 °C). KNN-based piezoelectrics have higher Curie temperatures thus a broader working temperature range (up to 400 °C) [113]. Recent breakthroughs on multisource energy harvesting also provide the KNN-based an opportunity to evolve towards multifunctional components [114, 120]. NBT-based piezoelectrics have the highest fracture toughness and strength, almost doubling that of the PZT family [121]. This feature is specifically beneficial in energy harvesting where high input kinetic energy (e.g. high acceleration) is present.

As mentioned above, piezoelectric energy harvesting is case-by-case design. This requires close collaboration among researchers of materials, devices and systems. Communal efforts should be made to answer research questions in the future:

- In what exact use cases can lead-free piezoelectric energy harvesters win, given that the material performance might not be excellent but the device and system can work better thanks to, e.g. higher fracture toughness, higher working temperature, and clever duty-cycle design [114]? Advanced computational methods will be a great stimulator in this progress.
- Can the development of novel processing methods, such as solid-state crystal growth and room-temperature densification of ceramics, be used to create industrially compatible piezoelectric energy harvesters that cannot be achieved by the lead-based counterparts? This question mainly considers the cost and energy efficiency of the material processing methods.

Concluding remarks

Lead-free oxide perovskite piezoelectrics promote sustainability and environmental friendliness. This can probably be a ground that, regulated by legislations and pushed by the global trend on climate actions, the industries and users could accept compromised device/system performances. However, lead-free

piezoelectric energy harvesting does not necessarily mean compromise as being thought. On the contrary, as lead-free piezoelectrics have not been deeply integrated in mature industrial value chains, energy harvesting is a market where they can take the timely lead from the beginning of the commercialization hype. To realize this, we need to expand materials research extensively into electronics and systems. Each new material should have had a defined use case in certain energy harvesting system already at the stage of material design and engineering.

3.3. Nanostructured inorganics for piezoelectric energy harvesting

Da Bin Kim and Yong Soo Cho
Department of Materials Science and Engineering, Yonsei University, Seoul 03722, Republic of Korea

Status

The technology for piezoelectric energy harvesting has traditionally evolved in microelectromechanical systems based on thin-film cantilevers composed of piezoelectric perovskite oxides on Si substrates, wherein vibrational mechanical sources are mainly concerned with specific resonance frequencies. Inorganic nanostructures with unique electrical and physical characteristics have been introduced as nonconventional alternatives for harvesting electromechanical energy, particularly using flexible polymer substrates that enable the utilization of unprecedented mechanical sources, such as bending, twisting, stretching, and pressing. Interestingly, the advantages of using various mechanical inputs in flexible environments have created an extensive range of state-of-the-art applications, including physiological power generation, self-powered flexible systems, wearable tactile devices, and biomedical sensors, all of which use electromechanical coupling with low-power generation in nanoscale materials [122, 123].
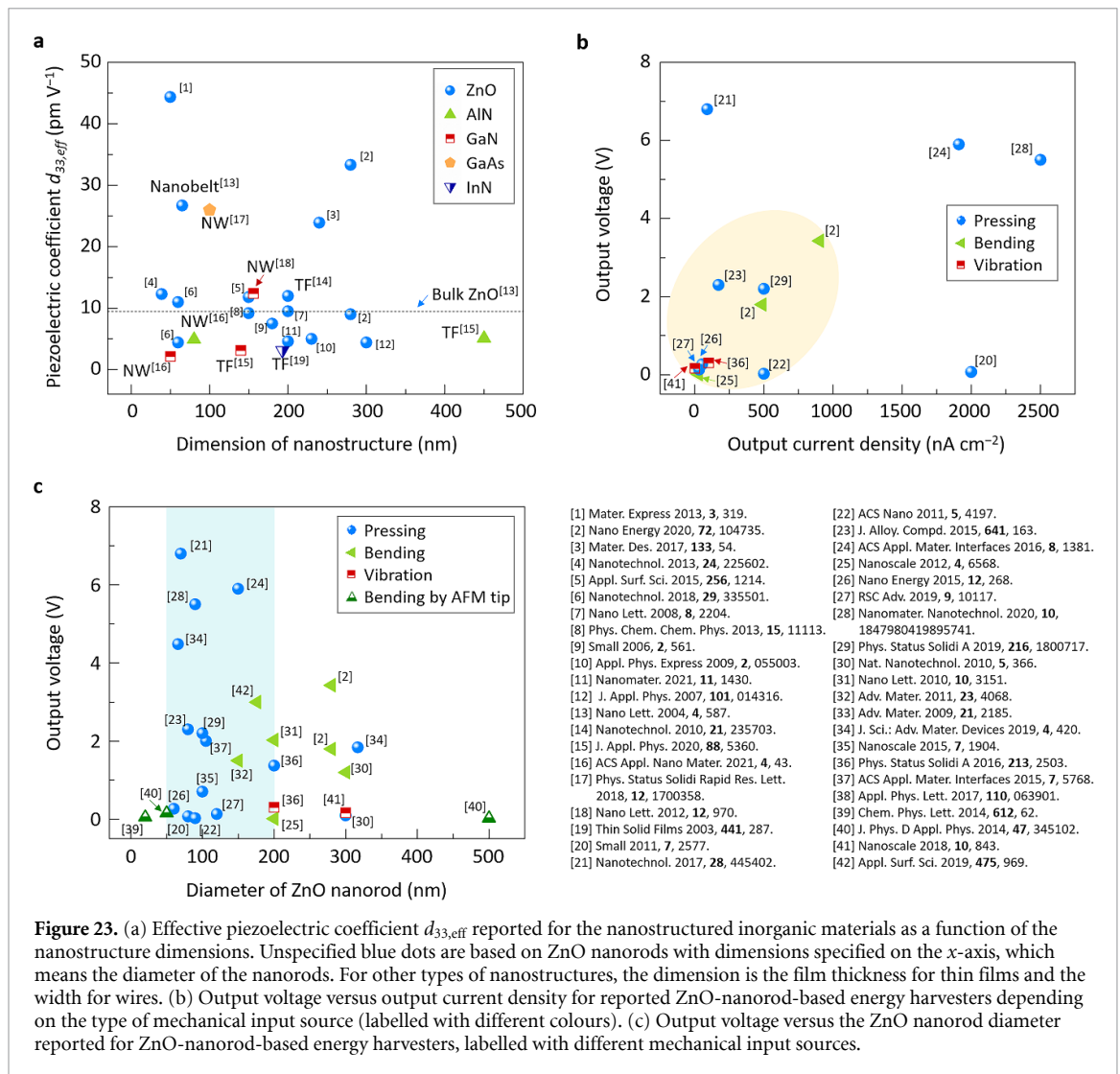
Piezoelectric energy harvesters based on nanoscale platforms are commonly called piezoelectric nanogenerators. For the last 20 years, nanoscale wurtzite ZnO has acted as a critical benchmark for representing earlier nanogenerators owing to its facile fabrication in the form of nanostructures, e.g. nanowires, nanorods, and nanofibers, its excellent crystallinity even at room temperature, and its high piezoelectricity. Harvesting outcomes in nanogenerators often outpace the output values of traditional thin-film cantilevers in terms of voltage and power density, accompanied by lower sensitivity to temperature and frequency owing to the non-ferroelectric nature of ZnO with no phase transition. Other inorganic piezoelectric materials, such as $Pb(Zr,Ti)O_3$, $(K,Na)NbO_3$, $BaTiO_3$, GaN, and perovskite halides, have also been employed in various nanoscale structures with promising power-conversion efficiencies [123, 124].

Because piezoelectricity is directly related to the enhanced dipole moments and polarization depending on the direction of the applied mechanical source, high-performance harvesters require the deliberate manipulation of the lattice strain in nanocrystals and the device architecture, as well as the proper adjustment of electrodes. The mechanisms that enable the extension of the lattice strain with applied stress in inorganic nanostructures may differ from the typical octahedral elongation of permanent dipoles in perovskite oxides, depending on the type of material and structure. For example, ZnO has a hexagonal structure without permanent dipoles and absorbs mechanical stress through the stretching of its ZnO_5 units [125]. For polymer-matrix nanocomposites incorporating inorganic nanoparticles, a more nuanced understanding of piezoelectricity and energy conversion with the contribution of individual constituents is required.

Current and future challenges

The choice of appropriate piezoelectric materials is critical for achieving high energy conversion. Because perovskite oxide materials must be processed above 700 °C for high crystallinity, stand-alone flexible harvesting systems using perovskite oxides on a plastic substrate have rarely been reported. Most common nanostructures for piezoelectric energy generation utilize an array of vertically aligned ZnO nanorods as fabricated from a seed layer by typical hydrothermal methods, which can be processed below 100 °C on a plastic substrate. This vertical nanostructure can be ideally utilized for out-of-plane lattice extension with applied tensile strain in structures with the top and bottom electrode layers. In figure 23(a), the effective piezoelectric coefficient $d_{33,\mathrm{eff}}$ values of the ZnO nanostructures are plotted with respect to the nanostructure dimensions, particularly for different ZnO morphologies and other nanomaterials. With some exceptions, the majority of $d_{33,\mathrm{eff}}$ values were less than 30 pm V^{-1}, regardless of the nanostructures or materials. Specifically, the performance projections of selected ZnO-nanorod-based nanogenerators in terms of the output voltage and current density are shown in figure 23(b), which are also classified by the mechanical input source, such as pressing, bending, and vibration. Most of the performance outcomes are less than 4 V and 1000 nA cm^{-2}, but some reach maximum values of ∼7 V and ∼2500 nA cm^{-2}. The harvesting output strongly depends on the type of mechanical input and the dimensions of the ZnO nanorods (figure 23(c)), where dimensions of ∼50–200 nm deliver viable performance outcomes owing to more effective energy conversion with higher deflectivity.

Because of the difficulty in forming nanorods or nanowires for flexible systems, other perovskite oxide materials have been commonly used as nanoscale fillers in polymer-matrix composites based on films or nanofibers. A higher content of piezoelectric filler induces a larger piezoelectric response while maintaining the resilience of the polymer matrix to accommodate a higher mechanical stimulus. For example, $Pb(Zr,Ti)O_3$ nanoparticles in a polymer matrix improved the harvesting characteristics, delivering outputs of 8.15 V and 956 μW cm^{-3} [126]. Particularly, with additional metallic inclusions, piezoelectric energy

Figure 23. (a) Effective piezoelectric coefficient $d_{33,eff}$ reported for the nanostructured inorganic materials as a function of the nanostructure dimensions. Unspecified blue dots are based on ZnO nanorods with dimensions specified on the *x*-axis, which means the diameter of the nanorods. For other types of nanostructures, the dimension is the film thickness for thin films and the width for wires. (b) Output voltage versus output current density for reported ZnO-nanorod-based energy harvesters depending on the type of mechanical input source (labelled with different colours). (c) Output voltage versus the ZnO nanorod diameter reported for ZnO-nanorod-based energy harvesters, labelled with different mechanical input sources.

generation was increased by extra space-charge polarization at the metal–polymer interfaces, in addition to the contributions of piezoelectric nanoparticles [127].

Advances in science and technology to meet challenges

Significant efforts have been made to overcome the limited energy-harvesting performance of inorganic nanostructures, which include the modulation of lattice strain, the modification of nanostructures, and the use of nonconventional piezoelectric materials (figure 24(a)). Strain engineering may be a promising approach for significant harvesting enhancement by inducing dipole extension under tensile strain. For example, a planar stretching strain of ∼4.87 % was reported to produce anisotropic lattice strain in a ZnO nanorod array, increasing the output voltage by ∼90 % [125]. Ideal generator devices must be designed with appropriate sample dimensions for optimal performance. In the case of nanocomposites, nonconventional nanoscale fillers, such as perovskite halides and carbon nanotubes, have recently been reported to exhibit outstanding performance. For instance, CsPbBr$_3$ halide nanocrystals embedded in polymer nanofibers delivered ∼103 V and ∼170 μA cm^{-2} with one-point pressing [127]. The performance of selected nanocomposites is projected in terms of their output voltage and current density in figure 24(b).

Perovskite halide materials have recently attracted significant interest as high-performance nanogenerators based on thin films or nanoscale constituents. For example, inorganic CsSnI$_3$ multi-layered films with the ∼100 nm Cu interlayers demonstrated impressive outcomes of ∼22.9 V and 1.2 μA[128]. As another recent example of inorganic nanostructures, two-dimensional dichalcogenide materials ranging in thickness from a single atomic layer up to a few nanometers have been introduced as potential piezoelectric nanogenerators. The energy-harvesting outcomes of a large-area monolayer MoS$_2$ film reached ∼0.4 V and ∼40.7 nA with optimal domain configurations relative to the position of the interdigitated electrodes [129].

[1] (ZnO nanorod/PVDF film) RSC Adv. 2019, **9**, 10117.
[2] (ZnO nanoflower/PDMS film) Mater. Lett. 2018, **230**, 207.
[3] (V:ZnO nanosheet/PDMS film) Nanoscale 2016, **8**, 1314.
[4] (ZnO nanosheet/PVDF-HFP nanofiber) Adv. Compos. Hybrid Mater. 2021, **1**.
[5] ($BaTiO_3$ nanotube/PDMS film) J. Phys. Chem. Lett. 2012, **3**, 3599.
[6] ($BaTiO_3$/CNT/PDMS film) Adv. Mater. 2012, **24**, 2999.
[7-1] (Random-$BaTiO_3$/PDMS film) ACS Appl. Mater. Interfaces 2016, **8**, 15700.
[7-2] (Vertical aligned-$BaTiO_3$/PDMS film) ACS Appl. Mater. Interfaces 2016, **8**, 15700.
[8] ($NaNbO_3$ nanowire/PDMS film) ACS Nano 2011, **5**, 10041.
[9] ($(K,Na)NbO_3$ nanoparticle/PDMS film) Nano Energy 2021, **82**, 105709.
[10] (PZN-PZT nanoparticle/Ag/UV polymer) Compos. Sci. Technol. 2022, **218**, 109151.
[11] (PZT microsphere/PDMS film) Nano Energy 2015, **11**, 1.
[12] ($CsPbBr_3$ nanocrystal/CNT/PVDF-TrFE nanofiber) Nano Energy 2022, **99**, 107421.
[13] ($FAPbBr_3$ nanowire/PDMS film) Adv. Funct. Mater. 2016, **26**, 7708.
[14] ($MASnI_3$ nanoparticle/PVDF film) Nano Energy 2019, **57**, 911.
[15] ($CsPbBr_3$ nanocrystal/PVDF nanofiber) Adv. Funct. Mater. 2021, **31**, 2011073.
[16] ($MAPbBr_3$/PVDF nanofiber) Nano Energy 2018, **49**, 380.
[17] ($MAPbI_3$/PVDF film) Nano Energy 2018, **53**, 46.
[18] ($FAPbBr_3$/PVDF film) Nano Energy 2017, **37**, 126.
[19] ($FAPbBr_3$/PVDF aerogel) Nanoscale 2020, **12**, 7214.
[20] ($Cs_3Bi_2Br_9$ nanocrystal/PVDF-HFP nanofiber) Adv. Mater. 2022, **34**, 2200042.
[21] ($TMCM_2SnCl_6$ nanoparticle/PDMS film) ACS Energy Lett. 2020, **6**, 16.

Figure 24. (a) Schematic illustration of recent experimental approaches using strain engineering, multifunctional nanocomposites, halide perovskites, and atomic-scale materials, in efforts to develop new piezoelectric energy harvesting platforms for upcoming applications such as physiological power generation, self-powered systems, wearable tactile devices, and biomedical use. (b) Projections of the output voltage and current density values reported for the nanocomposites incorporating inorganic nanoscale fillers.

Applications using inorganic nanostructures have been extended to self-powered wearable systems with diverse functionalities, which may also be suitable for artificial intelligence and machine learning systems interfacing with human motions and activities [130, 131]. Nanofiber-based composite generators have been extensively investigated as patches or woven fabrics for driving low-power devices or converting physical motion into electrical signals. In this regard, biocompatibility and long-term reliability must be seriously considered.

Concluding remarks

Piezoelectric energy harvesters based on nanostructured inorganic materials have a relatively short history. Since the early intensive investigations on adopting ZnO-based nanostructures based on different energy-conversion mechanisms, unprecedented device structures and inorganic nanomaterials have been extensively explored. Nanostructured inorganic materials may be the sole choice for developing flexible and wearable systems that require self-powered energy sources as a consequence of interactions to diverse mechanical inputs. The exploration of halide perovskite materials, novel nanocomposites, and atomic-scale structures in related fields is currently driving scientific efforts to understand piezoelectricity and the mechanism of electromechanical energy conversion in unexplored material systems. A critical issue in the field of piezoelectric energy harvesting may lie in the non-standardized measurements, which makes it difficult to compare widely scattered reported values, even in similar devices. Nanostructured inorganics are expected to provide unique solutions for future high-efficiency electromechanical energy-harvesting devices.

Acknowledgments

3.4. Nitrides for piezoelectric energy harvesting

Agnė Žukauskaitė[1,2] *and Stephan Barth*[1]
[1] Fraunhofer Institute for Organic Electronics, Electron Beam and Plasma Technology FEP, 01277 Dresden, Germany
[2] Institute of Solid State Electronics, Technische Universität Dresden, 01062 Dresden, Germany

Status
This section is focused on wurtzitic nitrides, i.e. aluminium nitride (AlN) and aluminium scandium nitride ($Al_{1-x}Sc_xN$, AlScN) as well as other similar ternary and quaternary AlN-based alloys. Piezoelectric nitrides are attractive for various applications, including the energy harvesting due to low dielectric constants, good mechanical properties, compatibility with complementary metal-oxide-semiconductor (CMOS) technology, as well as high temperature stability. The main method of synthesis is magnetron sputtering, which is very scalable and inexpensive. Furthermore, in contrast to PZT-like materials, piezoelectric nitrides with non-centrosymmetric wurtzite structure do not need to be poled as they exhibit permanent polarization along the *c*-axis (figure 25(a)). Until 2009, when the first paper about enhanced piezoelectric properties of AlScN was published [132], AlN was the main nitride considered for its piezoelectric properties. However, it suffered from relatively low d_{33} value of $\sim$4–6 pC N^{-1}. High acoustic velocity made it worthwhile for radiofrequency applications, but in energy harvesting it was not very competitive with lead zirconium titanate ($Pb(Zr_xTi_{1-x})O_3$, PZT)-like materials. Now, with the emergence of AlScN (up to $d_{33} = 31.6$ pC N^{-1} reported for $Al_{0.59}Sc_{0.41}N$ [133]), nitrides are also being considered a viable option for energy harvesting, especially where complementary-metal-oxide-semiconductor integration plays a role or where high-temperature poling step would damage a soft substrate so PZT cannot be used. Power generation output of AlScN harvesters can reach relatively high values, e.g. >1 mW in the 25–55 Hz range at Sc concentration of 39% [134]. An additional advantage is the possibility for use in high-temperature applications, as the Curie temperature of PZT materials is not so high (T_C of PZT < 400 °C, much lower for 'soft' material) whereas AlN or AlScN are stable at much higher temperatures [135]. AlScN and other ternary or quaternary nitrides with enhanced piezoelectric properties is a relatively new and very actively growing scientific field.

Current and future challenges
Due to high costs of Sc as a raw material, active search for alternatives is still ongoing, with various ternary and even quaternary nitrides being investigated (figure 26). However, they have not surpassed AlScN yet. Further theoretical and experimental search for other similar nitrides with enhanced properties is ongoing, with multiple research papers published every year.

Due to the metastability of AlScN [136], the material is prone to formation of abnormally oriented grains [137] as well as elemental segregation and parasitic cubic inclusions when Sc content is over 40%, so there is a physical limit for Sc incorporation before AlScN stops being wurtzite [136]. Other AlN-based ternary nitrides suffer from the same problems. As with all thin-film based piezoelectric materials, strain engineering and adhesion are also to be taken into consideration. So at the moment, the most effort is still concentrated in the material synthesis and the different aspects of it as well as understanding how to achieve highest material quality to assist with high-yield device fabrication.

Another challenge is actually the structuring of AlScN layers as the conventional methods used for AlN have a drop in etching rate (e.g. ion-milling) or significantly high lateral etching rate (e.g. KOH-based wet etching), so additional considerations have to be taken into account during the device fabrication. Even less is known about working with other ternary nitrides mentioned in the previous section. In the end, to maximize the output power will require new discoveries in material and process knowledge, improved device architecture and even the choosing of the right substrate for a specific frequency region. Moreover, for very high frequency applications the film thickness has to be decreased, so achieving high crystalline quality of the film would require additional attention.

Advances in science and technology to meet challenges
As the AlScN and other ternaries or quaternaries are still relatively new materials, discoveries about various material constants, behaviour under specific conditions or how the piezoelectric, mechanical, dielectric, optical, and other material properties are changing as a function of composition are still being made. For example, recently it was demonstrated, that due to the reduced energy barrier between the two polarization states of metastable AlScN the energy required for metal and nitrogen planes to switch their positions along *c* axis becomes very low, and as a result, under certain conditions AlScN is also ferroelectric [138] (figure 25(b)). As the switching is reversible, this would potentially allow to design hybrid cantilever-based energy harvesters that could dynamically switch between two modes: lower-output at higher frequency
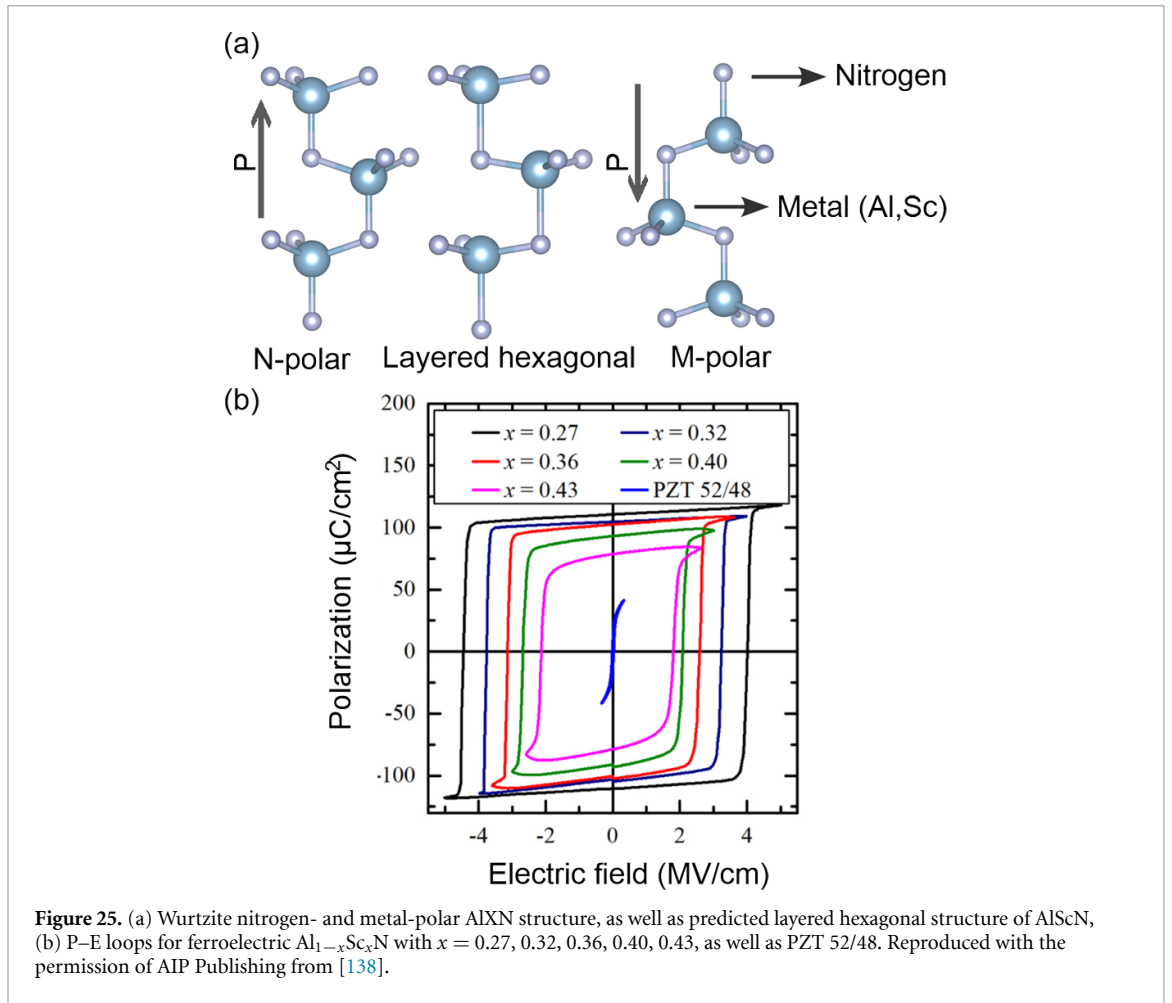
Figure 25. (a) Wurtzite nitrogen- and metal-polar AlXN structure, as well as predicted layered hexagonal structure of AlScN, (b) P–E loops for ferroelectric $Al_{1-x}Sc_xN$ with $x = 0.27, 0.32, 0.36, 0.40, 0.43$, as well as PZT 52/48. Reproduced with the permission of AIP Publishing from [138].
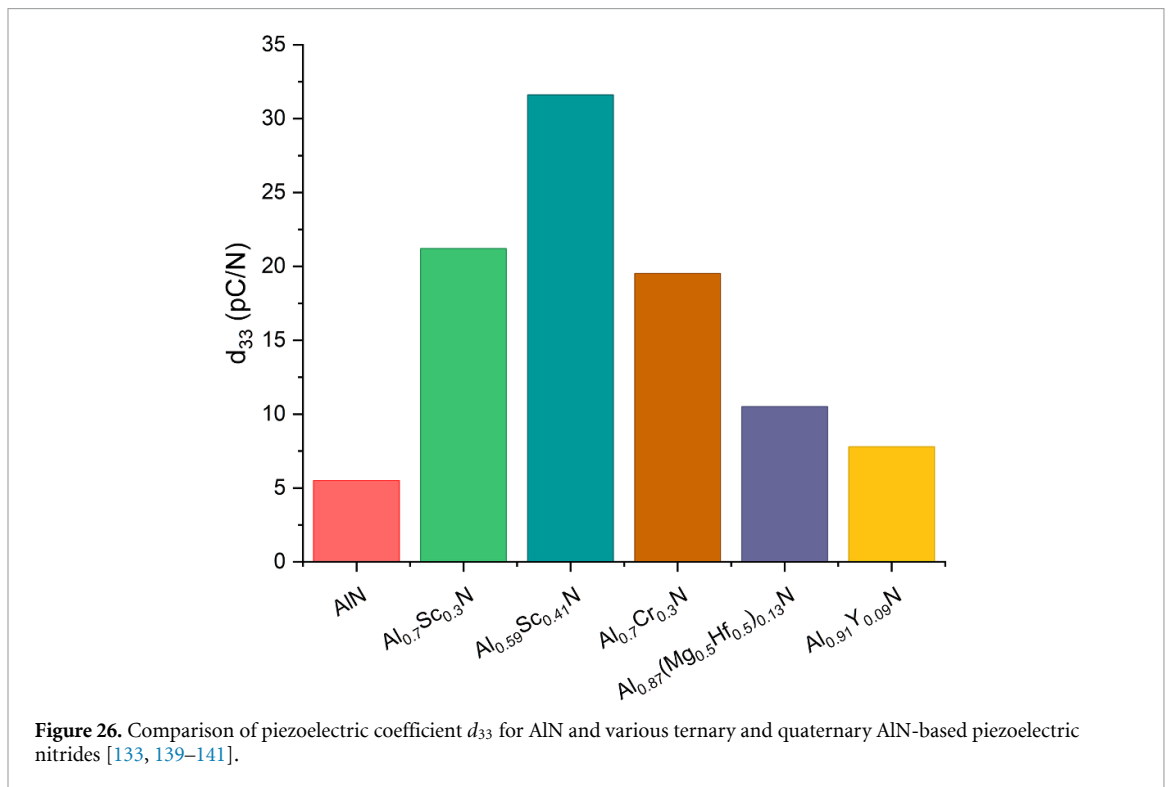

Figure 26. Comparison of piezoelectric coefficient d_{33} for AlN and various ternary and quaternary AlN-based piezoelectric nitrides [133, 139–141].

(unimorph) and higher-output at lower frequency (bimorph). For ultra-thin highly-crystalline nitride thin films, magnetron sputter epitaxy [133] is gaining more attention in the community as well. In addition, new and better harvester designs, e.g. hybrid piezoelectric-electromagnetic, multi-degree-of-freedom or nanowire energy harvesters are being developed where integration of nitride-based materials would be of relevance.

Concluding remarks

To conclude, the discovery of AlScN as the first nitride with such high piezoelectric coefficient and high electromechanical coupling triggered an avalanche in the studies of metastable nitrides for various applications, including energy harvesting. The challenges of fabrication of AlScN-based devices are being actively investigated by the scientific community as well as industry. Pronounced formation of abnormally oriented grains and potential for elemental segregation add additional limitations to the process window.

Under specific circumstances, where high-temperature stability, low environmental impact (lead-free) and complementary-metal-oxide-semiconductor compatibility play a dominating role, this new family of enhanced piezoelectric materials offers a lot of potential for compact, thin-film-based energy harvesters. New discovery of the ferroelectric properties of AlScN will also allow for designing more advanced and dynamic broadband harvesters.

Acknowledgments

3.5. Two-dimensional materials for piezoelectric energy harvesting

Feng Ru Fan[1] *and Wenzhuo Wu*[2]
[1] State Key Laboratory of Physical Chemistry of Solid Surfaces, College of Chemistry and Chemical Engineering, Innovation Laboratory for Sciences and Technologies of Energy Materials of Fujian Province (IKKEM), Xiamen University, Xiamen 361005, People's Republic of China
[2] School of Industrial Engineering, Purdue University, West Lafayette, IN 47907, United States of America
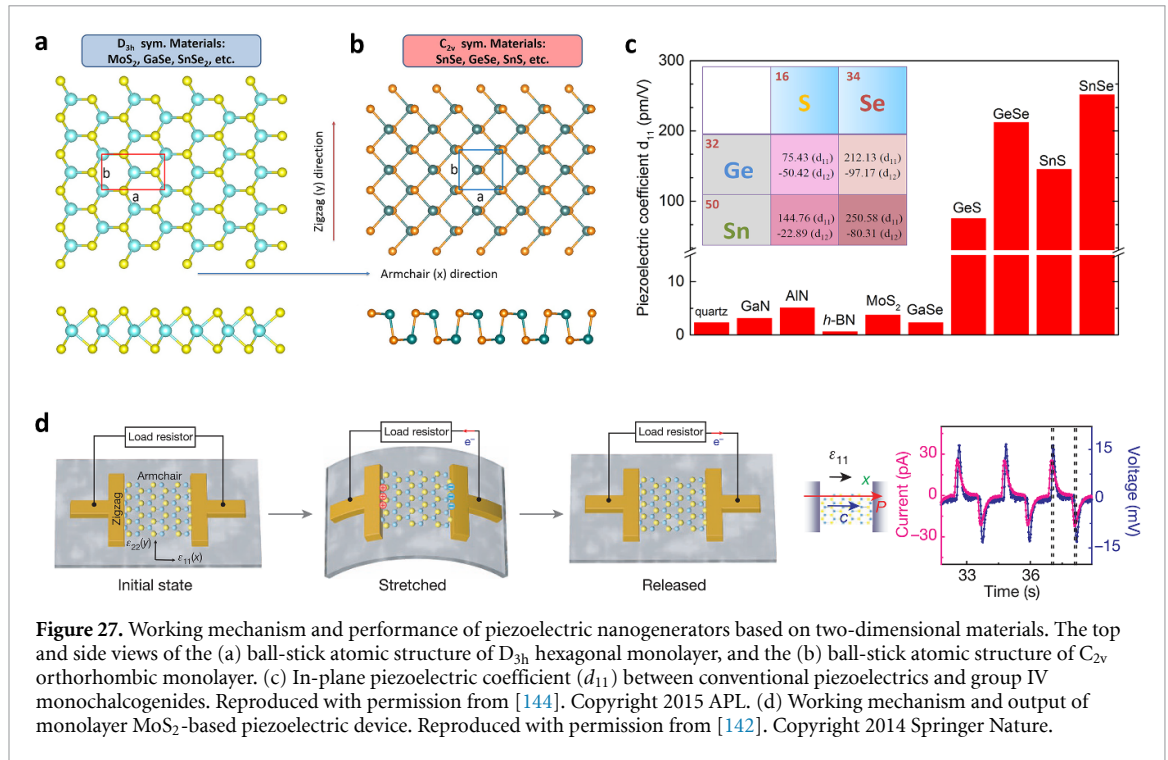
Status

Traditional piezoelectric energy harvesters fall short in several crucial respects that would make them ideal for the emerging applications in wearables, robotics, etc. Progress in piezoelectric nanogenerators has been aided by recent advances in both science and technology that leverage the unique characteristics of two-dimensional materials [142]. Unlike bulk or thin-film materials, two-dimensional materials can endure enormous strain and allow wide strain tunability due to their atomically thin geometries and superior mechanical features. Theoretical and experimental efforts suggest that many two-dimensional materials, including transition metal dichalcogenides (e.g. MoS_2), monochalcogenide group (e.g. SnS), and others, exhibit strong intrinsic piezoelectricity from their noncentrosymmetric lattices (figure 27a-c) [143]. The piezoelectric constant, a key piezoelectric figures of merit, for some two-dimensional materials (e.g. SnS, GeS, etc) is in the range of 75–250 pm V^{-1} [144], comparable to the piezoelectric constants of bulk piezoelectrics. The direct mechanical-to-electrical transduction of both static and dynamic signals makes these materials promising for application in piezoelectric nanogenerators with ultrathin form factors [145]. The reported power output for piezoelectric nanogenerators based on two-dimensional materials is in the range of mW m^{-2} (figure 27d) [146]. While there are many of recent papers that provide in-depth analyses of developments in related fields, our goal here is to give a more concise discussion focused on our perspectives on the potential and challenges in these areas.

Current and future challenges

Despite remarkable progress in related fields, challenges remain on the path toward the production, integration, and deployment of piezoelectric nanogenerators based on two-dimensional materials. Inducting consistent piezoelectric responses by applying external macroscopic mechanical strain is a significant challenge. The following elements contribute significantly to this problem: (1) most of these two-dimensional materials have symmetries that cause in-plane piezoelectricity [147]; (2) the ionic nature of these materials causes orientation-dependent piezoelectric responses; and (3) due to synthesis and/or assembly constraints, these materials are frequently placed on the host substrate with little or no control over the in-plane orientations. Even though a wide variety of two-dimensional materials have been predicted to exhibit intrinsic piezoelectricity, most of these materials have not yet been studied experimentally due to the challenges associated with current methods of preparing these materials [148]. The ability to scale up the preparation of related two-dimensional materials with the necessary yield and qualities is limited by constraints in growth substrates and process conditions. Furthermore, due to the material's symmetry, significant difficulties in process control arise when the thickness of a two-dimensional piezoelectric material varies by even a single atomic layer [142], rendering the material non-piezoelectric. Because of their atomic thickness, two-dimensional materials are highly sensitive to their surroundings (and possibly unstable). It has been found that the carrier concentration in two-dimensional materials may be dramatically altered by environmental doping, which in turn can have a profound effect on their piezoelectric behaviour due to charge screening [149].

Advances in science and technology to meet challenges

The above barriers also create a wealth of research opportunities. Due to the reduced dimensions of two-dimensional materials, their piezoelectricity is robust and easily accessible compared to its bulk counterpart. In contrast to conventional piezoelectrics, which are brittle and insulating, two-dimensional piezoelectric materials can host significant strain-induced electric field couplings due to the two-dimensional limit's extraordinarily high Coulomb interactions in the two-dimensional limit. The strong coupling of piezoelectricity to a variety of solid-state excitations including charges, photons, and spins in two-dimensional systems provide undiscovered prospects for pursuing fascinating science at the atomically thin limit. The hybridization of these processes within the operations of piezoelectric nanogenerators might promote interest in the study of new sciences and facilitate the creation of novel device designs. The thin thickness of two-dimensional materials also increases the occurrence of flexoelectricity, a physical phenomenon that can produce electrical polarizations with inhomogeneous deformation even in centrosymmetric lattices [150]. Understanding the impact of flexoelectricity on piezoelectric nanogenerators

Figure 27. Working mechanism and performance of piezoelectric nanogenerators based on two-dimensional materials. The top and side views of the (a) ball-stick atomic structure of D_{3h} hexagonal monolayer, and the (b) ball-stick atomic structure of C_{2v} orthorhombic monolayer. (c) In-plane piezoelectric coefficient (d_{11}) between conventional piezoelectrics and group IV monochalcogenides. Reproduced with permission from [144]. Copyright 2015 APL. (d) Working mechanism and output of monolayer MoS_2-based piezoelectric device. Reproduced with permission from [142]. Copyright 2014 Springer Nature.

based on two-dimensional materials is anticipated to facilitate the development of high-performance energy devices using a broader range of atomically thin materials.

Technology developments in material design and nanomanufacturing have opened the door to the possibility of mass-producing substrate-independent, high-performance two-dimensional materials with designer characteristics [151]. By combining theoretical and experimental examination of the interfacial characteristics of two-dimensional materials and electrode, we may get insight into phenomena such as the impact of metals and electrode configurations on charge transfer/transport in contacts involving a metal and a two-dimensional material. Such understanding is crucial for the rational design and optimization of future piezoelectric nanogenerators. The potential to allow innovative device ideas and applications in piezoelectric nanogenerators is only one of many reasons why it is crucial to understand the underlying doping process and defect chemistry in two-dimensional materials. The physics-based design and development of piezoelectric nanogenerators based on two-dimensional materials relies on quantitative *in situ* and *in operando* characterizations of two-dimensional materials under controlled straining circumstances to provide the vitally needed fundamental insights and experimental toolkit. Designing and fabricating two-dimensional heterostructured artificial crystals can generate new device physics and create a plethora of new functions. The ultrathin nature and robust mechanical properties of two-dimensional materials make them a candidate for three-dimensional devices, which might result in a myriad of unique capabilities and enhanced performance in comparison to their planar counterparts. For such three-dimensional integration, the discovery, development, and fabrication of two-dimensional materials with high out-of-plane piezoelectricity are desirable [149].

Concluding remarks

Theoretical and experimental progress in piezoelectric nanogenerators based on two-dimensional materials is expected to be sparked by the development of convergent techniques that bridge fields like advanced manufacturing, data science, material science, device physics, chemistry, etc. A concerted effort by the research community might assist several areas related to atomically thin materials' science and technology, such as piezoelectricity, semiconductor devices, ferroelectricity, and quantum physics.

Acknowledgments

3.6. Organics for piezoelectric energy harvesting

Pedro Costa[1,2], *Javier del Campo*[3,4] *and Senentxu Lanceros-Mendez*[1,2,3,4]
[1] Physics Centre of Minho and Porto Universities (CF-UM-UP), University of Minho, 4710–053 Braga, Portugal
[2] LaPMET-Laboratory of Physics for Materials and Emergent Technologies, University of Minho, 4710-057 Braga, Portugal
[3] BCMaterials, Basque Center for Materials, Applications and Nanostructures, UPV/EHU Science Park, 48940 Leioa, Spain
[4] OIKERBASQUE, Basque Foundation for Science, 48009 Bilbao, Spain

Status

Piezoelectricity was discovered by the Curie brothers in 1880 [152] while studying several materials, including organic ones such as cane sugar or tartaric acid. The piezoelectric effect is widely applied to sensor/actuator devices and to generate electricity. In this regard, wasted mechanical energy can be harvested to supply low-power electronic devices (μW to mW range) [152].

Piezoelectric materials, which typically display non-centrosymmetric crystalline structures, can be also present in specific amorphous organic materials. Generally, organic piezoelectric materials are characterized by lower piezoelectric constants, lower electromechanical coupling factors, and lower Curie temperature than their inorganic counterparts. In contrast, they present outstanding mechanical properties, can be processed in large areas, are flexible and can take a variety of shapes, including spheres, fibres or membranes [152].

Most piezoelectric polymers are semi-crystalline, though there are also amorphous ones. The piezoelectric effect in organic polymers is originated in the macromolecular structure and conformation together with their orientation and packaging [152], where a poling process is typically necessary to create or optimize their piezoelectric response.

The most studied organic piezoelectric polymers are polyvinylidene fluoride (PVDF) and its copolymers, which present the highest piezoelectric response to date (figure 28) [153]. Semicrystalline PVDF and their copolymers present distinct crystalline phases, being the β-phase the electroactive one with the highest dipolar moment per unit cell (8×10^{-30} C m) [153]. The piezoelectric coefficients of PVDF range from $8 < d_{31} < 30$ and $-24 < d_{33} < -140$ pC N^{-1}, respectively [153]. Other polymers with piezoelectric properties include polyamides (odd-nylons, being nylon-11 the most studied) with $d_{31} < 12$ pC N^{-1} [154].
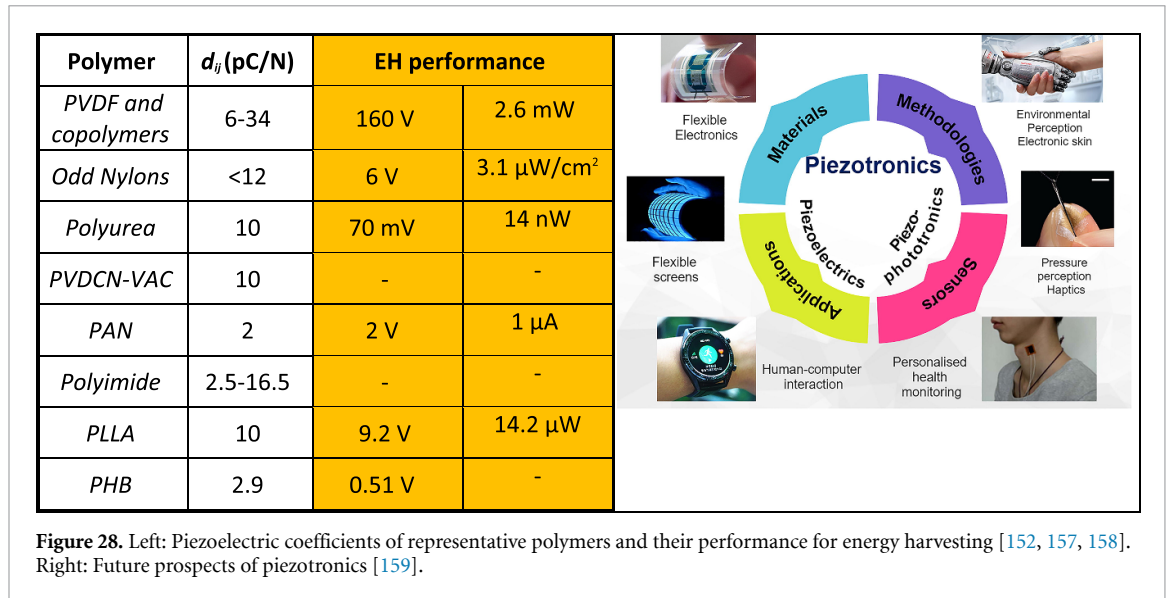
Biopolymers typically display piezoelectric coefficients between $0.1 < d_{14} < 2$ pC N^{-1}. These include polysaccharides (such as cellulose or chitin) and proteins (such as collagen or keratin) [155]. On the other hand, the piezoelectricity in amino acid single crystals can reach outstanding piezoelectric responses, such as 178 and 25 pC N^{-1}, respectively, for β-glycine and hydroxy-L-proline [156].

Piezoelectric polymers can be easily processed by solvent-based methods, including electrospinning, spin-coating, screen-printing or ink-jet printing, among others, but also from the melt: melt spinning, high-pressure melt crystallization, extrusion or injection provide a wide variety of shapes [152]. Among the different techniques, electrospinning provides larger piezoelectric coefficients because of the specific materials orientation during the process. Also, to optimize the piezoelectric coefficients and corresponding energy harvesting capability, poling (in order of MV m^{-1}) are usually applied in a post-processing step. The potential applications of the materials include energy harvesting from body movements, transportation, roadway, bridges, vehicles, tyres, engine or suspension, wind and ocean waves, among others.

Current and future challenges

Organic piezoelectrics show lower piezoelectric output than inorganic ones [152], but they are flexible, mouldable, can be processed by additive manufacturing in a variety of geometries, and are less expensive as they can be processed without advanced facilities.

The piezoelectricity of PVDF was first discovered by Kawai in 1969 [155] in stretched and poled films. In subsequent years, the research in PVDF and copolymers and in nylons was extensively performed [155]. Materials processing optimization led to piezoelectric coefficients (pC N^{-1}) for PVDF of $d_{33} = -24$ to -34 pC N^{-1}, and for the copolymers of poly(vinylidene fluoride-trifluoroethylene), PVDF-TrFE, $d_{33} = -25$ to -40 pC N^{-1}; poly(vinylidene fluoride-co-hexafluoropropylene), PVDF-HFP, $d_{33} = -24$ pC N^{-1}; poly(vinylidene fluoride-co-chlorotrifluoroethylene), PVDF-CTFE, $d_{33} = -140$ pC N^{-1}. Further, the introduction of small amounts (<2 mol %) of fluorinated alkyne monomers in the relaxor ferroelectric poly(vinylidene fluoride-trifluoroethylene-chlorofluoroethylene), PVDF-TrFE-CFE, terpolymer leads to an ultrahigh electromechanical coupling, with a $d_{33} > 1000$ pC N^{-1} [160], competitive with the ones of ceramic materials. For nylon-11 the piezoelectric response is $d_{31} < 12$ pC N^{-1} [154]. Poly(L-lactide) (PLLA), with $d_{14} = 12$ pC N^{-1} was discovered by Fukada in 1991 [152] and is relevant for medical applications due to

Polymer	d_{ij} (pC/N)	EH performance	
PVDF and copolymers	6-34	160 V	2.6 mW
Odd Nylons	<12	6 V	3.1 μW/cm²
Polyurea	10	70 mV	14 nW
PVDCN-VAC	10	-	-
PAN	2	2 V	1 μA
Polyimide	2.5-16.5	-	-
PLLA	10	9.2 V	14.2 μW
PHB	2.9	0.51 V	-

Figure 28. Left: Piezoelectric coefficients of representative polymers and their performance for energy harvesting [152, 157, 158]. Right: Future prospects of piezotronics [159].

their biodegradable characteristics. Natural materials with shear piezoelectric properties include silk and cellulose, with $d_{14} = -1.5$ and 0.2 pC N^{-1}, respectively [155], being biological piezoelectricity first reported for bone. Biological materials present lower piezoelectric coefficients (below 2 pC N^{-1}) and have been scarcely used for energy harvesting [156].

Organic biomaterials such as collagen can generate up to 10 V and 4.15 μW cm^{-2} [152] but most biomaterials working as energy harvesters show lower performance than traditional polymers. Nevertheless, their multifunctionality and sensing abilities are suitable for smart biomedical systems [156].

PVDF-based materials are the most explored materials as harvesting devices, mainly in cantilever beam geometry (unimorph or bimorph) and rotary harvesters but also in pressure or force modes, and the output power generated typically reach up to tens of μW to some mW [114, 152]. PVDF-TrFE is the most used polymer due to its improved piezoelectric coefficient [153]. The main advantage of these systems is the wide range of potential energy sources: rain over a PVDF film can generate several Volts and μW [114] while roadway applications may lead to 60 V, 18 μA and 0.2 W of output power [152] using electroactive PVDF.
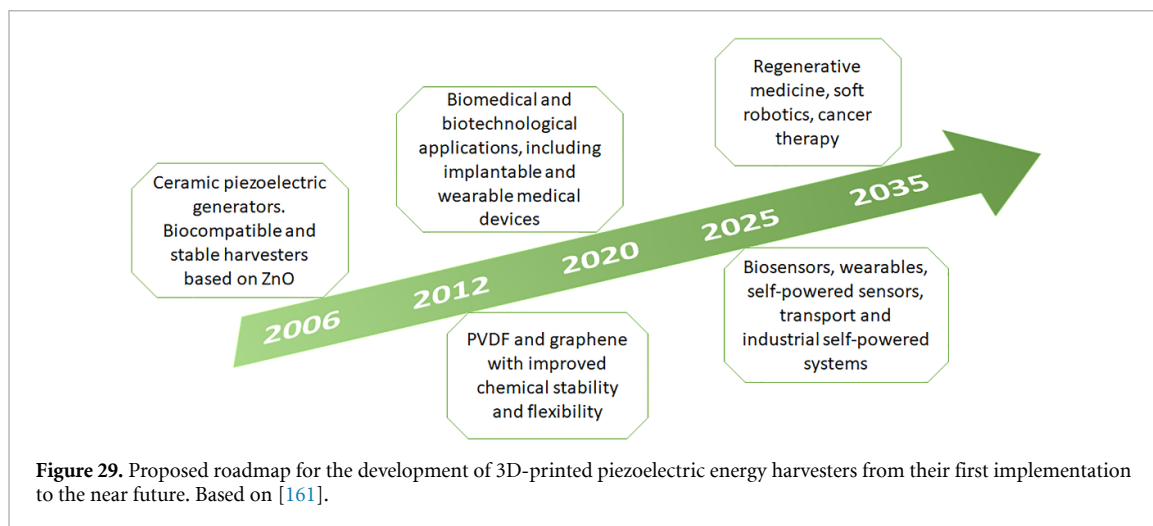
The need for flexible, low power energy harvesting systems has strongly increased in recent times due to market growth of small and autonomous electronic devices [152]. To optimize the generated energy harvesting devices it is mandatory combine two aspects: composite materials to maximize the energy per unit, and hybrid devices combining different active principles, such as the piezoelectric with triboelectric, pyroelectric or photovoltaic capabilities [159]. Lead-free piezoelectric ceramics with d_{33} larger than 100 [152] combined with ferroelectric polymers increase the device performance several times [152], while maintaining processability and flexibility. Polymer composites reinforced with ceramic fillers or nanocrystals can enhanced their performance several times generating of output power [158]. Poling the samples also increases the output performance of the devices.

Advances in science and technology to meet challenges

Three important areas where scientific advances will create opportunities for piezoelectric energy harvesters to meet societal and technological challenges (figure 29) are (i) materials and processes, (ii) integration into multifunctional components and (iii) more efficient devices with lower power demands.

Despite the advantages of organic or polymeric materials compared to ceramic ones, they face important drawbacks such as low piezoelectric coefficients, relatively poor thermal stability, and limited durability. These limitations define future avenues for new technology development. New composite materials combining polymeric piezoelectric materials, ceramics and metal oxides are one way forward to improve piezoelectric properties. Another intriguing opportunity is presented by the use of micro- and nano-patterned structures [159] as a means to improve both mechanical and electrical properties of these materials. Here the challenge rests in scaling up the process to enable large area applications.

Self-powered devices provide the third area where organic piezoelectric energy harvesters may find important opportunities. Current harvesting devices require the integration of several components such as the piezoelectric component, a rectifying unit, and a battery or other form of energy storage. The development of new materials and smarter device architecture could lead to the integration of several of these functions in a single component, which will lead to higher miniaturization levels and facilitate the

Figure 29. Proposed roadmap for the development of 3D-printed piezoelectric energy harvesters from their first implementation to the near future. Based on [161].

integration of piezoelectric energy harvesters particularly in small and autonomous devices. Self-powered sensors are a particular case in which the output of a piezoelectric energy harvester is actually used as the readout of an event of interest. For instance, in structural health monitoring, an important application area for piezoelectric materials, either alone or in combination with other energy generation and storage systems.

Last, one of the most cited limitations of organic piezoelectric energy harvesters is their low power output, but it can be expected to increase over the coming years though advance materials design and development, supported by machine learning strategies, among others. We often think about the improvements needed in one technology in relation to present circumstances, missing the parallel development occurring in other areas. Thus, advances in ultra-low-power electronics and energy storage will provide new opportunities for organic piezoelectric materials sooner than anticipated. While this kind of technological progress lies beyond piezoelectrics, it will eventually determine the most suitable opportunities.

Concluding remarks

Piezoelectricity has been a fruitful area of research and applications since its discovery over a century ago. Their ability to exchange mechanical and electrical energy makes piezoelectric materials extremely relevant in sensing and energy harvesting. Although organic piezoelectric materials display lower piezoelectric constants than their inorganic counterparts, their flexibility and compatibility with additive manufacturing processes makes them very attractive for a large variety of applications. The obvious way forward is improving piezoelectric response, thermal stability and durability. However, new architectures leading to multifunctional components, particularly self-powered ones, will open design avenues for new devices. Last, while performance gains in organic piezoelectric energy harvesters are important, one must keep an eye on the decreasing power needs of new low-power electronics and nanodevices, which may provide new opportunities sooner, or in areas other than expected. While most applications of piezoelectric sensors today may be in structural monitoring, applications in health and biomedicine will also play a decisive role in the future.

Acknowledgments

3.7. Bio-inspired materials for piezoelectric energy harvesting

Hamideh Khanbareh
Department of Mechanical Engineering, University of Bath, Claverton Down, Bath BA2 7AY, United Kingdom

Status

In the field of piezoelectric energy harvesting the term 'bio-inspired' has been referred to different groups of materials and systems depending on their origin or application. In recent years research has been focused on (i) biological piezoelectric materials (such as amino acids/peptides/proteins [162, 163], (ii) polysaccharides [164], (iii) animal-derived polymers such as silk [165] and collagen [166], (iv) biomimetic porous materials such as sea sponge and bone [167], (v) bio-waste [168] and (vi) energy harvesting mechanisms inspired by nature [169].

Cellulose is a biodegradable polymer with a piezoelectric coefficient of 26–60 pC N^{-1}. Mandal [165] fabricated a cellulose microfiber and polydimethylsiloxane (PDMS) composite piezoelectric generator. With hand punching, it produced an open circuit voltage of ∼30 V and short circuit current of ∼500 nA, and a power density of 9.0 μW cm^{-3}. Maiti *et al* [164] developed self-poled aligned cellulose fibrous with a piezoelectric coefficient of 2.8 pC N^{-1}. The fabricated generator produced a voltage, current, power density, and energy conversion efficiency of 18 V, 166 nA, 1.7 μW cm^{-2}, and 61.7%, respectively. Zheng *et al* [170] fabricated an aerogel cellulose and PDMS composite nanogenerator with an open circuit voltage of 60.2 V, a short circuit current of 10.1 μA, and a power density of 6.3 mW cm^{-3} at 10 Hz.

Sea sponge composed of soft fibrils and hard skeletons that combines high elasticity and toughness has inspired Zhang *et al* [171] to create a three-dimensional interconnected porous structure of $(Ba,Ca)(Zr,Ti)O_3$ piezoceramics and elastomer-based composite piezoelectric generator with enhanced mechanical and piezoelectric performance compared to those of a randomly dispersed particle-based composites. The output voltage, current density, and power density of 25 V, 550 nA cm^{-2} and 2.6 mW cm^{-2}, respectively, were achieved when compressed by 12%.

Ghosh [168] developed a piezoelectric nanogenerator based on fish swim bladder. It consisted of highly ordered self-aligned collagen nanofibrils and it could convert stress from a human finger (1.4 MPa) into electricity with an open circuit voltage, short circuit current, and power density of 10 V, 51 nA, and 4.15 μW cm^{-2}. Karan *et al* [172] showed that the bio-waste eggshell could be used to build a nanogenerator, with an output voltage of 26.4 V, 63% energy conversion efficiency, and 1.45 mA current with a power density of 238.2 mW cm^{-3} under 81.6 kPa. Alluri *et al* [173] used flexible and transparent aloe-vera films with a d_{33} of 6.5 pm V^{-1} to create an energy harvester and reported to generate sufficient electric charge to act as a self-powered sensor for human finger monitoring.

Current and future challenges

Bio-inspired natural materials exhibit promising piezoelectric properties as well as biocompatibility, biodegradability, flexibility, and durability. These are highly desired in most applications especially in healthcare and human-machine interface. However, this area of research is still in its infancy and open for the exploration of more novel biomaterials. These materials can help decrease toxic e-wastes generated by the use of electrochemical batteries or lead-containing piezoelectric materials.

Biomolecules like amino acids possess chiral symmetry, while protein-based polymers (silk and collagen) and polysaccharides (cellulose and chitin) have low-symmetric helical structures, exhibiting intriguing piezoelectric effect. Although most of these bio-inspired piezoelectric materials have an inferior piezoelectric performance compared to the classic counterparts, additional control over the orientation and polarization direction are expected to significantly improve their electromechanical coupling enabling future transducers with biodegradable properties.

Advances in science and technology to meet challenges

To overcome the inferior piezoelectric performance of bioinspired piezoelectric materials special attention has been given to uniaxial ferroelectric biomolecules with peculiar domain structure and record high piezoelectric voltage coefficients [162]. The key to significant improvement of properties in these materials lies in controlling nanoscale ferroelectricity in crystalline biomolecules as shown in the case of β-glycine [174, 175]. Self-assembly of organic ferroelectrics (such as β-glycine) with preferred orientation of polarization axes has been shown as an effective method in improving the materials properties [175]. The

importance of molecular simulations of polarization switching on nanoscale be over emphasized, which open pathways to creating novel classes of bioelectronic materials and devices.

Concluding remarks

In addition to widely researched organic and inorganic piezoelectric materials, plenty of biological materials are composed of piezoelectric components. In addition, their non-toxic, biocompatible, and recyclable nature, have paved the way for their application in energy harvesting devices. Due to the growing interest in mechanical energy harvesting for healthcare and implantable devices as well as the environmental concerns related to the inorganic piezoelectric ceramics, more and more designs have been inspired by the materials and processes that offer functionality as well as biodegradability and seamless interfacing with the human body. Bio-inspired materials are promising candidates for future transducers as they offer a unique combination of the desired features. Research is focusing on improving the electromechanical performance by means of controlling the materials crystal structure, microstructure and the polarization direction while maintaining biodegradability.

Acknowledgments

4. Materials for triboelectric energy harvesting

4.1. Introduction to materials for triboelectric energy harvesting

Zhong Lin Wang
School of Materials Science and Engineering, Georgia Institute of Technology, Atlanta, GA 30332–0245,
United States of America

Triboelectric nanogenerators
Triboelectric nanogenerators were first invented by Wang's group in 2012 for converting randomly distributed, irregular, and wasted low-frequency energy into electric power [176, 177]. A triboelectric nanogenerator relies on the coupling effect of contact-electrification and electrostatic induction that converts low-amplitude mechanical energy into electric power [178]. Different from the traditional electromagnetic generator, a triboelectric nanogenerator *uses Maxwell's displacement current as the driving force for effectively converting mechanical energy into electric power/signal.* According to the Science Citation Index, there are more than 8400 authors distributed across 62 countries and regions, who are engaged in triboelectric nanogenerator research. Triboelectric nanogenerator research is a truly multidisciplinary field with applications in many different areas, such as wearable electronics, medical science, security, environmental science, infrastructure monitoring, robotics and IoT.

Triboelectric nanogenerators have four basic working modes: the contact-separation mode, lateral sliding mode, single-electrode mode, and free-standing mode (see figure 30) [176, 177]. Triboelectric nanogenerators are highly versatile: they can be used as micro-nano power sources, self-powered sensors, blue energy generators, and high-voltage sources, covering applications in medical science, wearable electronics, flexible electronics, security, human-machine interfaces, and environmental science [179–185]. Let us take the contact-separation mode triboelectric nanogenerator shown in figure 30(a) as an example. Under the mechanical pull-press force acting in vertical direction, the two dielectric layers are periodically contacted and separated. The two surfaces have opposite electrostatic charges owing to contact electrification effect. A change in spatial distribution of the media, surface electrostatic charge density, as well as the distance between the two electrodes, results in a variation of electric field in space, which is a form of displacement current that generates an output conduction current across the load connected between the two electrodes. As a general case, the media boundaries here do vary with time, and we need to derive the Maxwell's equations for moving charged media.

Theory of triboelectric nanogenerators
The driving force for a triboelectric nanogenerator is the Maxwell's displacement current, which is caused by a time variation of electric field plus a media polarization term. In the case of triboelectric nanogenerators, triboelectric charges are produced on surfaces simply due to contact electrification between two different materials. To account for the contribution made by the contact-electrification-induced electrostatic charges in Maxwell's equations, an additional term $\boldsymbol{P}_s$, called mechano-driven produced polarization, was added in the displacement vector $\boldsymbol{D}$ by Wang in 2017 [186], that is:

$$\boldsymbol{D} = \varepsilon_0 \boldsymbol{E} + \boldsymbol{P} + \boldsymbol{P}_s. \tag{4}$$

Here, the first term polarization vector $\boldsymbol{P}$ is due to the existence of an external electric field, and the added term $\boldsymbol{P}_s$ *is mainly due to the existence of the surface charges that are independent of the presence of an electric field and the relative movement of the media.* Substituting equation (4) into Maxwell's equations, we define:

$$\boldsymbol{D}' = \varepsilon_0 \boldsymbol{E} + \boldsymbol{P} \tag{5}$$
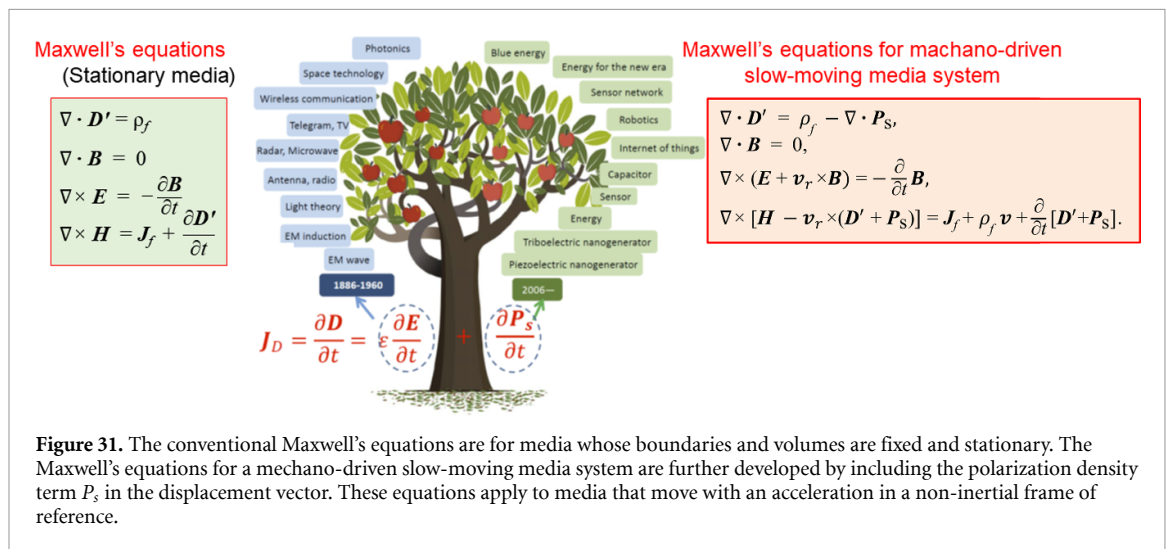
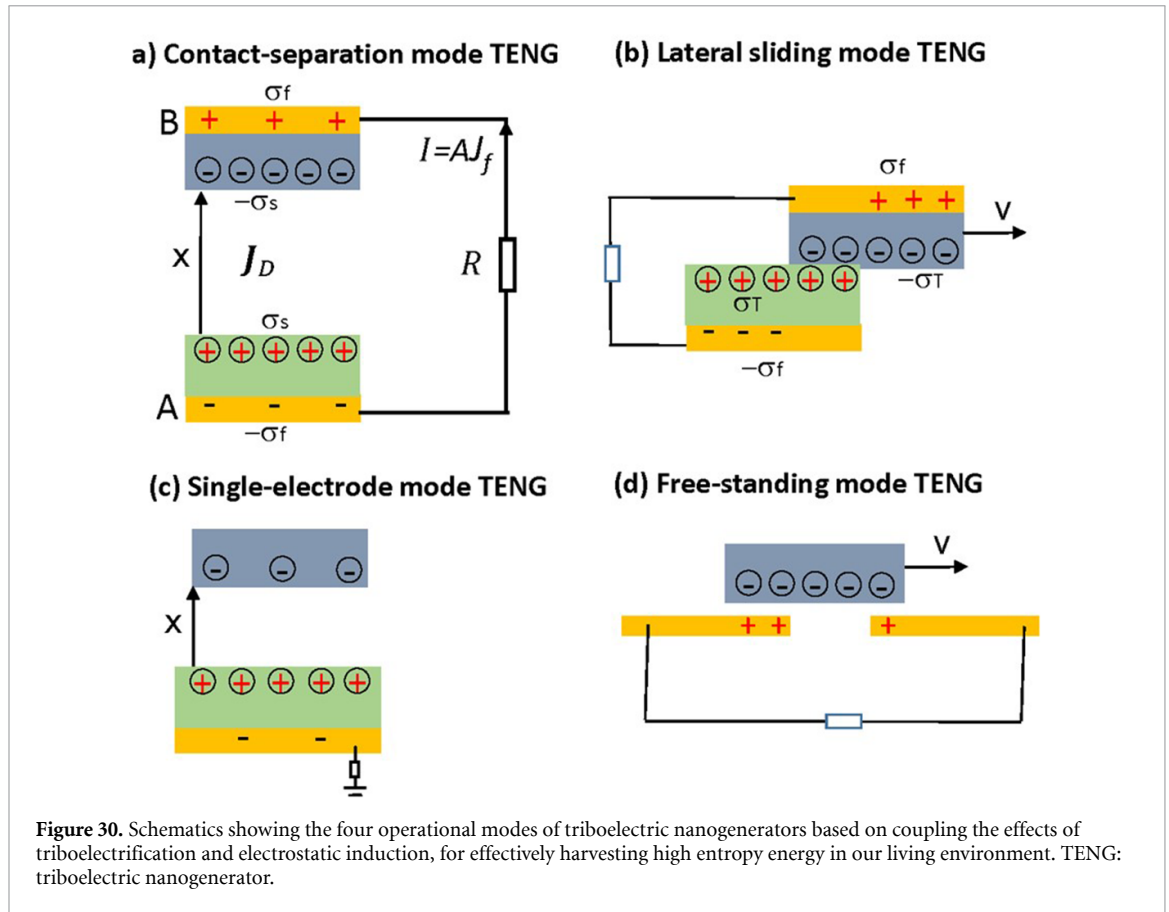The reformulated Maxwell's equations are [187]:

$$\nabla \cdot \boldsymbol{D}' = \rho_f - \nabla \cdot \boldsymbol{P}_s \tag{6}$$

$$\nabla \cdot \mathrm{B} = 0 \tag{7}$$

$$\nabla \times \mathrm{E} = -\frac{\partial \mathrm{B}}{\partial \mathrm{t}} \tag{8}$$

$$\nabla \times \boldsymbol{H} = \boldsymbol{J} + \frac{\partial P_s}{\partial \mathrm{t}} + \frac{\partial D'}{\partial \mathrm{t}} \tag{9}$$

Figure 30. Schematics showing the four operational modes of triboelectric nanogenerators based on coupling the effects of triboelectrification and electrostatic induction, for effectively harvesting high entropy energy in our living environment. TENG: triboelectric nanogenerator.

Figure 31. The conventional Maxwell's equations are for media whose boundaries and volumes are fixed and stationary. The Maxwell's equations for a mechano-driven slow-moving media system are further developed by including the polarization density term P_s in the displacement vector. These equations apply to media that move with an acceleration in a non-inertial frame of reference.

In equation (9), $\frac{\partial D'}{\partial t}$ represents the displacement current due to the time variation of the electric field and the electric field induced medium polarization. The second term $\frac{\partial P_s}{\partial t}$ is the displacement current due to non-electric field but owing to external strain field. The first term is dominant at high frequency for wireless communication, while the second term is the low frequency or quasi-static term that is responsible for the energy generation (figure 31). The term that contributes to the output current of a triboelectric nanogenerator is related to the driving force of $\frac{\partial P_s}{\partial t}$, which is simply named as the *Wang term* in the displacement current. In general cases, the two terms are approximately decoupled and can be treated independently. However, if the external triggering frequency is rather high, so that the two terms $\frac{\partial D'}{\partial t}$ and $\frac{\partial P_s}{\partial t}$ can be effectively coupled, the interference between the two term can be significant, but such case may occur in MHz–GHz range.
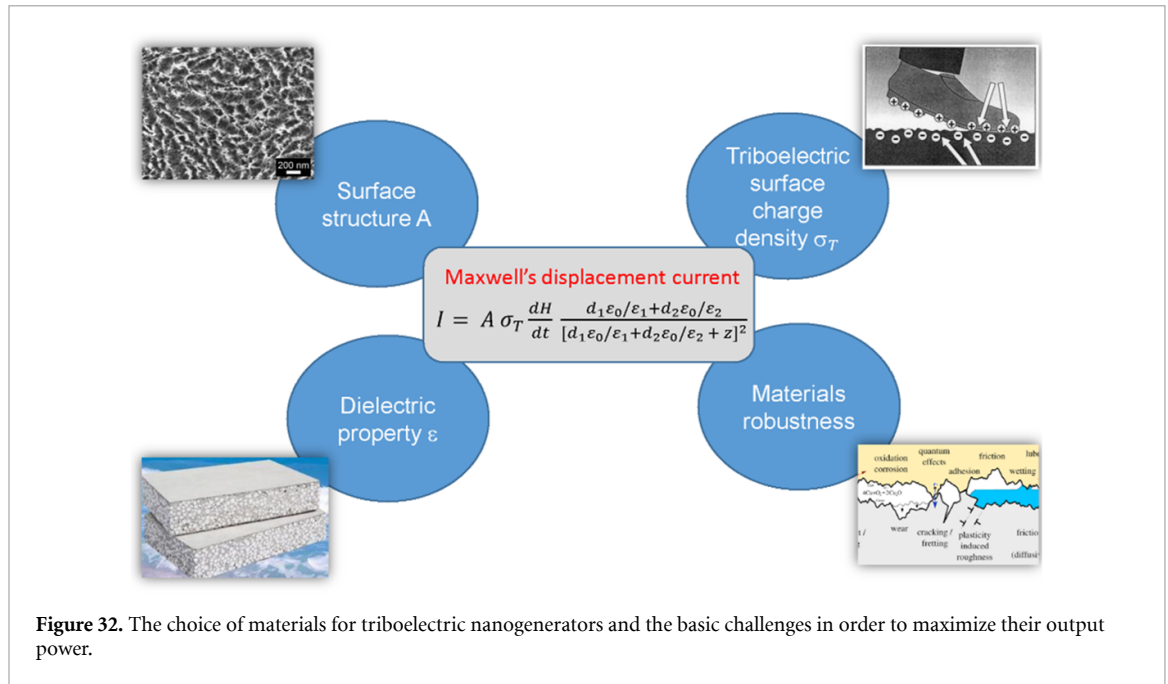
Figure 32. The choice of materials for triboelectric nanogenerators and the basic challenges in order to maximize their output power.

The conventional Maxwell's equations are for media whose boundaries and volumes are fixed and stationary. But for cases that involve moving media and time-dependent configurations, as in the case of triboelectric nanogenerators, the equations have to be expanded. Starting from the integral forms of the four physics laws, Wang has derived the expanded Maxwell's equations in differential form by assuming that the medium is moving as a rigid translation object with acceleration. If the relativistic effect is ignored, the Maxwell's equations for a mechano-driven slow-moving media system are given by [188]:

$$\nabla \cdot \boldsymbol{D'} = \rho_f - \nabla \cdot \boldsymbol{P_s} \tag{10a}$$

$$\nabla \cdot \mathrm{B} = 0 \tag{10b}$$

$$\nabla \times (\mathrm{E} - \boldsymbol{v} \times \boldsymbol{B}) = -\frac{\partial}{\partial \mathrm{t}} \boldsymbol{B} \tag{10c}$$

$$\nabla \times [\boldsymbol{H} + \boldsymbol{v} \times (\boldsymbol{D'} + \boldsymbol{P_s})] = \boldsymbol{J_f} + \rho_f \boldsymbol{v} + \frac{\partial}{\partial \mathrm{t}} \boldsymbol{P_s} + \frac{\partial}{\partial \mathrm{t}} \boldsymbol{D'}. \tag{10d}$$

These equations are most useful for describing the electromagnetic behaviour of moving media with acceleration. These expanded equations are the most comprehensive governing equations including electromagnetic interaction, power generation, and their coupling.

Materials for triboelectric nanogenerators

Since triboelectrification is a universal effect that applies to almost all materials and their related phases [189, 190]. The choice of materials for triboelectric nanogenerators is rather wide and unrestricted. In such a case, one can choose materials that fit the work environment the best, such as polymers, biodegradable materials, cellular materials etc. In general, choices of materials need to satisfy four requirements (see figure 32). First, rational design of the materials surface is important. We found that a flat surface may not give the highest triboelectric nanogenerator output because the contact between two flat surface may not reach atomic level, especially with the presence of some surface micro-size dust particles. A too rough surface will reduce the effective contact area at the atomic level. Therefore, an optimization has to be carried out to maximize the three-dimensional contact of the two surfaces, especially at atomic level contact, at which the charge transfer occurs. Secondly, from our theoretical analysis, the displacement current is related to materials permittivity so is the output voltage. A high-k material would result in stronger electrostatic screening, which may reduce the output power. A low-k material may not retain the required mechanical strength for the operation of the device.

Thirdly, the surface charge density is the most important factor that governs the output power, because the output power is proportional to the square of the surface charge density. In general, each material has its

own upper limit for holding the charges, which in most of the cases is limited by the strength of discharge in air. A great effort has been made to develop methodologies for enhancing the charge density on surfaces, including surface texturation [191] charge injection, oblique nanostructure construction [192], and charge transportation and storage along dielectric material [193] The surface charge density is normally limited by the breakdown voltage of a surface, so that it is normally in the order of $\sim$250 μC m^{-2}. Recently, a new strategy by binding charges in floating conductive layers is developed, and the bound charges are generated using a charge pump design that can be a normal triboelectric nanogenerator [194, 195]. The effective charge density can be greatly boosted to 1.02 mC m^{-2} in ambient conditions. Improved design of the pumping idea has further increased the charge density up to 2.38 mC m^{-2} based on optimization of contact status [196].

Lastly, a key challenge is to reduce the wear of materials and enhance the durability of triboelectric nanogenerators. With considering the facts that the tribo-charges would remain on insulator surfaces for hours at conventional condition, a continuous rubbing between the two surfaces is unnecessary. Therefore, by adopting a mechanical design that allows triboelectric nanogenerators to automatically switch between two modes depending on the rotation speed/frequency, the durability can be extensively extended [197, 198]. The second approach is to amplifying the operation frequency by structure design. The triggering energy from water wave can be stored as potential energy using a pendulum structure, so that an extended oscillation at a high frequency can largely enhance the energy conversion efficiency [199]. Such design has been extended for harvesting water wave energy, and an energy conversion efficiency over 28% has been achieved [200]. Lastly, by choosing an oil that has the smallest dielectric permittivity, such as squalene and paraffin oil, the performance of the lateral-sliding mode triboelectric nanogenerator is largely preserved and even improved. The lubricated triboelectric nanogenerator is able to give an output power that is 10 times of that of the unlubricated triboelectric nanogenerator [201]. This study opens a new approach for extending the lifetime and stability of triboelectric nanogenerators.

4.2. Synthetic polymers for triboelectric energy harvesting

Xiong Pu and Caofeng Pan
CAS Center for Excellence in Nanoscience, Beijing Key Laboratory of Micro-nano Energy and Sensor, Beijing Institute of Nanoenergy and Nanosystems, Chinese Academy of Sciences, Beijing 101400, People's Republic of China

Status
Synthetic polymers play a crucial role in triboelectric nanogenerators. A triboelectric nanogenerator typically contains triboelectric materials and electrode materials. Polymers can be designed to fulfill either of the two functions. Dielectric or insulating polymers are the most utilized triboelectric materials, as electrostatic charges on their surfaces are not easily dissipated. Semiconducting polymers have recently been found to generate triboelectric energy through the tribovoltaic effect, different from the electrostatic induction effect for insulating polymers [202]. Sliding motions were found to excite electron–hole pairs at the interfaces of the semiconductors, similar to the photovoltaic effect. Conducting polymers, either electronic conductors or ionic conductors, can be applied as the electrode materials in triboelectric nanogenerators. All-polymer or all-polymer-composite triboelectric nanogenerators have been reported. Therefore, it is easily understood that the properties of polymers can significantly affect the performance and functionalities of a triboelectric nanogenerator. Current research on triboelectric nanogenerators, from the perspective of polymer materials, has two trends. On the one hand, investigations are carried out to improve the electrical outputs of triboelectric nanogenerators by optimizing the polymer materials. The output voltage and power of a triboelectric nanogenerator are typically proportional to the static charge density maintained on the surface of triboelectric polymers. Materials engineering is then the core concern to boost the output of triboelectric nanogenerators. On the other hand, attention is also paid to enriching the functionalities of triboelectric nanogenerators through polymer design. Many functions can be obtained by appropriately designing the structures of the polymers used in a triboelectric nanogenerator, such as stretchability, wearability, transparency, self-healing capability, biocompatibility, and biodegradability.

Current and future challenges
The core challenge faced by triboelectric nanogenerators is to achieve high electrical power output. Therefore, it is of prime importance to increase the triboelectric charge density on the surface of triboelectric polymers. It was recently demonstrated that electron transfer between two different polymers accounts for contact electrification due to the difference in their work functions [203]. This charge transfer process leads to either positively or negatively charged surfaces. A larger distance between two materials in the triboelectric series leads to a possibly higher triboelectric charge density. However, this empirical rule does not provide reliable quantitative guidance for triboelectric nanogenerator design, and fundamental understanding on the relationship between the polymer structures and triboelectric properties remains challenging. Furthermore, the output of a triboelectric nanogenerator could also be determined by the air breakdown limit and the dielectric breakdown limit. The former factor is the reason why triboelectric nanogenerators are seriously degraded in a humid environment, as high humidity lowers the air breakdown limit and accelerates the dissipation of electrostatic charges; the latter factor could be attributed to the dilemma in electrification layer design, that improving the dielectric constant is beneficial to achieve a higher output from a triboelectric nanogenerator but also lowers the dielectric breakdown limit. Therefore, hydrophobic polymers could be considered to alleviate the effect of humidity, or a suitable waterproof package should be designed, which is very important for triboelectric nanogenerators applied to the harvesting of energy from water waves. Another challenge is the wear resistance of polymers, especially for sliding-mode triboelectric nanogenerators, though contact-separation-mode triboelectric nanogenerators have been demonstrated to be viable for long-term durability. As for functional polymers for triboelectric nanogenerators, such as stretchable and self-healable polymers, their durability and scalable fabrication are yet to be demonstrated.

Advances in science and technology to meet challenges
Progress in the following areas is needed to address the aforementioned challenges. First, fundamental studies are conducted to understand the mechanism of the electrification processes at the solid–solid, solid–liquid and solid–gas interfaces [189]. In the meantime, the origin of electricity generation in a triboelectric nanogenerator has been systematically investigated, finding that the output current is due to the Maxwell's displacement current, i.e. the time-varying electric field due to surface charges [186]. These efforts on fundamental understanding are crucial for future material or device optimizations. Second, quantitative descriptions of the relationship between materials/structures and the electrical outputs have been systematically studied. The figure of merit for triboelectric nanogenerators has been proposed [204]. The

triboelectric properties of a large number of polymers have been studied, trying to quantitatively establish the triboelectric series [205]. Fundamental studies have also been performed to correlate the polymer structures with their triboelectric behaviour [206]. Third, a series of different strategies have been attempted to improve the output performance of triboelectric nanogenerators. In order to increase the triboelectric charge density, triboelectric polymers can be chemically modified with the desired functional groups; their surfaces can be patterned with morphological features at different scales to increase the effective triboelectrification area; inorganic fillers with high dielectric constants can be added to polymer-based composites to enhance the outputs of triboelectric nanogenerators; approaches such as the corona discharge method were proposed to pre-charge the polymer surface with static charges; excitation circuits were designed to boost the surface charge densities [196]. Considering the importance of the triboelectric charge density, the output performance of triboelectric nanogenerators can be evaluated or compared based on it. The reported state-of-the-art triboelectric charge density reaches $\sim$8.8 mC m^{-2} [207]. Other than these advances, intensive studies have also been conducted to enrich the functionalities of triboelectric nanogenerators through innovations in polymer materials. Polymeric ionic hydrogels were designed to serve as either electrode or triboelectric materials, fulfilling multiple functionalities, such as stretchability, self-healing capability and transparency [208]. Biodegradable or bioabsorbable polymers were designed and fabricated to realize implantable energy harvesters. Through polymer materials engineering, triboelectric nanogenerators can be designed into fibres, yarns, thin films, fabrics, bracelets, eyeglass frames, swimsuits, socks, shoes, 3D-printed objects, and so on. The demonstrated versatility of triboelectric nanogenerators ensures their great potential for applications in a variety of areas.

Concluding remarks

In summary, a variety of polymer materials could play important roles in triboelectric energy harvesting. Not only improvement in output performance but also enrichment in the functionalities can be achieved through polymer engineering. The research field of triboelectric nanogenerators is attracting increasing attention worldwide, making it a hotspot and promoting fast advances. In particular, more polymer specialists are contributing to this field. As the challenges and opportunities are getting better understood, breakthroughs in practical applications are optimistically anticipated in the near future.

Acknowledgments

4.3. Nanocomposites for triboelectric energy harvesting

Renyun Zhang
Department of Natural Sciences, Mid Sweden University, Holmgatan 10 SE 851 70 Sundsvall, Sweden

Status

Traditional dielectric materials such as polymers have well-known mechanical and dielectric properties. These well-known properties allow us to study the mechanisms behind triboelectrification and apply them in triboelectric nanogenerators [189]. These properties are commonly found with pure polymer materials, and theoretical explanations could be developed due to the simplicity of the composition. These properties become more complicated if the pure polymers are composited with other materials, such as nanoparticles and nanowires. Despite the complex properties, nanocomposites bring new opportunities for studies of triboelectric nanogenerators because they enable tuning of the properties, such as dielectric constant, surface roughness, mechanical strength, conductivity, flexibility, and transparency.

The reasons why nanocomposite materials are so important for triboelectric nanogenerators can be explained with the theoretical model for the output current density [186]. The equation for current density can be divided into three parts [209] (figure 33). P_1 is the triboelectric charge on the surface that represents the charge affinity of a dielectric material. By forming a nanocomposite, the charge affinity can be changed so that more charges are transported during triboelectrification [210]. P_2 is related to operational aspects of triboelectric nanogenerators, such as force, frequency, and speed. The mechanical properties of the triboelectric materials can have a great impact on the operation of a triboelectric nanogenerator. By compositing with other materials, the mechanical strength, flexibility and friction constant of the dielectric material can be tuned [211]. P_3 is the electrostatic induction that decides directly how much induction charge can be created on the back electrode. The dielectric constant of the materials plays an important role here [212], and this is also a challenge for future studies.

Nanocomposites that have been studied in triboelectric nanogenerators have inorganic–organic (I–O), inorganic–inorganic (I–I), and organic–organic (O–O) compositions [213]. The I–O type of nanocomposites are mainly studied because the inorganic and organic parts of the composites have different properties that establish new properties in the nanocomposites and therefore enhance the output of triboelectric nanogenerators. The output power densities of nanocomposites constituting triboelectric nanogenerators are lower than those of pure polymeric materials, partly due to the emphasis placed on other advances, such as flexibility and durability. However, as our understanding of the properties of nanocomposites increases, higher output power densities are expected.

Current and future challenges

The challenges remaining for application of nanocomposites for triboelectric energy harvesting involve development of theories and fabrication of nanocomposite materials with desired triboelectric properties.

The challenge in developing theoretical models has two aspects: one is the understanding of charge transport during a triboelectrification process, and the other is the understanding of how the properties of a dielectric material change after it is composited with a nanomaterial. Current models built to explain charge transport were designed for materials with known band structures or orbitals that make electron transfer predictable. However, the complex chemical and physical compositions of nanocomposites make the band structures and orbitals difficult to define, especially when organic dielectric materials are composited with inorganic nanomaterials. Regarding the second challenge, it seems that there is no good theoretical model comparable to the empirical models derived from experiments for predicting the dielectric properties of nanocomposites. The theoretical models [214] most typically applied are used to simulate the dielectric constant of the nanocomposite, including the series mixing model and Lichtnecker logarithmic model. However, these models still generate errors in predicting the dielectric constants of nanocomposites. Figure 34 shows the P_3 value for a triboelectric nanogenerator using nanocomposites as triboelectric materials. As the figure shows, the two plotted models exhibit similar trends, but the P_3 values could be significantly different. That said, better models are needed to enable more accurate predictions.

The challenge that remains for the fabrication of nanocomposites with excellent triboelectric effects is in designing systematic experiments. Many studies have successfully produced nanocomposites for use in triboelectric nanogenerators. However, in most cases, one type of nanocomposite is made, despite the ratios of compositing parts being tuned. Such studies are successful but contribute relatively little to development of the theoretical models discussed above. On the other hand, a more systematic study demands more financial and human resources.

Figure 33. Deconstructed current density showing the three parts of the triboelectric effect; (P_1), device (P_2), and electrostatic induction (P_3). Reproduced from [209] under CC BY 4.0.
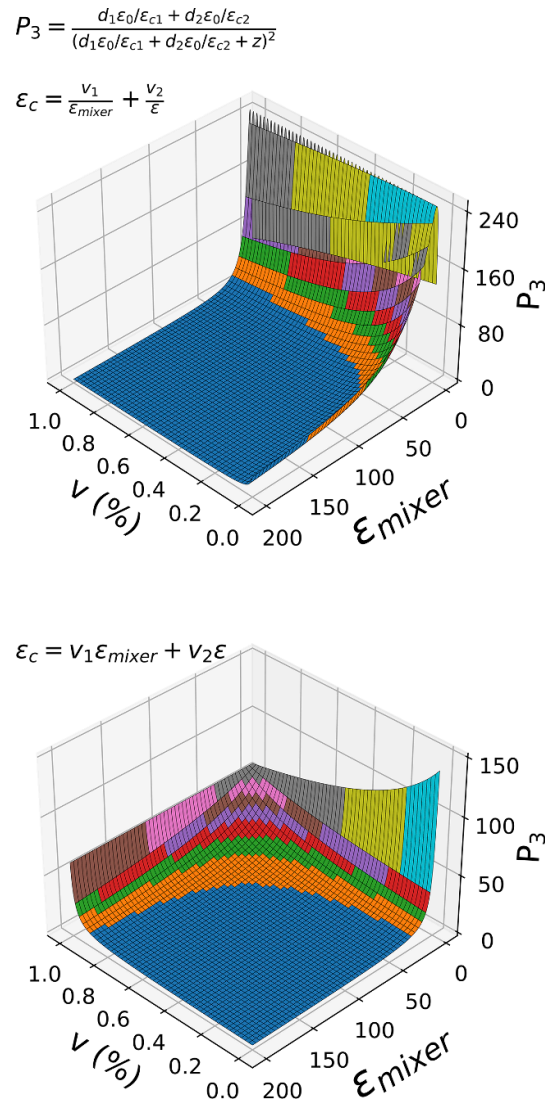

Figure 34. Simulated P_3 values based on the series mixing model (top) and the simplified model (bottom). v_1 and v_2 are the volume fractions of the components in a nanocomposite, and $v_1 + v_2 = 1$. The thicknesses of the dielectric materials, d_1 and d_2, were set at 0.1 mm, and the distance, z, between the triboelectric surfaces was set at 1 mm.

Advances in science and technology to meet challenges

Current nanocomposites studied for use in triboelectric nanogenerators are usually prepared by physically mixing their components. This procedure creates only physical contact between the components. A more advanced way is to create bonds between the components with or without linkages. Chemically, it is not very difficult to create such bonds, since many types of nanocomposites have been made from inorganic–inorganic, inorganic–organic, and organic–organic combinations. The question is whether the resulting nanocomposites could be processed further to develop good mechanical properties for use in triboelectric nanogenerators. A benefit of this strategy is that the properties of the nanocomposite become more predictable. Moreover, quantum chemical theories can be applied to simulate or calculate molecular

properties, such as the highest occupied molecular orbital and the lowest unoccupied molecular orbital [215]. The success of this strategy would contribute to our understanding of triboelectrification because one could design a nanocomposite, simulate its properties, and compare them with results from instrumental characterizations.

Modern characterization techniques, such as Kelvin probe force microscopy [216], could allow us to understand the triboelectric properties of nanocomposites. Kelvin probe force microscopy could provide information about the local dielectric properties of nanocomposites that would indicate how triboelectric charges are generated and distributed. Such information would lead to syntheses of nanocomposites with strong triboelectric effects.

Concluding remarks

Nanocomposite dielectric materials offer new opportunities to understand the fundamentals of triboelectrification and develop high-performance triboelectric nanogenerators for energy harvesting and self-powered sensing. Unlike pure engineering polymers that have limited ranges in which to tune the chemical composition, the methods for making nanocomposites allow researchers to design structures both chemically and physically. The outcomes of experimental studies will supply evidence needed to develop advanced theories and models. This will help to explain the mechanisms of triboelectrification and support the design of new nanocomposites for triboelectric nanogenerators exhibiting higher performance. To achieve such goals, there is a need for input from research areas other than material science and engineering, including chemical synthesis, quantum chemistry and electronics.

Acknowledgments

4.4. Surface texturing and functionalization for triboelectric energy harvesting

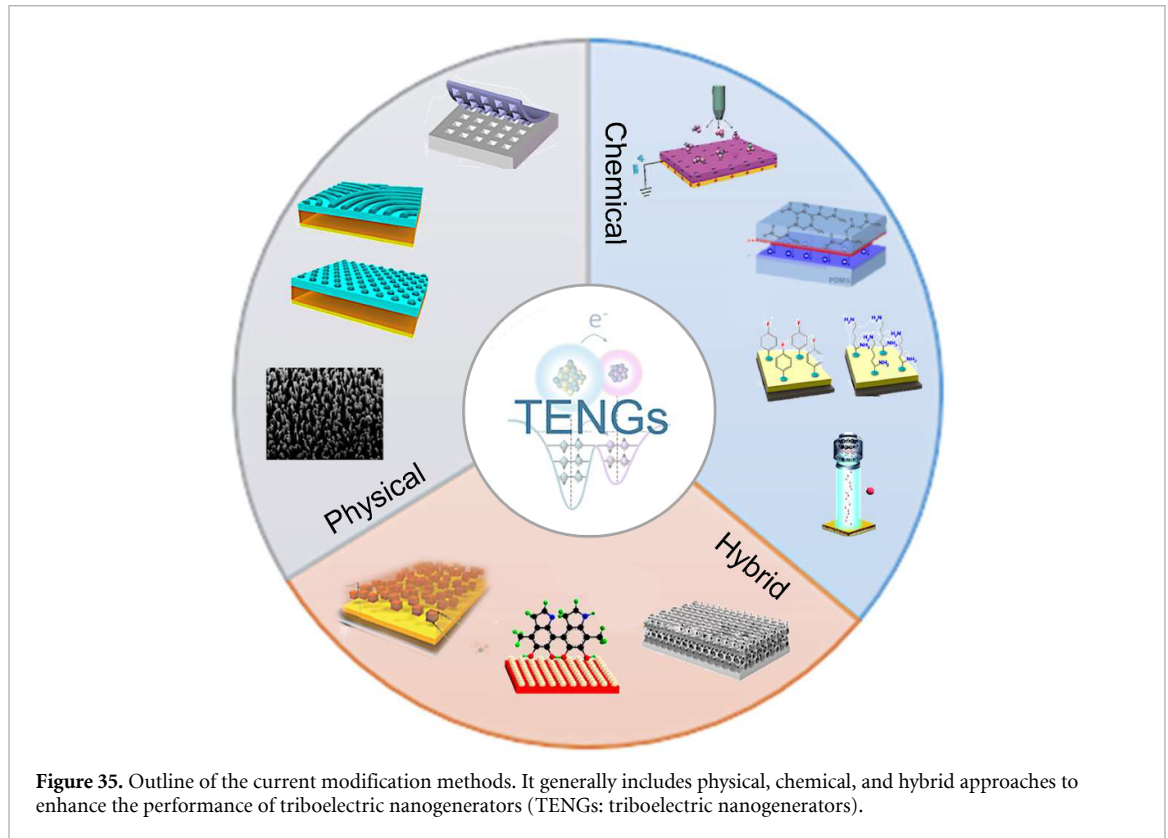*Jing Xu, Xun Zhao, Yihao Zhou, Guorui Chen, Trinny Tat, Il Woo Ock and Jun Chen*
Department of Bioengineering, University of California, Los Angeles, Los Angeles, CA 90095, United States of America

Status

The output performance of a triboelectric nanogenerator is determined by both multifaceted interface properties and material properties [217]. Therefore, nanoscale modifications that can manipulate the active interfacial area or electron transfer capacity of the materials are critical to ensuring high-performance triboelectric nanogenerators [218, 219]. Based on this, various physical, chemical, and hybrid strategies are proposed and developed substantially to engineer the tribo-materials at the nanoscale to improve the mechanical-to-electrical conversion of triboelectric nanogenerators, as shown in figure 35. Among them, *physical modifications* is the most widely adopted approach which includes two means: non-additive modifications and additive modifications. Non-additive physical modifications mainly refer to the morphology engineering of tribo-materials which can increase the effective contact area by introducing surface nanostructures and microstructures. Additive physical modifications can enhance the performance of triboelectric nanogenerators by introducing extra nanomaterials to increase the surface charge density. By using physical modifications, a relative voltage enhancement of >10 times can be realized, indicating that physical modifications are efficient strategies to increase the output performance of triboelectric nanogenerators. Another efficient strategy to improve the performance of triboelectric nanogenerators is *chemical modification*. Chemical modifications involve surface or bulk chemistry to tune the electron-donating or -accepting ability and thus increase the surface charge density. Basically, the most representative chemical modifications are functional chemical groups grafting and ion implanting [220]. Functional chemical groups with a higher possibility to accept or donate electrons can be grifted on the tribo-materials surfaces and change the surface charge density through self-assembled monolayers, wet chemical reaction, etc [221]. In addition, ion implantation can also effectively manipulate the surface charge density through direct ion injection or ion doping [222]. In this way, chemical modifications yield significant enhancement for both output current and voltage of triboelectric nanogenerators and maintain the desired performance for a long time, thereby expanding the available material choices in the triboelectric series to fabricate high-performance triboelectric nanogenerators. Besides these, the modifications involving more than one approach belong to *hybrid modifications*, which can combine the merits of different modification approaches and therefore can demonstrate a higher performance enhancement for triboelectric nanogenerators.

Current and future challenges

Even though efforts and developments have been made to enhance the output performance of triboelectric nanogenerators by introducing modifications at the nanoscale, there are still challenges and opportunities in this research direction. *Firstly,* for non-additive physical modifications, the correlation between the introduced surface nano/microstructure and output performance of triboelectric nanogenerators is not fully understood. Although in previous studies, introducing nano/microstructures to tribo-materials surfaces is thought to be able to improve the performance of triboelectric nanogenerators by increasing the effective contact area, more analysis of different geometric sizes and shapes (i.e. zero-dimensional nanoparticles, one-dimensional nanowires, two-dimensional nanoflakes, and more complex three-dimensional structures) should be performed to summarize a more universal strategy for triboelectric nanogenerator surface structure design. In addition, for additive physical modifications, the theories describing the enhancement effect of additives (e.g. nanoparticles, nanowires, nanoflakes) remain unverified. As summarized in some research, additives can increase the output performance of triboelectric nanogenerators by tuning the dielectric constant, preventing triboelectric loss, forming micro-capacitors, etc [221]. However, the true functions of additives can be more complex than consideration since the enhancement effects of one additive may come from more than one aspect. *Secondly,* for chemical modifications, the durability still needs to be improved in the future. The surfaces treated by chemical modifications, including functional group grafting, ion injection, etc are prone to lose efficacy during mechanical abrasions. Systematic studies on suitable operation modes and pre-prepared methods like post-packing may help to realize robust chemically modified triboelectric nanogenerators. *Last but not least,* comprehensive criteria for triboelectric nanogenerator performance evaluation have not been established yet which means it is still a challenge to directly compare the effectiveness of different modification approaches. Although various performance

Figure 35. Outline of the current modification methods. It generally includes physical, chemical, and hybrid approaches to enhance the performance of triboelectric nanogenerators (TENGs: triboelectric nanogenerators).

metrics, including output voltage, current, power density, etc have been reported in triboelectric nanogenerator modification studies, more comprehensive and scientific evaluation criteria need to be introduced which may take materials durability, cost, and other vital performance enhancement effects into consideration. These challenges coming with opportunities are worth exploring and will give valuable guidance to design efficient and robust triboelectric nanogenerators with high performance in the future.

Advances in science and technology to meet challenges

Significant progress has been made through physical, chemical, and hybrid modification methods to enhance the output performance of triboelectric nanogenerators. Challenges and opportunities coexist in this research direction which is favourable and promising in every triboelectric nanogenerator application from energy harvesting to personalized healthcare. Some perspectives can be proposed and discussed as follow to provide possible inspirations for future studies in this field:

1. *Theoretical guidance*. Theories require further development in order to guide the design of new modification methods. At the current stage, the correlation of nano/microstructures with output performance, the enhancement effect of additive nanomaterials, and the fundamental physics of the charge transfer process in contact electrification are still not fully understood. More calculations and simulations are required to provide a better understanding of both working principles and modification methods for the high-performance design of triboelectric nanogenerators.
2. *New materials introduction*. At present, most of the studies focus on adding various modifications to polymers and metals since they are typical tribo-materials that display excellent triboelectric properties and are indispensable in triboelectric nanogenerator design. However, many possible tribo-materials, i.e. semiconductors, remain largely unexplored. It is expected to see the introduction of more materials and new modification methods to triboelectric nanogenerator design in the future since it will be favourable for the development of multifunctional triboelectric nanogenerators with expanded application fields.
3. *Modification method combinations*. Although many hybrid approaches have been demonstrated in previous research, there are still opportunities in this field. How to wisely choose suitable combinations of various modification approaches that can not only maximize the performance but also create multifunctional triboelectric nanogenerators need further studies.

4. *Biotechniques and biomaterials.* With the rapid development of biotechniques and biomaterials, it will be exciting to see their applications in triboelectric nanogenerator research. For example, genetic engineering has shown its potential to tune the electron-donating ability of silk fibroin which may be helpful for tribo-materials modification. The development and exploration require the efforts of scientists across multidisciplinary fields.

5. *Evaluation criteria.* A unified and comprehensive assessment system of triboelectric nanogenerator modification approaches is urgently needed to evaluate their performance and give guidance to triboelectric nanogenerator design in the future.

Concluding remarks

Nanoscale modifications have been widely adopted to improve the performance of triboelectric nanogenerators, with paramount importance to mechanical-to-electrical energy conversion. Significant progress has been made through physical, chemical, and hybrid modification methods. Challenges and opportunities coexist in these research directions, including theoretical guidance, new materials introduction, modification methods combinations, biotechniques and biomaterials, and evaluation criteria. Therefore, more in-depth studies of nanoscale modifications for triboelectric nanogenerators are desirable and need the synergetic efforts of researchers from different backgrounds such as materials science, chemistry, physics, and engineering. It is hoped that this article can help beginners get familiar with modification methods for triboelectric nanogenerator research and provide possible inspiration for future studies in this field.

Acknowledgments

4.5. Nature-inspired materials for triboelectric energy harvesting

Sontyana Adonijah Graham and Jae Su Yu
Department of Electronics and Information Convergence Engineering, Kyung Hee University, 1732
Deogyeong-daero, Giheung-gu, Yongin-Si, Gyeonggi-do 17104, Republic of Korea

Status
Nature-inspired triboelectric materials are a potential candidate for the design of triboelectric energy harvesters due to their distinguishing characteristics such as triboelectricity, piezoelectricity, biocompatibility, biodegradability, and non-toxicity. However, using synthetic triboelectric materials is difficult to create an eco-friendly environment because they are mostly derivatives of petroleum products/plastic induced components. Thus, they have mostly low degradation ability, high recycling difficulty, poor remodelling ability, and toxicity [223]. Zheng *et al* first time reported a fully biodegradable triboelectric energy harvester, but this was fabricated using a synthetic polymer which is expensive and also may cause potential harm when implanted [224]. For this reason, the fabricated triboelectric energy harvester using nature-inspired triboelectric materials could efficiently reduce the cost and enhance biocompatibility and eco-friendliness. Nature-inspired triboelectric materials have been proven to be applicable in various nanogenerator applications to energy harvesting, medical treatments, self-powered systems, etc [225]. Triboelectric energy harvesters based on nature-inspired materials/hybrid devices can produce high power densities, making them applicable for powering electronic gadgets [223]. Generally, nature-inspired triboelectric materials can be classified into polysaccharides and proteins. Polysaccharides have a long chain of polymeric carbohydrates composed of monosaccharide units bound together by glycosidic linkages. They originate from various natural sources such as plants, algae, animals, bacteria, and fungal. Figure 36(a) shows various nature-inspired triboelectric materials previously reported to be employed in triboelectric energy harvesters [223, 225]. The other sources of nature-inspired triboelectric materials are proteins. Figure 36(b) shows various natural-inspired proteins used in the fabrication of triboelectric energy harvesters [226]. There are five different techniques for the fabrication of triboelectric energy harvesters using naturally-derived bio-materials, which include electrospinning, 3D printing, inkjet printing, spray pyrolysis, and casting. Investigating nature-inspired triboelectric materials to make them sustainable and reliable in triboelectric energy harvesters could promote the next-generation electronics to rely on renewable energy and create eco-friendly surroundings.

Current and future challenges
Compared to synthetic triboelectric materials, nature-inspired triboelectric materials have a great practical engineering application due to their low cost, simple production, high availability, etc. However, using nature-inspired triboelectric materials has a few challenges to be resolved for commercialization. Most of the commonly used triboelectric materials in the fabrication of triboelectric energy harvesters to achieve high performance are plastic products based on petrochemical production. For example, polytetrafluoroethylene, polydimethylsiloxane (PDMS), fluorinated ethylene propylene, and polyvinylidene fluoride (PVDF) have very unique characteristics of high durability, low density, high corrosion resistance, and many more [223]. It is well known that the work function of triboelectric materials is highly important for the electrical performance of triboelectric energy harvesters. However, the work function of nature-inspired triboelectric materials is low when compared to other synthetic materials used in the fabrication of triboelectric energy harvesters (figure 37(a)). This can be enhanced by hybridizing nature-inspired triboelectric materials with other materials [227–229]. Most of nature-inspired triboelectric materials are positively charged triboelectric materials and their electron affinity is also very low. The electrical performance can be enhanced by surface engineering, chemical modification, or combining nature-inspired triboelectric materials with biocompatible polymers (figure 37(b)) [229]. The output power density is considered the general criteria to facilitate the performance comparison among nature-inspired triboelectric materials. Figure 37(c) shows the output power densities of various triboelectric energy harvesters based on nature-inspired materials. The output power densities of most triboelectric energy harvesters based on nature-inspired materials are very low, which makes it very difficult for them to be used to power electronics. However, when nature-inspired triboelectric materials were combined with biocompatible polymers, enhanced electrical output was observed [229]. The currently used nature-inspired triboelectric materials shown in figure 36 lack high durability. Unfortunately, external environment conditions such as temperature and humidity also highly affect the electrical performance of triboelectric energy harvesters based on nature-inspired materials [227].
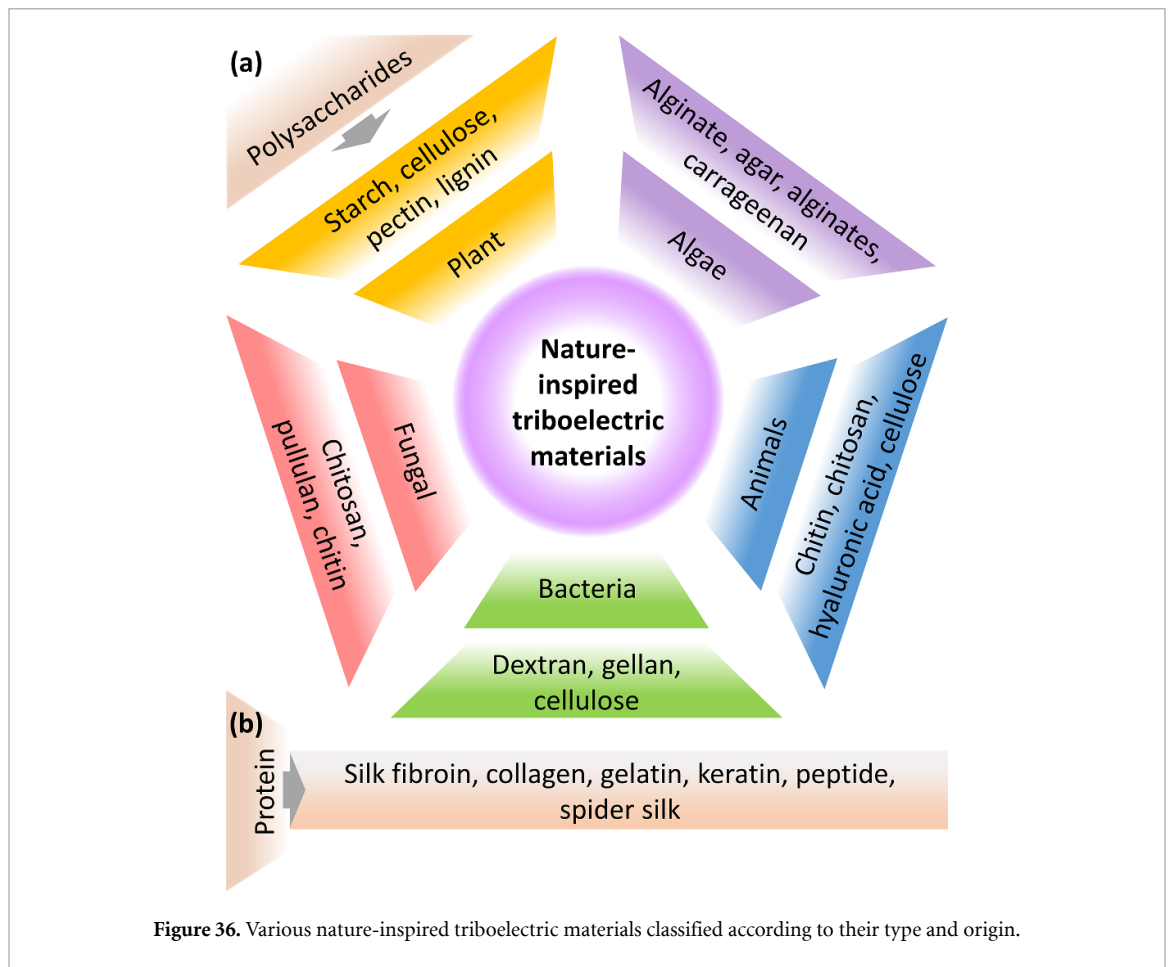
Figure 36. Various nature-inspired triboelectric materials classified according to their type and origin.

As shown in figure 37(d), the electric output of triboelectric energy harvesters further decreases with humidity, so making nature-inspired triboelectric materials or fabricating triboelectric energy harvesters that are sustainable in harsh environments is challenging [230]. Triboelectric energy harvesters can be protected from the environment by various techniques such as fully packing the device, functionalization, surface patterning, or making the film surface hydrophobic. On the other hand, environmental humidity can also be taken as a positive factor via chemical modifications to improve the electrical performance of triboelectric energy harvesters [231].

Advances in science and technology to meet challenges

Triboelectric energy harvesters based on nature-inspired materials have a few challenges that need to be resolved. Although these energy harvesters are made of nature-inspired triboelectric materials, most of their electrodes are made of synthetic materials, thus limiting the fabrication of complete biodegradable devices. Thus, bio-conductive electrodes could be investigated. Compared to the stable electrical performance and output power density of synthetic triboelectric energy harvesters, the performance of triboelectric energy harvesters based on nature-inspired materials is significantly low. This could be resolved by improving the triboelectric material properties and developing novel device fabrication techniques. There is a high potential for nature-inspired triboelectric materials to be applicable in implantable devices for *in-vivo* applications such as sensors and harvesters. However, the current investigations are not sufficient enough to reach the need. The limitations are due to the large size, not sustainability and compatibility. This issue can be overcome by integrating triboelectric energy harvesters based on nature-inspired materials with micro- and nano-electromechanical system technologies. Achieving high sensitivity and accuracy with triboelectric energy harvesters is still challenging, especially in biomedical applications. The slight discrepancy in the value could misdiagnose or misinform the patient's condition, which could be solved by improving the sensing accuracy and response time of triboelectric energy harvesters by modulating the nature-inspired triboelectric materials and the device structures. Since most of the nature-inspired triboelectric materials
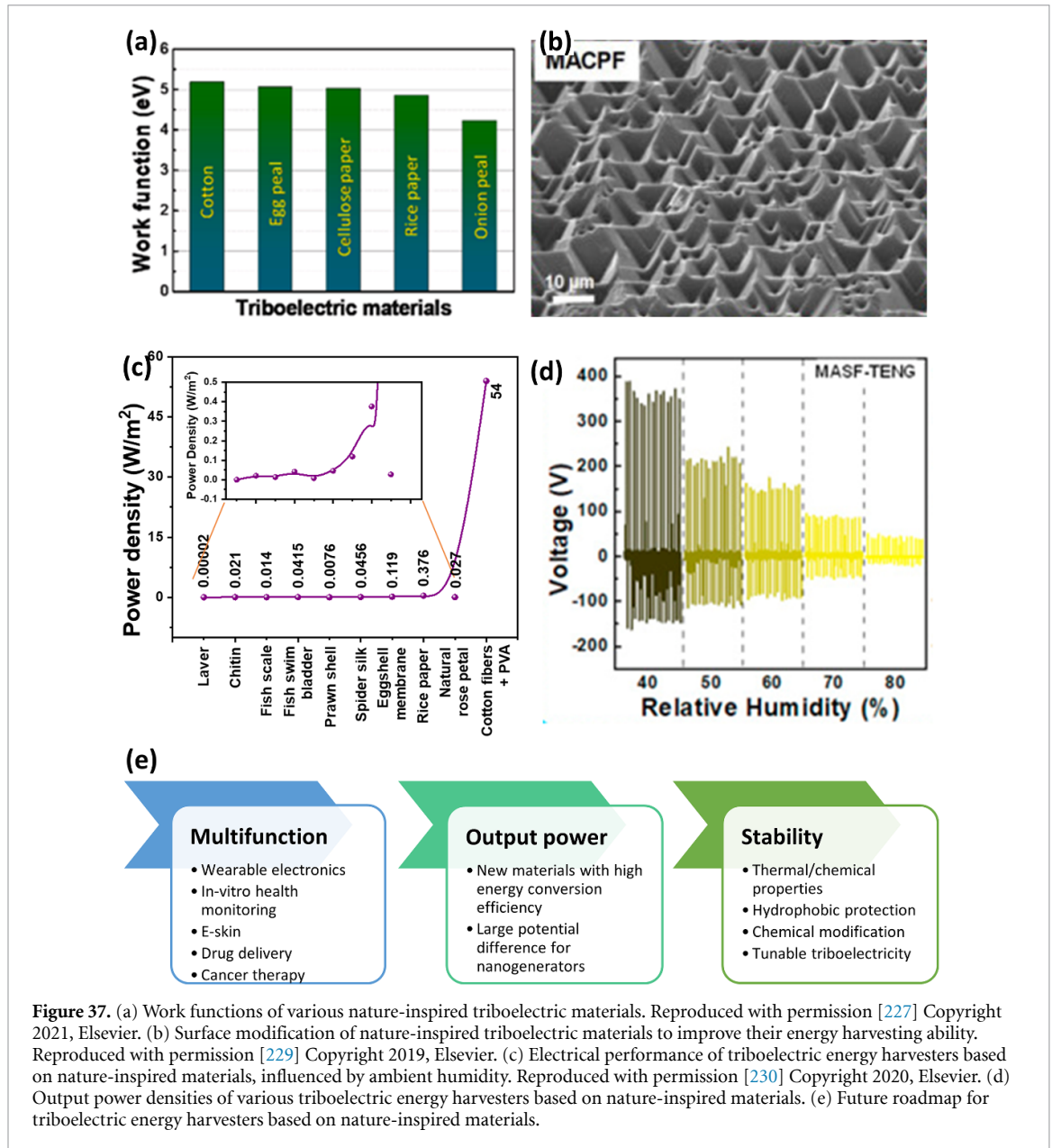
Figure 37. (a) Work functions of various nature-inspired triboelectric materials. Reproduced with permission [227] Copyright 2021, Elsevier. (b) Surface modification of nature-inspired triboelectric materials to improve their energy harvesting ability. Reproduced with permission [229] Copyright 2019, Elsevier. (c) Electrical performance of triboelectric energy harvesters based on nature-inspired materials, influenced by ambient humidity. Reproduced with permission [230] Copyright 2020, Elsevier. (d) Output power densities of various triboelectric energy harvesters based on nature-inspired materials. (e) Future roadmap for triboelectric energy harvesters based on nature-inspired materials.

functioning *in-vivo* or *in-vitro* produce low power, it is very difficult for them to be used in self-powered energy systems. Therefore, low energy consuming circuits can be investigated for integration with triboelectric energy harvesters producing low output power. Many of the biocompatible triboelectric energy harvesters are not fabricated with biocompatible materials [232]. The use of nature-inspired triboelectric materials could resolve this issue because of their non-toxic and biocompatible characteristics. Triboelectric energy harvesters based on nature-inspired materials have a high demand in the field of implantable medical devices for long-term *in-vivo* diagnosis and therapy. These can be applied in various fields including sensors, gastric simulators, cardiac pacemakers, and cardioverter-defibrillators as well as bone, deep brain, and nerve stimulation. The power source of most of the implanted devices has relied on rechargeable batteries, However, the internal heat, capacity loss, and battery failure are a series of problems. Replacing the battery in the implanted devices is also difficult, and efficient triboelectric energy harvesters based on nature-inspired materials could function as a continuous power source. Furthermore, the future roadmap for triboelectric energy harvesters based on nature-inspired materials is shown in figure 37(e) [232].

Concluding remarks

Energy harvesting systems using nature-inspired triboelectric materials that are biocompatible and eco-friendly would provide an advanced technology promoting a clean and sustainable environment.

Triboelectric energy harvesters based on nature-inspired materials have a high potential for mass production because of their eco-friendly feature, low cost, and abundantly available raw materials. Unfortunately, the current research may not be enough to commercialize nature-inspired triboelectric materials for energy harvesting due to the above-mentioned issues. Nevertheless, the incorporation of nature-inspired triboelectric materials in triboelectric energy harvesters could be very useful for eco-friendly energy harvesting systems and also to promote them for powering next-generation electronics. This future roadmap for triboelectric energy harvesters based on nature-inspired materials might provide a deep insight into the field of triboelectric energy harvesting and further benefit various other technologies.

Acknowledgments

## 4.6. MXenes materials for triboelectric energy harvesting

Ling-Zhi Huang, Dan-Dan Li and Ming-Guo Ma
Research Center of Biomass Clean Utilization, College of Materials Science and Technology, Beijing Forestry University, Beijing 100083, People's Republic of China

Triboelectric nanogenerators technology can directly convert irregular and tiny low-frequency mechanical energy in the environment into electrical energy [176]. MXenes are considered to be ideal candidates for triboelectric layers and conductive electrodes in triboelectric nanogenerators due to their high electrical conductivity, hydrophilic surfaces, and abundant surface functional groups (–OH, –O, and –F) [233]. For example, MXene was used as the active material and indium tin oxide (PET-ITO) film as the top electrode in triboelectric nanogenerators [234]. In addition, MXenes can also be used as effective filler together with other triboelectronegative materials such as polyvinylidene fluoride (PVDF), polytetrafluoroethylene (PTFE), and silicone rubber to improve dielectric property. For instance, Bhatta *et al* [235] prepared MXene-PVDF triboelectric nanogenerators with increased dielectric constants and surface charge densities. Moreover, MXenes can be used to replace metals as electrodes in triboelectric nanogenerators due to their high conductivity. Besides $Ti_3C_2T_x$ MXene-based triboelectric nanogenerators, V_2CT_x and Nb_2CT_x MXene were also applied to synthesize triboelectric nanogenerators. MXene-based triboelectric nanogenerators show great application potential in energy collection and self-powered sensors, as shown in figure 38. Combining various advantages of MXenes, triboelectric nanogenerators can be fabricated into lightweight and miniaturized devices to supply power for small electronic and meet the urgent needs of sustainable energy supply. In Cao's work [236], the cellulose nanofibers/MXene liquid electrode-based triboelectric nanogenerators (CM-TENGs) were obtained using elastic silicone rubber as both packaging material and triboelectrification layer. Flexible stretchable triboelectric nanogenerators were achieved using MXene/PVA hydrogels as electrodes [237]. MXene-based triboelectric nanogenerators can be utilized as self-powered tactile sensors to monitor body motions such as wrist, elbow, and finger movement. The self-powered sensors also need high sensitivity and stretchability to meet the requirements of practical applications. A fabric-assisted MXene/silicon nanocomposite friction nanogenerator (DSC-TENG) was developed for self-powered human-motion sensors and wearable electronics [238]. Cao *et al* [239] prepared pressure/strain sensors based on stretchable crumpled MXene-film triboelectric nanogenerators, demonstrating high sensitivity for wireless human motion detection. MXene-based triboelectric nanogenerators have promising applications in the fields of selective NH_3 or NO_2 gas sensor [240], humidity sensing [241], biomechanical sensing, personal thermoregulatory device, intelligent agriculture, etc. All the reports mentioned above indicate the immense potential of MXene-based triboelectric nanogenerators.

Current and future challenges
Although the exploration of MXene-based triboelectric nanogenerators only began about 5 years ago, this is a rapidly expanding field due to the application of MXenes as negative triboelectric materials and their replacement of traditional metal electrodes. Usually, the mechanical energy in the environment is intermittent, resulting in unstable output performance of MXene-based triboelectric nanogenerators, which affects the power supply for small electronic devices. Initially, the interest in MXenes was mainly for energy storage, conductive electrodes, electromagnetic shielding, etc. However, integration with energy storage devices such as supercapacitors is a promising development direction. Thereinto, triboelectric nanogenerators provide a new idea for the next generation of wearable electronic devices by converting the mechanical energy of human motion into electrical energy and storing it in electrochemical devices. However, the application of flexible functional MXene-based triboelectric nanogenerators for athlete health monitoring and auxiliary training has not widely reported yet. Secondly, MXenes usually undergo rapid oxidation/degradation reaction in air and water, mainly forming TiO_2. High stability is a necessary condition for the practical application of MXene-based triboelectric nanogenerators. Therefore, further research could pay more attention to improving the stability of MXene and its composites, so as to bring stable output performance and reliable stability to triboelectric nanogenerators. Moreover, besides $Ti_3C_2T_x$ MXene-based triboelectric nanogenerators, various other types of MXene-based triboelectric nanogenerators should be developed. In addition, fluorinated reagents are inevitably used in the synthesis process. Therefore, there is an urgent need to explore ways to control the morphology and termination groups of MXene and green and fluorine-free synthesis methods in the future. Third, we should carefully explore the stretching strategy for scalable production of wearable MXene-based triboelectric nanogenerators to meet the actual requirements for practical applications in wearable electronic devices. Fourth, self-powered sensors comprising MXene-based triboelectric nanogenerators face complex and diverse application contexts in practice, mainly

Figure 38. Overview of this research update for MXene-based triboelectric nanogenerators (MXene-based TENGs).
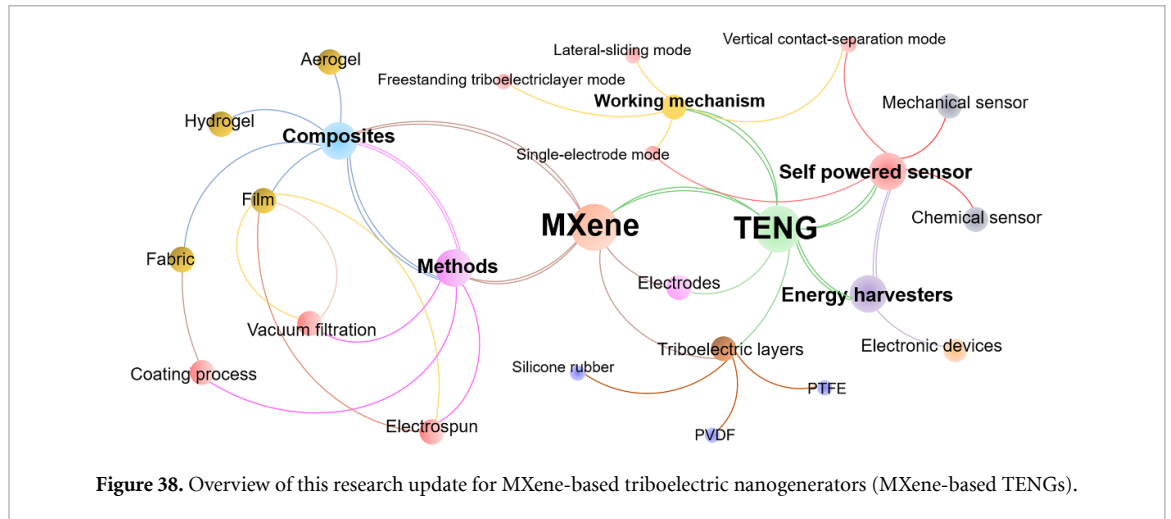
because the complex environment affects the stability of the output performance of triboelectric nanogenerators. For example, the presence of water vapour and temperature driving in the environment will lead to the loss of surface charge on the MXenes triboelectric materials, thus reducing the output performance of the sensors. It is still a great challenge to design wearable MXene-based triboelectric nanogenerators with long-term stability under extreme conditions such as severe cold. The limited stretching degree of composites and slow response to external stimuli greatly limit the practical application of MXene-based triboelectric nanogenerators. Therefore, it is necessary to continue to explore and solve these problems.

Advances in science and technology to meet challenges

So far, more than 30 kinds of MXenes have been synthesized experimentally, showing promising applications in MXene-based triboelectric nanogenerators. For example, a general Lewis acidic etching route was developed to prepare MXenes with enhanced electrochemical performance in non-aqueous electrolytes. MXene-based triboelectric nanogenerators with unique structure and excellent properties can be designed by simulation calculation. *In situ* characterization technologies, such as *in situ* X-ray diffraction, scanning electron microscopy, neutron diffraction, etc, are helpful to understand the change process of MXene-based triboelectric nanogenerators in real time. Theoretical calculation and experimental verification should be used to reveal the interaction mechanism among MXene-based triboelectric nanogenerators. The multi-scale delamination feature is related to the design strategies widely existing in nature, which means the toughening mechanism related to the micro/nano structural features of MXene-based triboelectric nanogenerators. Bionic strategies such as bionic materials, bionic structures, and functional bionics solves the problems by learning from nature. The bellow methods and types may effectively solve the problem that MXene-based triboelectric nanogenerators cannot be stretched. On the one hand, MXenes can be composited with flexible materials such as polydimethylsiloxane (PDMS), elastic silicone rubber, polymer, and biomass to prepare stretchable MXene-based triboelectric nanogenerators. On the other hand, MXene-based triboelectric nanogenerators displayed various types, such as hydrogel, aerogel, fibre, films, paper, and textile. Noteworthy, the construction of special structure (crumpled structure, Kirigami structure, and braided structure, sandwich structure, Janus structure, etc) can also endows the stretchability of brittle materials. Emerging preparation strategies help to obtain MXene-based triboelectric nanogenerators with ideal properties, such as 3D printing or additive manufacturing, spatially confined growth, surface imprinting technology, click chemistry, etc. The composite is a promising route to increase the stability of MXenes with graphene oxide, carbon nanotubes, metal–organic frameworks [240], noble metals, etc. Therefore, the development of appropriate packaging materials and packaging technology is one of the key issues to solve the problem of stability in the near future. MXene-based triboelectric nanogenerators based on scenario can better meet the requirements of practical applications. In view of the complex environmental factors, we suggest that MXene-based triboelectric nanogenerators should be endowed with various specific functions in future research. For example, the environmental stability can be enhanced by introducing the hydrophobicity, flame retardancy, oxygen barrier, and other functions, while the output stability can be improved by introducing the self-healing and charge-storage capacity functions. Up to now, the fundamental performance of MXene-based triboelectric nanogenerators for self-powered sensors was only explored. However, it is unrealistic for the whole IoT to work without any power supply. Therefore, we suggest to

develop a multi-functional self-powered IoT in the future, which can not only sense the stimulation in the external environment, but also obtain energy from the external environment.

Concluding remarks

In summary, MXene-based triboelectric nanogenerators has made a breakthrough in the research of energy collection and self-powered sensor. However, the common synthesis methods of MXenes will make the structure and surface functional groups out of control, further affecting the performance of MXene-based triboelectric nanogenerators. In addition, fluorinated reagents are inevitably used in the synthesis process of MXene-based triboelectric nanogenerators. Therefore, there is an urgent need to explore ways to control the morphology and termination groups of MXenes and green and fluorine-free synthesis methods in the future. Moreover, a major direction in the future is to select appropriate MXene-based triboelectric nanogenerators to obtain self-powered sensors with high sensitivity and wide response range for practical applications in health monitoring, sports monitoring, and wearable devices. In general, MXenes and their composites still have broad research prospects in the field of triboelectric nanogenerators. We believe that MXene-based triboelectric nanogenerators will have promising applications in the near future.

Acknowledgments

4.7. Perovskite-based triboelectric nanogenerators

Jikui Luo
College of Information Science and Electronic Engineering, Zhejiang University, Hangzhou 310027, People's Republic of China

Status

Perovskites, emerging as promising materials for electronic, optoelectronic and energy devices, have attracted considerable interests for the fabrication of triboelectric nanogenerators, because their variety of electronic band structures, crystal formats and tuneable material properties etc (figure 39(a)), and both the inorganic and hybrid organic–inorganic perovskites have been explored [242].

A triboelectric nanogenerator with a stretchable PVDF-copolymer nanofiber mambrane-Ag tribolayer delivered a high open-circuit voltage (V_{oc}) of ∼400 V. The nanofiber composite incorporated with $Cs_3Bi_2Br_9$ nanoparticles was obtained by electrospinning [243]. The perovskite nanoparticles served as efficient electron acceptors and nucleating agents for crystallization.

Inorganic perovskite $CsPbBaBr_3$/PVDF triboelectric nanogenerators showed significant dependence of outputs on the Ba content due to the corresponding variation of properties (figure 39(b)). A V_{oc} of 220 V was achieved with a 0.09% Ba [244]. $CsPbBr_3$ doped with I^- or Cl^- ions was further investigated for use in triboelectric nanogenerators. A V_{oc} of up to 257 V was obtained as displayed in figure 39(c)-(f), which can be attributed to the built-in electric field induced by the spontaneous polarization and alignment of dipoles [245]. However, the outputs are much smaller than expected. Four iron-based lead-free triple perovskites synthesized by sol–gel method were used to fabricate triboelectric nanogenerators paired with Kapton. Despite the very high relative dielectric constants of over 200, outputs of the triboelectric nanogenerators were very small with V_{oc} less than 80 V [246].

Hybrid perovskites ($MAPbI_3$) were utilized to fabricate triboelectric-nanogenerator-driven photodetectors paired with polytetrafluoroethylene (PTFE) and a mesoporous TiO_2 electron-transport layer. This triboelectric nanogenerator showed a V_{oc} of 10 V in dark, and a 11% enhancement in both current and voltage outputs once being exposed to light [247]. By using an ultrathin pentacene layer on top of $MAPbI_3$ as a hole transport layer, the outputs of the triboelectric nanogenerator were improved by 55%–58% [248]. $MA_xPb_{1-x}I_3$ paired with a PA6 or PTFE layer was utilized to fabricate triboelectric nanogenerators, as shown in figure 40(a)-(c). The perovskites showed either positive or negative triboelectric features, depending on the pairing tribomaterial. Polarization and mobile charges in the perovskites would modulate surface charge density significantly, increasing the V_{oc} from ∼550 to ∼780 V (reduced to ∼380 V) when being forward (reverse) polarized, as illustrated in figure 40(d)-(i). Similarly, the V_{oc} could be tuned largely from 380 V to 695 V when the MAI to PbI_2 ratio was changed from 0.4 to 3 due to the change of electron affinity etc [249, 250].
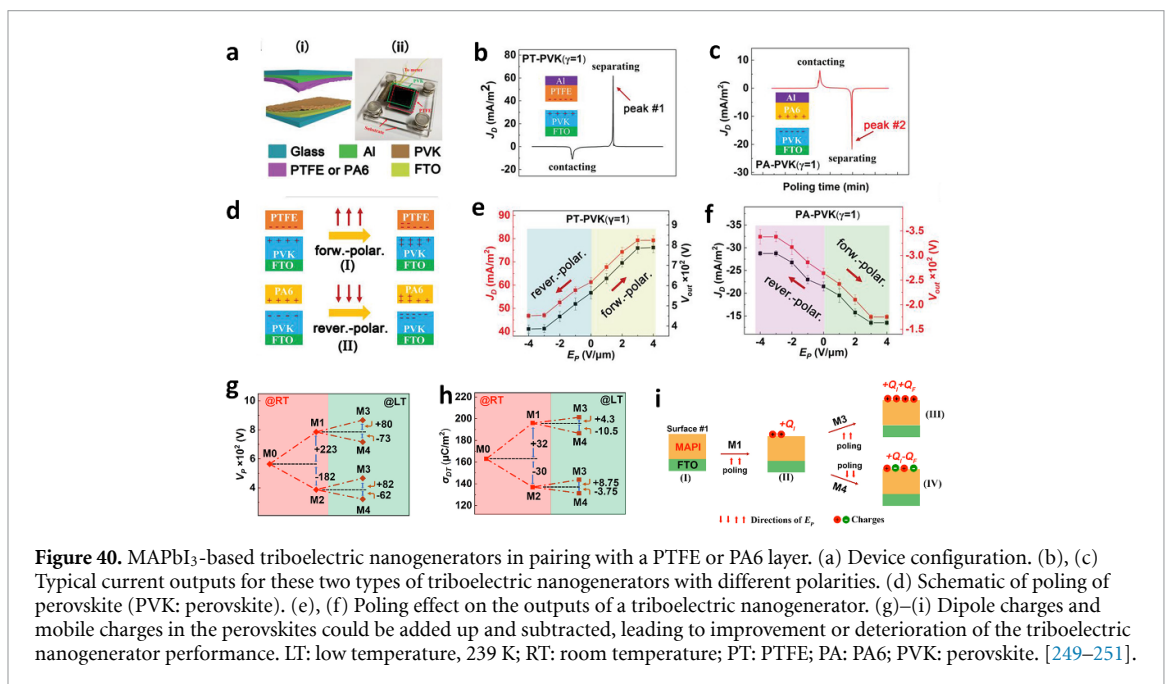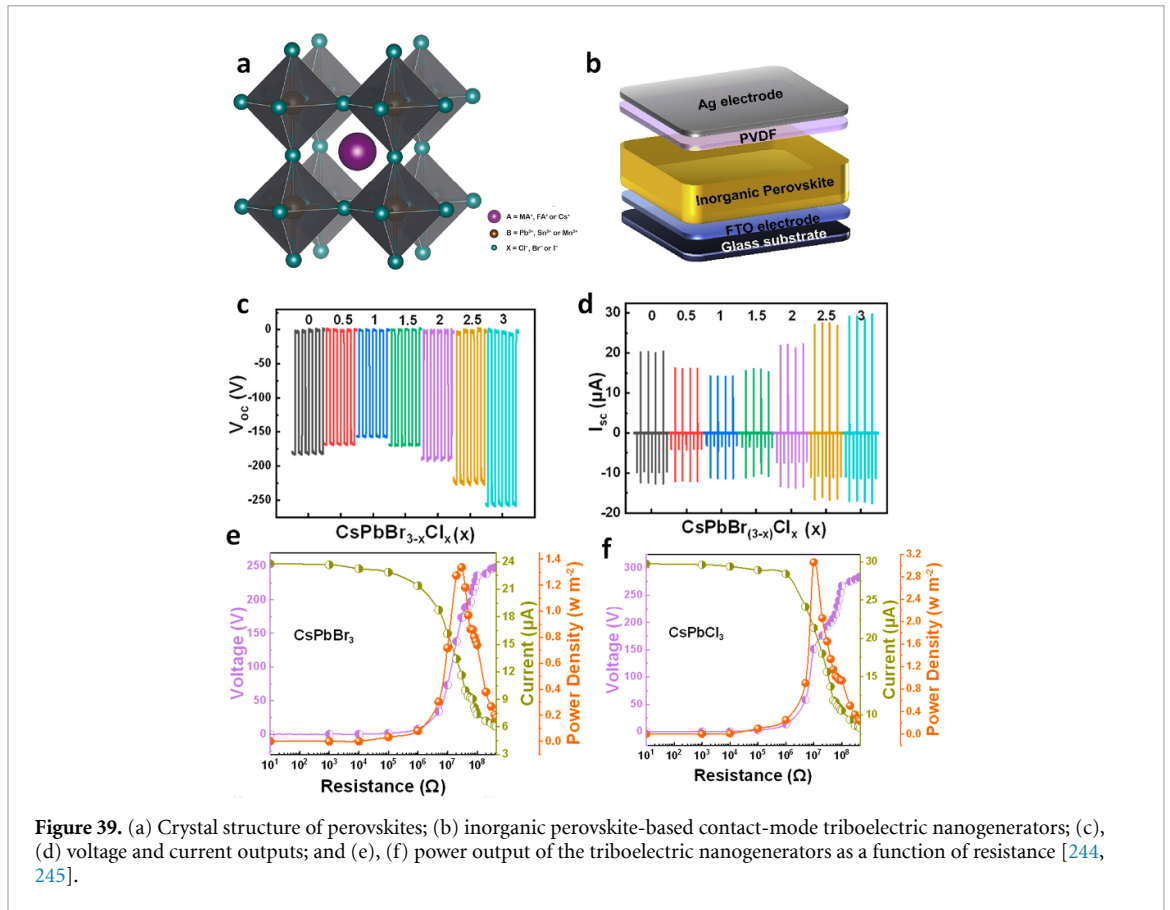
Current and future challenges

The outputs of triboelectric nanogenerators strongly depend on the tribomaterials. Perovskites possessing unique properties are expected to be the promising tribomaterials for triboelectric nanogenerators. However, from the vast types of perovskite materials point of view, the relevant research activities are sparse [242].

Varying composition ratio or percentage of metal ions of a perovskite could distinctly modify conductivity, electron affinity, piezoelectric property etc. These are anticipated to bring extra degrees of freedom to design new types of triboelectric nanogenerators and self-driven sensors, and they are very effective in altering material properties [251]. However, the lack of systematic investigation and fundamental research have inhibited its progress, and most of the research relied on the trial-and-error approach with no theoretical guidance for material and device development.

Perovskites possess excellent optoelectronic properties and have been utilized to fabricated self-powered triboelectric-nanogenerator-type photodetectors. However, the low sensitivity and high dark current are the serious drawbacks for the photodetectors [247]. Theoretically, photogenerated carrier concentrations are orders of magnitudes higher than the tribocharges, but the photo-enhanced triboelectric effect has not yet been clearly observed, requiring a thorough understanding of the mechanism and roles of the electron- and hole-transport layers, and optimal structural design.

Ferroelectricity is known to exist in some perovskites, and remnant polarization is in the range of a few mC cm^{-2} for $MAPbI_3$ [249, 250], which affects the piezoelectric property etc. Also, there are many mobile charges in perovskites. Change of both the dipoles and mobile charges under an electric field could modulate surface electronic state and potential of the perovskites. The challenges are how to generate a high density of these charges and fix them on surfaces, so as to further enhance and stabilize the performance of triboelectric nanogenerators.

Figure 39. (a) Crystal structure of perovskites; (b) inorganic perovskite-based contact-mode triboelectric nanogenerators; (c), (d) voltage and current outputs; and (e), (f) power output of the triboelectric nanogenerators as a function of resistance [244, 245].

Figure 40. MAPbI$_3$-based triboelectric nanogenerators in pairing with a PTFE or PA6 layer. (a) Device configuration. (b), (c) Typical current outputs for these two types of triboelectric nanogenerators with different polarities. (d) Schematic of poling of perovskite (PVK: perovskite). (e), (f) Poling effect on the outputs of a triboelectric nanogenerator. (g)–(i) Dipole charges and mobile charges in the perovskites could be added up and subtracted, leading to improvement or deterioration of the triboelectric nanogenerator performance. LT: low temperature, 239 K; RT: room temperature; PT: PTFE; PA: PA6; PVK: perovskite. [249–251].

Nanocomposites possess a range of excellent properties and have been utilized for fabricating high-performance triboelectric nanogenerators. Similarly, perovskites have a variety of nanostructures; however, their nanocomposites are barely explored for use in triboelectric nanogenerators, not even to mention very poorer performance. Some piezoelectric nanoparticles could assist polarization and crystallization of the piezo-phase of PVDF polymers, which has not been utilized for perovskite tribomaterials yet. The use of perovskite-polymer nanocomposites could boost the mechanical durability of perovskite triboelectric nanogenerators, enabling the development of flexible triboelectric-nanogenerator-driven energy sources and sensors.

Advances in science and technology to meet challenges

Although the application of perovskites has resulted in triboelectric nanogenerators with attractive performance and increased the portfolio of the tribo-series, the results have clearly indicated that the potential for perovskites-based triboelectric nanogenerators is not realized yet. Triboelectric nanogenerator performance largely depends on the electron affinity, surface charge density and permittivity of the tribomaterials. Piezoelectric coefficients are also positively related to both spontaneous polarization and permittivity, thus the piezoelectric and ferroeletric properties of perovskites provide much room for designing materials for high-performance triboelectric nanogenerators. The research on perovskites triboelectric nanogenerators is at the very early stage, and many discoveries and innovations are yet to be made, in terms of new types of perovskites, tribomaterial combinations, new physics phenomenon, novel device structures and applications. The challenges are as follows.

1. To design high-performance triboelectric nanogenerators, it is necessary to understand the fundamentals of perovskites, including electronic structures and dielectrics, piezoelectric and ferroelectric properties etc and their relationships with composition ratios. The first principle methods should be applied to clarify perovskites properties and design tribomaterials with desirable properties for high-performance perovskite-based triboelectric nanogenerators.
2. Perovskites is a material family with rich features, however, only a tiny portion of perovskites, mostly in the forms of thin films, have been studied for triboelectric nanogenerators development. More and systematic experimental investigations are needed to clarify perovskites in terms of electron affinity, band structure, conductivity etc, so that suitable materials could be identified for triboelectric nanogenerators.
3. Novel structural designs towards multifunctionalities with integrated electronic, optoelectronic, and piezoelectric effects are highly desirable for different application scenarios, particularly the self-driven sensors and photodetectors as perovskites have high light absorption coefficient and photoconversion efficiency, and are sensitivity to broad light spectrum. This requires device modelling for the structure optimization.
4. Nanocomposites possess excellent properties such as large effective surface area, tunable properties, high piezoelectric constants etc. Perovskite nanocomposites are hardly explored for triboelectric nanogenerators, thus there are great rooms for exploration and optimization. The material modelling and design approaches should be utilized for this research.
5. Further research could be conducted on lead-free perovskite for eco-friendly and sustainable development by replacing the lead element with other metals or even organic moieties.

Concluding remarks

Perovskites are a family of materials with numerous unique band structures, electronic, optoelectronic, piezoelectric and ferroelectric properties, thus, they could provide a rich source of materials for the exploration in multifunctional and high-performance triboelectric nanogenerators. Although some perovskites have been investigated for the fabrication of triboelectric nanogenerators, it is still at the very early stage, and much is yet to be done. Lack of fundamental understanding of the materials and systematic investigation of material properties are the obstacles that prevent the design of materials and triboelectric nanogenerators with desirable properties and application scenarios. On the other hand, this provides great opportunities for scientists and engineers to make efforts on fundamental theories for materials and devices, material synthesis methods, methodologies for device design and fabrication process. It is highly envisaged that great successes will be made soon in the relevant areas, that contribute to the research community and society markedly.

Acknowledgment

4.8. Towards self-powered woven wearables via triboelectric nanogenerators

Feng Jiang and Pooi See Lee

School of Materials Science and Engineering, Nanyang Technological University, 50 Nanyang Avenue, Singapore 639798, Singapore

Status

Fibres and textiles, serving as promising materials for triboelectric nanogenerators, endow the energy devices with excellent breathability, wearability, stretchability, and comfortability. The mature industrial production and abundant raw material selection also provide the fibre and textile-based triboelectric nanogenerators with a desirable platform for device fabrication and customized design. Compared to the thin film or bulk structures, fibres and textiles have more sophisticated patterns and higher surface roughness, which can further satisfy the functionality and aesthetic requirements of wearable applications with enhanced triboelectric output.

Figure 41(a) shows different forms of fibres and textiles based on their various structural dimensions and fabrication methods [252, 253]. Fibres are the basic building blocks, which can be coiled alone or twisted with other fibres to form yarns. Different yarns can be further processed to construct a hierarchical structure with better mechanical strength. Finally, textiles can be prepared by combining different yarns through woven and knitted methods [253]. The first fibre-based triboelectric nanogenerator was proposed in 2014, which utilized cotton, carbon nanotube, and polytetrafluoroethylene (PTFE) as raw materials to fabricate an entwined structure, conceptually confirming that fibres and textiles can be fabricated into efficient triboelectric nanogenerators [254]. Since then, tremendous efforts have been made to optimize the device structure, output performance, and application scenarios of fibre and textile-based triboelectric nanogenerators [255].

The textile-based triboelectric nanogenerators were not limited to traditional two-dimensional woven and knitted structures. The recently proposed three-dimensional fabric and multilayer stacking structure offered new opportunities for multifunctional integration and structure optimization [255]. Some non-woven methods, such as electrospinning and 3D printing, were also developed to improve the structure and expand the functions of textile-based triboelectric nanogenerators [252]. Apart from the structure design, electrical performance optimization is also significant to the fibre and textile-based triboelectric nanogenerators. Extensive improvement strategies, such as micro/nanopatterned structure design, charge trapping, as well as intermediate layer embedding, have been explored to promote the triboelectric output of the devices [253, 255]. Currently, fibre and textile-based triboelectric nanogenerators have also been widely applied in wearable electronics, self-powered sensors, as well as physiological health monitoring, exhibiting their huge potential in the field of smart textiles and human-machine interface [253].
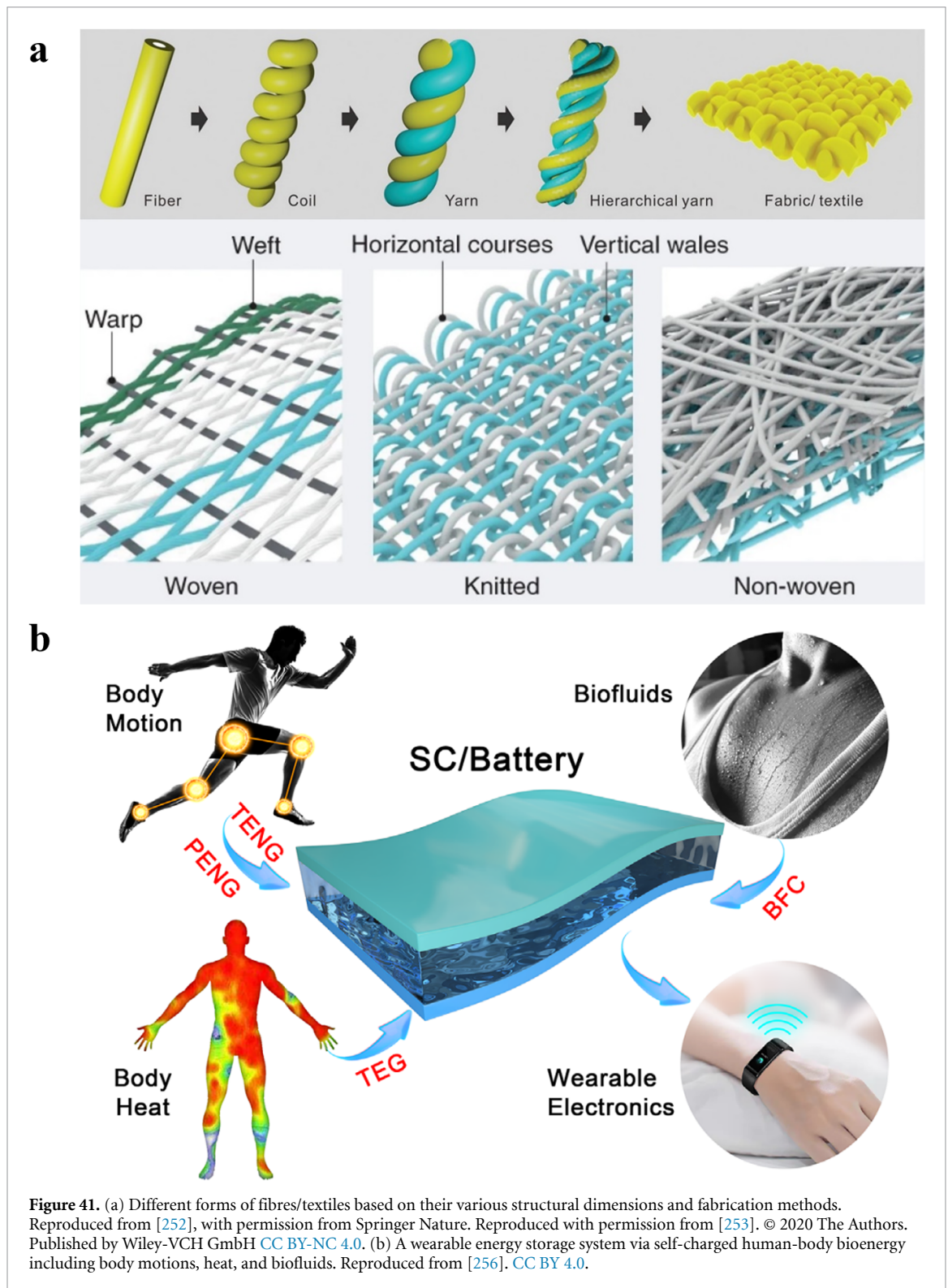
Current and future challenges

Material innovation

Fibre/textile-based triboelectric nanogenerators, despite excellent progress in structure design and performance enhancement, are primarily focused on traditional materials, such as metal, carbon materials, Kapton (polyimide), silicone rubber, PTFE, and polyethylene terephthalate (PET). Although these materials are low-cost and easy to obtain, they are difficult to meet the harsher requirements of multifunctional smart textiles in modern society. Therefore, developing new materials is of significant importance to address the emerging issues, including biocompatibility, washability, waterproofness, self-healing ability, as well as a complex integration of electronic devices. Furthermore, the new materials should also be low-cost, sustainable, eco-friendly, air/moisture permeable, and thermally and mechanically stable, in order to tackle new challenges for the future development of fibre/textile-based triboelectric nanogenerators.

A hybrid and sustainable energy platform

Fibre/textile-based triboelectric nanogenerators are effective technologies that convert mechanical energy into electricity. However, with the growing amount of energy consumption and urgent demands for denser device integration, sole reliance on mechanical energy is not sufficient to satisfy the present power supply. Hence, it is necessary to construct a hybrid and sustainable energy platform that simultaneously collects different forms of energy, such as mechanical, solar, thermal, and biochemical energy. The existing challenges are still centred on how to prepare the hybrid energy devices in the fibre/textile form and efficiently integrate them into one garment without affecting their original breathability and comfortability. An overview of the storage of energy via self-charged human-body bioenergy is shown in figure 41(b) [256].

Figure 41. (a) Different forms of fibres/textiles based on their various structural dimensions and fabrication methods. Reproduced from [252], with permission from Springer Nature. Reproduced with permission from [253]. © 2020 The Authors. Published by Wiley-VCH GmbH CC BY-NC 4.0. (b) A wearable energy storage system via self-charged human-body bioenergy including body motions, heat, and biofluids. Reproduced from [256]. CC BY 4.0.

Mass production

Low-cost and large-scale production of high-performance fibre/textile-based triboelectric nanogenerators is one of the most important goals in this research field. However, most works remain in the laboratory stage. To accelerate the practical applications of smart textiles, more efforts should be made to establish industry standards and develop modular production lines. On one hand, systematic evaluation of device fabrication methods and performance measurements should be determined, serving as guidelines for the future design of fibre/textile-based triboelectric nanogenerators. On the other hand, new equipment and manufacturing methods should also be developed for the mass production of fibre/textile-based triboelectric nanogenerators. Even though traditional textile production is mature and industrialized, some novel

Figure 42. Schematic illustration of a smart textile platform for multiform energy harvesting and storage. Reprinted with permission from [255]. Copyright (2020) American Chemical Society.

processing requirements, such as conductive textile fabrication as well as assembly of conductive and functional textiles, still need further optimization and improvements.

Advances in science and technology to meet challenges

The electric output of fibre/textile-based triboelectric nanogenerators is determined by the intrinsic physicochemical properties, surface roughness or micro/nanopatterns, as well as charge trapping or retention capacity of materials. Surface functionalization/modification via coating or printing is an effective method that bestows textiles with better performance and novel functions. For example, the surface of PET could be more negative and positive by functionalizing it with more fluorinated (electron-accepting elements) and aminated (electron-donating elements) molecules, respectively [218]. Moreover, the waterproofness and charge trapping capacity of fabric could be also enhanced by modifying their surface with functional fillers (e.g. hydrophobic cellulose oleoyl ester nanoparticles for waterproofness improvement and black phosphorus for electron-trapping enhancement) [257]. Therefore, designing new functional materials and combining them with textiles are prospective ways that endow triboelectric nanogenerators with higher output performance and more advantageous properties.

Integrating multiform energy harvesting and storage systems into one fabric is also promising for future smart textiles, allowing users to charge their electronic gadgets such as cell phones and laptops through their garments whenever and wherever they like. An ideal textile platform for multiform energy harvesting and storage is shown in figure 42. Some pioneer works have been done to combine the fibre/textile-based triboelectric nanogenerators with other energy generation and storage devices, including fibre/textile-based solar cells, lithium-ion batteries, as well as supercapacitors [258, 259]. However, these research works are still in the preliminary stage. Some critical challenges, such as high-efficiency power conversion, structural design, and device packaging, still need long-term exploration.

Advanced manufacturing processes are also needed to supplement traditional textile production and tailor to the new era of 5G, the IoT, and artificial intelligence. At present, some preliminary efforts have been made to use 3D printing to directly fabricate porous and fibre-shape triboelectric nanogenerators with high electric output and ultra-high flexibility [260]. These new manufacturing technologies not just make the fabrication process of fibre/textile-based energy devices more efficient and precise, but also provide a new platform for customized designs of smart textiles, bringing unprecedented opportunities and revolutionary progress to the whole textile industry.

Concluding remarks

Overall, much inspiring progress, from structure design and performance optimization to application development, has been made in the field of fibre/textile-based triboelectric nanogenerators. Beyond the structure and performance improvement, more efforts should be focused on material innovation, hybrid energy system construction, multifunctional device integration, as well as the mass production of these fibre/textile-based energy devices. In the future, this emerging field will pave a fresh avenue toward the next-generation wearable electronics and smart textiles. These fibre/textile-based triboelectric nanogenerators are easily combined with other energy technologies mentioned in this roadmap, including photovoltaic, piezoelectric, thermoelectric, and wireless radiofrequency devices, to construct a sustainable, safe, eco-friendly, and hybrid wearable energy system, offering new application scenarios in self-powered sensors, wearable power source, and personal healthcare.

Acknowledgments

4.9. Theoretical investigations towards the materials optimization for triboelectric nanogenerators

Bhaskar Dudem[1], Venkateswaran Vivekananthan[1,2] and S Ravi P Silva[1]

[1] Advanced Technology Institute, Department of Electrical and Electronic Engineering, University of Surrey, Surrey GU2 7XH, United Kingdom
[2] Department of Electronics and Communication Engineering, Koneru Lakshmaiah Education Foundation, Andhra Pradesh, 522302 India

Status

Triboelectric nanogenerators are at the forefront in terms of promising technologies for next-generation energy harvesting to power IoT electronics and self-powered sensing devices. Triboelectric nanogenerators generally work with four different modes, namely contact-separation mode, linear sliding mode, single electrode mode, and free-standing mode. For each different mode, optimizing with the different counter triboelectric materials is key to high performance. Further, multifunctionality aspects such as energy storage, voltage regulation, and power modules can all be integrated with different components and comprise systems engineering of materials to external functionality. These triboelectric nanogenerators have several advantages such as high output generation under low frequency, cost-effectiveness, and simple fabrication techniques. The mechanism of power generation of triboelectric nanogenerators is based on contact electrification and electrostatic induction by the charge separation between the triboelectric contact layers. Therefore, the two counter triboelectric materials in contact are crucial for high performance. So far, triboelectric nanogenerators have been utilized for various applications such as bio-mechanical energy harvesting, water wave energy harvesting, vibration detection, photodetection, human-machine interfacing, chemical sensing, and the IoTs. In each system, specific and unique materials have been used as counter triboelectric surfaces. In addition, triboelectric nanogenerators have been coupled with piezoelectric energy harvesters and electromagnetic generators for boosting the electric output performance as well as coupled with the supercapacitors for extending its application in continuous powering up applications. As triboelectric nanogenerators can be used in a set of wide applications, it is important to understand the underlying mechanism of power generation and material evaluation. In view of a better cost-effective analysis, the design of materials for a high throughput triboelectric nanogenerator is necessary prior to manufacturing. To achieve this, the present section discusses theoretical models such as the parallel-plate capacitor model (*V–Q–x* relationship), distance dependent electric field model (DDEF), and figures of merit as leading concepts together with any specific materials requirements. The parallel-plate model is the most fundamental theoretical model which can be used to simulate the power generation of triboelectric nanogenerators under a planar working configuration. Whereas the non-planar modes and configurations can be simulated using the DDEF models in which the distance dependence is considered rather than uniform all over the space. Figures of merit are introduced to standardize the evaluation of the output performance of triboelectric nanogenerators, which influence the output performance of triboelectric nanogenerators with different parameters analysis. These models contribute towards the theoretical investigations of triboelectric nanogenerators for the better optimization of parameters in triboelectric nanogenerators, which would help boost the electrical output performance of triboelectric nanogenerators towards their utilization in various applications in the future. For each of these scenarios, specific materials would be needed, and the performance optimized based on the active materials in use.

Current and future challenges

The current and future challenges are dependent on boosting the electrical output of triboelectric nanogenerators with accurate figures of merit by the influence of configuring the device parameters. The charges generated in the triboelectric layers move to the metal electrodes and transfer through the external circuit to balance the potential difference [186]. The parallel-plate model can be applied to triboelectric nanogenerators having planar configurations, which can be constructed upon two factors such as (1) the generated charges are distributed evenly on the counter triboelectric materials surface and (2) the electrical field component, which is parallel to the plate, should be neglected and there is one electric field perpendicular to the plate inside the dielectric [263]. In this case, the *V-Q-x* relationship is an important factor for the parallel plate capacitor model of a triboelectric nanogenerator:
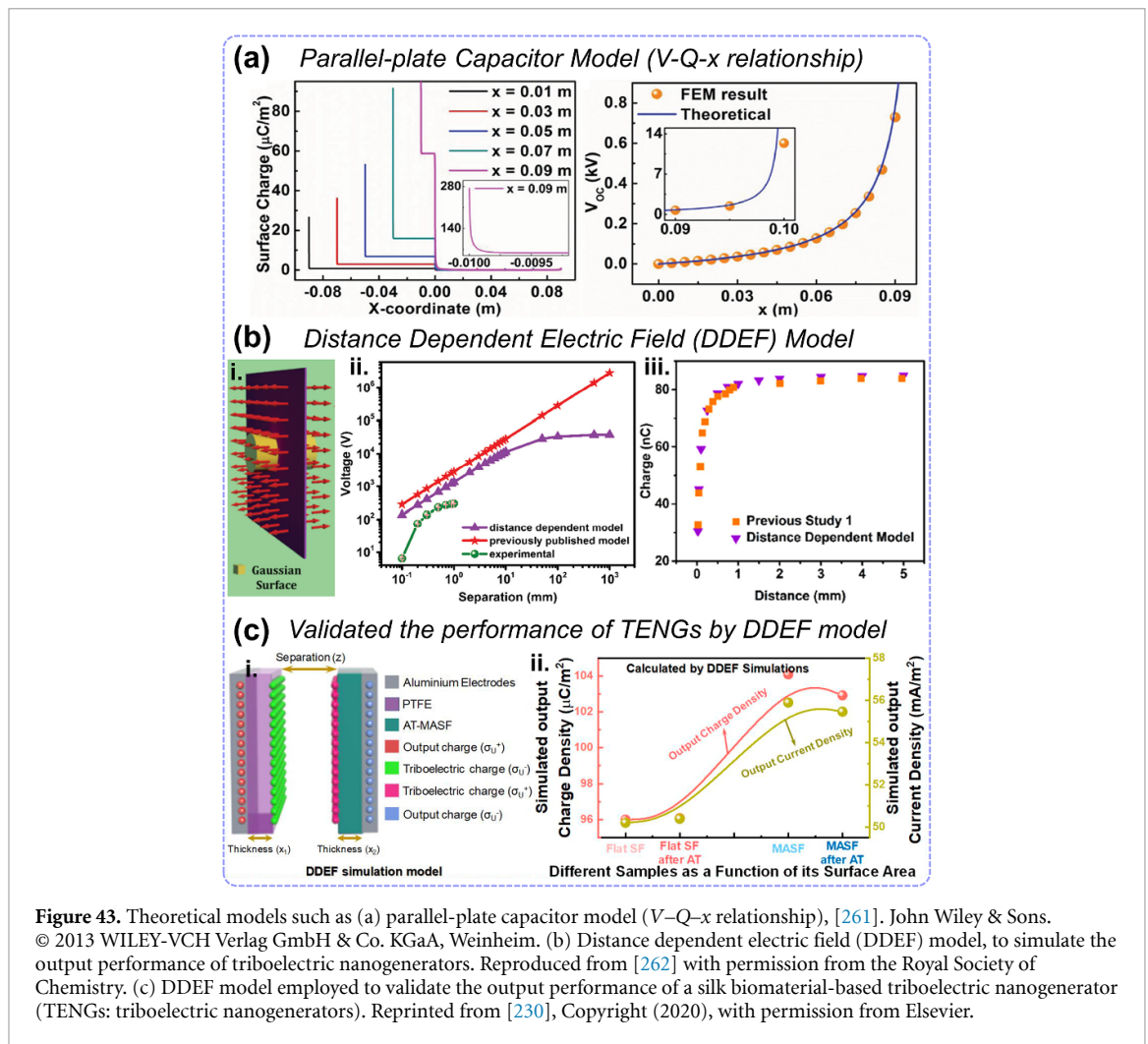
$$V = -\frac{1}{C(x)}Q + V_{OC}(x) \tag{11}$$

Figure 43. Theoretical models such as (a) parallel-plate capacitor model (V–Q–x relationship), [261]. John Wiley & Sons. © 2013 WILEY-VCH Verlag GmbH & Co. KGaA, Weinheim. (b) Distance dependent electric field (DDEF) model, to simulate the output performance of triboelectric nanogenerators. Reproduced from [262] with permission from the Royal Society of Chemistry. (c) DDEF model employed to validate the output performance of a silk biomaterial-based triboelectric nanogenerator (TENGs: triboelectric nanogenerators). Reprinted from [230], Copyright (2020), with permission from Elsevier.

Figure 43(a) shows the dielectric-to-dielectric model sliding mode triboelectric nanogenerator: with the increase of x (lateral separation direction), the open circuit voltage (V_{OC}) between the two electrodes also increases, and the V_{OC}–x curve increases higher when x is approaching l (longitudinal direction). So, the peaks are higher when $x = 9$ cm, which is shown in figure 43(a) indicating that the edge effect is more severe when x approaches to l [261]. Figure 43(b) shows the DDEF model, with figure 43(b-i) showing the electric field distribution perpendicular to an infinitely large, charged sheet which is derived from Gauss's law. Figure 43(b-ii) shows the comparison of prediction with the DDEF model compared with the previous models [262]. The DDEF model is further verified by comparing the electrical response of the metal-dielectric triboelectric nanogenerator reported against the DDEF model shown in figure 43(b-iii) in which the output from both cases agrees with the DDEF predictions. As shown in figure 43(c), the electrical output performance of a typical triboelectric nanogenerator developed through biowaste counter triboelectric materials like silk cocoons was further validated by the DDEF model, where the electrodes responding to the induced charges on the other side of the triboelectric contact surfaces [264, 265]. The validation of performance was analysed with different silk polymers as a function of their surface area by recording the surface charge density and output current [230]. These studies are well matched with the experimental output performance, confirming that the output of triboelectric nanogenerators increases with an increase in triboelectric material's surface roughness owing to the increased surface area.

Advances in science and technology to meet challenges
The challenges may be overcome by adopting proper power transfer equations and parameters in designing triboelectric nanogenerators. The power transfer equation was used to predict the output behaviour of triboelectric nanogenerators under the contact separation working model,

$$K(t)_{eff} = \frac{LW}{G(t)} = \left[\frac{1}{LW\pi} \left(\frac{1}{\varepsilon_a} + \frac{1}{\varepsilon_b} \right) \int_0^y f(x)\, dx \right]^{-1} \tag{12}$$
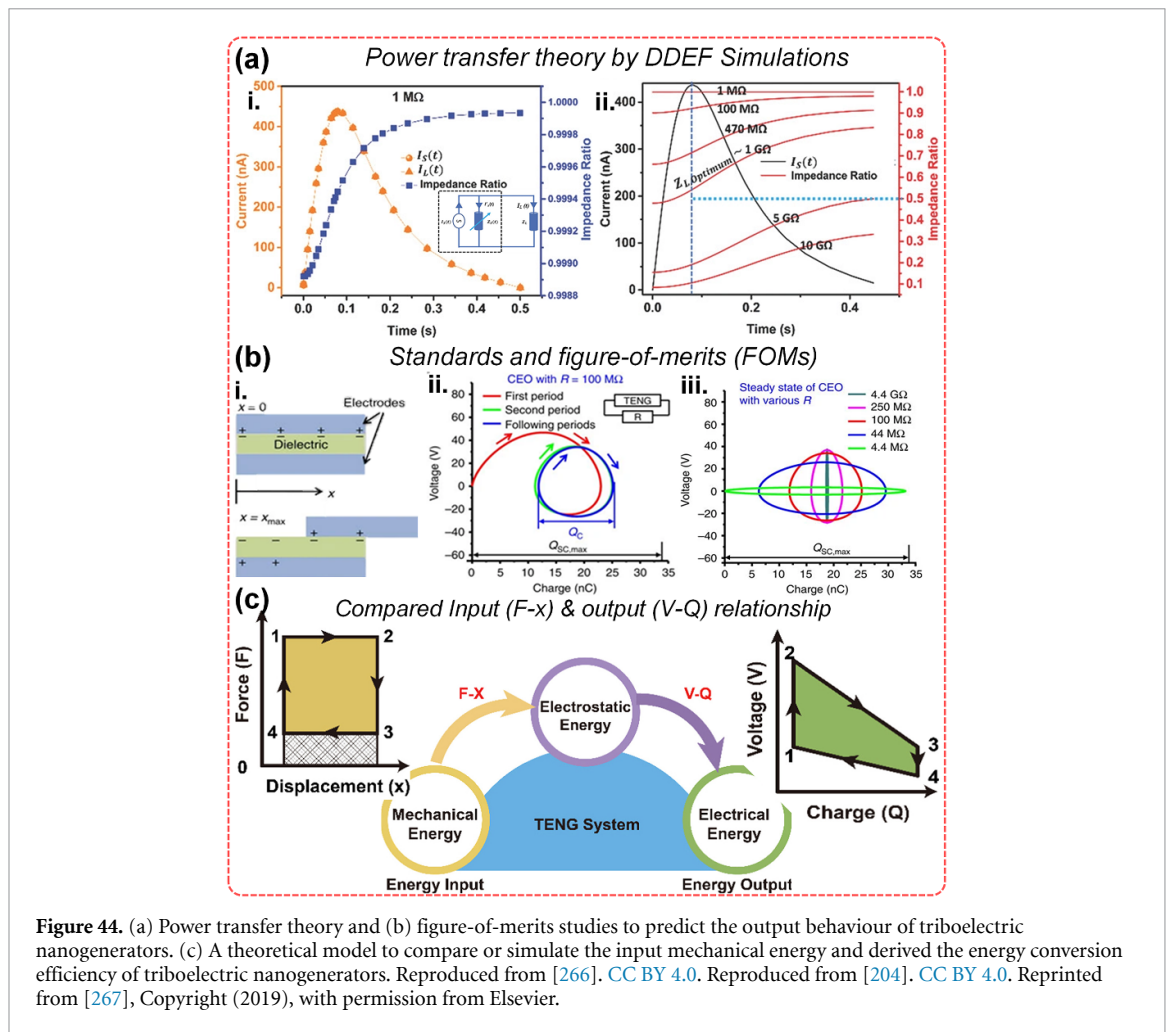
Figure 44. (a) Power transfer theory and (b) figure-of-merits studies to predict the output behaviour of triboelectric nanogenerators. (c) A theoretical model to compare or simulate the input mechanical energy and derived the energy conversion efficiency of triboelectric nanogenerators. Reproduced from [266]. CC BY 4.0. Reproduced from [204]. CC BY 4.0. Reprinted from [267], Copyright (2019), with permission from Elsevier.

The accuracy of the triboelectric nanogenerator power transfer equation was evaluated by comparing the output predictions with the DDEF model, and by directly solving the power transfer equation. Figure 44(a-i) describes the parameters of triboelectric nanogenerators in the power transfer equation [266]. Changing the load resistance causes the impedance ratio to vary and as a result the output current changes according to the change in load resistance, which is predicted in the power transfer theorem shown in figure 44(a-ii).

Another challenge is quantifying the output performance of triboelectric nanogenerators by adopting proper figures of merit. The figures of merit are usually comprised of structural and material figures of merit, the corresponding method is described in figure 44(b). Consider a linear-sliding-mode triboelectric nanogenerator in which both the absolute short-circuit transferred charges $Q_{SC}(x)$ and the absolute open-circuit voltage $V_{OC}(x)$ at $x = 0$ position are set to be 0. The definitions of the displacement x and the two electrodes for a linear-sliding-mode triboelectric nanogenerator are illustrated in figure 44(b-i). The maxima of $Q_{SC,\max}$ and $V_{OC,\max}$ are expected to be reached at $x = x_{\max}$ for these basic-mode triboelectric nanogenerators. From the V–Q plot, we noticed that the operation of the triboelectric nanogenerator will go to its steady state after only a few periods as shown in figure 44(b-ii), and thus we can directly focus on the output of the steady-state operation [204]. In figure 44(b-iii) we noticed that for each 'cycles for energy output' (CEO), the total cycling charge Q_C was always less than the maximum transferred charges $Q_{SC,\max}$, especially for cycles with large external load resistances. If we could maximize the Q_C to be $Q_{SC,\max}$ for these cycles, the output energy per cycle would be further enhanced. Figure 44(c) shows the force–displacement (F–x) plot and voltage–charge (V–Q) plot in triboelectric nanogenerators with maximum energy output under infinite resistance [267]. The encircled area in the F–x plot equals the mechanical energy input per cycle.

Concluding remarks

In summary, the present section briefly introduces the distinct theoretical models. These models are a guide to the optimization of materials and their structural features, fabrication processes, and experimental analysis of triboelectric nanogenerators, which could further be proposed for successful commercialization.

The parallel-plate capacitor and DDEF models suggest the use in the simulation of planar and non-planar materials-based triboelectric nanogenerators. The power transfer theory with DDEF models suggests the consideration of the impedance of the device and edge effects on counter materials to solve the problems in triboelectric nanogenerator design. In addition, the influence of triboelectric material's surface roughness in improving the electrical performance of triboelectric nanogenerators is studied through DDEF and materials figures of merit. Supplementing to energy harvesting, triboelectric nanogenerators have a great potential to use in self-powered sensing and IoT applications, which warrants development in theories of working.

Acknowledgments

5. Materials for thermoelectric energy harvesting

5.1. Introduction on materials for thermoelectric energy harvesting

Mercouri G Kanatzidis and Hongyao Xie
Department of Chemistry, Northwestern University, Evanston, IL 60208, United States of America

In the past few decades, the realization has set in that over 65 % of the energy we generate is wasted in the form of heat and low-cost effective technologies to reduce the losses are desired [268–270]. Thermoelectric materials offer an attractive solution for directly converting thermal energy into electrical power. If they can be successfully employed on a broad scale in waste heat harvesting, they will improve the efficiency of fossil fuel utilization. Moreover, thermoelectric materials can be used to sustainably charge portable/wearable electronics based on the temperature differences found indoors or between the human body and the ambient environment.

A thermoelectric device is a fully solid-state electronic device that can generate electricity from a hot source using the Seebeck effect. Vice versa, electricity can drive a thermoelectric device in reverse to work as a solid-state heat pump for refrigeration through the Peltier effect [271]. Thermoelectric devices are free of moving parts, run quietly, and can have excellent reliability and scalability in size and power. These advantages make it compatible with other energy-conversion technologies [270].

A typical device utilizing this effect is shown in figure 45(a). It is composed of one pair of n- and p-type thermoelectric materials. When a temperature gradient is applied across a material, the free charge carriers on the hot side absorb energy and tend to diffuse to the cold side. This migration of charge carriers builds up a net charge at the cold side until an equilibrium is reached between the diffusion potential and the electrostatic repulsion caused by the build-up of charge. Thus, an electric potential difference is produced between the hot side and cold side of the material. The performance of thermoelectric materials is defined by the dimensionless figure of merit $ZT = S^2 \sigma T/\kappa$, where S is the Seebeck coefficient, σ is the electrical conductivity, T is the specific operating temperature and κ is the thermal conductivity [272]. The maximum power conversion efficiency/ZT relationship is shown in equation (13). The maximum power conversion efficiency of a thermoelectric device depends on the temperature difference between the hot source (T_h) and the cold source (T_c), as well as the performance of the materials as follows [273]:

$$\eta = \left(\frac{T_h - T_c}{T_h} \right) \left[\frac{\sqrt{1 + ZT_m} - 1}{\sqrt{1 + ZT_m} + (T_c/T_h)} \right]. \tag{13}$$

Here the ratio of the temperature difference between the hot end and the cold end to T_h is the Carnot efficiency, and the ZT_m is the average ZT value between T_h and T_c. Thus, in practical applications, a large ZT averaged over a wide temperature range is more pragmatic than a high maximum ZT at a narrow temperature range. To make thermoelectrics competitive with other energy generation technologies, an average ZT value of ∼3–4 is needed [269]. If they are achieved, game-changing conversion efficiencies near 30% or more could be possible. However, although the maximum ZT values of 3.0 have been reached in such materials as SnSe [274], the average ZT for most advanced thermoelectrics materials is below 1.0 and the record-high value is about 1.7 in recent reports (figure 45(c)) [275].

Improving the ZT value of materials is the key to the application of thermoelectrics. Based on the ZT expression, it is obvious that good thermoelectric materials should have a large Seebeck coefficient (S), high electrical conductivity (σ), and poor thermal conductivity (κ). The actual scientific challenge is that these transport properties are strongly interdependent through the carrier concentration (n) and the carrier effective mass (m^*), and maximizing one transport parameter would inevitably lead to the diminishing of the others [273]. On the other hand, the total thermal conductivity is generally composed of the lattice part (κ_l) and the electronic part (κ_e) as $\kappa = \kappa_l + \kappa_e$, and increasing the σ would also unavoidably leads to an increase in the κ_e [273]. Thus, the strong correlation between the heat and electronic transport properties makes the optimization of the average ZT challenging. The key to achieving high ZT values must be a synergistic optimization of these transport properties by tuning the carrier concentration to an optimized value, see figure 45(b).

In the past two decades, tremendous progress has been made in understanding how to increase ZT leading to many promising materials, with ZT values exceeding 2, figure 45(c) [268]. The most successful strategies in improving performance have been those that minimize thermal conductivity. The most well-known is the formation of *in-situ* nanostructured inclusions, figure 45(g) [276]. This was first demonstrated in the lead chalcogenide and then has been widely employed in many other material systems as a universally valid method. Since then, other important strategies have also been proposed to optimize the
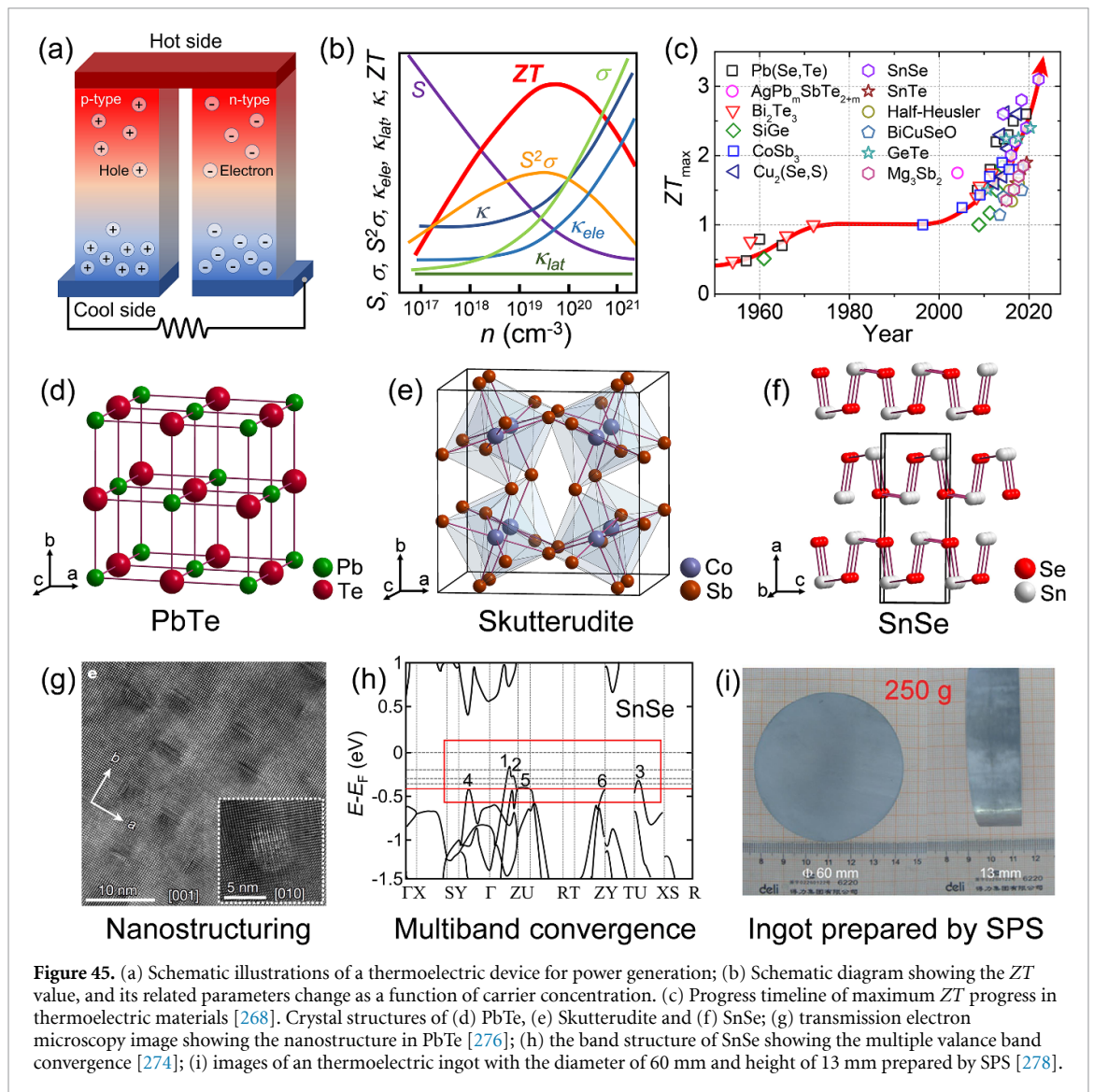
Figure 45. (a) Schematic illustrations of a thermoelectric device for power generation; (b) Schematic diagram showing the *ZT* value, and its related parameters change as a function of carrier concentration. (c) Progress timeline of maximum *ZT* progress in thermoelectric materials [268]. Crystal structures of (d) PbTe, (e) Skutterudite and (f) SnSe; (g) transmission electron microscopy image showing the nanostructure in PbTe [276]; (h) the band structure of SnSe showing the multiple valance band convergence [274]; (i) images of an thermoelectric ingot with the diameter of 60 mm and height of 13 mm prepared by SPS [278].

thermal conductivity for several specific materials, such as the rattling atom filling, liquid-like lattice, weak chemical bonding, and recently, the discordant atom doping [270, 277]. Moreover, exploiting new materials with intrinsic low thermal conductivity is always an important research area for thermoelectrics.

For electronic property optimization, the most successful concept in the past decades could be the presence of several electronic bands of the same carrier type near the Fermi energy, also known as multiband convergence. When all these bands host multiple carrier pockets that participate in the electronic transport (figure 45(h)), they can enhance the Seebeck coefficient and the electrical conductivity [269]. This band convergence strategy has been widely implemented to achieve high performance, including in PbTe, PbSe and PbS, $Mg_2(SiSn)$, SnSe, $CoSb_3$, and GeTe to name but a few examples (see figure 45(d)–(f) for representative crystal structures) [269].

Among these compounds, PbTe is an outstanding mid-temperature range thermoelectric material in the past decades. Because of its unique electronic band structure and the successful application of nanostructuring strategy, PbTe exhibits a very high thermoelectric performance in both p-type ($ZT > 2.6$) and n-type ($ZT > 2$) forms [268]. On the other hand, the world record of *ZT* has recently been pushed to 3.1 by the SnSe compound. Because of the intrinsic ultralow thermal conductivity and the multiple electronic band structure. The maximum *ZT* value of $\sim$3.0 has been obtained in both p-type and n-type SnSe, raising expectations for SnSe-based thermoelectric devices in the near future [268].

However, to further broaden the application of thermoelectric energy harvesting and make it a more competitive technology, future research should not simply focus on improving the maximum *ZT* of the material. Other important challenges that must be addressed are improving the average *ZT* of the materials, enhancing their mechanical strength and thermal stability, raising their toughness and fracture strength,

exploring the approach for large-scale and high-quality material production (figure 45(i)), as well as developing the new device structure and fabrication techniques [268].

Acknowledgments

5.2. Chalcogenides for thermoelectric energy harvesting

Xiao-Lei Shi and Zhi-Gang Chen
School of Chemistry and Physics, Queensland University of Technology, Brisbane, QLD 4000, Australia

Status

Chalcogenide-based thermoelectric materials are important members of the thermoelectric family. Conventional thermoelectric chalcogenides such as $Bi_2Te_{3-x}Se_x$, $Bi_{2-x}Sb_xTe_3$, and PbTe, have been widely applied in thermoelectric devices for various purposes such as commercial thermoelectric modules and radioisotope thermoelectric generators [279]. In the last few years, a few thermoelectric chalcogenides with high experimental *ZT* values of >1.5, including SnX, Cu_2X, Ag_2X, ZnX, $In_\delta X$, and GeX, have been considerably developed (X = S, Se, Te). Especially, some chalcogenides have exhibited outstanding *ZT*s of >2 (figure 46) or even reached *ZT* > 3 [275, 280]. For example, GeTe is a promising material with high *ZT*s of >2 within a wide temperature range from 500 K to 800 K, and the reported GeTe-based single-leg device showed a high η of 14% [281]. Cu_2Se is one of the most cost-effective thermoelectric materials with high *ZT* of up to 2.7 [282], and the reported prototype Cu_2Se-based thermoelectric device showed a η of 9.1% [283], indicating great potential for practical applications. High-entropy alloys based on chalcogenides are also rapid developed with potentially high *ZT*s [284].

Current and future challenges

The supreme thermoelectric performance of advanced chalcogenides is mainly derived from their manipulable band structures with relatively narrow bandgaps, which are important to achieve high electrical conductivity and Seebeck coefficient. As well, chalcogenides usually exhibit relatively low thermal conductivity due to their unique crystal structures. However, despite their high *ZT*s, there is still a huge gap in employing them in practical devices for commercial use. The current and future challenges mainly include: (i) low mechanical properties. Compared to other thermoelectric materials such as skutterudites, oxides, half Heuslers, and silicides, chalcogenides usually exhibit relatively low mechanical properties due to their relatively weak bonding between metal cations and chalcogenide anions [279]. Considering that mechanical robust thermoelectric materials are significant for ensuring performance stability during device service, their mechanical properties must be further improved; (ii) high cost. A few high-performing thermoelectric chalcogenides such as GeTe possess high costs derived from the expensive Ge that limits its future applications, therefore some alternatives need to be developed to reduce the cost but keep the high performance; (iii) relatively low stability. Some chalcogenides such as Cu_2Se and SnSe are not stable at very high temperatures because selenium is easily volatile, which limits their applications. Phase transition engineering should be a good resolution, but still needs a long-time attempt; (iv) difficulties in applying these advanced chalcogenides into devices. Designing a useful thermoelectric device with both high performance and stability is tricky due to the coupled factors such as topology, structural optimization, electrode material selection, interlayer, n/p-materials pairing, filling material, and the reduction of internal thermal/electrical resistance. Such a device design is especially challenging when using newly developed chalcogenides because most of the above factors need to be re-adapted to exert the high thermoelectric properties of advanced chalcogenides. For example, it is difficult to pair p-type GeTe and Cu_2Se with suitable n-type legs in the devices because it is considerably difficult to realize n-type GeTe and Cu_2Se with similar *ZT*s to their p-type counterparts. Therefore, considering the discussed challenges, developing practical thermoelectric devices composed of newly developed advanced chalcogenides is still a long way to go.

Advances in science and technology to meet challenges

To achieve the goal of developing high-performance, cost-effective, and mechanically robust thermoelectric chalcogenides and related devices, there are many advances in science and technology to meet the challenges discussed above, as summarized below and in figure 47:

1. Further improving the thermoelectric performance of chalcogenides to enhance the performance of their devices. Various band manipulation approaches such as alloying and doping with secondary elements/compounds can be applied to enhance the power factors by tuning appropriate electrical transport properties [285], and structure engineering can be used to strengthen the multi-wavelength phonon scattering and in turn, suppress the thermal conductivity [277]. Computational methods such as modelling and first-principles have been employed to design thermoelectric chalcogenides with promising *ZT*s or guide the improvement of current thermoelectric chalcogenides [286].
2. Boosting the mechanical properties as well as the stability of advanced chalcogenides to enhance the practical application values of their devices. As discussed above, phase transition engineering by doping
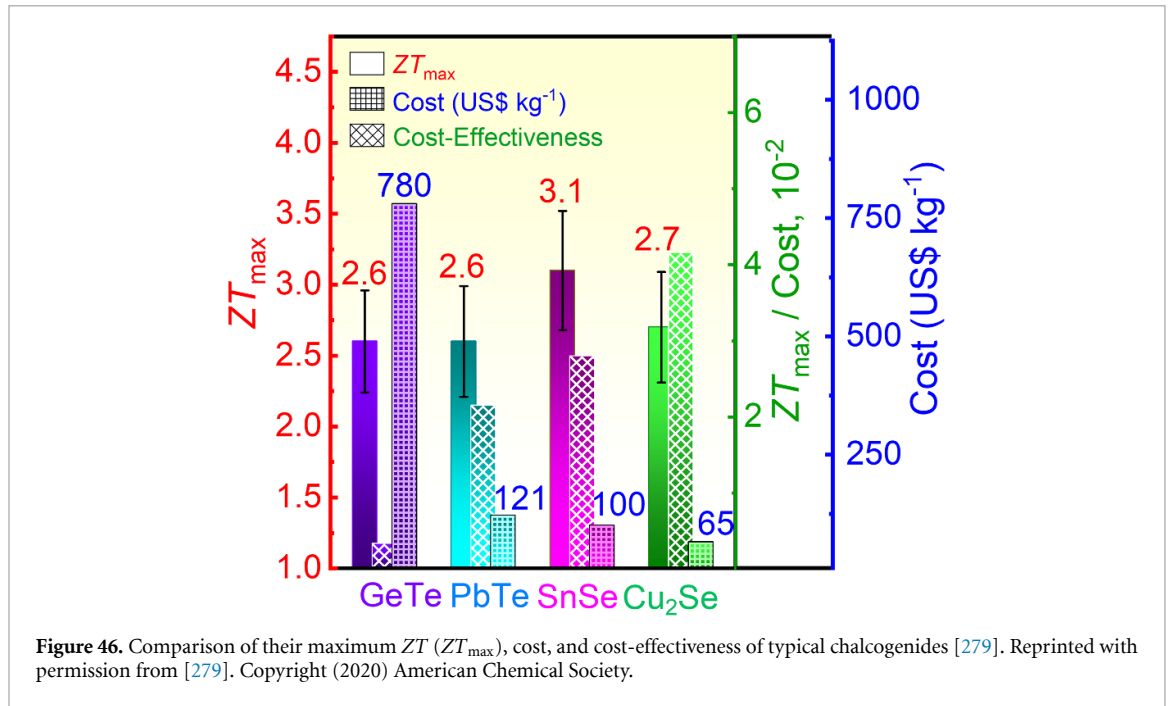
Figure 46. Comparison of their maximum *ZT* (ZT_{max}), cost, and cost-effectiveness of typical chalcogenides [279]. Reprinted with permission from [279]. Copyright (2020) American Chemical Society.
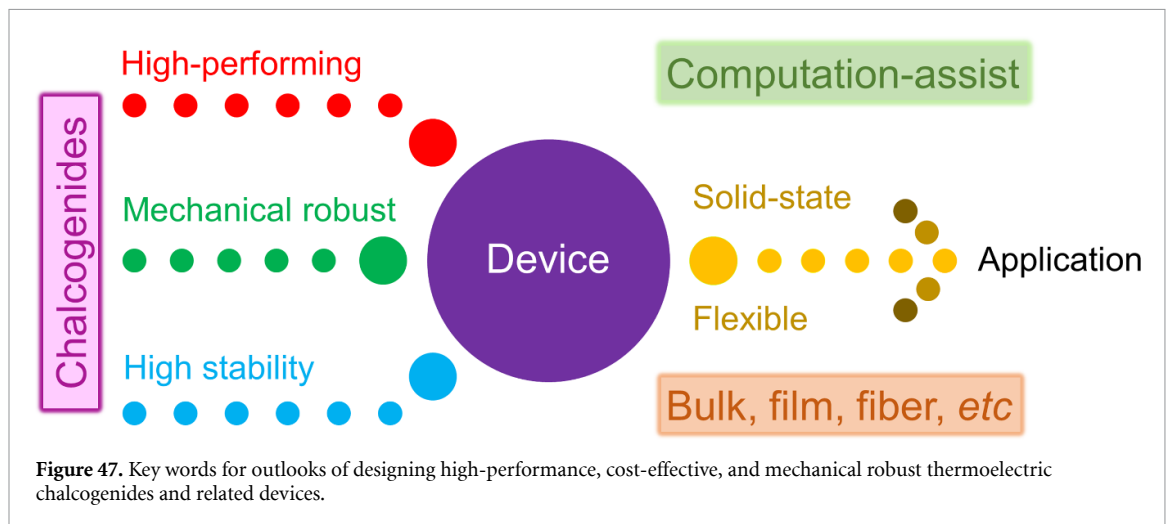

Figure 47. Key words for outlooks of designing high-performance, cost-effective, and mechanical robust thermoelectric chalcogenides and related devices.

or alloying is a good resolution to tackle the stability issue, while the routes to further improve the mechanical properties of chalcogenides can be referred to the strengthening mechanisms of conventional alloys, such as grain refinement, vacancy-induced dispersion hardening, and alloying with carbon nanotubes to strengthen the adjacent grain bonding like steel-reinforced concretes [279].

3. Rationally designing chalcogenides-based thermoelectric devices with both high performance and stability to meet the requirement of practical applications. Such a design needs to satisfy many coupled factors, including topological structures, electrode materials, transition layers, n/p-chalcogenides pairing, fillers, and stability test methods. Fortunately, mature commercial thermoelectric devices composed of conventional chalcogenides such as Bi_2Te_3 can provide enough valuable experience to design the new-generation chalcogenides-based thermoelectric devices, while the rapid developed computational assist tools such as ANSYS can also help guide the device designs in terms of the electrical/thermal transport.

4. Broadening the types of chalcogenides-based thermoelectric devices for various application scenarios. In addition to conventional solid-state thermoelectric devices, high-performing chalcogenides can be developed to fabricate miniature or flexible/wearable thermoelectric devices, which target various application scenarios such as sustainably charging low-grade wearable electronics, or realize solid-state localized chip thermal management.

Concluding remarks

Up to now, the performance of conventional thermoelectric chalcogenides has been considerably improved, while many advanced chalcogenides with significant thermoelectric potential have been newly found and developed, both benefited from the advanced strategies based on electronic band engineering and structural manipulation theories. Although there are still many issues that impede the practical appellations of these advanced chalcogenides in devices such as stability, mechanical property, and high cost, most of these challenges are expected to be resolved soon based on the already established knowledge and experience in device engineering as well as the continuously developed techniques from physics, chemistry, engineering, computer science, and data science.

Acknowledgments

5.3. Full Heuslers for thermoelectric energy harvesting

Alexander Riss, Michael Parzer, Fabian Garmroudi and Ernst Bauer
Institute of Solid-State Physics, TU Wien, A-1040 Wien, Austria

Status

In 1905, Friedrich Heusler submitted a manuscript entitled '*Über magnetische Manganlegierungen*', where he first demonstrated that three non-magnetic elements (Cu, Mn, Al) form a ferromagnetic material in the X_2YZ stoichiometry [287]. Since then, thousands of cubic X_2YZ full-Heusler and XYZ half-Heusler compounds have been found, as their unique and simple crystal structure allows to host a large range of elements from the periodic table. As a result, Heusler compounds represent a material class which exhibits a multitude of interesting physical phenomena and tunable properties, such as band topology, half-metallicity, superconductivity or thermoelectricity. It was demonstrated that for both full-Heusler and half-Heusler compounds, the electronic properties are strongly dependent on the valence electron concentration n_V. The Slater–Pauling rule states that Heusler compounds with $n_V = 6$ are non-magnetic semiconductors. Following this rule, many half-Heusler semiconductors were identified, with gap sizes up to several eV, making them excellent candidates for thermoelectric explorations, whereas full-Heusler compounds have been mostly studied with respect to their peculiar magnetic properties and half-metallicity [288]. Previously, however, the discoveries of a giant anomalous Nernst effect in several full-Heusler compounds sparked enormous interest [289]. While numerous full-Heusler semiconductors with excellent thermoelectric performance have been predicted theoretically, experiments so far identified only semi-metallic Fe_2VAl as a potential thermoelectric material.
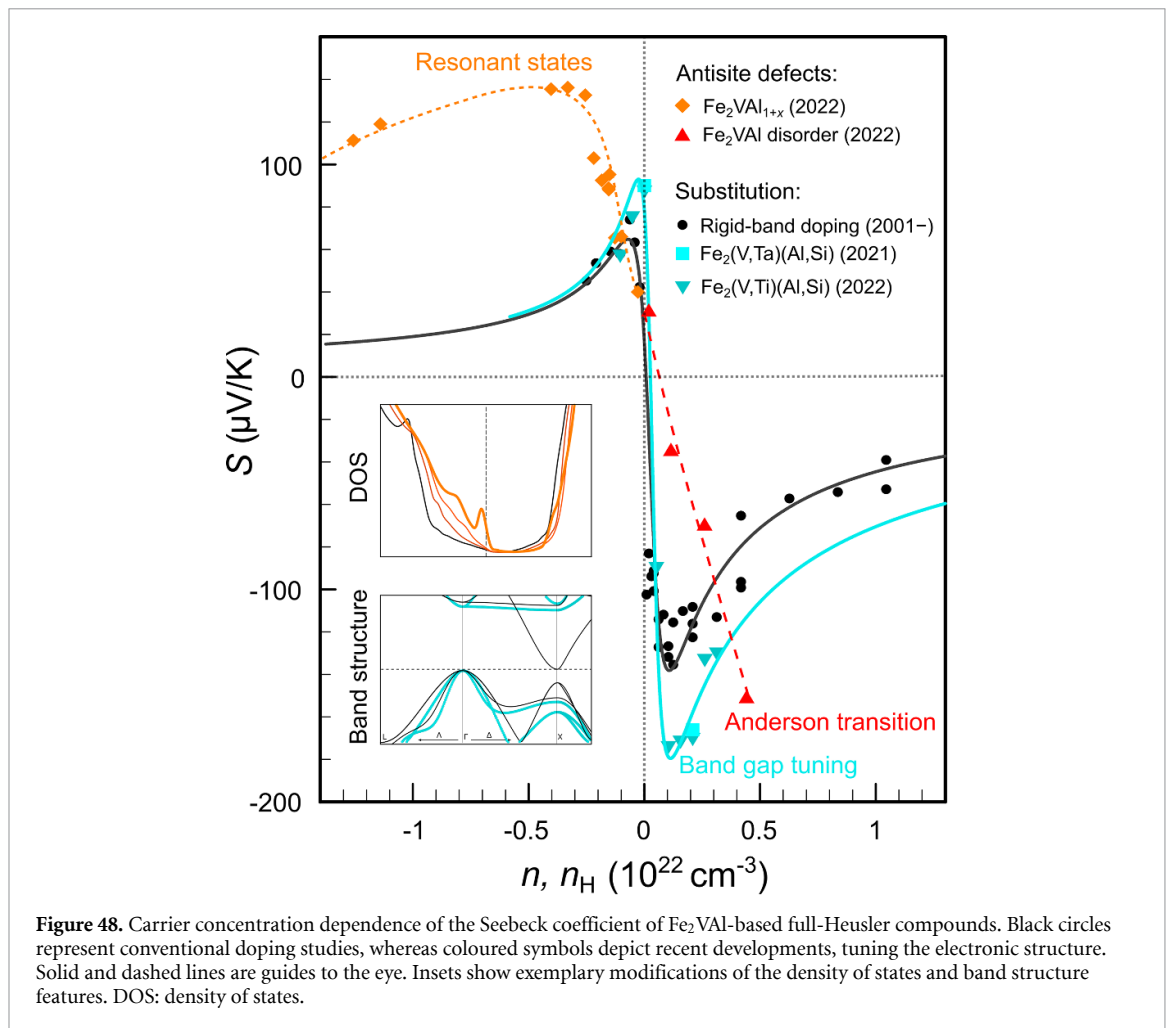
Already in the early 2000s, Nishino and co-workers obtained large values of the Seebeck coefficient S and power factor PF in Fe_2VAl which they attributed to a deep pseudo gap in the vicinity of the Fermi energy E_F [290]. Over the years, doping studies showed that the position of E_F of Fe_2VAl can be readily tuned by changing the carrier concentration n, depicted as black circles in figure 48. Only recently, it has been demonstrated that the electronic structure itself can be severely modified, exhibiting remarkable tune-ability. By either opening the band gap [291] or incorporating narrow resonant or semi-localized impurity states at E_F [292, 293], the Seebeck coefficient was significantly enhanced, compared to the conventional $S(n)$ behaviour (see coloured symbols, deviating from the black solid line in figure 48). Consequently, thermoelectric power factors 2–3 times larger than those of optimized Bi_2Te_3 systems in the 0 °C–100 °C range have been achieved [291].

Current and future challenges

Although full-Heusler systems possess excellent power factors (see figure 49(a)), well above those of other state-of-the-art thermoelectric materials, and exhibit excellent mechanical and chemical properties, the overall thermoelectric performance of full Heuslers is suffering from their large thermal conductivity, l, prevalent in most of the full-Heusler family members. This is primarily a result of the simple crystal structure and stiff lattice, reflected in high values of the sound velocity v_s. As an example, Fe_2VAl demonstrates an average $v_s = 5500$ m s^{-1}, while the sound velocity of Bi_2Te_3 is $v_s = 1750$ m s^{-1}, leading to a lattice thermal conductivity, l_{ph}, being intrinsically at least 3 times larger for the full-Heusler compound.

Disorder and substitutions can lower l_{ph} owing to scattering processes originated from mass and volume differences of the various ions on the respective lattice sites [294]. Reducing the dimensionality of full-Heusler compounds by thin film deposition or manipulating the nano- and microstructure can further decrease l_{ph}. As shown in figure 49(b), l_{ph} drops, from about 25 W m^{-1} K^{-1} in pristine Fe_2VAl, to around 4 W m^{-1} K^{-1} for severe off-stoichiometry [292] or heavy-element substitution [294], around 2 W m^{-1} K^{-1} for thin films [295] and even down to 1.2 W m^{-1} K^{-1} for severe plastic deformation [296]. However, the total thermal conductivities are still several times larger than those of other high-performance thermoelectric materials, owing to a sizeable electronic contribution l_{el}, hindering the realization of high ZT values ($ZT_{max} \approx 0.4$) [296]. A future challenge to improve ZT will therefore be to combine the novel electronic enhancement concepts for increasing the Seebeck coefficient with the above-mentioned strategies to substantially reduce l_{ph}.

Apart from Fe_2VAl-based full-Heusler systems, current and future challenges involve the experimental realization of other theoretically predicted full-Heusler compounds with semiconducting properties. For instance, Fe-based full Heuslers, such as Fe_2YZ ($Y = $ Ti, Zr, Hf; $Z = $ Si, Ge, Sn) [297] and Fe_2TaZ ($Z = $ Al, Ga, In) [298], have been predicted to be semiconductors with very promising thermoelectric properties. Moreover, ultralow thermal conductivities and $ZT = 2$–5 were predicted theoretically for a novel class of

Figure 48. Carrier concentration dependence of the Seebeck coefficient of Fe_2VAl-based full-Heusler compounds. Black circles represent conventional doping studies, whereas coloured symbols depict recent developments, tuning the electronic structure. Solid and dashed lines are guides to the eye. Insets show exemplary modifications of the density of states and band structure features. DOS: density of states.

full-Heusler semiconductors X_2YZ (X = Ca, Sr, Ba; Y = Au, Ag; Z = Sn, Pb, As, Sb, Bi) [299, 300]. These predictions have yet to be confirmed experimentally.

Advances in science and technology to meet challenges

Record-high power factors and ZT values have been recently reported for Fe_2VAl-based full-Heusler compounds, and new enhancement concepts were proposed over the last couple of years. In 2019, Hinterleitner *et al* reported $ZT > 5$ in a metastable Heusler thin film, due to a severe reduction of l_{ph} and an anomalously large Seebeck effect [295]. In the same year, Tsuji *et al* showed that spin fluctuations can be utilized to increase the Seebeck coefficient of ferromagnetic Heusler alloys [301]. In 2022, Fukuta *et al* demonstrated that high-pressure torsion is an effective and reproducible tool to reduce the grain size of Fe_2VAl-based systems towards the nanoscale, resulting in record-low values of l_{ph} [296]. Shortly after, Parzer *et al* found ultrahigh solubility of Al antisites, leading to low l_{ph} and simultaneously to a promising enhancement of the Seebeck coefficient due to resonant states [292]. Later that year, Garmroudi *et al* proposed a disorder-driven Anderson transition in an impurity band as a novel route to obtain high thermoelectric performance in Fe_2VAl [293]. This was achieved by an innovative approach of freezing the high-temperature disordered structure via thermal quenching. Both the deposition of thin films as well as the rapid thermal quenching technique can also be explored to potentially stabilize other full-Heusler-based semiconductor phases (see previous section) with theoretically promising thermoelectric properties that have not yet been experimentally realized.

In addition, recent progress in fundamental thermoelectric research has identified significantly reduced Lorenz numbers L and violations of the Wiedemann–Franz law as a means of reducing the electronic part of the thermal conductivity l_{el} in several nano-structured systems but also in topological materials. For instance, it has been estimated that L decreases by almost an order of magnitude in the ferromagnetic Weyl semimetal full-Heusler compound Co_2MnAl [302]. Since full-Heusler compounds often also have
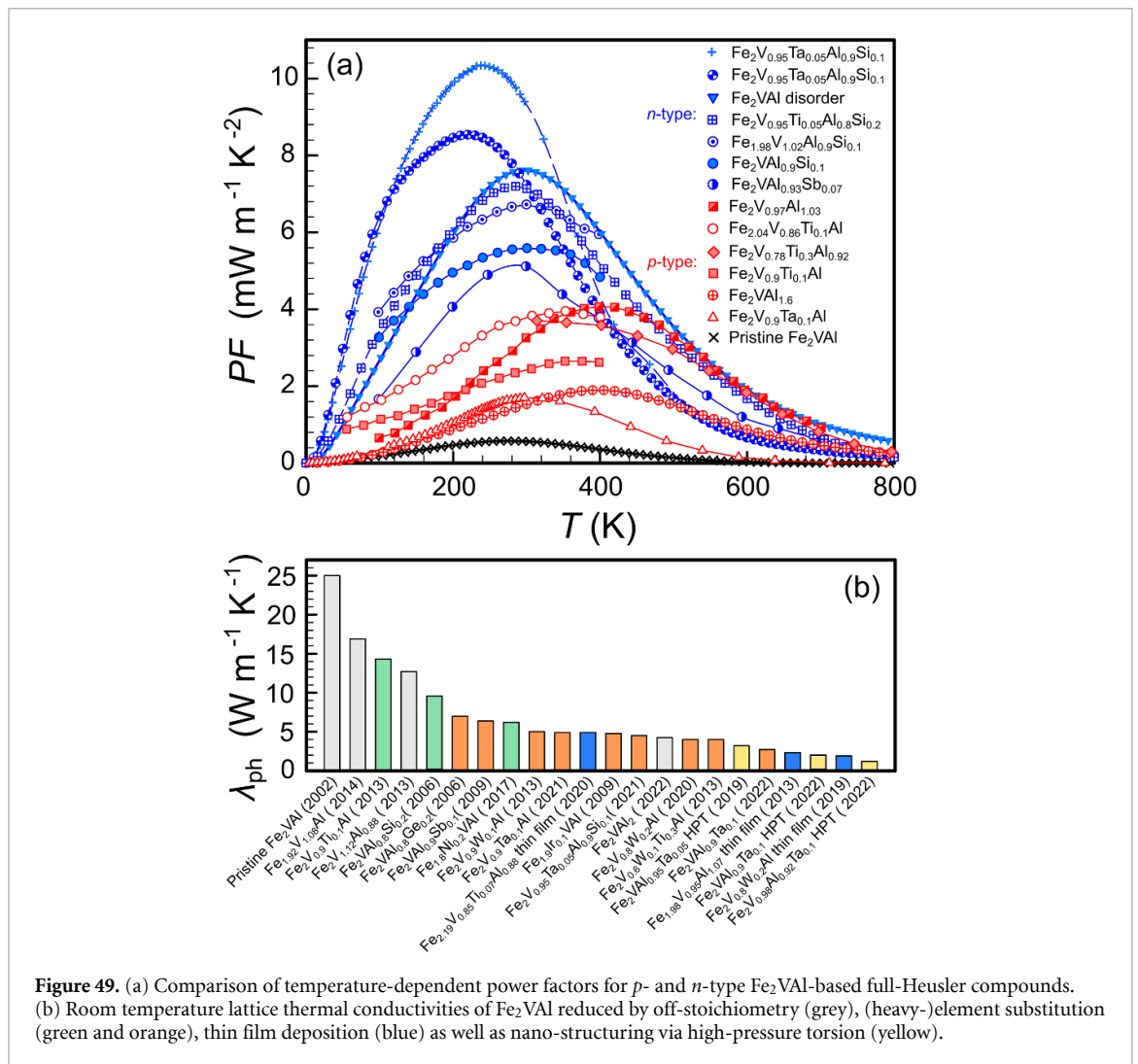
Figure 49. (a) Comparison of temperature-dependent power factors for *p*- and *n*-type Fe$_2$VAl-based full-Heusler compounds. (b) Room temperature lattice thermal conductivities of Fe$_2$VAl reduced by off-stoichiometry (grey), (heavy-)element substitution (green and orange), thin film deposition (blue) as well as nano-structuring via high-pressure torsion (yellow).

intrinsically large values of l_{el} in addition to l_{ph}, violations of the Wiedemann–Franz law can be an especially promising approach to tackle the issue of high thermal conductivities in this material class. Upcoming research on full-Heusler thermoelectric materials would have a successful breakthrough if the electronic tuning concepts discussed in this review as well as a further reduction of l can be combined effectively.

Concluding remarks

Full-Heusler thermoelectric materials based on Fe$_2$VAl turn out to bear large potentials for being used in the 100 °C temperature range for power generation, cooling, or wireless sensing in near future, thereby supersede today's commercially available materials based on Bi$_2$Te$_3$. Superior power factors and excellent mechanical properties, the easy synthesis and the non-poisonous and reasonably priced constituting elements, as well as their respective abundance will outplay Bi$_2$Te$_3$ in this temperature regime, where globally the largest share of waste heat accumulates.

The flexibility of tuning the electronic structure of full Heuslers, such as the band gap size or the density-of-states effective charge carrier mass and promising theoretical predictions concerning other full-Heusler compounds, which still remain to be experimentally verified, are outstanding assets of full Heuslers. These encouraging results motivate further research on combining the established electronic-engineering and nano-structuring strategies—thus paving the road towards high *ZT* in full-Heusler systems.

Acknowledgments

5.4. Half Heuslers for thermoelectric energy harvesting

Duncan Zavanelli, Madison K Brod, Muath Al Malki and G Jeffrey Snyder
Department of Materials Science and Engineering, Northwestern University, Evanston, IL 60208, United
States of America

Status
There are many classes of materials that are currently pursued as promising thermoelectric materials. The focus of most of these studies is improving the material figure of merit, *ZT*, as a proxy for device efficiency. One promising group of potential materials are the half-Heusler alloys with the formula XYZ, where X and Y are transition metals and Z is an element in the p block. The structure of half-Heusler alloys is shown in figure 50 along with the *ZTs* of state-of-the-art alloys. The current best performance gives *ZT* values of up to 1.5 at high temperatures, showing excellent thermoelectric performance competitive with other materials [303]. These *ZT* values arise from very large power factors, with alloying crucial to reduce thermal conductivity (κ) [303]. Current alloying strategies focus on increasing mass contrast to reduce κ, leading to high performance in alloys such as $Ta_xV_{1-x}FeSb$ and $Zr_xHf_{1-x}NiSn$ [303]. Their high power factors make half Heuslers attractive for applications where total κ is fixed by geometric constraints.

Beyond their *ZT*s, half-Heusler alloys provide other advantages over other thermoelectric systems that make them more important than just their *ZT*. Other thermoelectric materials, such as PbTe, have limited usage despite reported *ZT*s much higher than can be obtained with half Heuslers. This is often a result of the inherent brittleness of many semiconductors, or a limited temperature range prohibiting high ΔT values. Half-Heusler alloys have been shown to have the highest creep resistance of all measured thermoelectric materials as well as excellent thermal stability [303, 304]. As a result, half-Heusler alloys have their niche as the usable thermoelectric materials that have a unique combination of non-thermoelectric properties that make them much more practical than other materials. This ensures that they remain of great interest despite not being able to reach with some of the recently reported *ZT*s of greater than 2 in other materials such as SnTe or PbTe. Future work into half-Heusler alloys is poised to focus on further understanding and optimizing the electronic structures, microstructures, alloying strategies, and mechanical properties of these alloys.

Current and future challenges
The biggest challenge facing half-Heusler alloys is their comparatively poor thermoelectric performance in relation to current high performing materials. A promising route for improvement for both n-type and p-type half-Heusler thermoelectrics is via band engineering through alloying. Band engineering can improve the valley degeneracy (NV) of half-Heusler alloys. NV is a characteristic of an electronic dispersion that describes the number of carrier pockets that contribute to electronic transport, and higher values of NV lead to better performance. Electronic bands with higher NV require band extrema at lower symmetry points in the Brillouin zones (BZs) of higher symmetry crystals and convergence between band extrema at different (or the same) $\boldsymbol{k}$-points in the BZ [306].

There are opportunities to achieve high NV in both n-type and p-type half-Heusler thermoelectrics. For half-Heusler alloys, there are two competing conduction band minima (CBMs) at the X-point and three possible locations for the valence band maximum (VBM) at different $\boldsymbol{k}$-points, Γ, L or W [305, 307, 308]. There are three symmetrically equivalent X-points, four L-points, six W-points, and one Γ-point in the BZ of an fcc crystal. Thus, the valley degeneracy of the CB edge can be improved engineering the bands such that the two competing CBMs at X are converged in energy, and the valley degeneracy of the VB edge can be improved by promoting a VBM at L or (ideally) W rather than at Γ, and/or by converging multiple of the competing VBMs [305, 308].

High-throughput density-functional-theory studies have discovered chemical trends describing the relative energy of the competing CBMs and VBMs that can help predict both end-member compounds and solid-solution alloys that have high NV based on the group number (valence) or electronegativity of the X, Y, and Z sites [307, 308]. In alloys, the average group number difference can be tuned through aliovalent substitutions, while both aliovalent and isoelectronic substitutions can be used to tune the electronegativities. The chemical guidelines for engineering high NV can be understood by studying the chemical bonding that dominates the band edges [305]. Thus, the current challenge for improving half-Heusler alloys is to predict and synthesize these alloys predicted to have enhanced NV, such as p-type NbCoSn.

Advances in science and technology to meet challenges
Along with the band engineering approach outlined above, alloying and microstructure strategies are needed to further reduce κ and optimize electronic properties. From figure 50, the highest performing half-Heusler
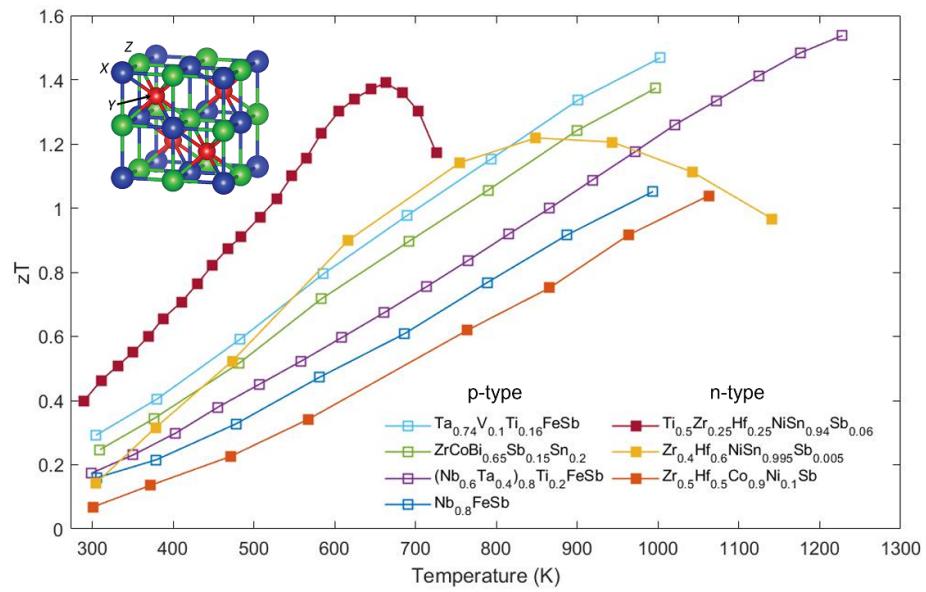
Figure 50. *ZT* of highest performing p-type and n-type half-Heusler alloys from Quinn *et al* [303] with an insert showing the half-Heusler structure adapted from Brod *et al*. Reproduced from [303]. CC BY 3.0. [305] John Wiley & Sons. © 2022 Wiley-VCH GmbH.
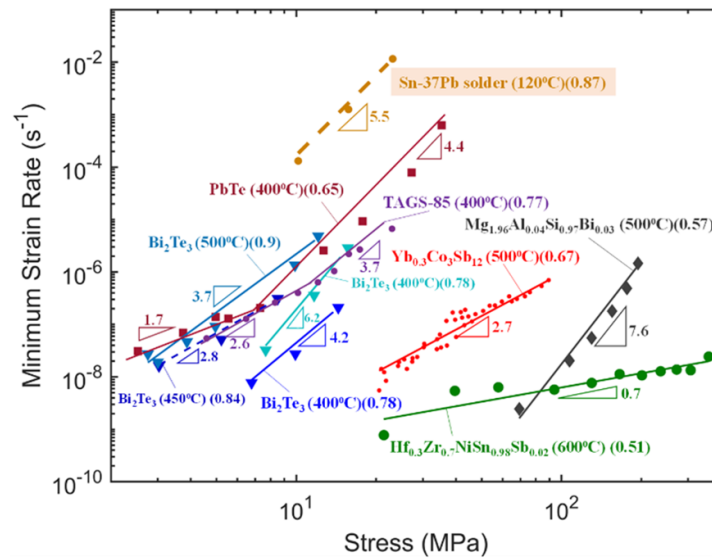

Figure 51. Comparison of creep rates between the half-Heusler ZrNiSn and other thermoelectric materials. Reproduced based on Malki *et al*. Reproduced with permission from [304]. CC BY-NC-ND 4.0.

alloys contain alloying elements, such as Ta on the Nb site in NbFeSb [303]. While many alloys have been explored, there are opportunities for systematic probes of the large compositional space open to half-Heusler alloys. Computational work has emerged to present alloy strategies, particularly showing that increasing the number of alloying elements does not necessarily lead to further reductions in κ [309]. The alloying elements need to increase mass contrast on a sublattice to reduce κ. These strategies could be combined with high throughput methods to rapidly screen promising compositions and discover optimal stoichiometries. However, this approach can be complicated by the presence of significant site disorder, particularly on the interstitial site, seen in half-Heuslers like ZrNiSn [310].

Aside from alloying, half-Heusler alloy performance can be improved through microstructural understanding and control. Recent studies have shown dopant segregation to grain boundaries (GB) in half-Heusler alloys, with corresponding reduction of GB scattering. For example, Pt dopants in NbCoSn segregate to GBs, increasing the room temperature weighted mobility [311]. Dopant segregation can be used as a tool to enable GBs to reduce κ without harming electrical transport.

Until the performance of half-Heusler alloys is improved, their main advantage as thermoelectric materials is their mechanical properties. Superseding other classes of thermoelectric materials, half Heuslers are known for their mechanical robustness and thermal stability in the mid-high temperature range [312]. This is depicted in high resistance to elastic deformation (average Young's modulus $\sim$187 GPa)[312] and the best reported creep resistance in thermoelectric materials (see figure 51) [304]. However, half-Heusler alloys, among most of the thermoelectric materials, lack the required fracture resistance that is essential to minimize the impact of expanding cracks initiated during processing or operation of thermoelectric devices. Toughening mechanisms established for brittle ceramics, including fibre bridging, transformation toughening and crack tortuosity, can be applied to half Heuslers and thermoelectric materials in general to enhance their fracture toughness without compromising the electronic properties.

Concluding remarks

Half-Heusler alloys feature competitive thermoelectric properties, as well as a path for further improvements through engineering their band structure. Despite not quite matching the current best reported *ZT* values, the other inherent advantages of half-Heusler alloys make them the target of considerable interest for designing full thermoelectric modules. Their mechanical stability makes them more inherently usable than most brittle thermoelectrics. However, the high operating temperatures of half-Heusler modules and resulting thermal stresses means there are challenges in creating stable robust modules. In summary, the current and past research has identified several high performing half-Heusler alloys based on NbFeSb and ZrNiSn and highlighted their anomalously good mechanical properties for thermoelectric materials. Future work should concentrate on further improving these alloys through band engineering strategies as well as improving the module stability with toughening strategies and an investigation of the interfaces between half Heuslers and other components.

Acknowledgments

5.5. Clathrates for thermoelectric energy harvesting

Kirill Kovnir[1,2] *and Susan M Kauzlarich*[3]
[1] Department of Chemistry, Iowa State University, Ames, IA 50011, United States of America
[2] US DOE Ames National Laboratory, Ames, IA 50011, United States of America
[3] Department of Chemistry, University of California, Davis, CA 95616, United States of America

Status

Clathrates are cage structures with various guest occupying the centres of 20–28 vertex polyhedra. Inorganic clathrates can be comprised of almost all the elements from the periodic chart and the diversity of structures provide materials with properties ranging from semiconducting to superconducting with applications in energy conversion and storage [313–315]. This brief highlight will focus on thermoelectric energy conversion. Inorganic clathrates can be considered the quintessential 'phonon-glass electron-crystal' (PGEC) materials as proposed originally by Slack because the large unit cell covalent framework can provide effective transport of charge carriers while guest atoms in the oversized polyhedra can rattle giving rise to scattering of heat-carrying phonons [316]. The tetrahedrally coordinated clathrate framework suits elements from group 14 well. Filling the clathrate cages with guest ions requires aliovalent substitution in the framework to maintain charge balance (figure 52(a)). Conventional clathrates feature group 13 (or lower) and 14 elements in the framework with guest alkali, alkaline-earth, or rare-earth cations. Inverse clathrates host anionic guests from group 16 or 17 inside a framework composed of elements from group 14 and 15 or 16. In these two examples, the frameworks composed of group 13–14 elements can be considered electron deficient, and a cation is necessary to fill the guest sites, whereas in frameworks containing group 14–15 elements, an anion is necessary to compensate charge. The Si-containing clathrates are earth abundant lightweight compounds where the guest cation can have significant impact on the structure and properties. Depending on polyhedral cage types and connectivity the structure of clathrates is divided into different classes and most abundant and studied are type I ($A_2B_6E_{46}$) and type II ($A_{16}B_8E_{136}$) clathrates, A and B—guests, E—framework atoms (figures 52(b) and (c)). The clathrates free from group 14 elements have been called 'unconventional clathrates'. Their frameworks are based on combination of group 11 or 12 or 13 and 15 elements allowing for substantial deviations from tetrahedral coordination of the framework resulting in structural and properties flexibility [317]. Unconventional clathrates show a variety of framework structures with guest ions (figures 52(d) and (e)) and hold the promise of high figure of merit, *ZT*, while being prepared from light elements with tunable transport properties.

Current and future challenges

Inorganic clathrates have structures that exhibit phonon glass electron crystal behaviour. The framework provides a conduction path while the guest atoms scatter phonons and significantly reduce thermal conductivity. In addition, alio- and isovalent substitutions allow for band structure engineering and various elemental combinations providing a variety of adjustable band gaps. Many clathrate phases have been shown to have good thermoelectric properties (figure 53) [314, 318] with the highest thermoelectric figure of merit, *ZT*, reported to date of 1.35 for $Ba_{16}Ga_{16}Ge_{30}$ at 823 K [319]. Several Sn-based clathrates exhibited similar *ZT* in 1–1.3 range albeit at lower temperatures of 500–550 K. A significant number of conventional, inverse, and unconventional clathrate crystal structures have been reported and a limited number of properties investigated. Because many of these framework structures undergo significant expansion with temperature, obtaining dense pellets for measurement is a challenge. Another challenge is to organize the data to provide a signpost toward the best compositions that may provide further improvements in thermoelectric conversion efficiencies. Zintl rules, electron transfer between the framework and guest atoms and the fulfillment of the electron octet, provides an excellent roadmap for proposing new combinations of elements but lack of detailed understanding of guest-host interactions limits the predictive property outcomes of this simple electron counting formalism. Compositions and structural features of the frameworks are well understood by covalent or polar covalent bonding between atoms. For clathrates based on group 14 elements, frameworks stability (and thermoelectric application temperature) correlates with strength of homoatomic covalent E-E bond: Si-based frameworks are stable up to 900 °C–1200 °C while most of Sn-based clathrates decomposes above 600 °C. This is emphasized by the absence of high-temperature Sn-based clathrate thermoelectrics (figure 53). Si clathrates readily form charge-unbalanced compositions, which prevents widespread investigations of Si clathrates for thermoelectric applications, as control over carrier concentration is difficult to achieve. Unconventional clathrates with polar-covalent bonding exhibit intermediate stability in the range of 600 °C–900 °C. The understanding and interpretation of defects and their interplay with stability and transport properties remains a challenge [320]. As mentioned above, guest-host interactions are a key issue for study. PGEC concept postulates the independence of the heat and
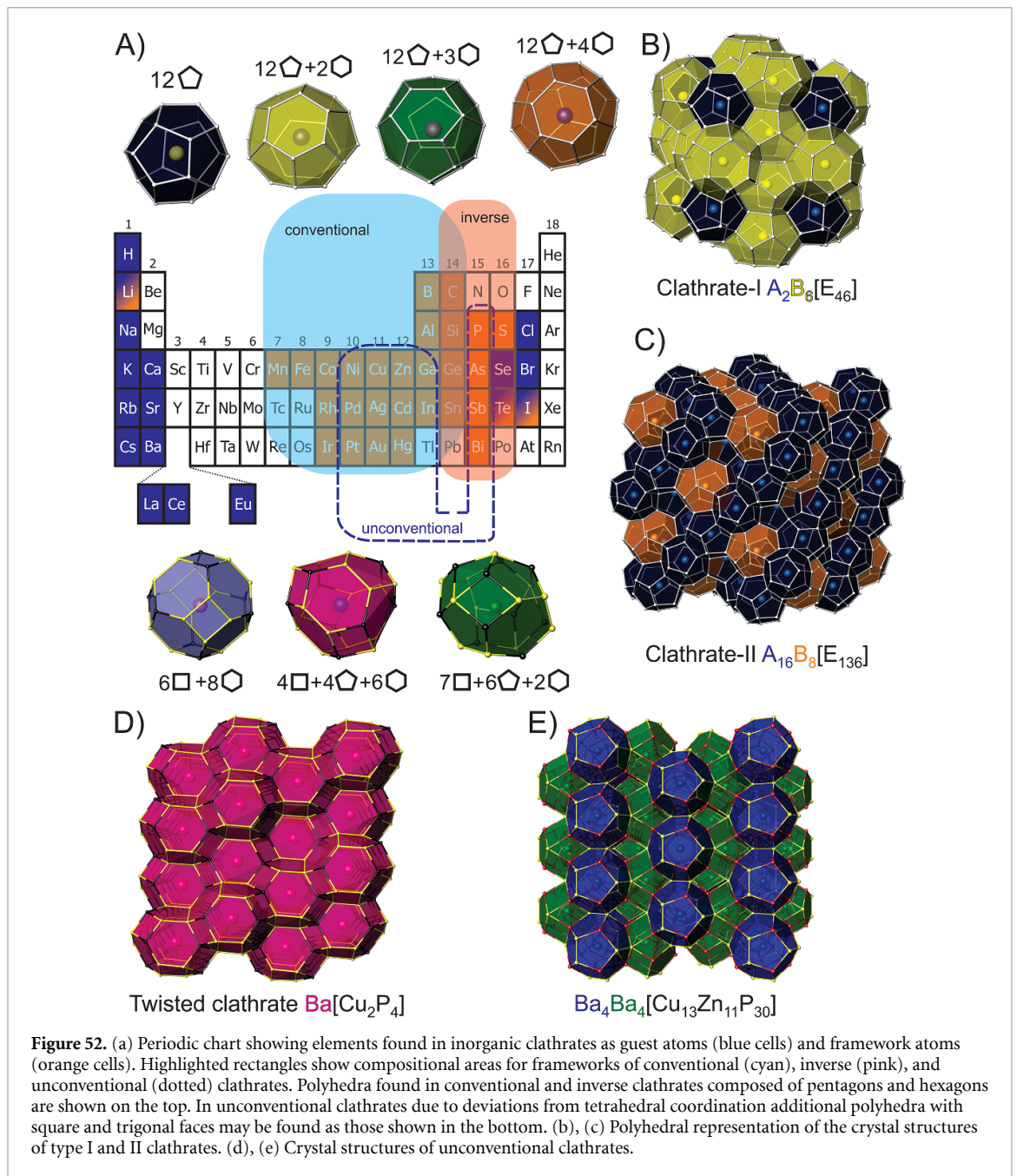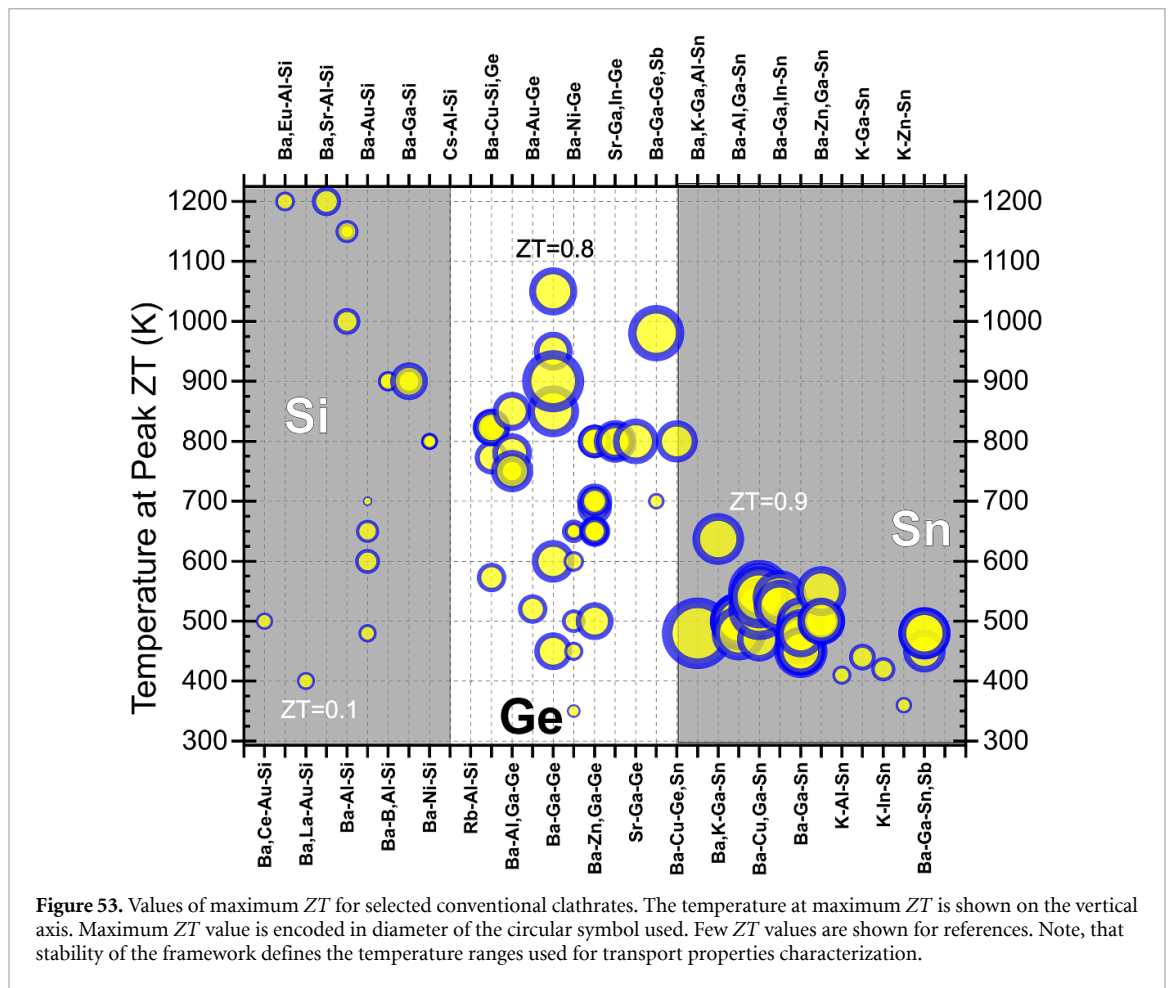
Figure 52. (a) Periodic chart showing elements found in inorganic clathrates as guest atoms (blue cells) and framework atoms (orange cells). Highlighted rectangles show compositional areas for frameworks of conventional (cyan), inverse (pink), and unconventional (dotted) clathrates. Polyhedra found in conventional and inverse clathrates composed of pentagons and hexagons are shown on the top. In unconventional clathrates due to deviations from tetrahedral coordination additional polyhedra with square and trigonal faces may be found as those shown in the bottom. (b), (c) Polyhedral representation of the crystal structures of type I and II clathrates. (d), (e) Crystal structures of unconventional clathrates.

charge transport, but in clathrates strong host-guest interaction may arise and affect properties [321]. Even with these caveats, an exciting challenge is to design new materials with earth abundant elements that may provide high thermoelectric efficiencies at high temperatures and are stable in air.

Advances in science and technology to meet challenges

Although clathrates display a large diversity of structure and properties, most are restricted to low temperatures and modest *ZT* values. Therefore, an important challenge for the field is to design and synthesize materials with better properties, eventually leading to applications. An important fundamental science priority is a development of new synthetic approaches to high purity materials where composition can be controlled with high fidelity [322]. Theoretical calculations on the defect structures and understanding their impact on properties is a challenge. Clathrates are often described as highly symmetric cubic structures with some disorder in the framework due to the presence of either vacancies or two or more elements of different chemical nature. More thorough studies shown that bonding preferences of the framework forming elements results in either short-range or long-range ordering which impacts the electronic structure and transport properties. Proper modelling of such complex structures requires a detailed characterization where X-ray and neutron high resolution powder and single crystal diffraction in

Figure 53. Values of maximum *ZT* for selected conventional clathrates. The temperature at maximum *ZT* is shown on the vertical axis. Maximum *ZT* value is encoded in diameter of the circular symbol used. Few *ZT* values are shown for references. Note, that stability of the framework defines the temperature ranges used for transport properties characterization.

combination with total scattering and local probes such as EXAFS and scanning-transmission electron microscopy may reveal true structure. The latter is crucial for the proper computational description of electronic structure and properties prediction. High throughput theoretical calculations may provide a breakthrough by identifying underlying components of these complex framework structures that can lead to high thermoelectric efficiencies.

Concluding remarks

There is a myriad combination of possible elements that give rise to clathrate phases and progress has been considerable. A good understanding of electron counting requirements of compounds synthesized to date frames the design of semiconducting properties that may provide good thermoelectric properties. Theory has a significant role to play in providing guideposts towards new materials with good thermoelectric properties. However, there is still a significant phase space unexplored with high prospects of finding efficient thermoelectric materials. In addition, because of the possibilities of superconductivity, photovoltaic and energy storage applications, these properties are also worthy of investigation.

Acknowledgments

5.6. Skutterudites for thermoelectric energy harvesting

Ctirad Uher
Department of Physics, University of Michigan, Ann Arbor, Michigan 48109, United States of America

Status

In 1994, Prof. Slack pointed out that skutterudites are an excellent example of his Phonon-Glass-Electron-Crystal (PGEC) paradigm [323]. Since that time, researchers worldwide have focused on the development of this interesting class of thermoelectrics [324]. Moreover, many car-manufacturing companies saw a great potential in capturing the waste heat from engines, converting it to electricity, and, ultimately, improving the millage. Further appeal of skutterudites has been their non-toxic and readily available chemical elements. Skutterudites are binary compounds MX_3, with M being column 9 transition metals Co, Rh, and Ir, while X are pnicogen elements P, As, and Sb. All nine combinations of M and X exist, and they crystallize in the bcc structure in the space group Im [325].

The prominent feature of skutterudites are two large structural voids. When filled with foreign ions, filled skutterudites result [325] that are of interest to thermoelectricity due to their outstanding electronic properties. Moreover, filling, particularly with multiple kinds of filler species, is exceptionally effective in suppressing the thermal conductivity by affecting a broader range of phonon frequencies. Combining excellent electronic properties and very low lattice thermal conductivities makes filled skutterudites outstanding thermoelectric materials for power generation applications. Although the interest of the car companies in thermoelectricity has recently fizzled out as they shifted their attention to electrically driven cars, filled skutterudites maintain their position as premier thermoelectrics for waste heat recovery in the temperature range between 500 K–850 K, where there are plentiful sources of waste industrial heat waiting to be captured, figure 54.

Current and future challenges

The current state-of-the-art skutterudites developed in the laboratories worldwide have achieved outstanding thermoelectric performance with $ZT \sim 1.8$ for n-type skutterudite [326, 327], further enhanced to $ZT \sim 2$ upon applying high-pressure torsion [328]. The best p-type forms of the structure have attained a somewhat lower but still very competitive $ZT \sim 1.3$ [329]. Moreover, skutterudites are mechanically very robust and machineable. A long-standing puzzle concerning n-type skutterudites, namely their high Seebeck coefficients at high carrier densities of $\sim 10^{21}$ cm^{-3}, has been solved recently by density-functional-theory calculations combined with detailed measurements of the temperature dependent optical absorption [330, 331]. The data revealed the existence of a nearby-lying second conduction minimum that descends with temperature and converges with the G-point conduction band minimum, figure 55. The convergence dramatically enhances the valley degeneracy and the density-of-states effective mass, thus assuring high electrical conductivity with no penalty to the Seebeck coefficient. Concerns regarding sublimation of Sb and oxidation when operated in air at elevated temperatures have been mitigated by applying thin protective electrically insulating coatings, such as aerogels and enamels. The major problem concerning skutterudites is the inability to transfer the outstanding laboratory results to a large-scale manufacturing setting and fabricate highly efficient skutterudite-based thermoelectric modules. This is partly due to the poorer performance of materials prepared in large batches and due to high contact resistances introduced during the assembly of modules. Nevertheless, modules with the efficiency exceeding 10% have been demonstrated [332].

Advances in science and technology to meet challenges

To improve the thermoelectric energy conversion of skutterudites, advances must be made on several fronts. The performance of p-type skutterudites should be improved to match closely the performance of their n-type cousins. Detailed density-functional-theory calculations combined with doping studies should explore a possibility of band convergence within the valence band manifold. For all forms of skutterudites, optimal microstructures should be identified (grain size and its orientation) that minimize electrical resistivity yet very effectively scatter the heat conducting phonons, and ways to realize such microstructures in actual samples should be explored. The key point is that such optimal microstructures must be stable at temperatures where skutterudites are expected to operate. An understanding must be gained why the performance of gram quantities of skutterudites prepared in laboratories are not replicated when the identical skutterudite is fabricated in kilogram quantities in a production setting. In the past, the bulk of research efforts have focused on finding the best performing skutterudite compounds with little regard how such outstanding materials will function in efficient thermoelectric modules. The much less glamorous tasks of finding how to metallize skutterudites, how to make low resistance contact, how to mitigate differential thermal expansion between n- and p-type elements, and how to protect the couple's legs in a hostile
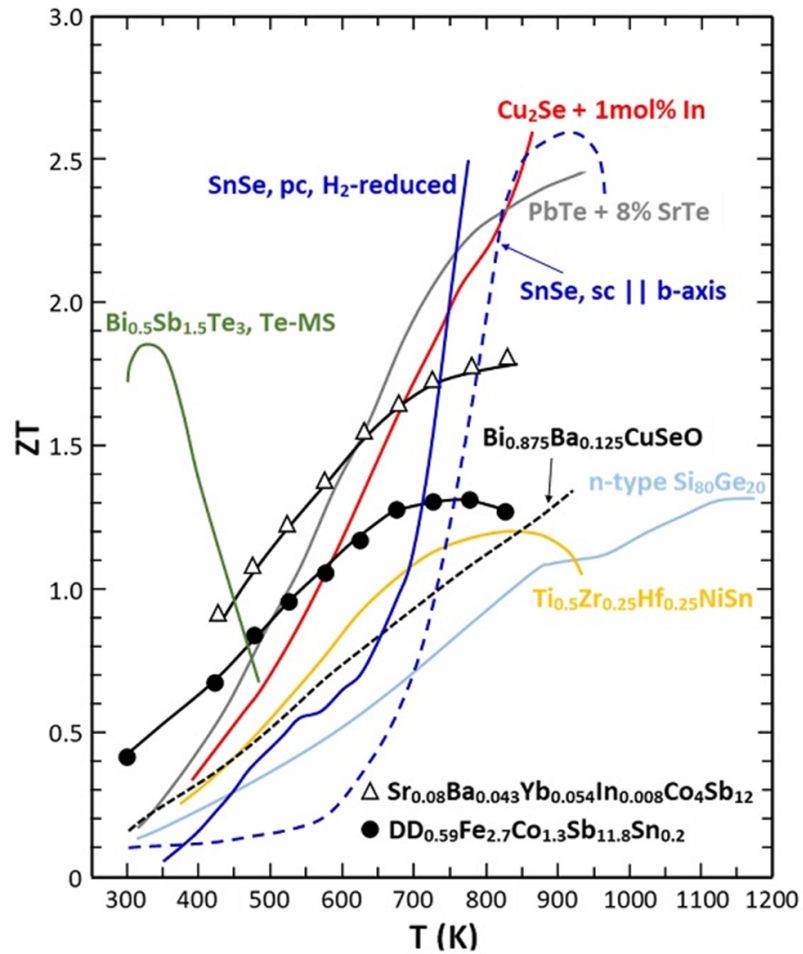
Figure 54. Comparison of the best n-type skutterudites, designated with upside unfilled triangles, Rogl *et al Acta Mater.* 95 (2015) 201, and the best p-type skutterudites indicated by black solid circles, Rogl *et al Acta Mater.* 91 (2015) 227, with other high-performing thermoelectrics. In the mid-temperature range 500 K–900 K, skutterudites are an excellent choice for thermoelectric modules.
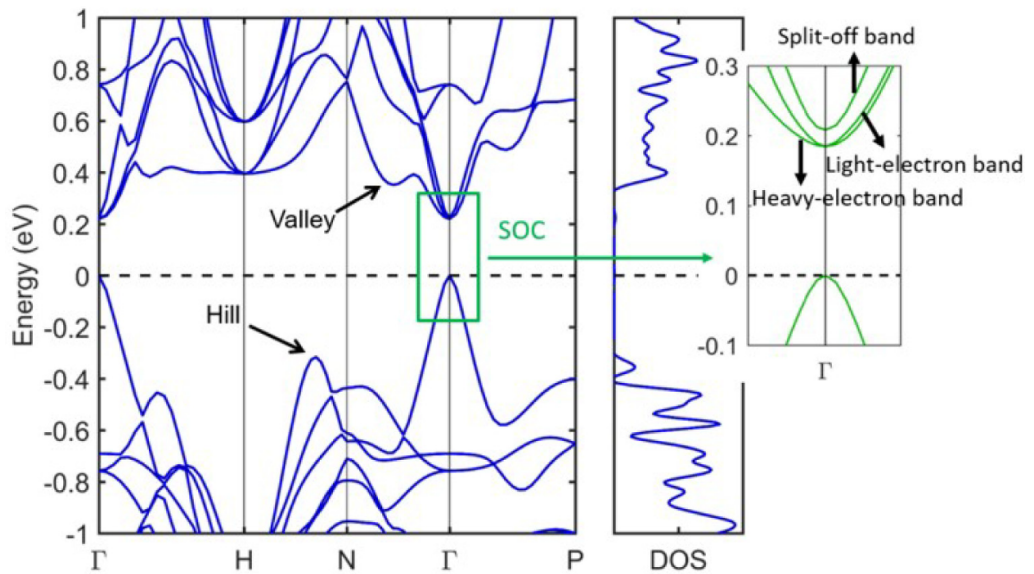

Figure 55. Band structure of skutterudites highlighting the closely lying conduction bands, the band edges of which converge with increasing temperature to the G-point conduction band. Reproduced from Hu *et al Phys. Rev.* B 95 (2017) 165 204. [330] 2017, reprinted by permission of the publisher (Taylor & Francis Ltd, www.tandfonline.com).

environment when operating in air at high temperatures were not adequately considered. These more engineering tasks must become of prime focus to fully utilize the great potential of skutterudites and fabricate efficient, reliable, and inexpensive skutterudite-based thermoelectric modules.

Concluding remarks

Some twenty-five years of research have resulted in n- and p-type skutterudites that have the thermoelectric figure of merit greatly exceeding values of unity. Moreover, skutterudites are among the best thermoelectrics as far as the mechanical properties are concerned and are even machineable. Thin protective electrically insulating coatings, such as aerogels and enamels, solved problems with Sb sublimation and oxidation. These are outstanding laboratory achievements. The problem is that they have not transferred readily to a large-scale manufacturing setting where detailed issues concerning the assembly of elements into reliable thermoelectric couples are dealt with. Indeed, one cannot buy skutterudite modules off the shelf because, simply, no one is manufacturing them. Yet, the modules fabricated by some of the larger research groups perform very well with efficiencies in excess of 10%. The shift of interests of the car manufacturers from gasoline engines to fully electric cars has been a major blow to funding of research on skutterudites. Nevertheless, there are numerous other sources of waste industrial heat in the temperature range between 500 K and 900 K where the efficient performance of skutterudites could make a great impact.

Acknowledgments

5.7. Oxides for thermoelectric energy harvesting

Jinle Lan[1] and Yuan-Hua Lin[2]
[1] State Key Laboratory of Organic-Inorganic Composites, College of Materials Science and Engineering, Beijing University of Chemical Technology, North Third Ring Road 15, Chaoyang District, Beijing 100029, People's Republic of China
[2] State Key Laboratory of New Ceramics and Fine Processing, School of Materials Science and Engineering, Tsinghua University, Shuangqing Road 30, Haidian District, Beijing 100084, People's Republic of China

Status

To date, state-of-the-art thermoelectric materials usually contain toxic, scarce and expensive metal elements (e.g. Pb, Te, and Sb). The practical applications of these materials are restricted by the poor thermal and chemical stability at high temperature as well as high cost. After the discovery of $NaCo_2O_4$ single crystals with high thermoelectric potential performance by Terasaki *et al* [333], many oxides such as $Ca_3Co_4O_9$ [334], ZnO, $CaMnO_3$ and $SrTiO_3$, were carefully investigated for thermoelectric applications. These types of oxides have proven to be very promising for high-temperature thermoelectric applications, as they are thermally and chemically stable in air at high temperatures. These oxides are easy to prepare, rely on low-cost raw materials and are eco-friendly, thus drawing considerable attention in the thermoelectrics community. However, the thermoelectric performance of oxides, especially in polycrystalline form, is characterized by relatively low ZT values, which is ascribed to low electrical conductivity and high thermal conductivity caused by high grain boundary resistance and strong ionic bonding (figure 56). So far, some layered-structure oxides have delivered outstanding performance, giving some hope for further development. Amongst p-type oxide thermoelectric materials, Co-based oxide material $Ca_3Co_4O_9$ has been intensively investigated due to its low thermal conductivity originating from its misfitted structure and high Seebeck coefficient by the plus spin entropy. The highest ZT value of $Ca_3Co_4O_9 \sim 0.90$ at 1073 K was achieved by grain boundary engineering [335]. BiCuSeO oxyselenides have been reported to exhibit intrinsic low lattice thermal conductivity and high ZT value [336]. Recently, thermoelectric performance with $ZT > 1.5$ at 873 K has been achieved for Pb,Ca-dual-doped BiCuSeO oxyselenide ceramics [337].

Current and future challenges

In the field of oxide-based thermoelectric materials, several challenges need to be tackled. Here, we highlight a few key challenges:

- The strong ionicity in the bonds between light oxide atoms with other atoms leads to intrinsically small carrier mobility μ and carrier concentration n. Besides, strong bonds in oxides also make the lattice distortions be suppressed, and the vibrations of atoms are rarely disturbed, which further results in relatively high lattice thermal conductivity κ_1. Thus, except $Ca_3Co_4O_9$ [334], Bi_2O_2Se [338], and BiCuSeO [336], most oxide thermoelectrics exhibit poor ZT values of around 0.1–0.4. Therefore, it is an open question for the thermoelectrics community to design the proper crystal structure for the novel oxide materials.
- Grain boundary engineering with dopant segregations or carbon addition (e.g. graphene, carbon nanotubes and graphite) have been proved to be a robust strategy to achieve 'phonon glass- electron crystal' behaviour in oxides, which even outperform single crystal-like charge transport in polycrystalline oxides. The open question is how to clearly resolve and manipulate the atomic structure of grain boundaries to achieve desirable properties [339, 340].
- To decouple the electrical and thermal properties, the 'phonon glass- electron crystal' concept proposed by Slack can be realized in the materials with layered structures. Two-dimensional layered materials exhibit artificial super-lattice structure, which possess short phonon mean free paths due to the strong phonon scattering in lattice-scale without deteriorating the electric transport. The layered oxygen-containing thermoelectric materials (e.g. $Ca_3Co_4O_9$, BiCuSeO and Bi_2O_2Se), were intensively investigated due to their low κ value originated from misfitted structures and impressive high carrier mobility. Nevertheless, the electronic and phonon mechanism has not been fully understood, especially in the effect of in-plane and out-plane structures of the sublayers in the materials.
- In non-oxide thermoelectric devices, the effects of air and high temperatures have always limited their practical applications. Oxide ceramics are considered promising for high-temperature applications due to their excellent thermal stability and strong oxidation resistance. The first prototype of an all-oxide thermoelectric device was fabricated using Gd-doped $Ca_3Co_4O_9$ p-type legs and La-doped $CaMnO_3$ n-type legs on a fin in
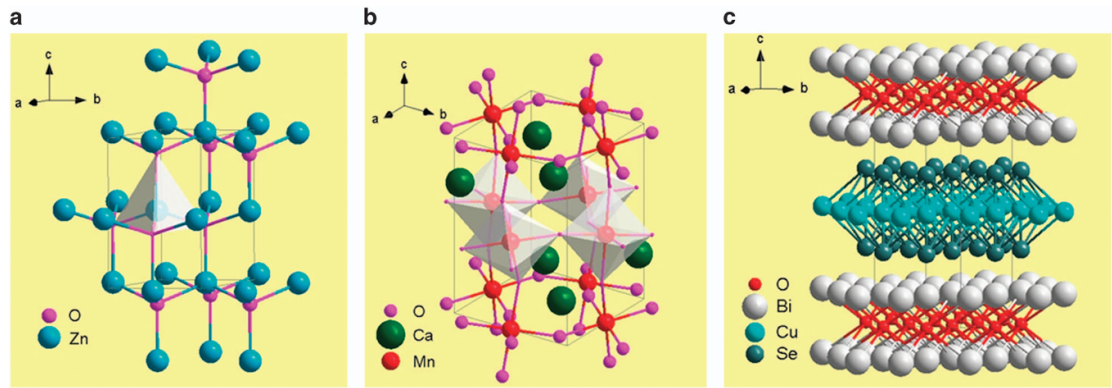
Figure 56. The crystal structure of (a) simple wurtzite oxide-based materials: ZnO (P63mc), (b) perovskite oxides: CaMnO$_3$ (Pbnm) and (c) layered oxides: BiCuSeO (P4/nmm).
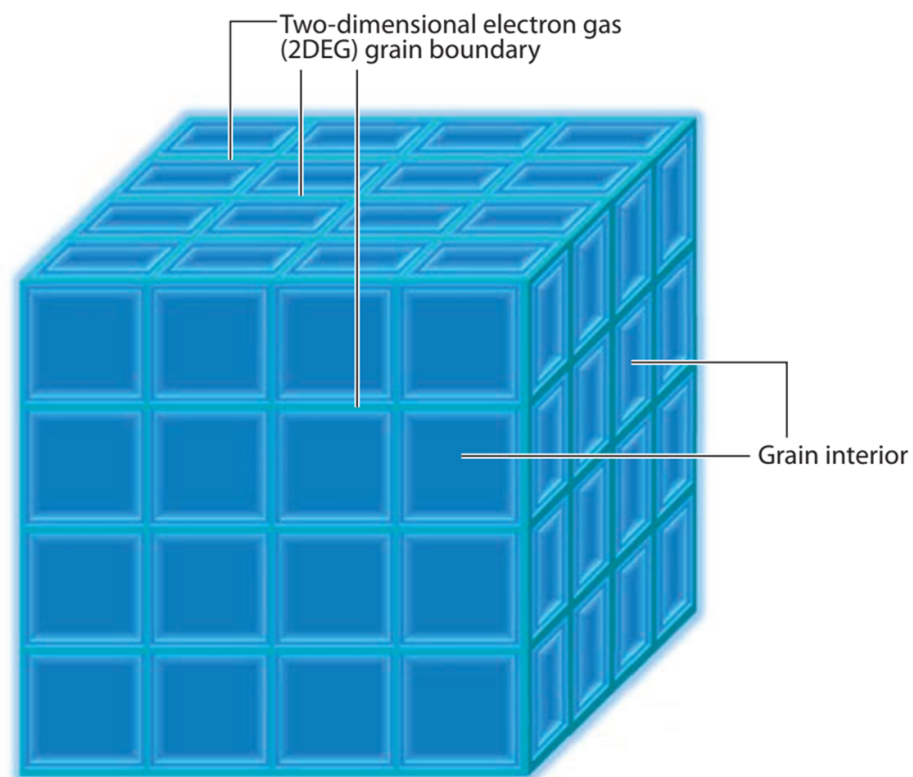

Figure 57. Brick-and-mortar-type structure of SrTiO$_3$ nanoceramics. Two-dimensional-electron-gas grain boundaries are shown in light blue. Grain interiors are shown in deep blue [342].

2001 [341]. This device proved to be operable for more than two weeks in air showing high durability. The challenge is that few new works concerning oxide thermoelectric devices have been reported during the last decade.

Advances in science and technology to meet challenges

To address the challenges mentioned above, key strategies are required to boost the development of oxide thermoelectrics. Efforts must continue to design and synthesize new materials with complex structure and high bonding covalency, searching beyond oxyselenides and cobaltites.

To shed more light on the optimized properties for the existing materials system, strategies including band gap tuning, modulation doping, texturing and nanocompositing should be carefully investigated. A brick and mortal type structure of ceramics with two-dimensional electron gas grain boundary (figure 57)

are introduced to SrTiO$_3$ system [342]. The predicted *ZT* value of this material can reach 1.13 at room temperature, an order of magnitude higher than the bulk value. This assumption may be realized through the fine-tuning of grain boundaries by two-dimensional materials (e.g. graphene) in the future.

In terms of technological advances, efforts should continue to intertwine interfacial and local properties characterization tools (e.g. atomic structure of grain boundaries). All-oxide thermoelectric devices should be rationally designed and tested in real-world waste-heat source conditions in air.

Concluding remarks

During these two decades, great efforts have been made in the oxide thermoelectrics field, allowing their *ZT* values to surpass 1. Future work must combine the new crystal/bonding design concept and proper interfacial manipulation to achieve carrier mobility maximization and lattice thermal conductivity minimization. It is no doubt that oxide thermoelectrics are becoming more and more important in the big thermoelectric family. With unique features like good chemical and thermal stabilities, oxide thermoelectric materials and devices are promising candidates for high-temperature thermoelectric applications.

Acknowledgments

5.8. SiGe for thermoelectric energy harvesting

Luis Fonseca[1], Alex Morata[2], Marisol Martin-Gonzalez[3] and Giovanni Pennelli[4]
[1] Instituto de Microelectrónica de Barcelona (IMB-CNM, CSIC), C/Til·lers s/n (Campus UAB), Bellaterra, Barcelona, Spain
[2] Catalonia Institute for Energy Research (IREC), Jardins de Les Dones de Negre 1, 08930, Sant Adrià de Besòs, Barcelona, Spain
[3] Instituto de Micro y Nanotecnología (IMN-CNM-CSIC), C/ Isaac Newton 8, PTM, E-28760 Tres Cantos, Spain
[4] Dipartimento di Ingegneria dell'Informazione, Università di Pisa, Via G. Caruso, I-56122, Pisa, Italy

Status

SiGe is an alloy of semiconductor nature and a very stable material that offers a good thermoelectric figure of merit ($ZT = S^2 \cdot \sigma \cdot T \, \kappa^{-1}$) in the mid-high temperature range. It is the paramount example of the advantages thermoelectricity offers as a solid-state approach to robust, low maintenance and reliable heat harvesters without moving parts, providing long-term, unattended, autonomous supply of energy: Voyager 1 and 2, already in interstellar space (>18 000 million km), are still reporting thanks to the power supplied by them after 40 years of mission.

Back on Earth, SiGe is an environmentally friendly alternative to the materials that require exotic or even toxic elements, e.g. B, Te or Pb-containing materials, which are currently used in the market dominant devices. However, while SiGe systems are much superior to systems based on pure silicon, due to the alloy phonon scattering effect, germanium is not a very cheap material, so that conventional bulk monocrystalline SiGe systems do not offer future prospects for large-scale applications. SiGe belongs to the suite of the silicon family materials, though, and thus can be incorporated into mainstream silicon technology, which is the champion of scalable, miniaturized, and high-density features device making. This is a particularly worth avenue to explore in 'install & forget' IoT scenarios to fulfil the promise of smarter (and more sustainable) environments. In these scenarios heat harvesters could replace primary batteries (or complement secondary batteries) for the provision of the desirable long-term energy autonomy given the widespread of waste heat sources. Since SiGe performance peaks at mid-high temperatures, industrial IoT may be the appropriate market to address.

There are current efforts about going micro and even nano with SiGe. One approach is internally *nanostructuring bulk SiGe* to lower the Ge content, but still preserve or enhance *ZT*, and use it in the assembly of thermoelectric modules with dimensions comparable to commercial Bi_2Te_3 ones. Another, it is engineering it into thinner holey membranes or nanomeshes [343] (e.g. using nanoporous alumina templates), as well as thin films, and low dimensional objects such as nanowires arrays [344, 345] or bundles of *nanotubes* [346], as shown in figure 58. This second approach better suits the silicon integration route and enables the possibility of *on-chip microfabricated thermoelectric generators*.

Current and future challenges

In a microenergy 'harvesting for IoT' scenario, *efficacy* (getting what it is needed from the ambient) prevails over *efficiency* (getting as much as possible). While there is still margin for improvement both at the materials processing level (e.g. optimum doping and nanostructure, homogeneity etc.) and at the device level (e.g. low thermal and electrical contact resistances, reduced thermal strain etc.), the feasibility of *effective* thermoelectric devices based on SiGe is not questioned. The main hindrances to take SiGe technologies out of their niche applications are the high Ge cost and the lack of scalable processing routes.

The integration of SiGe in silicon technologies has been pointed as a solution for mass production, while acutely reducing critical materials usage. The two available routes are Si micro-electromechanical systems (MEMS) and standard complementary-metal-oxide-semiconductor fabrication. In MEMS, *Silicon micromachining* can be used to fabricate silicon microplatforms able to convert vertical temperature gradients into internal lateral ones. These devices feature the so-called transversal architecture where low dimensional SiGe instances can be integrated flexibly [347], as shown in figure 59. Alternatively, *entirely complementary-metal-oxide-semiconductor-compatible* approaches can be used for on-chip thermoelectric generators replicating the π-architecture of standard modules [348]. In this way, scalability of silicon technologies is fully exploited, but the length of the thermoelectric legs is functionally constrained to the range of thickness compatible with planar mainstream technologies.

One of the key points for the progress of thermoelectricity, also the one based in SiGe, is improving the default *performance of the material of choice* by optimizing the (normally mutually depending) magnitudes of *ZT*. Local low dimensionality has been shown to *decrease thermal conductivity* due to phonon scattering without affecting electric conductivity [349]. *Increasing the power factor* ($S^2 \cdot \sigma$) will be much convenient, too.
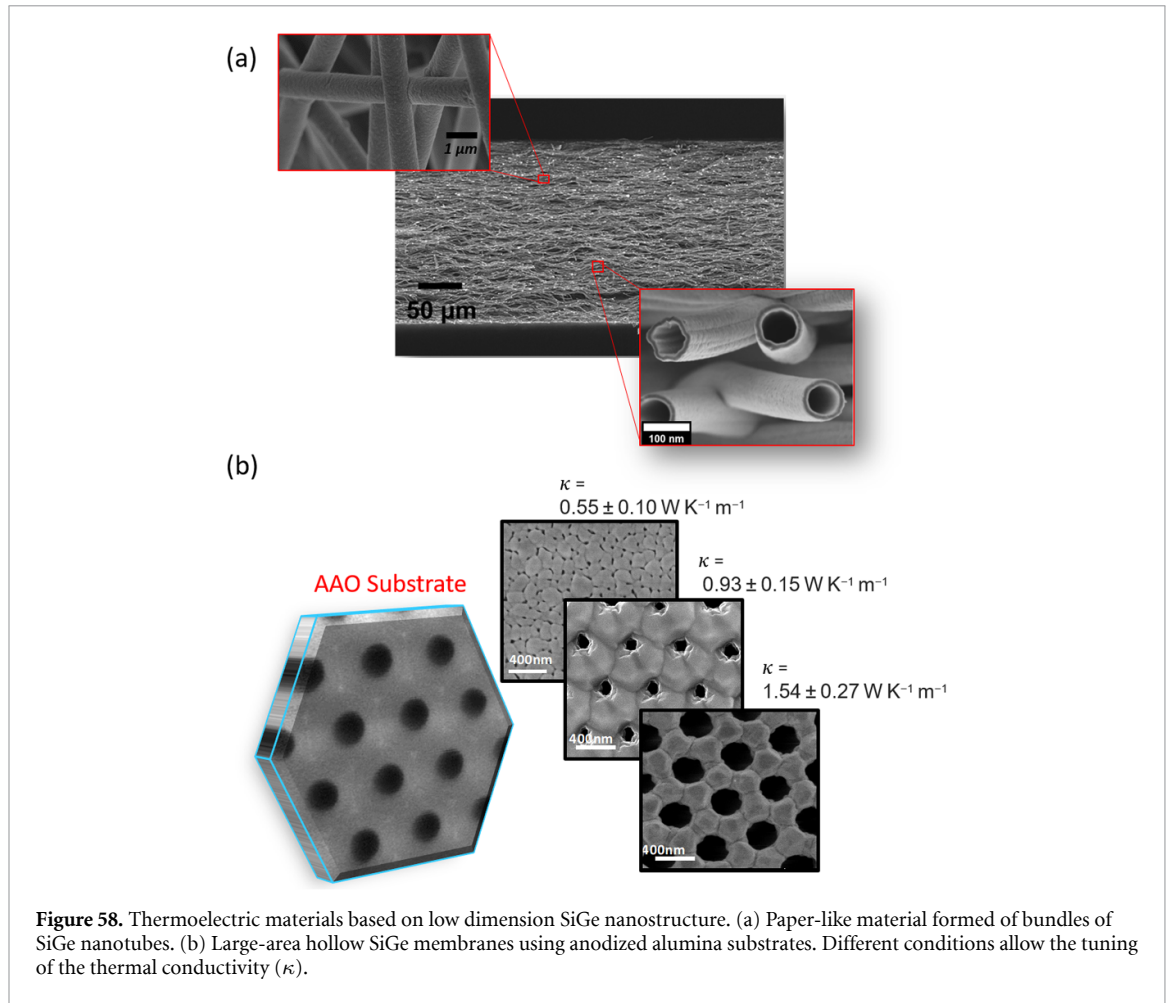
Figure 58. Thermoelectric materials based on low dimension SiGe nanostructure. (a) Paper-like material formed of bundles of SiGe nanotubes. (b) Large-area hollow SiGe membranes using anodized alumina substrates. Different conditions allow the tuning of the thermal conductivity (κ).
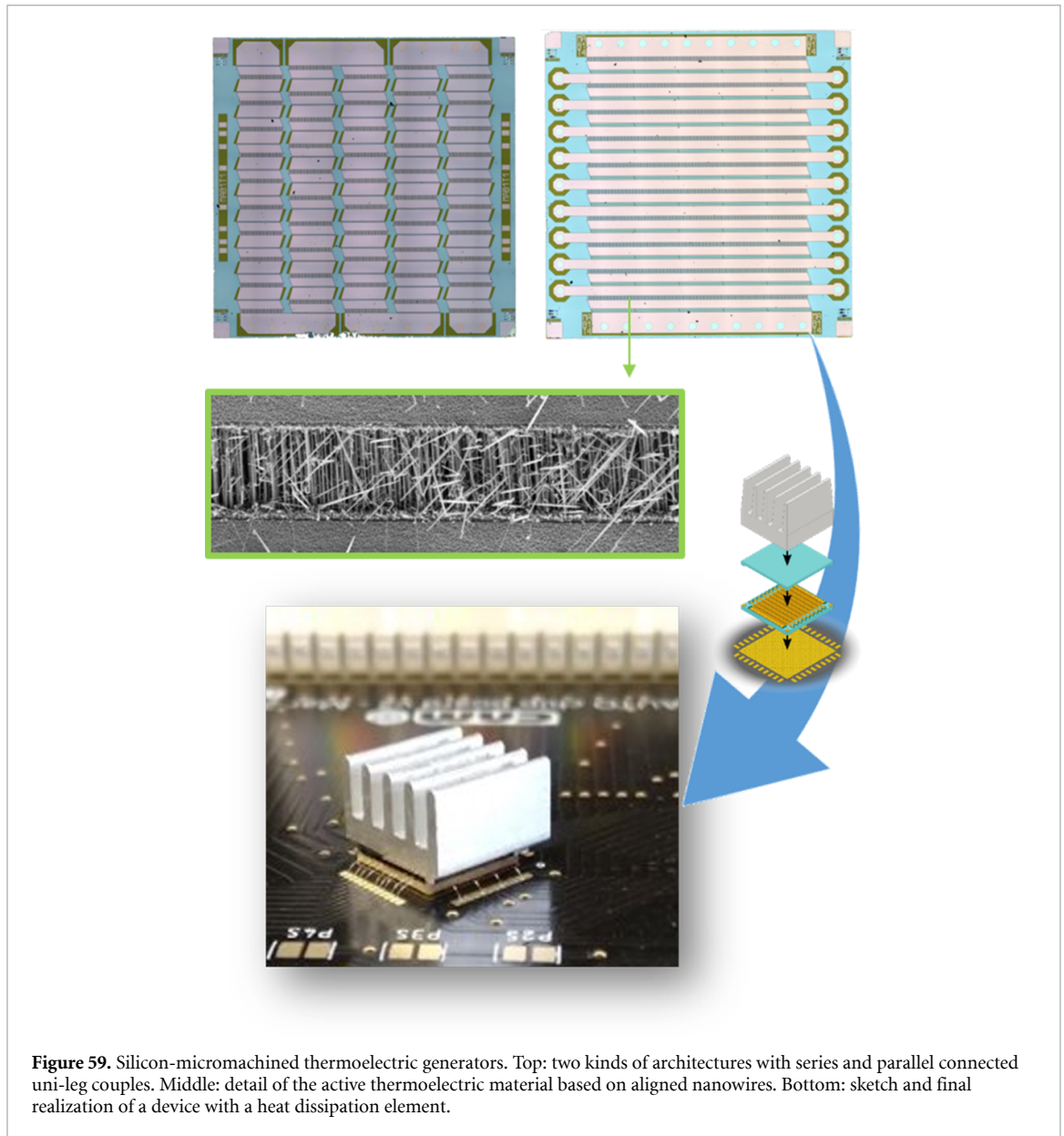
There are many theoretical and experimental advances in science and technology needed to relate material features (e.g. nanocrystallinity, defects, grain boundaries, alloying effects, meshing, metal decoration, and roughness) that could be engineered towards the *energy filtering* of carriers [350] and *phonon suppression* [351] leading to the independent optimization of *ZT* parameters.

Advances in science and technology to meet challenges

Interdisciplinary and complementary skills, ranging from semiconductor physics, chemistry, material science and nanotechnology, to the design, nanofabrication, and (thermal and electrical) characterization of advanced nanodevices and nano-electromechanical systems (MEMS-NEMS) are required to succeed with the design, assembly and testing of SiGe-based prototypes completed with heat exchanger systems for green energy approaches.

Multi-scale, multi-physics modelling of thermal and electrical transport for the different avenues considered is needed. At current stage of development, improving the power factor and decreasing the internal resistance of the device should take precedence over lowering the thermal conductivity, which has a low starting value for SiGe. Theoretical predictions need to be validated. They will provide the precise guidelines for the fabrication of devices with maximized performance, either in micro or macromodule format. Such fabrication needs to be put to a test by defining a feasible *technological route*, using the toolbox of *bottom-up* and *top-down* processes accessible to silicon technologies, integrating the engineered materials into the appropriate architectures to transduce the available thermal gradients into usable power. The new materials and devices need to be characterized with refined versions of standard procedures or adhoc methods that are better adapted to the low dimensionality of the materials.

Of particular importance is the part of the technological route that assures a *good thermal coupling* with the heat source and the heat sink. The exposed surfaces are very small to be cooled off effectively by natural convection, so a *mesoscale assembly of a heat exchanger* is required. For on-chip micromachined approaches, which feature transverse architectures, both hot and cold areas are on the same surface level. This means that the assembly of the heat exchanger needs to be precise and mechanically controlled to make a gentle physical contact only with the cold parts of the suspended platforms [352].

Figure 59. Silicon-micromachined thermoelectric generators. Top: two kinds of architectures with series and parallel connected uni-leg couples. Middle: detail of the active thermoelectric material based on aligned nanowires. Bottom: sketch and final realization of a device with a heat dissipation element.

Concluding remarks

Thermoelectric generators based on nanostructured SiGe materials will eventually offer a wide variety of possible applications in the fields of microenergy harvesting and waste heat recovery. On the material side, they build up on availability, environmental sustainability and stability with aging. On the other hand, combining low-dimensional SiGe material systems with the maturity of silicon technologies paves the way of device integration, miniaturization and production scalability. A long and interdisciplinary route of theoretical and experimental work is still required in order to establish the guidelines that can lead to adequate performance improvements. These advances have to combine low thermal conductivity and high power factor ($S^2 \cdot \sigma$) and must sort out the full chain of nano-micro-meso integration issues that will allow such thermoelectric generators to reach technological maturity and thermally couple to the environment in the most productive way possible.

5.9. Mg₂IV (IV = Si, Ge and Sn)-based systems for thermoelectric energy harvesting

David Berthebaud[1] and Takao Mori[2,3]
[1] CNRS-Saint Gobain-NIMS, IRL 3629, LINK, National Institute for Materials Science (NIMS), 1–1 Namiki, Tsukuba 305–0044, Japan
[2] National Institute for Materials Science (NIMS), WPI International Center for Materials Nanoarchitectonics (WPI-MANA), 1–1 Namiki, Tsukuba 305–0044, Japan
[3] Graduate School of Pure and Applied Sciences, University of Tsukuba, Tennoudai 1-1-1, Tsukuba 305–8671, Japan

Among potential thermoelectric materials for applications, $Mg_2IV(IV = Si$, Ge and Sn)-based compounds have attracted a great deal of interest in the last couple decades as they combine great advantages such as versatility between n and p-type, in addition with their *ZT* value also able to reach unity or above, while they also are relatively light-weight and are composed of low-cost and abundant elements for the silicides and stannides [353, 354]. They usually have been considered to be manufactured as an n-type leg associated with their p-type manganese counterpart; higher manganese silicide (HMS) [355], since until recently the thermoelectric properties of p-type Mg_2IV materials were deemed to be rather low to be implemented in thermoelectric generators [353]. Until the recent advances on p-type Mg_2IV materials, tentative manufacturing of thermoelectric generators was mainly carried out with Mg_2Si-based/HMS modules [355] which is a challenging task due to large differences in the mechanical properties of these two materials, as well as poorer resistance to oxidation under working conditions for the magnesium-based materials. The main disadvantage of using a manganese counterpart [356] to the Mg_2Si-based materials in thermoelectric generator fabrication is their large differences of coefficient of thermal expansion (CTE) which under high temperature differences cause a high level of mechanical stress ultimately leading to the reduction of the thermoelectric efficiency or its complete failure [355]. Various strategies have been considered to address these issues such as for example the fabrication of Mg_2Si unileg structure thermoelectric modules. Since such modules are only made of n-type Mg_2Si legs therefore they did not meet the mechanical failure issues due to CTE differences between n-type and p-type materials [357]. The unileg concept initially drew some interest for industrial application, but was ultimately not propelled forward, as the complex geometry involved in the unileg design appeared to greatly affect the power output of the module in a diminishing way [357]. Fortunately, in the last few years, the improvement of p-type $Mg_2(Si,Sn)$ thermoelectric properties [353] has revived interest in this material system with future hope of fabrication of a fully Mg_2IV-based thermoelectric generator.

Current and future challenges
Even if the future of low-cost, lightweight, fully Mg_2IV-based thermoelectric generators is hopeful, many challenges remain to be overcome and addressed regarding these materials. Among those challenges, the trade-off between the improvement of the thermoelectric properties and the chemical stability, remains one of the most important, as it defines the final power output of the working modules. Indeed, in the Mg_2IV-based materials, in order to control the n-type or p-type behaviour [353] or to achieve high figure of merit [354], complex doping strategy have been used involving for example 3 or 4 different elements on the anionic position [354], which comes with a cost concerning the chemical stability of the materials during working conditions or under temperature cycles, leading to phase segregations or decomposition of the involved materials. Sensitivity of Mg_2X based materials toward oxidation has also been pointed out as an issue preventing these materials to be operable for a long period of time [355]. To address oxidation issues, coatings strategies have been considered to protect Mg_2X against corrosion, such as for example a promising coating based on amorphous silicon oxycarbide SiOC which exhibit good mechanical and chemical stability [358]. If the current challenges concerning chemical stability and efficiency are overcome, large scale synthesis/production of magnesium-based materials will also need to be further addressed. Indeed, magnesium metal can be explosive and flammable, therefore production with fast, safe and efficient methods need to be developed. So far classic solid state chemistry method or mechanical synthesis have shown to be efficient at a laboratory scale but are unpractical at the industrial scale. More exotic production techniques such as self-propagating high-temperature synthesis (SHS) or synthesis under microwave irradiation have been demonstrated as fast and efficient synthesis method, but these methods still come with high uncertainty concerning their reproducibility, up scalability, and safety.

Advances in science and technology to meet challenges

The energetic development and application of various enhancement principles and processes continue to promise further increase in the performance of thermoelectric materials in general. In addition to higher degree of control over various nano-microstructuring, defect engineering, etc to achieve improved selective phonon scattering, better understanding of various band engineering to enhance the Seebeck coefficient, there have recently also been multidisciplinary efforts such as utilizing magnetism to enhance the thermoelectric properties. In this backdrop it is expected that the *ZT* of Mg$_2$IV-based materials themselves will continue to show further improvement. As the different tools for property enhancement increase, it is also hoped that the requirement of stability mentioned above can be satisfied more readily.

The development of Mg$_2$IV-based bulk thermoelectric generators at mid-high temperatures for energy saving is an increasingly important target, because of the recent carbon neutral goals. In regard to the oxidation problem, the further development of protective coatings such as recently demonstrated [358], is a promising direction as mentioned above. As has been reviewed recently [359], the scientific issues and strategies regarding fast and energetically efficient synthesis methods such as solution-based, solvothermal, microwave-assisted, and mechanochemical synthesis are becoming clearer, and hopefully can be applied further for the mass production of the Mg$_2$IV-based materials.

One new applicative direction which is not plagued by the oxidation problems described above, is the relatively low temperature IoT energy harvesting applications [360]. For an elementally abundant, light-weight system, which is starkly in contrast to conventionally used Bi$_2$Te$_3$-type materials, a quite high room temperature power factor of close to 2 mW m^{-1} K^{-2} has been obtained for bulk and thin film Mg$_2$Sn-based materials [361]. Typically, thin film materials exhibit significantly lower electrical conductivity and thereby lower power factors than their bulk counterparts, so this is a promising development. Toward IoT applications, an in-plane miniaturized thermoelectric generator using Mg$_2$Sn-type thin film was constructed utilizing industrially compatible microfabrication techniques of photolithography and dry etching. The microfabricated thermoelectric generator exhibited a relatively high output voltage of 0.58 V and output power of 0.6 mW [362]. Further IoT-oriented developments of the Mg$_2$IV-based systems should continue.

Concluding remarks

The Mg$_2$IV (IV = Si, Ge and Sn)-based systems, especially for the silicide and stannide-based materials, represent attractive thermoelectric systems, for their high *ZT* reaching unity and above, versatility between n and p-type, while being relatively light-weight and composed of low-cost and abundant elements. In this section we have laid out several technological challenges for these materials which are expected to be possible to overcome, and to be a promising material to be applied, not just for the mid-high temperature energy saving power generation, but also energy harvesting to power the innumerable IoT sensors and devices.

Acknowledgments

5.10. Zintl phases for thermoelectric energy harvesting

Robert J Quinn and Jan-Willem G Bos
Institute of Chemical Sciences and Centre for Advanced Energy Storage and Recovery, School of Engineering and Physical Sciences, Heriot-Watt University, Edinburgh EH14 4AS, United Kingdom

Status

Zintl phases can be defined as materials with ionic and covalently bonded substructures [363]. The presence of two types of bonding results from the transfer of valence electrons from electropositive metals to covalently bonded elements. Ideal Zintl phases (e.g. NaSi) are valence precise with all elements achieving either empty (Na^+) or filled valence shells (tetrahedral $[Si_4]^{4-}$ clusters). This directly leads to semiconducting behaviour, a key requirement for good thermoelectric properties.

Many of the known good thermoelectric materials, including the clathrates, half-Heuslers and skutterudites discussed elsewhere in this roadmap can be understood within the Zintl concept. The term Zintl thermoelectrics is, however, largely synonymous with antimonide materials [363, 364]. Sb-based thermoelectrics first generated attention in the early 2000s and have $ZT > 1$ values for a wide range of compositions, as summarized in figure 60. $Yb_{14}MnSb_{11}$ (p-type) is one of the best materials for high temperatures, whilst n-type $Mg_3(Sb/Bi)_2$ is competitive with Bi_2Te_3 near room temperature. Lower mass compositions based on P are starting to attract attention [365], whilst As is likely of limited use due to its toxicity. Alloying with heavy Bi has been exploited to introduce mass disorder and to manipulate the electronic band structure. However, there are relatively few Bi-based Zintl compounds reported in structural databases.

The first widely investigated high-ZT compositions were Zn_4Sb_3 and $Yb_{14}MnSb_{11}$, achieving $ZT = 1.3$ at 670 K and at 1220 K, respectively (figure 60) [368, 370]. Both materials have complex structures with low lattice thermal conductivity, enabling good ZT values from modest power factors $S^2/\rho = 0.5–1.5$ mW m^{-1} K^{-2}. $Yb_{14}MnSb_{11}$ has a large unit cell, leading to many optical phonon modes with low heat propagation. Zn_4Sb_3 is non-stoichiometric and contains interstitial Zn atoms that effectively reduce the thermal conductivity through structural disorder. Both materials have been the subject of intensive optimization studies but are limited by their unique structures that limit the possibilities for chemical substitutions. By contrast, the layered AZn_2Sb_2 (A = Ca, Sr, Ba, Eu, Yb) phases are a large class of materials that offer wider opportunities for electronic and phonon engineering, achieving peak $ZT = 1.2$ at 700 K in samples with designed p-orbital degeneracy (figure 60) [369]. The most recent breakthrough in the field of Zintl thermoelectrics is the discovery of high $ZT = 1.5$ at the relatively low temperature of 650 K in n-type Mg_3Sb_2 in 2016 (figure 60) [367, 371]. This was remarkable because Mg_3Sb_2 usually forms as a p-type material and careful control of the defect chemistry was required to achieve this. Current optimized Bi-rich compositions approach $ZT = 1$ at room temperature (figure 60) and may be a possible replacement for Bi_2Te_3. This is an exciting development, both for ambient temperature waste heat harvesting and thermoelectric cooling [366].

Current and future challenges

The reported ZT and power factors (S^2/ρ) can be used to estimate an upper limit on power output and efficiency of harvesting devices [372]. This is based on the 'leg' performance of a single material with the performance reduced in generators, e.g. due to the imperfect matching of n- and p-type legs, parasitic losses due to electrical and thermal contacting, and the reduced fill fraction needed to avoid contact between legs. An overview of calculated power outputs and efficiencies for near ambient harvesting (300–310 K) and up to the stability limit of the materials is given in figure 61. This shows that high efficiencies are possible for large temperature differences, and that $Mg_3(Sb/Bi)_2$ is promising for near ambient harvesting, both in terms of efficiency and power output. The relatively modest power output of the Zintl materials reflects the dominant impact of a low thermal conductivity, which in combination with modest S^2/ρ, enables the observed high ZT values. Improving the electrical properties, whilst maintaining $ZT,$ would enable improved device power at comparable efficiency.

Two key challenges are to improve ZT and the power output of the Zintl materials and to find matched n- and p-type pairs for use in generators. Achieving better power factors is linked to finding optimal electronic structures, enabling high mobilities and large Seebeck coefficients, and control of doping levels. Controlling the carrier-type is often difficult due to the presence of compensating 'killer' defects. In the layered 122 phases, first principles calculations guided the preparation of band converged compositions, leading to increased power factors [369]. In Mg_3Sb_2, calculations identified a favourable conduction band structure with a highly degenerate pocket away from the usual high-symmetry directions, which underpins the outstanding n-type performance [367, 371]. Progress has been made in controlling n-/p-type doping though
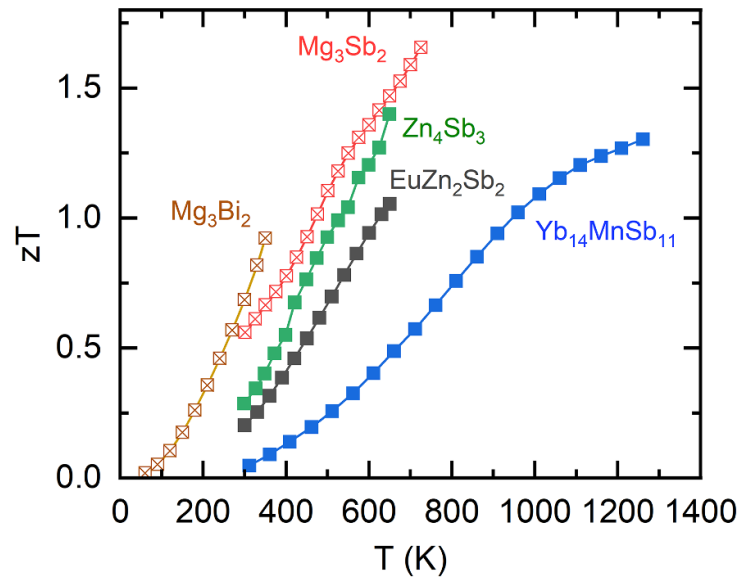
Figure 60. Thermoelectric figure of merit (*ZT*) for high performance Sb-based Zintl phases. Mg_3Bi_2 (n-type) $= Mg_{3.2}Bi_{1.28}$ $Sb_{0.7}Te_{0.02}$ [366]; Mg_3Sb_2 (n-type) $= Mg_3Sb_{1.48}Bi_{0.48}Te_{0.04}$ [367]; Zn_4Sb_3 (p-type) $= (Zn_{3.98}Pb_{0.02}Sb_3)_{0.97}(Cu_3SbSe_4)_{0.03}$ [368]; $EuZn_2Sb_2$ (p-type) $= EuZn_{1.8}Cd_{0.2}Sb_2$ [369]; $Yb_{14}MnSb_{11}$ (p-type) $= Yb_{14}Mn_{0.2}Al_{0.8}Sb_{11}$ [370].
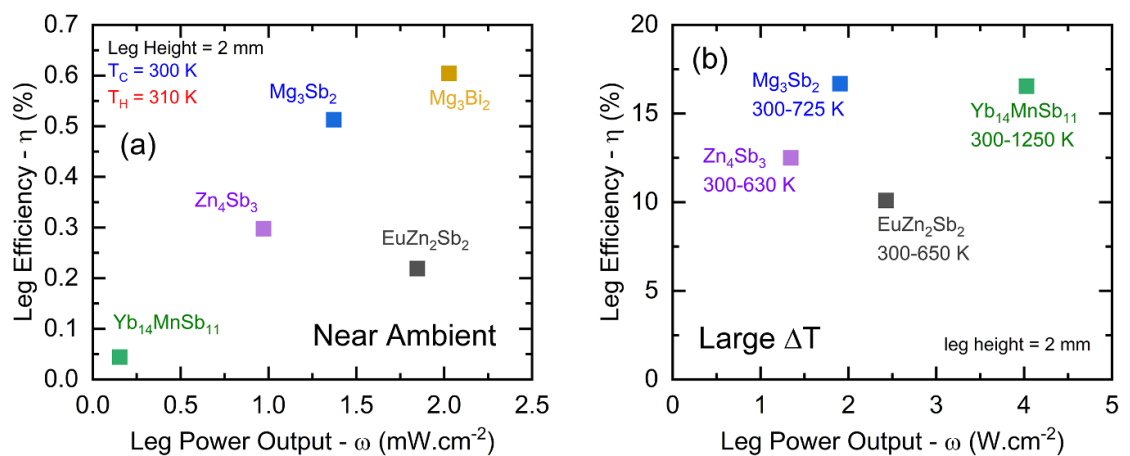

Figure 61. Calculated leg efficiencies and power outputs for the Sb-based Zintl compositions shown in figure 60. Panel (a) shows calculated values for utilization of a 300–310 K gradient. Panel (b) shows leg efficiencies and power outputs up to the stability limit of the materials. Note that these values will be substantially reduced in generator devices and only reflect an upper limit on performance (based on the properties of a single material).

improved materials growth, guided by defect chemistry calculations. This is illustrated by n-type Mg_3Sb_2: as grown, this composition is p-type, and it is difficult to access n-type compositions due to the presence of compensating Mg vacancy acceptor defects. The synthetic innovation was to grow the materials in Mg-rich conditions [371], which suppresses formation of Mg vacancies, enabling the material to be n-type doped through chemical substitution.

Advances in science and technology to meet challenges

The challenge in discovering the next generation of ultra-high performance Zintl phases is like other classes of thermoelectrics. At the fundamental level this boils down to finding materials that have highly favourable electronic and phonon band structures, and that allow for synergistic optimization of the individual thermoelectric parameters. To some extent this is exemplified by the band engineered AZn_2Sb_2 phases and Mg_3Sb_2 [367, 369, 371], where calculations were used to guide experimental work. At a lower level of accuracy first principles calculations are used to screen structural databases and electronic band structures of materials are now readily available (e.g. from the Materials Project). The next step is to combine this with electronic transport calculations that go beyond the constant relaxation time approximation, enabling better predictions of S^2/ρ. *Ab initio* calculation of the thermal conductivity remains challenging but access to

calculated elastic properties and velocity of sound data is a useful proxy for materials selection. Another area where first principles calculations can have a big impact is in the area of defect energetics. Here energy calculations can be used to identify favourable growth conditions (suppressing compensating defects) that enable highly controlled and targeted carrier doping. This has the potential to greatly reduce the amount of experimental work, especially for chemical systems with many components. From the experimental side, control of defect energetics in the Ca–Zn–Sb system has been explored, leading to a doubled $ZT = 1.1$ at 875 K for $Ca_9Zn_{4+x}Sb_9$ [373]. A notable feature of recent work is that many high-performance materials have been prepared by a route involving mechanical milling/alloying followed by rapid consolidation [366, 367, 371]. Further work developing alternative routes for materials growth, including low-temperature routes targeting metastable phases, is highly desirable. Another challenge that was highlighted by Mg_3Sb_2 is the need to identify and eliminate grain boundary resistances, which can be achieved by exposure to Mg vapour [374]. This approach was directed by atom probe tomography that showed Mg deficiencies at grain boundaries, illustrating the need for detailed structural analysis to fully understand and optimize materials. Finally, there is a clear need for continued materials discovery, expanding the library of Zintl compounds and testing their properties.

Device fabrication and testing is the final step in the validation of a thermoelectric material. Several Zintl phases have been tested in laboratory generator test devices (e.g. p-type $Yb_{14}MnSb_{11}$ and Zn_4Sb_3, and n-type Mg_3Sb_2) [366]. None are currently commercially applied and there is a need to develop matching n- and p-type pairs, including in terms of performance, mechanical properties and stability. The low thermal conductivity of Zintl phases is compatible with small temperature gradients in harvesting, whilst some of the difficulties of contacting Sb-based materials have been resolved in the extensive work on skutterudite generator modules.

Concluding remarks

Major advances have been made since the first investigations in the early 2000s and a range of high-performing Zintl phases is available as illustrated in figures 60 and 61. Based on efficiency, the Zintl phases are amongst the leading thermoelectric materials and further work is therefore warranted. This should also focus on non-Sb systems, in particular phosphides that may support good electrical properties.

Acknowledgments

5.11. Molybdenum-based cluster chalcogenides as high-temperature thermoelectric materials

Christophe Candolfi[33], Patrick Gougeon[2], Philippe Gall[2] and Bertrand Lenoir[33]
[1] Institut Jean Lamour, UMR 7198 CNRS – Université de Lorraine, 2 allée André Guinier-Campus ARTEM, BP 50840, 54011 Nancy Cedex, France
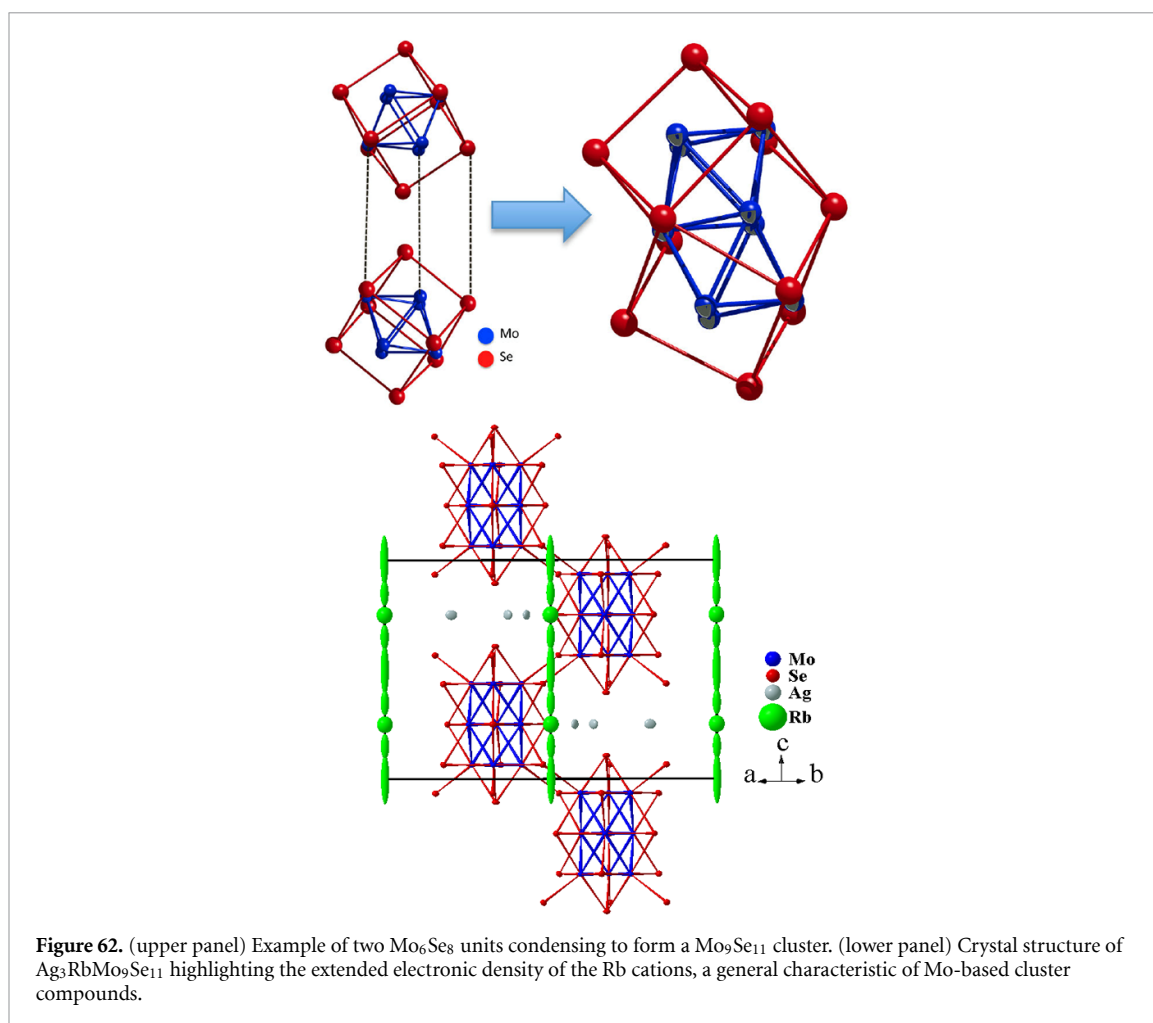[2] Institut des Sciences Chimiques de Rennes, UMR 6226 CNRS – Université de Rennes 1 - INSA de Rennes, 11 allée de Beaulieu, CS 50837, F-35708 Rennes Cedex, France

Status

Thermoelectric materials provide a versatile way to convert waste heat into electrical power from room to high temperatures. While most of them reach their optimum efficiency between 500 and 700 °C, only a handful are able to operate beyond due to their limited thermal stability and/or melting point. Over the last two decades, several rare-earth-containing Zintl phases were demonstrated to outperform the state-of-the-art $Si_{1-x}Ge_x$ alloys used in space applications [375–378]. Identifying novel materials with high thermoelectric performance and high melting points is desirable for both terrestrial and space applications. While the former would benefit from higher temperature differences yielding enhanced output power, such materials would also allow to reduce the amount of radioisotope heat-source fuel embarked in spacecrafts. In this context, Mo-based cluster compounds are particularly appealing due to their very high melting points, typically above 1800 °C, and their promising thermoelectric properties [379–384], as first pointed out in Chevrel phases [383]. The crystal structure of these compounds are built up by a three-dimensional arrangement of $Mo_{3n}X_{3n+2}$ clusters ($X = $ S, Se or Te; n is an integer), the size and geometry of which can vary from 3 to more than 36 atoms. The intercluster voids can be filled by various cations such as alkali (Li, Na, K, Rb or Cs), alkaline-earth (Ba) or transition metals (Ag, In, Fe, Ti or Cu) with a strongly disordered character (figure 62). Additional inserted cations (Ag or Cu) contribute to both tuning the p-type electronic properties and lowering the lattice thermal conductivity down to extremely low values on the order of 0.3–0.5 W m^{-1} K^{-1} at high temperatures (figure 63) in several compounds such as $Ag_xMo_9Se_{11}$ ($3.4 \leq x \leq 3.9$), $Ag_2Tl_2Mo_9Se_{11}$, $Ag_3RbMo_9Se_{11}$ or $Ag_3In_2Mo_{15}Se_{19}$ [379–382]. With these values being similar to those achieved in the best-performing p-type Zintl phases, improving the power factor of quaternary molybdenum chalcogenides through a careful selection of inserted cations and band-structure-engineering tools (resonant levels, band convergence etc.) offers interesting prospects to design rare-earth-free compounds with thermoelectric performance rivalling the best thermoelectric materials operating above 900 °C.

Current and future challenges

The key advantages of these phases—chemical richness and flexibility, high melting points, inherently poor thermal conductors—are counterbalanced by several drawbacks that need to be addressed in future works. A first difficulty is related to the complex synthesis route required to produce phase-pure samples, which usually involves high-temperature solid-state reactions of powdered, mixed binary or ternary precursors followed by ion-exchange reactions to insert alkali or alkaline-earth elements. This complexity in the synthesis process contrasts with more direct, time-efficient techniques typically employed such as powder metallurgy or high-energy ball-milling. Whether some of these cluster materials can be obtained in high yield by such techniques remain to be investigated. A second challenge to address is tied to their lower thermoelectric performance with respect to optimized Zintl phases, with maximum ZT values remaining limited to 0.7 at 800 K [379–382] due to their moderate power factors. Being inherently p-type metals, inserting cations drives the electronic properties towards a highly-doped semiconducting state. However, the hole concentrations achieved remain too high which, combined with the multiband character of transport, contributes to lower the thermopower values. Further adjustment of the hole concentration through aliovalent substitutions or insertions will be important to make them competitive with Zintl phases. Although rare examples of n-type Mo cluster compounds have been reported [384], the fundamental question of n-type dopability remains another issue that will require more thorough investigations. In addition to these materials-related issues, their integration into thermoelectric legs will also face challenges. While most of these materials are relatively immune against sublimation up to the sintering temperature (1000 °C–1200 °C), they remain sensitive to oxidizing atmospheres, as the vast majority of thermoelectric materials. Efforts to determine their aging behaviour in such environments and in contact with other types of materials used in thermoelectric generators will be worthwhile to fully assess their potential for power generation applications.
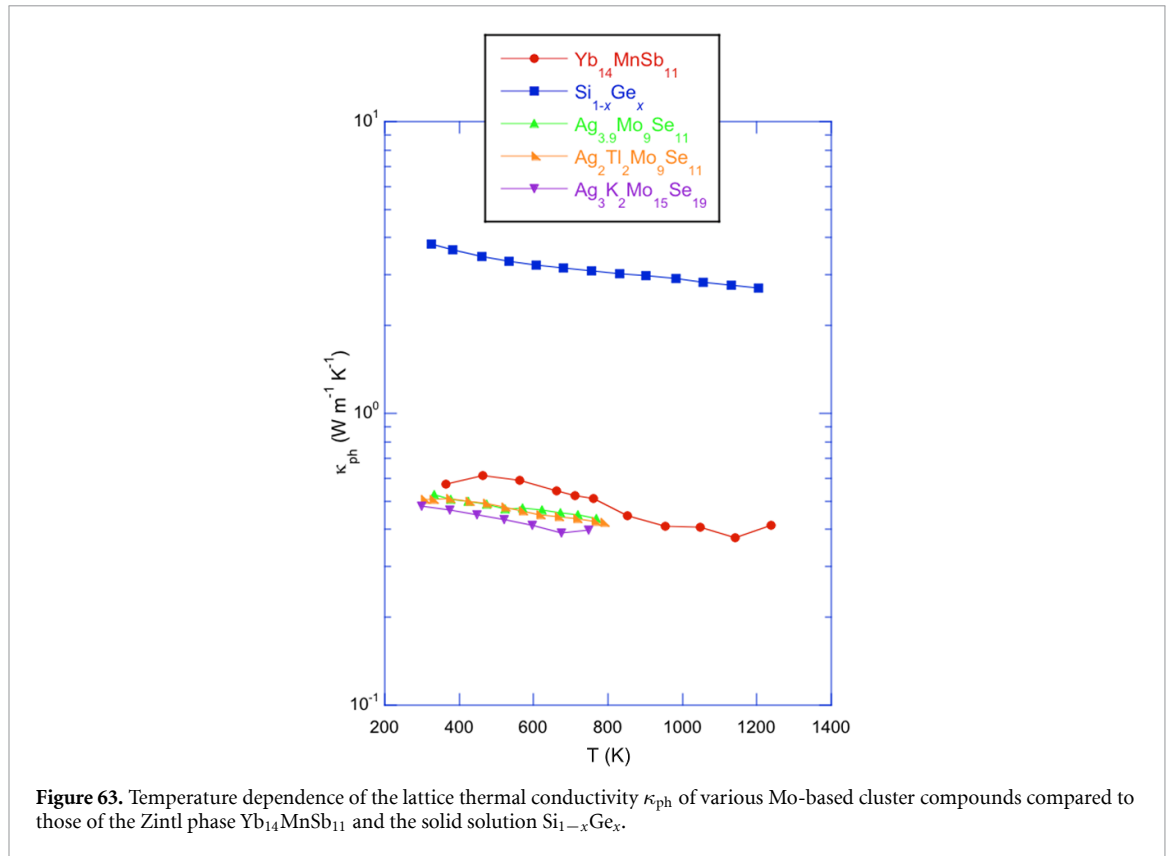
Figure 62. (upper panel) Example of two Mo_6Se_8 units condensing to form a Mo_9Se_{11} cluster. (lower panel) Crystal structure of $Ag_3RbMo_9Se_{11}$ highlighting the extended electronic density of the Rb cations, a general characteristic of Mo-based cluster compounds.

Advances in science and technology to meet challenges

Overcoming the above-mentioned challenges will be facilitated by the recent progress realized in the synthesis of complex thermoelectric materials and their integration into devices. High-energy ball milling may be employed to synthesize various precursors prior to a second annealing step of mixed powders. Alternatively, efforts should also be devoted to replace this second, time-consuming step by a direct ball-milling reaction. A successful synthesis of these cluster compounds by this technique would speed up the identification of novel phases with potentially superior thermoelectric properties, thereby contributing to address the second challenge related to their still moderate *ZT* values. Deploying the arsenal of band-structure-engineering tools will be an interesting line of research to pursue in parallel, which will require electronic band structure and transport property calculations as a theoretical guide. An inherent difficulty of such calculations is the proper modelling of the cationic disorder that characterizes these compounds. Recent efforts towards this goal have shown a good agreement between the thermopower values computed and the experimental data. Further calculations will allow for a full screening of the rich landscape of possible chemical compositions, offering valuable insights into the most judicious dopants and cations to be investigated. Detailed characterizations of the thermal stability of these materials under oxidizing atmospheres and under vacuum should be performed using state-of-the-art techniques. This will enable to determine the temperature range over which these materials are thermally stable with respect to mass loss and oxidation. Finally, first attempts to fabricate thermoelectric legs would be worthwhile to identify the main issues to be solved for the development of p-type, and possibly n-type, legs. This might require the identification of diffusion barriers and braze to minimize the electrical contact resistance and the thermomechanical stresses undergone under operating conditions. In this regard, determining the mechanical properties of these materials will be necessary.

Concluding remarks

With the remarkable ability for crystalline materials to poorly conduct heat and high melting points, multinary molybdenum cluster chalcogenides offer an interesting playground to design and optimize novel phases for thermoelectric applications at very high temperatures. Despite the growing number of studies

Figure 63. Temperature dependence of the lattice thermal conductivity κ_{ph} of various Mo-based cluster compounds compared to those of the Zintl phase $Yb_{14}MnSb_{11}$ and the solid solution $Si_{1-x}Ge_x$.

devoted to these materials, the surface of the vast landscape of chemical compositions has only been barely scratched. Further manipulating the types of clusters and cations inserted may open up new avenues for achieving improved *ZT* values. Solving issues identified herein will pave the way to the development of rare-earth free, highly efficient Mo cluster compounds that can be integrated in thermoelectric generators for both space and industry-related applications.

Acknowledgments

5.12. Organic thermoelectrics

Deepak Venkateshvaran[1] and Bernd Kaestner[2]
[1] Cavendish Laboratory, University of Cambridge, JJ Thomson Avenue, Cambridge, CB3 0HE, United Kingdom
[2] Physikalisch-Technische Bundesanstalt (PTB), Abbestrasse 2–12, 10587, Berlin, Germany

Status

Organic semiconductors are relevant for applications in thermoelectrics owing to their low thermal conductivities (κ), relatively large and tuneable Seebeck coefficients (S) and their ability to conduct charge carriers with reasonably high electrical conductivities (σ). Since the thermoelectric figure of merit is defined as $ZT = \left(\frac{S^2 \sigma}{\kappa} \right) T$, an organic semiconductor having $\kappa = 0.3$ W m^{-1} K^{-1} and a power factor $S^2 \sigma \sim 10^{-3}$ W m^{-1} K^{-2} should effortlessly demonstrate the benchmark figure in thermoelectrics of $ZT \sim 1$ at 300 K [385]. Experimental evidence shows that such values of the thermal conductivity and the power factor lie within the parameter space accessible by organic semiconductors, justifying their search in the effort to maximize ZT.

An organic semiconductor's low thermal conductivity arises from the intrinsic nature of van der Waal's bonding and molecular vibration-induced phonon scattering. Their large Seebeck coefficients (i.e. several times $\frac{k_B}{e}$) are a consequence of configurational entropy, and their electrical conductivities spur from rapid hopping of charge carriers along the polymer backbone, along the inter-molecular $\pi - \pi$ stacking direction, or along both simultaneously. The hopping rates are influenced by intra-molecular torsion as well as disorder in the manner molecules pack within the solid state. A picture that connects both molecular conformation and structural properties with the thermoelectric transport coefficients is starting to evolve [386]. Such an interdependence demands comprehensive investigation and validation through the design of new organic molecules. Figure 64 shows the power factors of a selection of organic semiconductors as a function of their conductivity [387, 388]. The heuristic trend is clear; an increasing electrical conductivity gives rise to an increasing power factor.

By modulating the carrier density, n, over three orders of magnitude from 10^{18} to 10^{21} cm^{-3}, the Seebeck coefficient of an organic semiconductor decreases from 100 s of μV K^{-1} to 10 s μV K^{-1}. Its electrical conductivity increases by several orders of magnitude over the same range. The boost in the power factor got by increasing the electrical conductivity in these soft electronic systems is known to outweigh the accompanying reduction in the Seebeck coefficient. For this reason, the last few years have focused on charge carrier doping as a route to increase the power factor, and thus ZT of organic semiconductors.

Current and future challenges

1. An understanding of the transport coefficients κ, S and σ, and their influence on the power factor continues to rapidly develop. Empirical trends such as $S \propto \sigma^{-\frac{1}{4}}$ and $S^2 \sigma \propto \sigma^{\frac{1}{2}}$ have been found, but a foundational description of why these scaling laws arise is still lacking [389]. In addition, although polaronic transport theories at high charge carrier densities are known to explain the behaviour of the Seebeck coefficient and the power factor in the 'near-degenerate' transport regime, more experimental evidence is necessary to validate their use. In general, S decreases with increasing n, and σ is proportional to both n and the carrier mobility μ. Thus, increasing μ beyond its current benchmark of 1 cm^2 Vs^{-1} is another prospective route to increasing the overall power factor [390]. Progress in this direction has been sluggish.

2. Efficient doping techniques that guarantee increases in the charge density of organic semiconductors are currently possible only through the incorporation of additional dopant molecules within the lattice. This can cause changes to the rigidity of molecular packing [385, 386]. In other words, the original organic system needs to gradually distort to be able to show improved thermoelectric performance. In so doing, the pristine properties of the original semiconductor are not preserved.

3. Very high carrier densities upon doping instil 'metallic transport' properties in organic semiconductors. This causes its thermal transport to sport a strong electronic contribution in addition to its lattice contribution. Although intermediate doping densities under controlled conditions can preserve a low thermal conductivity, such is not the case for very high electrical conductivities [391]. The simultaneous increase in the electrical and thermal transport coefficients in the organic semiconductor imposes a limit on the maximum achievable ZT. The common belief that organic semiconductors can embody a 'phonon-glass electron-crystal' necessary for high-performance thermoelectrics is thus invalidated at very high carrier densities [385]. One workaround in overcoming the intrinsic limits to ZT within organic systems is to actualize 'phonon stack electron tunnel composites' using selective interfaces [390]. In such
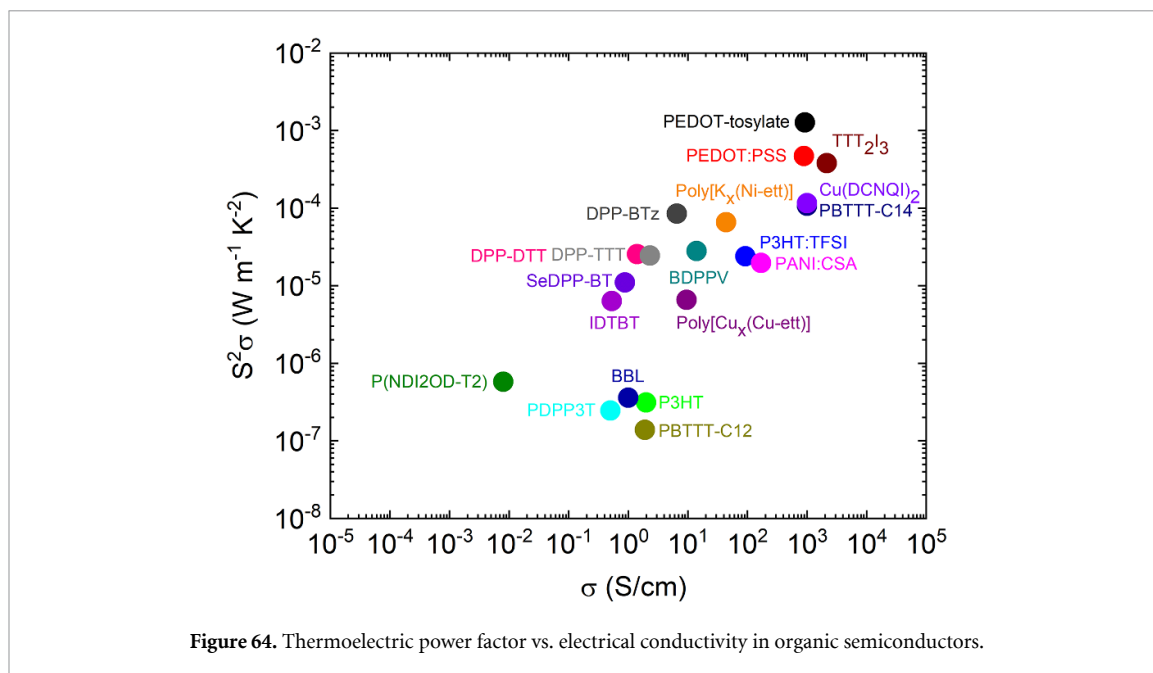
Figure 64. Thermoelectric power factor vs. electrical conductivity in organic semiconductors.

composites, conductive carbon nanotubes are incorporated within the matrix of organic semiconductors to ensure that charge carriers preserve high mobility pathways through carbon nanotubes. Phonons on the other hand continue to be scattered, ensuring reduced thermal conductivities [392].

4. There is also a lack of stable, high-performance, n-type organic thermoelectric materials beyond the fullerenes, which makes impedance-matched all-organic thermoelectric generators very complex to realize.

5. Evolving the optimum properties for thermoelectric conversion within single-component organic films, without the incorporation of additional dopant molecules or without building carbon-based composites, remains a challenge. One way to preserve the compositional purity of organic semiconductors for science and applications of heat to voltage conversion is to augment ongoing research (that focuses majorly on *ZT* optimization) with novel devices and measurement techniques that use the efficient heat flow within molecular films under infrared vibrational resonance [393]. Doing so unravels the nature of thermal transport within molecular systems and evolves new applications of organic polymers in ultrafast bolometers and nanoscale heat switches.

Advances in science and technology to meet challenges

To probe the scattering characteristics of electrons and phonons within composite micro- and nanoscale organic polymer matrices, as well as within semicrystalline polymer films containing grain boundaries, advanced metrology tools need to be developed. Performing measurements on composite materials is a challenge because of the sample complexity and the requirement for doing measurements with very high spatial, temporal, and energy resolution. Complex device geometries such as organic-inorganic multilayer structures can make use of multi-modal analytic tools like Infrared Scanning Nearfield Optical Microscopy (IR-SNOM), which when employed within the spectral region containing molecular fingerprints, permits chemical and crystallinity characterization [393]. IR-SNOM also makes contactless electrical characterization possible over a limited conductivity range. Despite having a wavelength range in micrometres, its spatial resolution is not sacrificed since it is governed by the tip geometry. Hence, such a multi-modal tool can be used in understanding the role of grains and domain boundaries within thin films for thermoelectrics. It also allows one to characterize time-resolved degradation phenomena that are expected to start at the grain boundaries simultaneously with their influence on electronic transport.

For accurately mapping the temperature distribution in organic semiconductors, techniques such as Scanning Thermal Microscopy (SThM), Time Domain Thermoreflectance or Frequency Domain Thermoreflectance can be used. Thermoreflectance makes use of the change in the reflectance of the surface upon heating to derive the thermal properties. The probe in SThM is sensitive to local temperatures, and therefore acts like a nano-scale thermometer. SThM measures the local thermal conductivity with an uncertainty of 20% for low thermal conductivity materials at room temperature. The spatial resolution can be down to a few tens of nanometres. Thermoelectric characterization using raster-scanned lasers also have sub-wavelength, nanometre-scale resolution, as demonstrated using near-field enhancement of metallized

scanning probes [394]. The above techniques make possible an evaluation of the thermoelectric transport coefficients within single ordered domains, without the drawbacks presented by domain boundaries in polycrystalline films.

Concluding remarks

$ZT = 1$ is yet to be demonstrated in the field of organic thermoelectrics. Despite tremendous progress at characterizing various macromolecular systems over the last decade, several roadblocks continue to prevail. These roadblocks are linked to factors such as dopant stability, doping efficiency, control of microstructure and molecular conformation, a limit on the achievable charge carrier mobility, a lack of sufficient competitive n-type organic materials, a difficulty in describing transport within disordered systems having an abundance of domain boundaries, and the absence of strategies which decouple σ from κ at large carrier densities. Consistent and precise measurements of thermoelectric transport coefficients at the nanoscale and molecular scale are only starting to be pursued. Such techniques might ultimately yield the clarity required to build a framework to understand and describe the fundamental limits on thermoelectric efficiency using organic semiconductors and organic semiconductor-based hybrids.

Acknowledgments

5.13. Two-dimensional materials for thermoelectric applications

Yunshan Zhao[1] *and Gang Zhang*[2]
[1] NNU-SULI Thermal Energy Research Center (NSTER) and Center for Quantum Transport and Thermal Energy Science (CQTES), School of Physics and Technology, Nanjing Normal University, Nanjing 210023, People's Republic of China
[2] Institute of High Performance Computing, A*STAR, Singapore 138632, Singapore

Status

Although the commercial bulk thermoelectric materials were well developed around 1960s, the research interest in low-dimensional thermoelectrics traces back to 1990s, where the effect of quantum-confinement was proposed to modulate the thermoelectric coefficients in a nearly independent way [395]. Among the low-dimensional materials for thermoelectric energy harvesting, the family of two-dimensional materials is one of the largest and latest groups, which becomes the subject of intense study in last decade.

In contrast with the traditional bulk thermoelectric materials, two-dimensional materials represent a discretized electron density of states due to the quantum size effect [395], which is beneficial for an enhanced Seebeck coefficient [396, 397]. In bulk forms, the charge carriers are normally introduced during the process of materials growth, while for two-dimensional materials, the carrier concentrations could be easily tuned by intercalating ions or an electric gating. Meanwhile, layered two-dimensional materials can be exfoliated into few layers, with a dimension close to the mean free paths of phonons, therefore, the electrical conductivity or thermal conductivity could be tuned individually. Moreover, the bandgap of two-dimensional materials is easily tuned by the strategy of 'thickness engineering'. All of these advantages of two-dimensional materials are beneficial for a high ZT [396, 397].
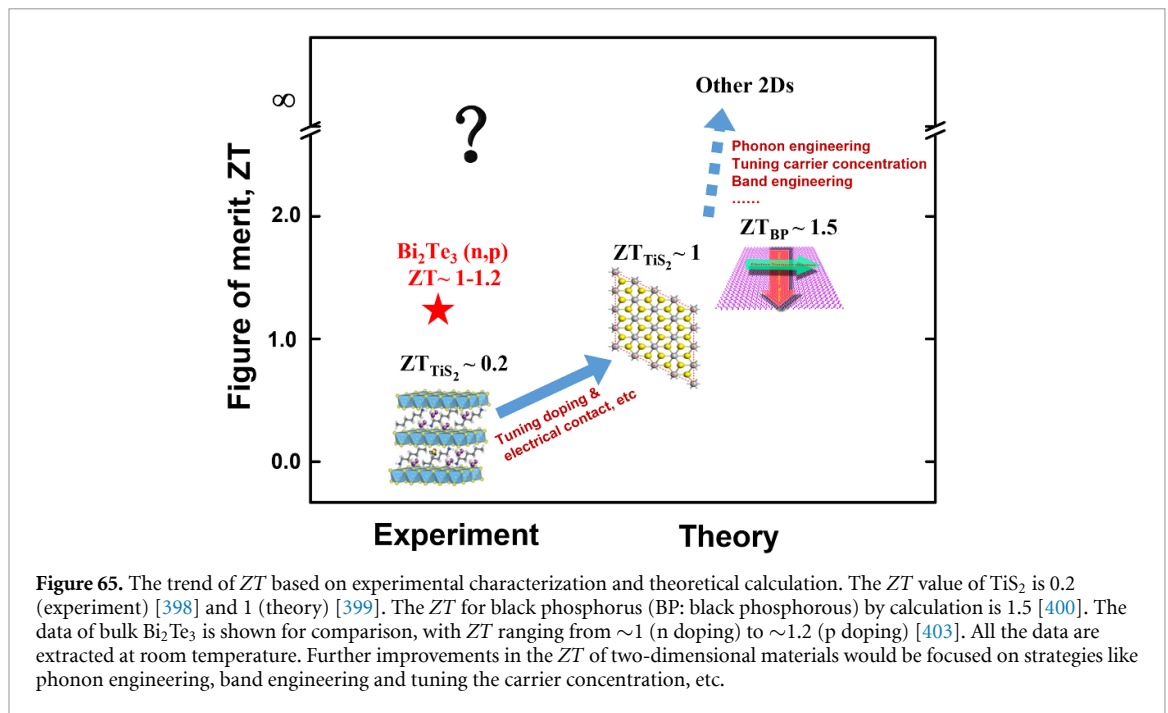
Current and future challenges

With the advancement of nano-fabrication and nano-characterization, a series of thermoelectric devices based on two-dimensional materials have been developed and investigated, showing outstanding thermoelectric energy conversion potential, such as TiS_2 with a ZT value 0.2 [398] at 300 K, which is nearly comparable to that of bulk thermoelectric forms at room temperature. While for even higher temperature regime that bulk thermoelectric materials typically outperform, there is lacking experimental data related to the thermoelectric performance of two-dimensional materials.

Currently, strategies of exploring two-dimensional thermoelectric materials are dominated by theoretical calculations and simulations. By constructing a monolayer lattice structure, S, σ and κ can be obtained through atomistic simulations, and the optimized ZT is achieved, like TiS_2 [399] and BP [400] with ZT values around 1 and 1.5, respectively, as shown in figure 65. Compared to the theoretical high ZT under a much high carrier concentration, the current experimental treatments like top- or back-gate are insufficient to achieve a high charge concentration in the system, thus the optimization of ZT in two-dimensional materials is far from being satisfactory for potential applications. Some experimental approaches like thickness engineering, tunability of carrier scattering mechanisms and defects engineering [401, 402] are proposed, while the tunability of thermoelectric conversion efficiency is limited.

Moreover, there is lacking study for the measurement of each ZT parameter, especially for the evaluation of power factor. A high ZT value and thus improved heat-to-electricity energy conversion efficiency is the key challenge for two-dimensional thermoelectric materials in the current and future study. Since the thermoelectric performance of two-dimensional materials is based on field-effect-transistor devices, a better electrical ohmic contact is desirable to extract the intrinsic transport property of the measured materials. On the other hand, considering the sensitivity to environment and super tiny scale of each thermoelectric device based on two-dimensional materials, their integration into thermoelectric units is another key consideration for their practical use. Further advances on two-dimensional thermoelectric materials should be focused on the design of new materials and new contacts to achieve optimal thermoelectric properties. Physically, the phonon and electron transport mechanisms in two-dimensional materials should be clarified as well to further manage their contributions in ZT.

Advances in science and technology to meet challenges

Following graphene, numerous two-dimensional materials with unique transport properties have been discovered. The family of two-dimensional materials and the subsequent in-plane and out-of-plane heterostructures provide a new platform to explore thermoelectric performance. Among them, two-dimensional semiconductors with a tunable bandgap and high electron/hole mobilities have shown superior thermoelectric properties [396, 397], which even disgraces the thermoelectric performance of bulk forms in the low temperature range. These two-dimensional semiconductors with rich physical properties

Figure 65. The trend of *ZT* based on experimental characterization and theoretical calculation. The *ZT* value of TiS$_2$ is 0.2 (experiment) [398] and 1 (theory) [399]. The *ZT* for black phosphorus (BP: black phosphorous) by calculation is 1.5 [400]. The data of bulk Bi$_2$Te$_3$ is shown for comparison, with *ZT* ranging from ∼1 (n doping) to ∼1.2 (p doping) [403]. All the data are extracted at room temperature. Further improvements in the *ZT* of two-dimensional materials would be focused on strategies like phonon engineering, band engineering and tuning the carrier concentration, etc.

would be further explored for thermoelectric applications. Meanwhile, more interesting two-dimensional semiconductor materials and their complex heterostructures should be fabricated and further designed for thermoelectric application.

As for the huge family of two-dimensional semiconductors, it is challenging to conduct measurement for *ZT* value of each sample and the high-throughout machine learning techniques should be developed to search for the appropriate two-dimensional materials with high *ZT*s [404]. Machine learning, well known for its data-analysis capability, provides an efficient and convenient tool to discover the appropriate thermoelectric candidates before conducting experimental measurements. By evaluating each parameter in *ZT*, machine learning accelerates the exploration of the thermoelectric properties of two-dimensional materials by linking their various unique characteristics. On the other hand, the current theoretical and modelling tools should be developed as well to better simulate the thermoelectric transport properties and thus advance thermoelectric performance.

Moreover, advanced nano-fabrication technologies during sample growth and the subsequent thermoelectric device fabrication based on two-dimensional materials should be considered carefully. As for the characterization of the thermoelectric properties of two-dimensional materials, standard commercialized techniques should be developed, which are still lacking and need more attention for future study. Different from that of bulk thermoelectric materials, both the quality of substrate and the environment would significantly affect the thermoelectric performance of two-dimensional materials. Two-dimensional materials with super-high crystallinity supported on a clean substrate (normally treated with a dielectric *h*-BN) are necessary for thermoelectric measurements. For device-level applications, factors such as electrical shock, electrical contact and moisture are the main considerations for integrated thermoelectric devices based on two-dimensional semiconductors. These strategies for modifying the *ZT* of two-dimensional materials are shown in figure 65.

Concluding remarks

To conclude, we briefly introduce the current status of two-dimensional materials for thermoelectric applications, together with their challenges and their advancement in science and technology. Although numerous two-dimensional materials have been designed and fabricated, the attempt at using them for thermoelectric application is scarce. Two-dimensional materials with high *ZT*s have potential for thermoelectric energy conversion. In experiments, improved techniques that enable thermoelectric devices based on two-dimensional materials need to be developed, such as achieving better electrical contact and high carrier doping. These are both necessary and beneficial for overall thermoelectric performance optimization. Lastly, with the advent of a library of two-dimensional materials, even more two-dimensional semiconductors appropriate for thermoelectric applications can be filtered and selected with the help of high-throughout machine learning studies.

Acknowledgments

5.14. Carbon nanotubes for thermoelectric energy harvesting

Yoshiyuki Nonoguchi

Faculty of Materials Science and Engineering, Kyoto Institute of Technology, Kyoto 606–8585, Japan

Status

The thermoelectric properties of carbon nanotubes are of interest in both the fundamental researches of physical properties, and the development of advanced power generators [405]. Particularly, single-walled carbon nanotubes (SWCNTs) show unique thermoelectric properties compared to conventional thermoelectric materials. Due to their chemically stable structures, SWCNTs are recognized as a platform for studying low-dimension-derived thermoelectric transport [406]. Additionally, due to their mechanical stability, SWCNT-based materials are candidates for the components of flexible thermoelectric power generators [407]. SWCNTs are seamless cylinders made from graphene sheets, and their electronic structures vary depending on the chiral (rolling) angles of graphene. Dependent on the periodic condition, SWCNTs possess semiconducting and metallic electronic structures. Rather than single nanotubes, due to their limited scaling, most studies deal with sheets made from SWCNT networks. In this context, secondary structures such as orientation and inter-tube contacts are highly dominant for thermoelectric properties, along with primary structures (e.g. electronic type and bandgap (diameter), crystallinity).

So far, tremendous efforts have been made for seeking excellent thermoelectric properties of carbon-nanotube-based materials. A growing body of evidence suggests that the films composed of enriched semiconducting SWCNTs show superior thermoelectric properties upon viable chemical doping, compared to metal-enriched SWCNT networks [408]. The state-of-the-art work reported the dimensionless figure of merit *ZT* as high as 0.12 around room temperature, for sorted semiconducting SWCNTs made by the Hipco method [409]. Multi-walled carbon nanotubes (MWCNTs) exhibit advantages for the preparation of structured materials. For example, their yarns and webs can be prepared by the direct spinning of MWCNT products in chemical vapour deposition synthesis [410], where these materials are robust, and show excellent thermoelectric power factor exceeding 2000 μW m^{-1} K^{-2}. For the elucidation of physical properties, various emerging chemical processes had yet to be developed, including chemical and electrochemical doping. To optimize their thermoelectric properties, heavy doping of SWCNTs is highly demanded along with the improvement of the anti-oxidation capability of their doped state, particularly n-type SWCNTs. In this context, various approaches to stable n-type doping were reported. Simple electron transfer, hydride transfer, and also supramolecular complexation were examined for this purpose [411, 412]. All these efforts would contribute to the further development of practical power generators as well as the exploration of emerging physical properties.

Current and future challenges

This carbon-nanotube-based field has shown a rapid evolution in the past 15 years, leading to the generation of new physics idea, chemical treatments, and emergent applications in energy harvesting. Despite such progress, the structure-property relationships of carbon nanotubes in thermoelectrics have yet to be explored. Methods of increasing the efficiency of thermoelectric conversion are extremely paradoxical. Usually, there is a trade-off between electrical conductivity and the Seebeck coefficient, from which the optimal power factor must be found. In the case of carbon nanotubes, controlling their inherently huge thermal conductivity is also a challenge.

The understanding of physical and chemical aspects in the thermoelectric properties of SWCNTs should be obtained by preparing single-phase materials, although the sorting of uniform, high-quality SWCNTs is still under investigation. SWCNTs usually show significant inhomogeneity in their forms (figure 66). As-synthesized carbon nanotubes vary in their diameter and chiral angle (called 'chirality'), and these physical variations result in significant changes in their electronic/thermoelectric transport. Controlling the degree of structural perfection and defect density (crystallinity) is crucial for determining the electronic structures and the corresponding transport properties. Additionally, the thermoelectric properties of SWCNT assemblies are of interest for most applications. In this case, the length of SWCNTs could limit the transport properties (i.e. electrical and thermal conductivity), and the morphology of SWCNT networks

Figure 66. Possible key parameters for the determination of thermoelectric transport in SWCNT films.
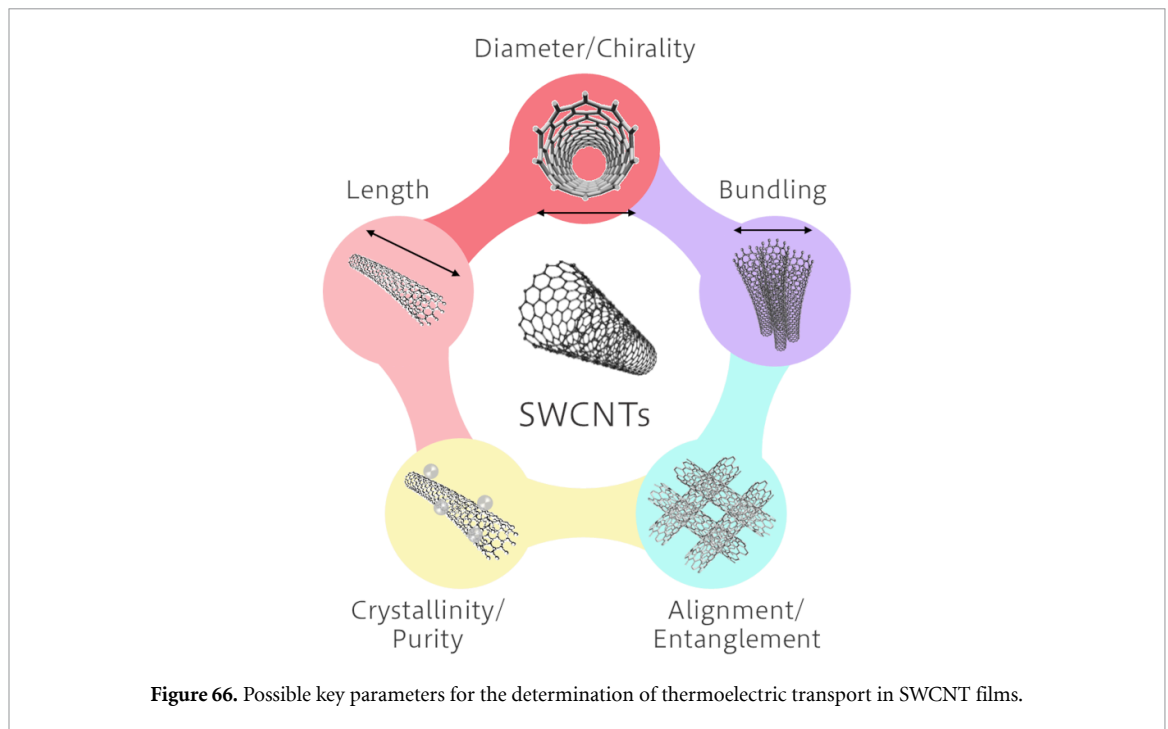
might play an important role [409]. The morphology includes the degree of nanotube bundling and entanglement. The thermoelectric properties of aligned SWCNT thin films showed isotropic Seebeck coefficient and anisotropic electrical and thermal conductivity. It is still difficult to independently control each structure, where procedures for the sophisticated sorting and the morphological control of SWCNTs without degradation have yet to be explored. In this context, there still remain many requirements for thermoelectric applications with carbon nanotubes, including the controlled growth, the postsynthesis sorting and morphological control, and the characterization techniques.

Advances in science and technology to meet challenges
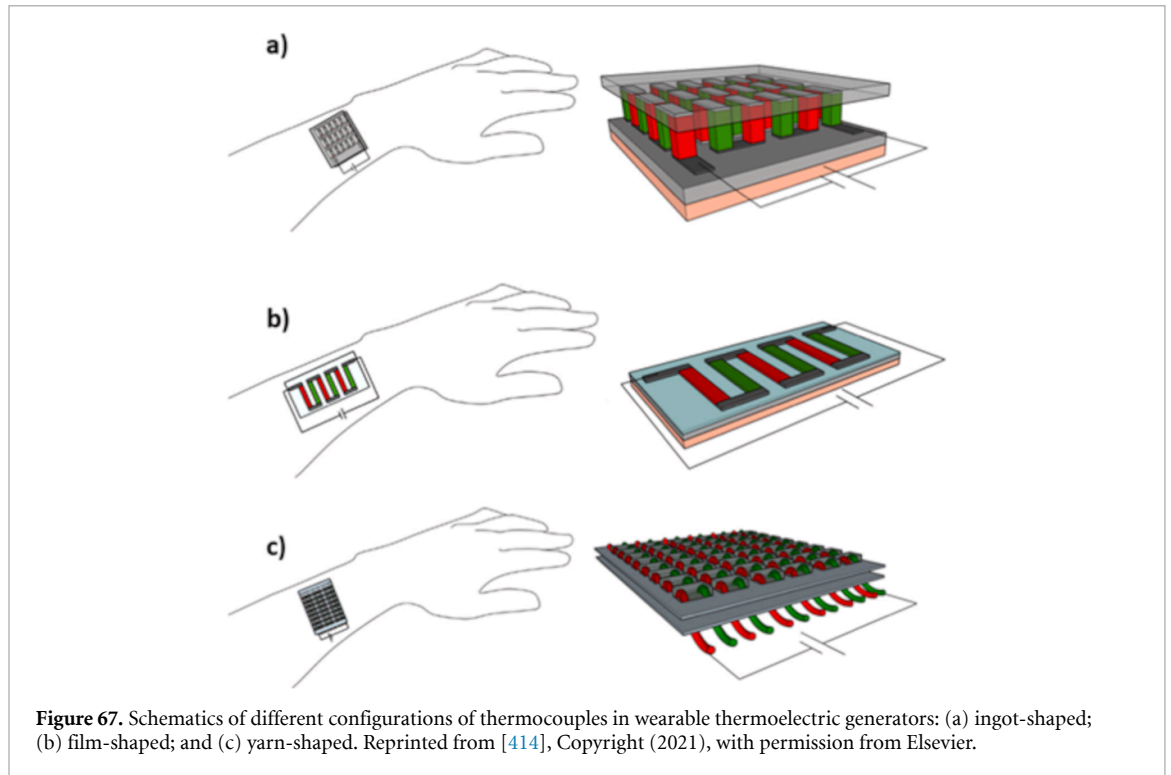*Theoretical approaches*
Keeping pace with structural sorting, it is necessary to clarify desirable materials design at an individual SWCNT and SWCNT networks levels. Theoretical knowledge is becoming increasingly important, including calculations on phonons and lattices, calculations on heat transfer, and theoretical depictions of various correlations such as linear response theory, as well as calculations on electronic states and band structures [413].

Composite science
Various approaches for high-performance thermoelectric composites with carbon nanotubes have been proposed, where thermoelectricity enhancement effects originating from inhomogeneous materials are proposed. For more details, see section 5.15.

Power generator design
Most thermoelectric generators are composed of the series circuit of p-type and n-type components (figure 67). Their conventional geometry enables power generation in (1) cross-plane and (2) in-plane directions [414]. Due to the shape of nanotubes, it is easy to fabricate their cast film, non-woven sheets, and composite materials where carbon nanotubes are oriented two-dimensionally. These sheets show excellent mechanical flexibility, which can be readily applied for the development of in-plane-type thermoelectric generators (figure 67(b)). Additionally, flexibility in the fabrication of SWCNTs might expand the module design; for example, SWCNTs and MWCNTs can be fabricated into flexible yarns (strings), where the

Figure 67. Schematics of different configurations of thermocouples in wearable thermoelectric generators: (a) ingot-shaped; (b) film-shaped; and (c) yarn-shaped. Reprinted from [414], Copyright (2021), with permission from Elsevier.

knitting of a fabric is an emerging procedure for the fabrication of thermoelectric generators (figure 67(c)) [410]. The optimal structures for thermoelectric generators would rely on the applications and should further be investigated.

Concluding remarks

The study of thermoelectric conversion with carbon nanotubes are still providing new science including physics, thermal engineering, and chemistry, as well as applications in flexible power generators. Regarding the former, in other words, new thermoelectric conversion mechanisms and effects may be discovered by exploring complex fields. In the latter, the price of SWCNTs has dropped significantly over the past two decades due to the realization of mass production, and large-area sheets and longer wire rods are available. This may lead to the development of a completely new type of thermoelectric device. In recent years, environmental power generation through thermoelectric conversion has been attracting attention toward the realization of IoT and physical cyber systems. Carbon nanotubes, which show relatively low environmental impact, are expected to be used as a realistic thermoelectric material for this purpose.

Acknowledgments

5.15. Polymer-carbon composites for thermoelectric energy harvesting

Bob C Schroeder[1] and Emiliano Bilotti[2]
[1] Department of Chemistry, University College London, 20 Gordon Street, London WC1H 0AJ, United Kingdom
[2] Department of Aeronautics, Imperial College London, Exhibition Road, London SW7 2AZ, United Kingdom

Status

Low dimensional materials, such as fullerenes (zero-dimensional), carbon nanotubes (one-dimensional) and graphene (two-dimensional), have long been considered for thermoelectric applications as interesting materials to increase the figure of merit *ZT*. In particular, low dimensionality has been shown to increase the boundary scattering of phonons without significantly increasing electron scattering and to allow for manipulating the density of states near the Fermi energy level [415].

Despite these theoretical advantages of carbon allotropes, their high thermal conductivities (>2000 W m^{-1} K^{-1} for carbon nanotubes and graphene) and often poor processing characteristics limit their application in thermoelectrics. To overcome these drawbacks, carbon nanomaterials can be combined with a polymer matrix (either electrically insulating or conjugated) into polymer nanocomposites [416]. The introduction of a polymer allows to reduce the aforementioned high thermal conductivity, due to phonon scattering over the extended interfacial area without compromising the electrical conductivity for percolated nanoparticle networks. Moreover, several authors have reported an even improved thermopower due to the phenomenon of energy filtering; unique interfaces, with controlled interfacial energy barriers, can act as an energy filter that allows high-energy charge carriers to preferentially cross the energy barrier at the interface, while deterring low-energy charge carriers [417].
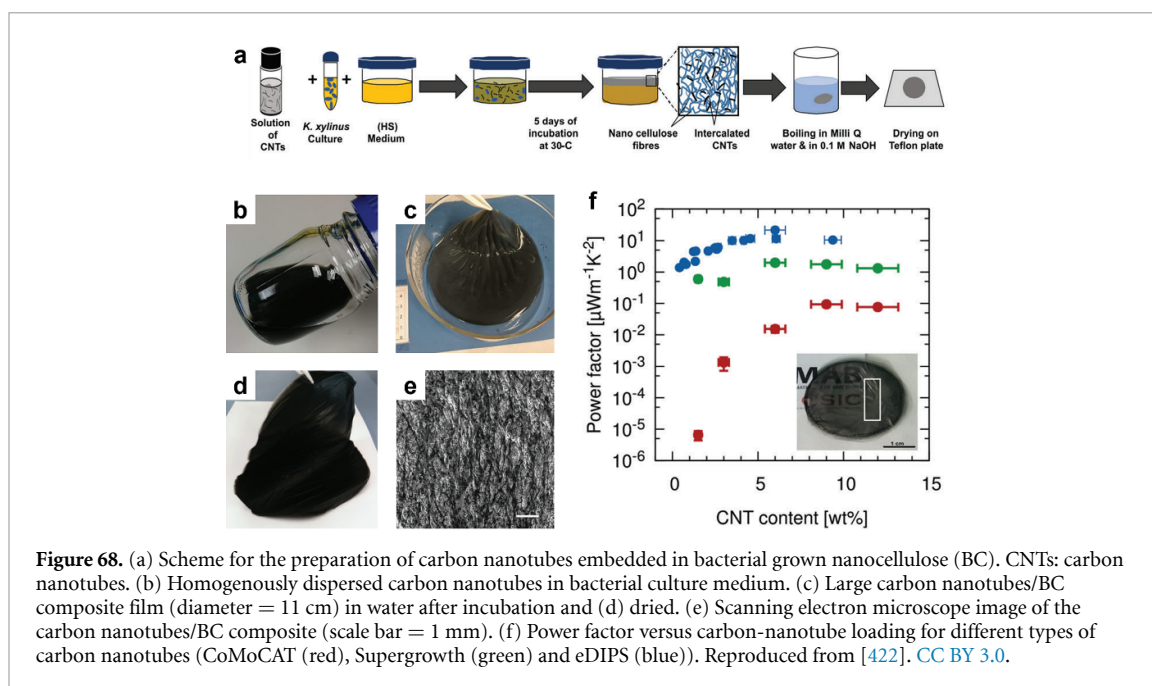
The formation of carbon-polymer composites however is not only advantageous to tune the thermoelectric properties, but also to modulate the mechanical properties. The often-poor solubility and brittle nature of carbon allotropes makes it a challenge to process them into continuous large area thin films and, even more, into thicker thermoelectric elements and generators, a prerequisite for efficient thermal energy recovery. By blending and dispersing the carbon nanomaterials with a polymer, the processing is facilitated, and the resulting composites display enhanced mechanical properties [418], which is of particular interest for applications requiring conformal, tough and flexible thermoelectric generators.

Over the past decades, tremendous effort has been dedicated in understanding and optimizing the unique thermoelectric properties of carbon nanomaterials, yet more advances are needed to explore their full potential in thermoelectric generators. The further development of carbon-polymer composites offers the opportunity to unite the promising thermoelectric properties of carbon allotropes with the distinctive mechanical and thermal characteristics of polymers in the quest to develop high-performing thermoelectric composites.

Current and future challenges

While the electrical conductivity values presented in the scientific literature are often high, simultaneously suppressing the intrinsically high thermal conductivity of carbon nanomaterials, remains difficult. Moreover, the Seebeck coefficients of carbon-composites are still significantly lower than for the best performing inorganic thermoelectric materials despite the promising theoretical values predicted [419]. Furthermore, carbon-polymer nanocomposites are anisotropic materials with orders of magnitude higher electrical and thermal conductivities in plane, than the corresponding out-of-plane (normal direction) values [420]. Anisotropy however is both an opportunity and a challenge for thermoelectric generators, yet only one of several aspects to consider.

The chemical composition of both the carbon allotrope and polymer must be controlled to achieve consistent thermoelectric properties. While it is technically possible to separate and purify carbon nanotubes to a very high degree, considering different chiralities, diameters and lengths, this remains a challenge for graphene; in particular for chemically modified graphene, such as reduced graphene oxide, where batch to batch variations can be severe. Similarly the polymer composition depends on the synthetic pathway, particularly if the composite is formed via *in-situ* polymerization, in which case monomers are directly polymerized on the carbon allotrope surface [421] or grown with the help of bacteria around the carbon nanomaterial (figure 68) [422].

Figure 68. (a) Scheme for the preparation of carbon nanotubes embedded in bacterial grown nanocellulose (BC). CNTs: carbon nanotubes. (b) Homogenously dispersed carbon nanotubes in bacterial culture medium. (c) Large carbon nanotubes/BC composite film (diameter = 11 cm) in water after incubation and (d) dried. (e) Scanning electron microscope image of the carbon nanotubes/BC composite (scale bar = 1 mm). (f) Power factor versus carbon-nanotube loading for different types of carbon nanotubes (CoMoCAT (red), Supergrowth (green) and eDIPS (blue)). Reproduced from [422]. CC BY 3.0.

Flexibility and mechanical robustness are other desirable features often reported and emphasized. Flexible thin films under bending are relatively simple to achieve, whereas tensile deformations remain a challenge. The best performing materials used (e.g. PEDOT:PSS and carbon-nanotube networks) are brittle and will only withstand little tensile strain before breakage. The use of mechanically robust polymer matrices hosting functional nanofillers has been demonstrated to be a very efficient strategy to achieve flexibility and stretchability as well as improved processability [423].

Recently, it was demonstrated that the electrical conductivity and thermopower of semiconducting single-wall carbon nanotube networks tend to increase with temperature, whereas the thermal conductivity decreases [405]. These findings indicate an opportunity of maximizing the thermoelectric efficiency at temperatures above ambient. The challenge remaining however is the limited availability of appropriate dopants to boost electrical conductivity. The dopants must not only be stable under ambient conditions, which is particularly difficult to achieve for n-type dopants, but also resistant to prolonged exposure to elevated temperatures, both with regards to chemical decomposition and morphological instabilities.

Advances in science and technology to meet challenges

Carbon-polymer nanocomposites have demonstrated their potential for thermoelectric power generation, yet significant challenges remain and will require a concerted and multidisciplinary effort to promote key scientific and technological advances.

Ease of processability is one of the features often brought forward in favour of organic electronics, yet this is not necessarily true, particularly if bulk thermoelectrics are the target. Numerous techniques have been developed to process carbon-polymer composites, from simple mixing to liquid-phase exfoliation to more advanced layer-by-layer deposition, achieving a thermoelectric power factor of up to 1825 μW m^{-1} K^{-2} [424]. A true commercial breakthrough in bulk organic thermoelectric materials and carbon-polymer composites would come from finding a way to process the materials via continuous melt extrusion or injection moulding without compromising the thermoelectric properties.

Optimizing the often-contrasting physical properties in carbon-polymer composites is possible only by finely controlling structure at different hierarchical length-scales, from nano to macro. As such the dispersion and orientation of long carbon nanotubes or large graphene sheets is of paramount importance, together with the precise control of the conductive percolated (electrical and thermal) networks and the polymer/nanofiller interface. Moreover, the above will be ideally achieved utilizing processing routes that are compatible with large-scale production, of both thin films and bulk components.

Another often overlooked factor is the thermoelectric module design and fabrication, which so far has been inspired by the established designs used in commercial inorganic thermoelectric devices. These device structures require millimetre to centimetre thick bulk material to maintain sufficient temperature gradients.
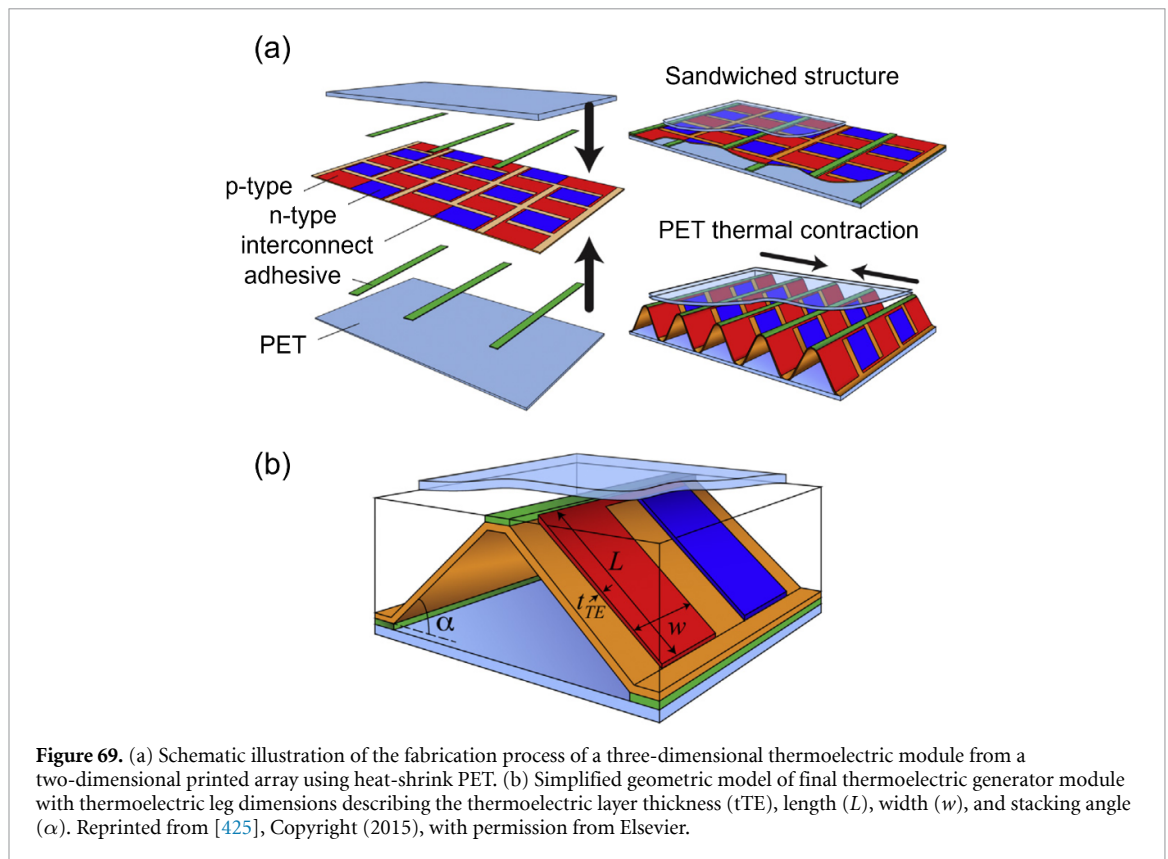
Figure 69. (a) Schematic illustration of the fabrication process of a three-dimensional thermoelectric module from a two-dimensional printed array using heat-shrink PET. (b) Simplified geometric model of final thermoelectric generator module with thermoelectric leg dimensions describing the thermoelectric layer thickness (tTE), length (L), width (w), and stacking angle (α). Reprinted from [425], Copyright (2015), with permission from Elsevier.

This approach however is unsuitable for many organic materials currently processed into thin films and difficult to translate into thicker bulk processing without negatively altering the thermoelectric properties. Novel device architectures and fabrication methods will be needed to ideally convert two-dimensional printed arrays of thin-film composite legs into three-dimensional module architectures (figure 69).

Concluding remarks

Carbon-polymer composites have demonstrated their potential for thermoelectric applications. While they are currently unsuitable for large scale energy generation due to the prohibitively high costs of the carbon nanomaterials, they hold great promise for self-powered and wearable sensors. Numerous researchers have demonstrated the mechanical flexibility of composite materials and incorporated the materials into wearable thermoelectric generators by exploring new module geometries and more sustainable and biocompatible materials (e.g. gelatine and cellulose). In order for carbon-polymer composites to successfully power wearable electronic devices however, it is paramount to develop new and bespoke electronic components (e.g. energy storage, wireless communication), able to operate at lower power and, at the same time, be lightweight, compact and flexible. Once these technological challenges are overcome, polymer-carbon composites can showcase their full potential and spearhead the development of self-powered wearable electronics.

Acknowledgments

5.16. Hybrid organic–inorganic thermoelectrics

Akanksha K Menon[1] *and Jeffrey J Urban*[2]
[1] George W. Woodruff School of Mechanical Engineering, Georgia Institute of Technology, Atlanta, GA 30332, United States of America
[2] The Molecular Foundry, Lawrence Berkeley National Laboratory, Berkeley, CA 94720, United States of America

Status

All thermoelectric materials enable the direct conversion of thermal energy into electrical energy via the Seebeck effect. There are, however, different classes of thermoelectric materials covered in this Roadmap and elsewhere—the choice of which thermoelectric material to pursue is driven by the end use (i.e. the temperature of heat available). Given that heat is a (by)product of any non-isentropic 'real-world' process, it represents a natural resource existing from just a few degrees above room temperature all the way to high-temperature processes. Historically, thermoelectrics research has largely focused on inorganic materials for power generation using higher-temperature sources, but about 10–15 years ago a strong interest began to develop in organic and hybrid thermoelectrics. This was driven to some extent by academic interest in the new physics being exhibited by these materials, as well as their inherently low thermal conductivity and/or decoupled electronic and thermal transport [426]. Compared to single-phase inorganic and organic thermoelectric materials, hybrids promise 'the best of both worlds' and are comprised of inorganic nanostructures chemically conjoined with organic materials to form something fundamentally new. The main appeal of hybrids is that interfacial effects enable tuning the thermoelectric properties beyond what is otherwise attainable with single-phase materials or even composite mixtures. For example, PEDOT:PSS with Tellurium (Te) nanowires has been shown to overcome the conventional S–σ–κ tradeoffs prevalent in both inorganic and organic thermoelectrics to achieve ZT values as high as 0.4 at room temperature [427].
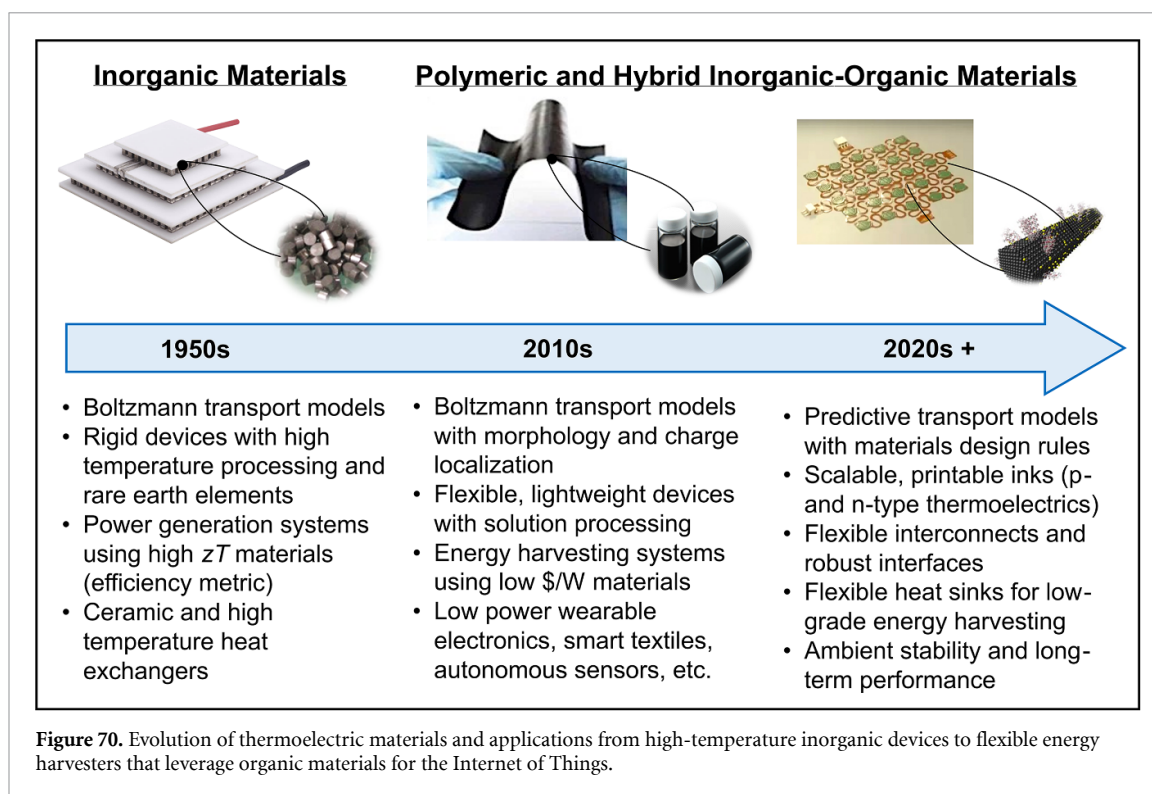
In addition to the interesting physics, hybrid materials retain the solution processability of their organic constituents for low-temperature energy harvesting ($<150\,°C$), thereby enabling new application spaces—wearable electronics, remote sensing, interactive displays, functional textiles, and biomedical devices. For these use cases, we argue that optimizing device efficiency is less important as these applications typically only require a low power density ($\sim$mW cm^{-2}) for operation. Instead, the focus should be on developing lightweight and flexible devices with high reliability and minimal maintenance [428]. This also changes the equation in terms of what constitutes viability for these materials—rather than chasing a high material ZT (as a proxy for efficiency), a fit-for-purpose technoeconomic analysis or \$/W metric that includes scalability and stability considerations may be more appropriate [429]. In this roadmap, we outline the opportunity space for hybrid thermoelectrics and project the anticipated material and system-level breakthroughs needed to render them competitive with their inorganic and organic counterparts, as shown in figure 70.

Current and future challenges

One central challenge with hybrid thermoelectrics is understanding the non-linear interactions that occur between the two phases at the interface. Effective medium models (e.g. Bergman–Levy) do not apply, and hybrid material performance can exceed that of either pure component even without any extrinsic doping. To explain these results, mechanisms such as energy filtering due to the different work functions of Te and PEDOT:PSS have been incorrectly posited since there are no methods to directly probe the interface. Recent work on single nanowire hybrids has revealed that it is the interfacial interactions at the nanoscale that are at play, leading to self-assembly or templating of the organic phase along the crystalline inorganic nanowire [427]. This however is a purely morphological effect dependent on nanowire diameter rather than true hybrid behaviour, as there is no change in the electronic structure or scattering mechanisms. Thus, synthesis routes that can harness effects like energy filtering to enable new materials with vastly improved properties remains a challenge.

The other enduring challenge is that the structure and bonding of standard organic elements (C, H, N, O) has resulted in primarily p-type hybrids with a high thermoelectric performance. In theory, hybrids can be potent owing to seamless introduction of new electronic states via an inexhaustible library of inorganic materials to generate unforeseen n-type materials that retain the flexibility of organic thermoelectrics. For example, the Seebeck coefficient of Te nanowires can be tuned via interfacial charge transfer (i.e. resonant doping) to achieve an n-type hybrid material. However, design of materials beyond Te is yet to be practically realized.

At the device level, the overall stability of these materials to oxidation, thermal cycling, and mechanical strain has not been thoroughly studied. There is thus considerable opportunity to take advantage of the

Figure 70. Evolution of thermoelectric materials and applications from high-temperature inorganic devices to flexible energy harvesters that leverage organic materials for the Internet of Things.

ability to lithographically work with hybrid materials to create incredibly robust structures mimicking those in nature by using hard/soft concepts and hierarchical design principles such as negative Gaussian curvature and tensegrity [430, 431].

One of the elements favouring hybrid materials is their processability and manufacturability using pre-existing infrastructure developed for other stretchable electronics. However, this advantage brings with it several important research questions that are yet to be adequately solved: the role of processing when applying the material in a given form factor to a device for energy harvesting can result in properties that are very different from the hybrid single nanowire or thin film form, then there are real needs for flexible interconnects that enable the materials to retain their function over multiple bending or strain cycles, and there is also a need for flexible heat exchangers. While there has been some recent work in this space [432, 433], there is significant room for improvement and innovation.

Advances in science and technology to meet challenges

Currently, hybrid thermoelectrics are at the research stage, with some development through industrial partnerships and small startups. Long-term it will be important to understand if extant materials are maximizing their potential, or if we are limited by current materials science, syntheses, and manufacturing principles. For example, there is no thermoelectric equivalent of the Shockley–Quiesser evaluation for soft thermoelectrics and it is unclear exactly how good they can become (e.g. nothing physically prevents a *ZT* of infinity). Charge transport models can set some bounds on these materials, but only recently has there been reconciliation of vastly different physical models (e.g. hopping- to metal-like transport) using a generalized charge transport model and the semi-localized transport (SLoT) model [434, 435]. However, these models are predicated on insight from temperature-dependent measurements to infer the energetic landscape, as a result of which they cannot be predictive and have limited utility.

For hybrid organic-inorganic thermoelectric devices, the clear target is cost-effective harvesting of low-grade thermal energy for low-power electronics (mW cm^{-2}). Therefore, the motivation is no longer chasing high-*ZT* materials but is instead oriented towards making the entire device robust, reliable, and capable of being manufactured in arbitrary geometries at scale. This will require a paradigm shift from the status quo (i.e. synthesizing novel organic materials/dopants and characterizing them in an inert environment) to thinking in terms of integrating the material in a device. Here, processing and scale-up parameters will need to focus on consistency (both batch-batch and at scale), along with minimizing the adverse impact of any binders/additives necessary for fabricating large-area devices, and measuring thermoelectric performance in the direction in which the device experiences a temperature gradient.

Other prominent technological challenges are flexible heat exchangers to partner with the flexible thermoelectrics and enable the most efficient use of the small thermal resources available. This area has seen little interest, but it is a substantial need as traditional ceramic heat exchangers for high-temperature semiconductor thermoelectrics will not be viable. It is also strongly recommended that thermoelectric devices be tested for months and not days (like in most academic papers) and under various environmental conditions.

Concluding remarks

Research in hybrid thermoelectrics is, in many ways, still in its infancy. Despite having limited time and investment relative to traditional inorganic semiconductor thermoelectrics, this field has made several landmark discoveries (both in terms of the physics and material performance) and demonstrated accelerated development on an annual basis. However, to realize the promise of what has been achieved thus far, directed investments into fundamental aspects of materials science, the charge and thermal transport physics of these materials, and translational innovations into the processing and implementation of these 'soft thermoelectrics' are desperately needed. Flexible and stable n- and p-type hybrid thermoelectrics that can be woven together into arbitrary geometries can be impactful to a future where distributed low-power electronics and sensors will play a prominent role.

Acknowledgments

5.17. Halide perovskites for thermoelectric energy harvesting

Oliver Fenwick and Ceyla Asker
School of Engineering and Materials Science, Queen Mary University of London, Mile End Road, London E1
4NS, United Kingdom

Status
The reason for low uptake of thermoelectric technology lies in the combination of device efficiency and low elemental abundance, cost and often toxicity of the materials from which current thermoelectric generators are made. A new generation of thermoelectric materials is needed, which addresses some or all of these issues. Halide perovskites are materials that have promise to address three or more of these challenges simultaneously. Halide perovskites are crystalline semiconductors with an ABX_3 stoichiometry and can be fully inorganic or organic-inorganic hybrids. The B-site is a metal cation (e.g. Pb^{2+}, Sn^{2+}), the X-site a halide anion and the A-site can be an organic or inorganic cation (e.g. Cs^+, $CH_3NH_3^+$, $CH_5N_2^+$) (figure 71). They have been widely studied as absorbers in solar cells and can be processed by low-cost methods from solution or by mechanochemical synthesis and low temperature sintering. A wide range of elements can be used on the A-, B- and X-sites which can be abundant and (when Pb is avoided) non-toxic.

Thermoelectric figure of merit ZT values of $MABI_3$ (MA = methylammonium, B = Pb^{2+} or Sn^{2+}) are predicted to be between 1 and 2 [436]. The mixed-halide version, $CsPb(I_{1-x}Br_x)_3$, is predicted to have $ZT = 1.7$ [437], whilst the low-dimensional $Cs_3Cu_2I_5$ perovskite derivative is predicted to have $ZT = 2.6$ at 600 K (figure 72) [438]. This therefore puts the predicted thermoelectric performance of halide perovskites alongside the state-of-the-art in the low to mid temperature range and offers the possibility of high-performance sustainable thermoelectric materials.

Current and future challenges
Despite high predicted thermoelectric performance in halide perovskites, experimental results have only shown low to modest thermoelectric figure of merit ZT. Understanding this discrepancy is key to developing the field. On the positive side, halide perovskites have been identified as 'phonon glass electron crystals' where there is a role of the A-site cation in phonon scattering, resulting in thermal conductivities that are in (or close to) the ultralow regime, which is defined as <0.5 W m^{-1} K^{-1}. Charge mobilities in these materials are known to be quite reasonable, in the range of tens to hundreds of cm^2 V^{-1} s^{-1} [439] and Seebeck coefficients are commonly >100 μV K^{-1}, depending on doping level.

Nonetheless, electrical conductivities of halide perovskites in their intrinsic state are low. Extrinsic doping, self-doping, off-stoichiometry doping and charge transfer doping have been applied experimentally to improve the electrical conductivities and the overall ZT value. The greatest success in terms of figure of merit has been in the Sn-perovskites, where the oxidation of Sn^{2+} to Sn^{4+} provides a route to self-doping. ZT values of $CsSnI_3$ have been reported in several studies, with a ZT of 0.11 achieved at 320 K [440]. However, since oxidation is the source of charge carriers, stability of Sn-perovskites is a potential issue. Self-doping of $CsSnI_{3-x}Cl_x$ has achieved hole-doping concentrations of 10^{18}–10^{19} cm^{-3} and ZT of 0.14 at 345 K, where Cl-dopants enhanced the stability as well as acting as a sacrificial source of free charges [441]. The highest ZT value of 0.19 (at room temperature) was achieved with charge transfer doping of thin films using the molecular dopant F4TCNQ [442].

Doping of more stable (non-Sn-containing) perovskite systems for thermoelectrics has been achieved, but the low doping efficiency [443] results in low electrical conductivities and low ZT. The main current challenge is therefore to improve doping efficiencies in this class of materials where doping is a challenge due to ionic compensation of point defects in addition to an electronic structure that is tolerant of defects.

Advances in science and technology to meet challenges
The potential for halide perovskites as sustainable high-ZT thermoelectric materials has therefore been demonstrated computationally and only partly realized experimentally. These authors believe that the principle 6 challenges to realize high thermoelectric performance in halide perovskites are:

1. *To understand electrical doping better in these materials.* They have been developed mostly as solar cell absorbers, where a low density of free charges is advantageous, and there has still been relatively little work on ways to achieve doping densities >10^{18} cm^{-3}.
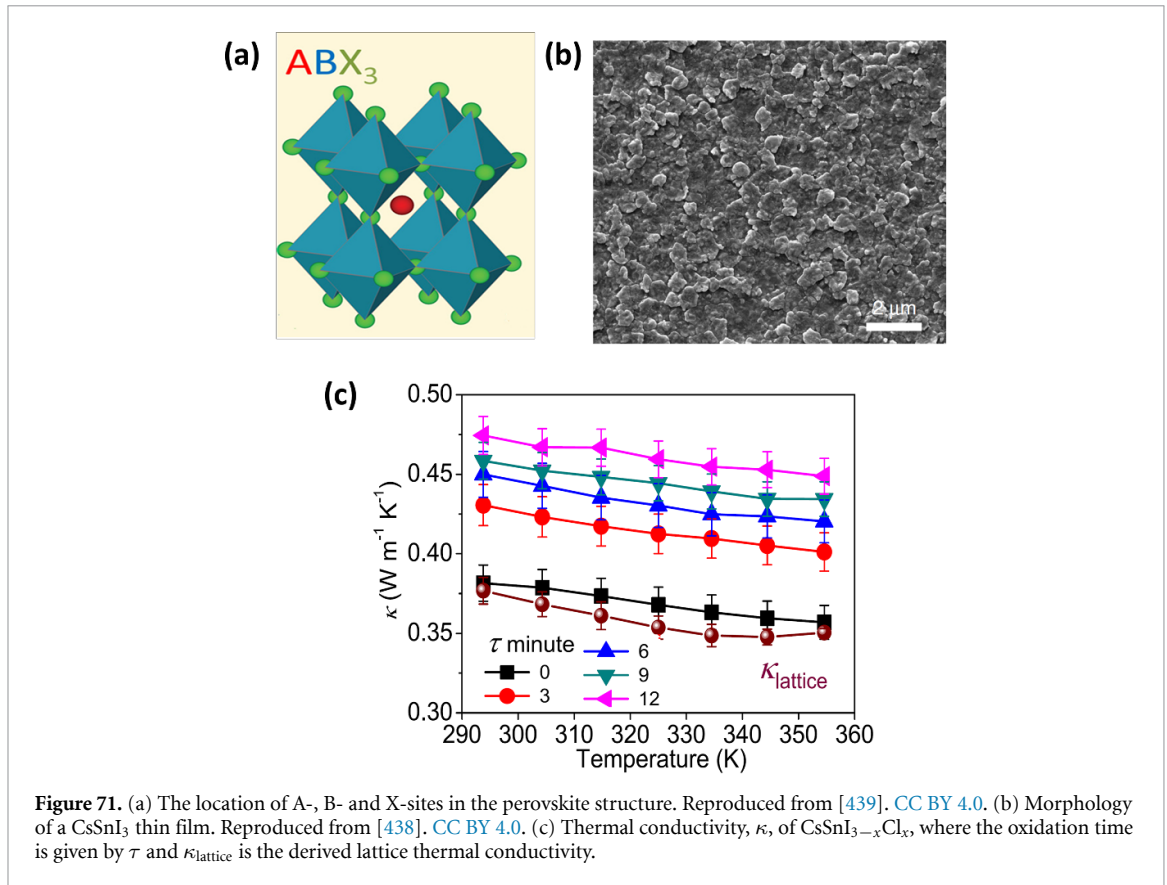
Figure 71. (a) The location of A-, B- and X-sites in the perovskite structure. Reproduced from [439]. CC BY 4.0. (b) Morphology of a CsSnI$_3$ thin film. Reproduced from [438]. CC BY 4.0. (c) Thermal conductivity, κ, of CsSnI$_{3-x}$Cl$_x$, where the oxidation time is given by τ and $\kappa_{lattice}$ is the derived lattice thermal conductivity.
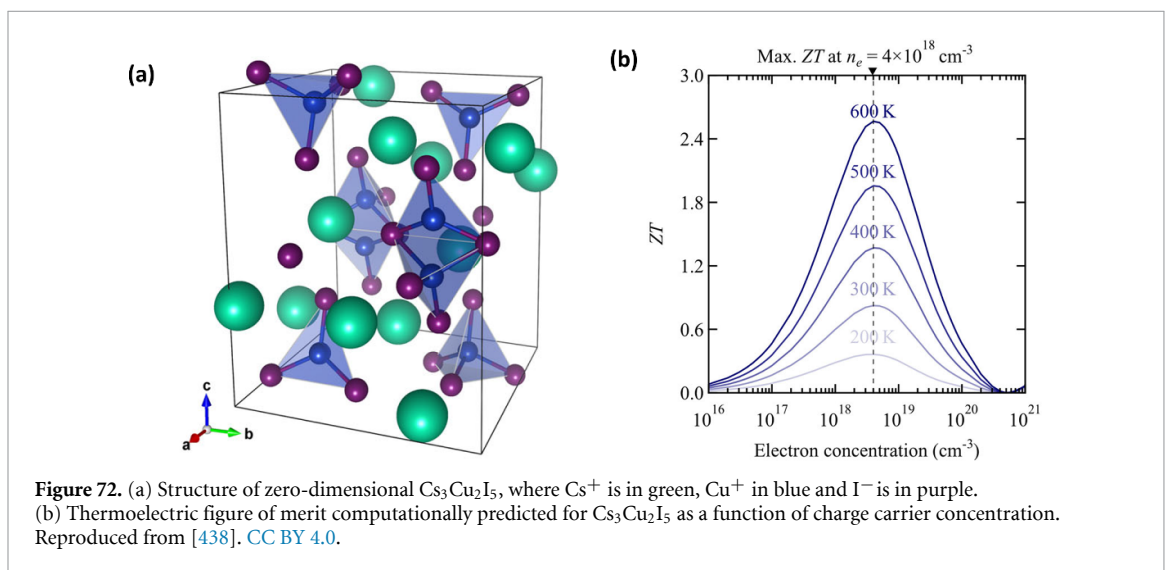

Figure 72. (a) Structure of zero-dimensional Cs$_3$Cu$_2$I$_5$, where Cs$^+$ is in green, Cu$^+$ in blue and I$^-$ is in purple. (b) Thermoelectric figure of merit computationally predicted for Cs$_3$Cu$_2$I$_5$ as a function of charge carrier concentration. Reproduced from [438]. CC BY 4.0.

2. *To balance conductivity and stability.* Currently, the best halide perovskite thermoelectric materials are Sn-based, which are among the least atmospherically stable of the material class. Methods to achieve similar doping densities in more stable halide perovskites will be needed.

3. *Computational materials discovery.* Currently, relatively few of the thousands of possible halide perovskites have been explored, and this is experimentally time-consuming. Computational approaches to explore the materials space for the best candidates and the best doping strategies is much needed.

4. *Exploring lower dimensional analogues.* Halide perovskites have low-dimensional counterparts which comprise metal halide clusters separated by organic or inorganic cations (figure 72). These halide perovskite derivatives have shown potential for further reduced thermal conductivity and even higher Seebeck coefficients.

5. *Balancing cost and scalability.* Halide perovskites have been developed as thin film (sub-μm) materials in photovoltaic devices. Thermoelectric generators would typically require millimetre thicknesses (i.e. bulk material). Avoiding costly or toxic elements in the composition is therefore important, as well as considering solid-state synthesis approaches to avoid solvent cost and solvent waste.

6. *Incorporating them into prototype thermoelectric generators.* Many processes can occur in thermoelectric generators that are not captured by a *ZT* measurement of the material in isolation. These may include electrode reactions that may require passivation by organic interlayers and careful choice of electrode material. There may be contact resistances, ionic migration and Joule heating effects to name a few. On the other hand the processability of these materials may enable innovative device geometries that are not possible with conventional ceramic thermoelectric generators.

Concluding remarks

Halide perovskite materials are well known in the research community and increasingly to industry through their development in high-efficiency single- and multi-junction solar cells. Whilst they remain underexplored for thermoelectrics, interest is certainly increasing. This is perhaps unsurprising due to their intrinsically low thermal conductivity that is comparable to polymers, decent charge mobility and large Seebeck coefficients. Experimental reports of $ZT > 0.1$ and computational predictions of $ZT > 2$ have given researchers some confidence. If the challenge of doping to achieve charge carrier densities $>10^{18}$ cm^{-3} can be achieved in a wider range of halide perovskite materials, then we would expect to see much higher *ZT* values in the future and perhaps halide perovskite thermoelectric generators operating with high power conversion efficiencies.

Acknowledgments

5.18. Metal organic frameworks for thermoelectric energy conversion applications

A Alec Talin
Sandia National Laboratories, Livermore, CA 94551, United States of America

Status

Metal organic frameworks (MOFs) are extended, crystalline compounds consisting of metal ions interconnected by organic ligands, forming scaffolding-like structures that are sometimes referred to as 'molecular tinker toys' [444]. These porous coordination polymers have attracted considerable attention for traditional applications of microporous materials, such as gas storage and separation. More recently, the discovery that certain MOFs conduct electrons by virtue of the electronic coupling within their structures or by interactions with guest molecules (Guest@MOF) that facilitate charge delocalization and hoping, has sparked interest in using MOFs in thermoelectric applications [445]. The interest in MOFs, and coordination polymers more broadly, is motivated by the practical need for thermoelectric materials that are low-cost, non-toxic, mechanically flexible, and can conform over complex shapes. A potential advantage of MOFs and Guest@MOF materials compared to organic polymers is their synthetic and structural versatility [444]. Specifically, the choice of metal, ligand, and guest molecule enables tuning of the electronic transport, and therefore promote high charge mobility because of the long-range crystalline order inherent in these materials while maintaining low thermal conductivity. In this section, we briefly review the recent advances in development of MOFs, Guest@MOFs and coordination polymers for thermoelectric applications and discuss how the Seebeck coefficient, electrical conductivity and the thermal conductivity could be tuned to further optimize their thermoelectric performance.

Current and future challenges

Irrespective of the material type, the efficiency of a thermoelectric device is determined by the *ZT* figure of merit, $ZT = S^2 \sigma T \kappa^{-1}$, where S is the Seebeck coefficient, σ is the electronic conductivity, T is temperature, and κ is the thermal conductivity [445]. Because the parameters are interdependent, finding materials with $ZT \gg 1$ has been a major challenge for developing practical thermoelectric systems. The Seebeck coefficient, or thermopower, is the voltage difference that arises when a temperature gradient exists across a slab of material [445]. Its sign indicates the majority carrier, positive for hole conductors and negative for electron conductors, and its magnitude ranges from a few μV K^{-1}, typically for metals, to over 1 mV K^{-1}, observed in lightly doped semiconductors. Seebeck coefficient values for several p-type and n-type MOFs and non-porous coordination polymers are included in table 2.

The second factor that is needed to realize thermoelectric systems with high efficiency is low thermal conductivity. Indeed, MOFs exhibit a low thermal conductivity, typically ~0.2 W m^{-1} K^{-1}, which is ~10× lower compared to Bi$_2$Te$_3$ (see table 2 for a few representative examples). The low thermal conductivity for MOFs is consistent with their weak bonding (metal-ligand coordination bonds are generally weaker compared to covalent bonds), complex atomic structures, and high anharmonicity, which decrease the amount of energy carried per vibrational mode, the phonon propagation speed and the phonon mean-free path.

The electronic conductivity is the third factor that determines *ZT*. In general, high electronic conductivity is observed in solids with strong electronic coupling between neighbouring atoms leading to large band dispersion and delocalization of carriers across many lattice sites [444]. Most MOFs, on the other hand, have little or no band dispersion due to low atomic density and strong localization of the electron wave function characteristic of Werner-type coordination complexes. Because electronic conductivity is key to so many potential applications (e.g. electronics, sensors, energy conversion and storage), designing electronically conducting frameworks has been a major research thrust in the MOF community [444]. In general, electronic conduction mechanisms in MOFs can be classified as either intrinsic or guest induced (see figure 73). Examples of intrinsically conducting MOFs include Ni$_3$(HITP)$_2$ and Cu$_3$(HHTP)$_2$, examples of guest induced conductivity include TCNQ@Cu$_3$(BTC)$_2$ [445] and carbon nanotubes@ZIF-67[447], and an example of a conducting non-porous coordination polymer is Cu-BHT [449]. Note that while adsorption of guest molecules or nanostructures can dramatically boost electronic conductivity, it can also increase the thermal conductivity by increasing phonon modes and depending on the guest-host interaction, the framework rigidity (see table 2).

Advances in science and technology to meet challenges

Although the two-dimensional MOF Ni$_3$(HITP)$_2$ has a relatively high electrical conductivity (compared to other MOFs) of ~60 S cm^{-1} and a very low thermal conductivity of ~0.2 W m^{-1} K^{-1}, exhibits a very low *ZT* of ~10^{-3}, well below the typical values of $ZT \sim 1$ for inorganic thermoelectric materials. This is in part

Figure 73. Tetracyanoquinodimethane (TCNQ) above a $Cu_3(BTC)_2$ with arrow pointing to the pore. Colour code: white, H; blue, N; cyan, C; red, O; ochre (light brown), Cu. Reproduced from [445], with permission from Springer Nature. (b) A portion of the crystal structure of $Ni_3(HITP)_2$ showing multiple stacked two-dimensional layers. Orange, green, gray, and white spheres represent Ni, N, C, and H atoms, respectively. (c) TEM micrographs of $Ni_3(HITP)_2$ nanoparticles viewed along the pores. Reprinted from [446], Copyright (2017), with permission from Elsevier.
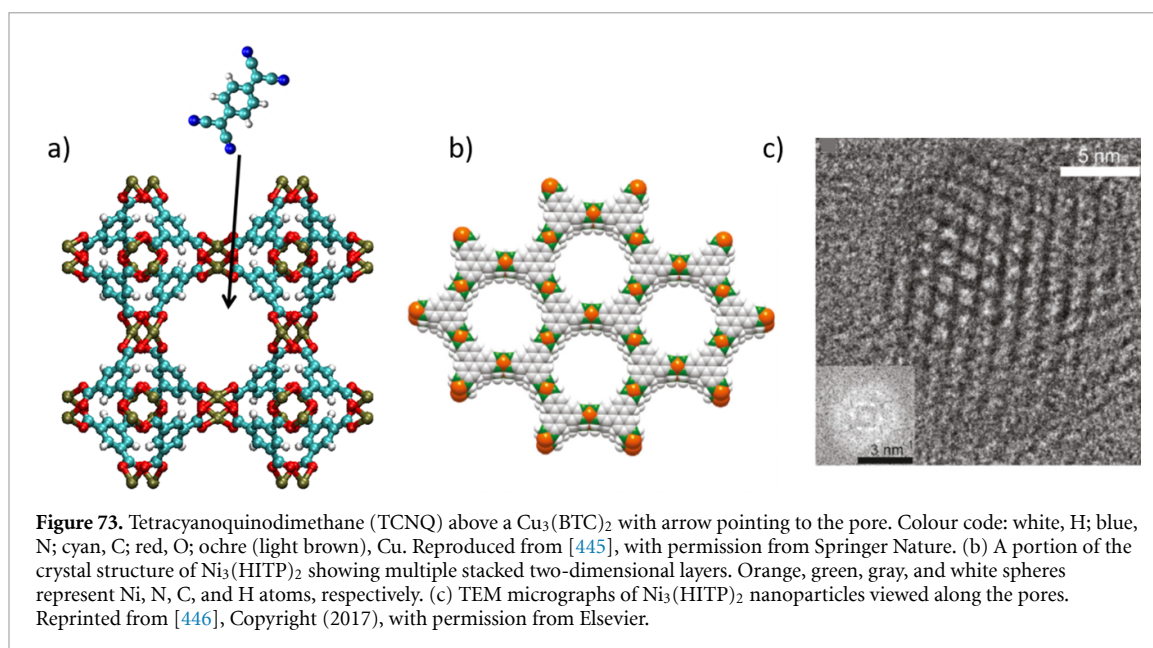
Table 2. Thermoelectric properties of selected MOF, Guest@MOF, coordination polymer and organic polymer materials. PF: thermoelectric power factor.

Material	S (μV K^{-1})	σ (S cm^{-1})	κ (W m^{-1} K^{-1})	PF (μW m^{-1} K^{-2})	ZT	References
$Ni_3(HITP)_2$	-11.9	58.8	0.2	0.83	1.2×10^{-3}	[446]
CNT@ZIF-67	55.6	825.7	4.1	255.6	0.02	[447]
TCNQ@$Cu_3(BTC)_2$	375	4.5×10^{-3}	0.25	0.06	10^{-4}	[448]
Cu-BHT	-21	2000	1.99	88	0.013	[449]
PEDOT:PSS	76	9×10^5	0.24	480	0.42	[450]

due to this framework's relatively low Seebeck coefficient of -11.9 μV K^{-1} and an electrical conductivity that is considerably lower compared to values observed for inorganic and organic polymer thermoelectric materials. The nanocrystalline character of the $Ni_3(HITP)_2$ used in [446] likely contributed to the lower value of the electrical conductivity. Indeed, Wu *et al* reported electron mobility as high as $\sim$50 cm^2 V^{-1} s^{-1} for field-gated $Ni_3(HITP)_2$ thin films fabricated using an alternative route based on liquid-air interface method, resulting in much better crystalline quality [451]. This mobility is well above the values typically observed for hopping conduction associated with small polaron formation and indicates substantial delocalization of the electron wave function [444]. The fact that much higher charge mobilities of >200 cm^2 V^{-1} s^{-1} have been reported for single crystals two-dimensional MOF such as $Fe_3(THT)_2(NH4)_3$ [452] suggests that there is ample opportunity to improve thermoelectric characteristics using two-dimensional conducting MOFs. It is also worth noting that while Sun *et al* reported a negative Seebeck coefficient for $Ni_3(HITP)_2$, the transfer characteristics observed by Wu *et al* for nominally the same material suggest that this framework is ambipolar (i.e. can conduct both electrons and holes), which is encouraging for developing practical thermoelectric conversion systems where elements with majority electron and hole carriers are necessary.

To achieve MOF thermoelectrics with $ZT > 1$ will require both increases in the electronic conductivity and the Seebeck coefficient. Since $S \propto \frac{dn(E)_{E=E_F}}{dE}$ where $n(E)_{E=E_F}$ is the density of states at the Fermi level, materials with higher S typically result in lower electronic conductivities due to fewer carriers at the Fermi level [445]. In traditional thermoelectrics like Bi_3Te_2 and its alloys, low bandgap and high doping concentrations enable a compromise to optimize S and σ. Recent demonstrations of continuously tunable bandgap of 0.3–0.8 eV in the binary alloy system $(M_xM')_{3-x}(HITP)_2$ (MM' = CuNi, CoNi, and CoCu) suggests that such an approach could also work with MOFs [453].

Concluding remarks

In summary, MOFs offer tremendous opportunity to tune the electronic structure, electronic transport and thermal conductivity via their composition, bonding character and three-dimensional assembly (including structural porosity). Thus, MOFs are excellent candidate materials both for fundamental exploration of thermoelectric phenomena as well as for discovery of novel thermoelectrics that combine high performance with low cost, low toxicity and mechanical flexibility.

Acknowledgments

6. Materials for radiofrequency energy harvesting

6.1. Introduction to materials for radiofrequency energy harvesting

Thomas D Anthopoulos
King Abdullah University of Science and Technology (KAUST), KAUST Solar Center (KSC), Thuwal
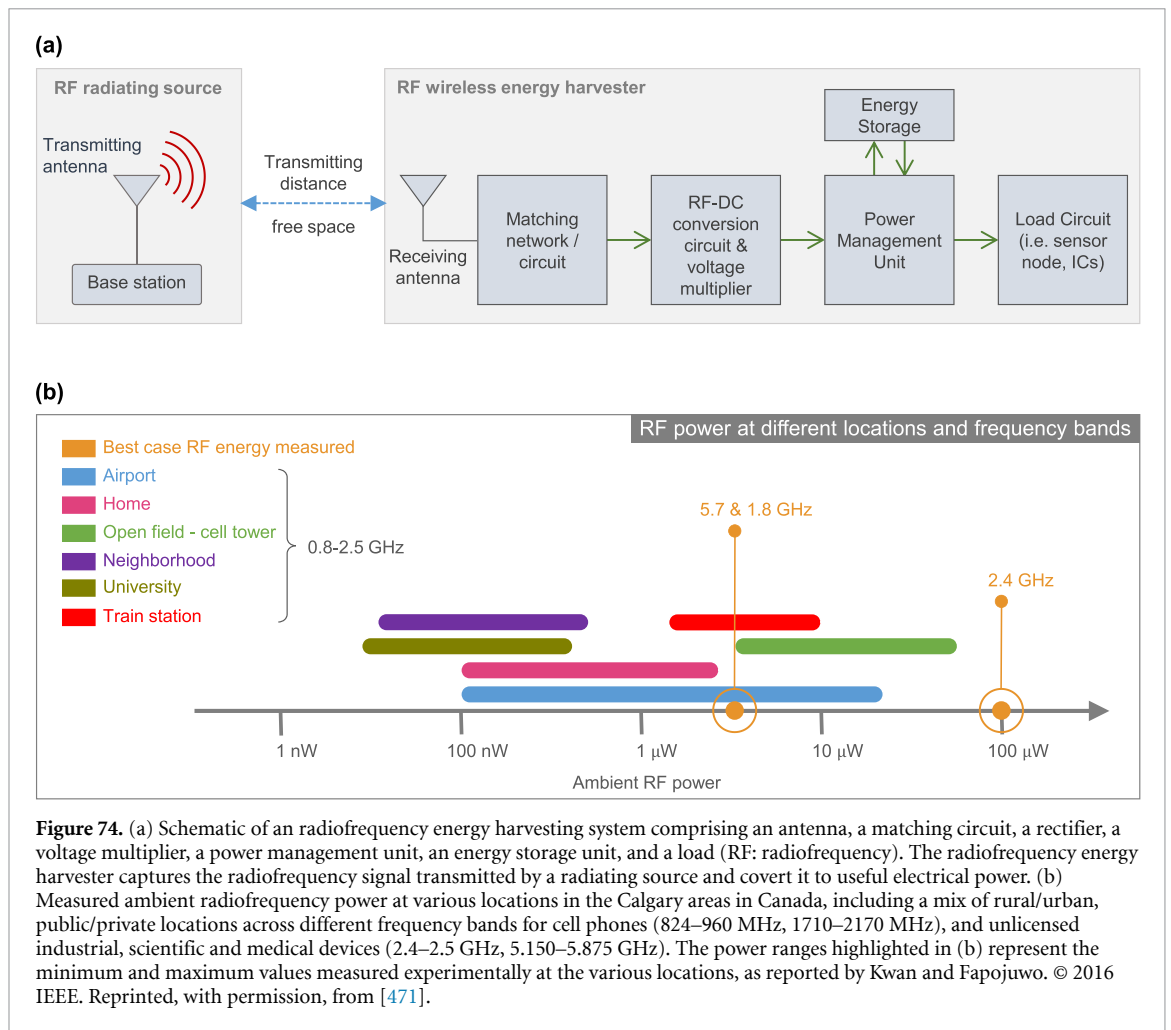23955–6900, Saudi Arabia

Electromagnetic signals in the radiofrequency range are ubiquitous and originate from various sources, including wireless networks, broadcast transmission antennas, mobile base stations and mobile phones, Wi-Fi signals, and dedicated radiofrequency base stations, among others. Harvesting the energy of such signals has recently emerged as a promising method for powering electronic devices wirelessly including distributed sensor networks and more broadly the rapidly expanding IoT device ecosystem. In 2022 alone, the total number of connected IoT devices grew by 18 % to 14.4 billion and is predicted to reach 27 billion globally by 2025 [454]. Each physical 'Thing' (sensor node, etc) is identifiable within the IoT ecosystem and can exchange information wirelessly. Powering this rapidly increasing number of devices is now recognized as a major techno-economic challenge with no obvious solution in sight. This is precisely where radiofrequency wireless energy harvester (RF-WEH) technologies offer a promising alternative to conventional batteries by enabling the autonomy required by the IoT nodes. Moreover, RF-WEHs can be operated 24 h indoors and outdoors and supply enough energy for the periodical operation of IoT devices.

The prospect of energy-autonomous operation of distributed IoT devices has also highlighted RF-WEH technologies as a more sustainable and greener option that promises to reduce the environmental impact associated with the manufacturing, maintenance, and disposal of conventional electrochemical batteries. The environmental impact of emerging electronic technologies is now becoming a major concern since the continuously increasing availability of electronics has fuelled the generation of electronic waste (e-waste), making it the fastest-growing waste stream globally [455]. Thus, developing technologies that can help address this timely issue has become a strategic priority for the electronic industry.

A typical wireless radiofrequency energy harvesting system consists of several components the most critical of which is the rectenna, as it determines the radiofrequency to direct current (DC) conversion efficiency (figure 74(a)). The rectenna comprises an antenna which is responsible for capturing the radiofrequency signal and a rectifier circuit that converts it into DC, which is then used to power the load (sensor, microcontroller, etc.). An impedance-matching network is often used to connect the antenna with the rectifier circuit, ensuring optimal transfer of the captured radiofrequency power. The most critical component within the radiofrequency-to-DC unit is the diode element that rectifies the electromagnetic signal collected by the antenna [456]. Along with the required high-frequency response, a critical parameter that describes the ability of a diode to rectify an electrical signal is the short circuit current responsivity (in A/W). The latter can be calculated directly from the second-order derivative of the experimentally measured current–voltage $I(V)$ characteristic and is broadly used to quantify and compare the performance of the various rectifier technologies.

Traditionally, Schottky diodes have dominated the application landscape, but other technologies have been demonstrated, including backward tunnel (Esaki) diodes, tunnel diodes, and spin diodes [457]. The use of metal-oxide-semiconductor transistors as the rectifying element has also been explored extensively in complementary-metal-oxide-semiconductor circuitry as well as in several other transistor technologies [458–463]. Although simpler to integrate, the intrinsic characteristics of conventional transistors often result in inferior rectification compared to the corresponding Schottky diode technologies [464]. To maximize the radiofrequency-to-DC power conversion efficiency of an RF-WEH, the impedance matching network connecting the antenna and the load circuit needs to be carefully designed to avoid signal reflection back to the environment. Additional circuit elements, such as a voltage multiplier and a power management module, are also required to increase the output voltage of the rectenna so it can drive the load module and charge the energy storage unit, often consisting of a battery or a capacitor. The efficiency of each block determines the overall power conversion efficiency of an RF-WEH; therefore, all elements are equally important to achieve optimal performance [457].

Despite the exploding interest in RF-WEHs, numerous challenges still need addressing before the technology can be fully embraced commercially. One such challenge is the limited radiofrequency power in the ambient environment (figure 74(b)). The steady progress in developing low-power circuitry and the continuously increasing abundance of radiofrequency signals have partially helped alleviate this issue. Another challenge relates to the system's physical shape and size. As the size of the IoT node continues to reduce, its integral components also need to be miniaturized and integrated cost-efficiently. The silicon

Figure 74. (a) Schematic of an radiofrequency energy harvesting system comprising an antenna, a matching circuit, a rectifier, a voltage multiplier, a power management unit, an energy storage unit, and a load (RF: radiofrequency). The radiofrequency energy harvester captures the radiofrequency signal transmitted by a radiating source and covert it to useful electrical power. (b) Measured ambient radiofrequency power at various locations in the Calgary areas in Canada, including a mix of rural/urban, public/private locations across different frequency bands for cell phones (824–960 MHz, 1710–2170 MHz), and unlicensed industrial, scientific and medical devices (2.4–2.5 GHz, 5.150–5.875 GHz). The power ranges highlighted in (b) represent the minimum and maximum values measured experimentally at the various locations, as reported by Kwan and Fapojuwo. © 2016 IEEE. Reprinted, with permission, from [471].

industry has responded to this challenge by developing manufacturing processes that enable the integration of the load circuitry with the radiofrequency components, such as the antenna, to deliver system-on-chip solutions [465]. In parallel, research on new materials for substrates, dielectrics, semiconductors, and conductors has propelled these emerging technologies to the forefront of research in emerging RF-WEH technologies [466–470]. The rapid pace of recent progress shows that harvesting ambient radiofrequency energy could offer unique solutions and lead to truly enabling technologies for the IoT device ecosystem of the future.

This chapter discusses recent progress in radiofrequency energy harvesting technologies with a primary focus on emerging materials and their integration into devices and systems for IoT applications. Caironi *et al* (section 6.2) and Georgiadou (section 6.3) discuss the prospects of organic and metal oxide semiconductors in radiofrequency rectifying devices processed via scalable manufacturing techniques. Peng *et al* (section 6.4) and Lemme *et al* (section 6.5) summarize recent advances in radiofrequency rectennas based on low-dimensional materials, such as carbon nanotubes and two-dimensional materials, and highlight the need for appropriate modelling tools. Finally, Wagih and Beeby (section 6.6) underline the importance of emerging conductors for the development of radiofrequency antennas, the critical role of material-induced losses, and the importance of new rectenna designs.

6.2. Organic semiconductors for radiofrequency rectifying devices

Tommaso Losi, Fabrizio Viola and Mario Caironi
Center for Nano Science and Technology@PoliMi, Istituto Italiano di Tecnologia, Via Pascoli 70/3, 20133 Milano, Italy

Status

One of the most exploited methods to wirelessly power *smart objects* for IoT without the use of batteries is the coupling with radiofrequency waves incoming from a transmitter. Such waves resonate with a suitably designed antenna, following which a rectifying electronic device performs the AC–DC field rectification, as required to operate the load (sensors, circuits etc). Target frequencies span from the high-frequency (HF) range—from 3 to 30 MHz—to the ultra-high frequency (UHF) range—from 300 MHz to 3 GHz—depending on the final application. UHF is suited for *far-field* powering and communication protocols (with a read range up to 100 m) typically employed for security, while HF allows *near-field*, cm-range, communication and powering. In this scenario, different semiconductor technologies and scalable manufacturing processes have been investigated with the goal of ensure cost-effective fabrication of radiofrequency rectifiers, capable to be integrated with everyday objects at viable costs. Organic semiconductors are one of the most promising technologies to achieve such goal, since they can be deposited through cheap, low-waste and energy efficient techniques, such as printing [472]. Furthermore, organic materials do not need high temperature processing, thus being compatible with flexible substrates [472]. In the last decade, a lot of efforts has been devoted to the improvement of organic semiconductors performance, achieving the *operational frequency* in the HF regime when integrated in rectifiers. The latter are typically based on two-terminal devices, such as organic diodes, or three-terminal ones, such as organic field-effect transistors (OFETs) connected in trans-diode mode (figure 75a). Thanks to the development of scalable fabrication processes for device footprint reduction and for the deposition of high quality organic semiconducting layers with outstanding charge transport properties, supported by metal-semiconductors interface engineering to reduce contact resistance effects, operational frequency of both OFETs and organic diodes increased in the recent past: several demonstrations are available in the tens of MHz range [473, 474], with the record value so far of 160 MHz for the OFETs [475], and 14 GHz for the organic diodes [476] (figure 75b and c). Such progresses renewed the interest in this field towards the adoption of organic rectifiers for a plethora of applications, such as remote healthcare and distributed sensing, which require a technology integrating wireless-powered and large-area electronics with radiofrequency-communication capabilities.

Current and future challenges

Despite recent improvements in operational frequency of organic rectifiers, there are still several limitations which prevent the unlocking of their full potential, especially for UHF operation. Refined radiofrequency design of optimized rectifiers for efficient energy harvesting typically requires the use of transistors, while a diode-only technology poses limits in this sense. Therefore a technology enabling both diodes and transistors is preferable, with the additional advantage of allowing integration of electronic circuits with the same process. On the one side, current high-frequency organic diodes for which a multi-GHz cut-off frequency (f_C) was demonstrated [476], are based on ad-hoc two-terminal Schottky diode architectures. However, there are still major technological limitations (such as limited-throughput and scalability, as well as limited compatibility with large-area production), which do not allow the massive adoption of the reported multi-GHz cut-off frequency diodes. On the other, owing to a higher complexity, the achievement of high speed operation has proven more difficult for OFETs. One of the main reasons that has limited the achievement of UHF operation for OFETs so far, is inefficient charge injection or, in other words, a too high *width-normalized contact resistance* ($R_C W$) [477], rather than a low *charge carrier mobility* μ that is now comparable with that of low-temperature metal oxides ($\sim$10 cm^2 V^{-1} s^{-1}). As a matter of fact, only few works report $R_C W$ values <100 Ωcm, which are order of magnitudes higher compared to other thin-film technologies [477]. The detrimental effect of contact resistance becomes critical when high mobility semiconductors are employed in downscaled OFETs structures. However, the combination of high mobility semiconductors and downscaling is crucial for (i) the reduction of the *capacitive parasitism* related to the gate-to-source and gate-to-drain geometrical overlap (C_g), and for (ii) maximize *channel transconductance* (g_m), thus improving transition frequency according to:

$$f_T = g_m / 2\pi C_g = \mu_{\text{eff}} \left(V_g - V_T \right) / 2\pi L_c \left(L_c + 2L_{\text{ov}} \right) \tag{14}$$

where μ_{eff} is the *effective carrier mobility*, while L_c and L_{ov} are *channel* and *overlap length*. Another important limit is related to heat generation (or *self-heating*) during OFETs high-frequency operation. For example,
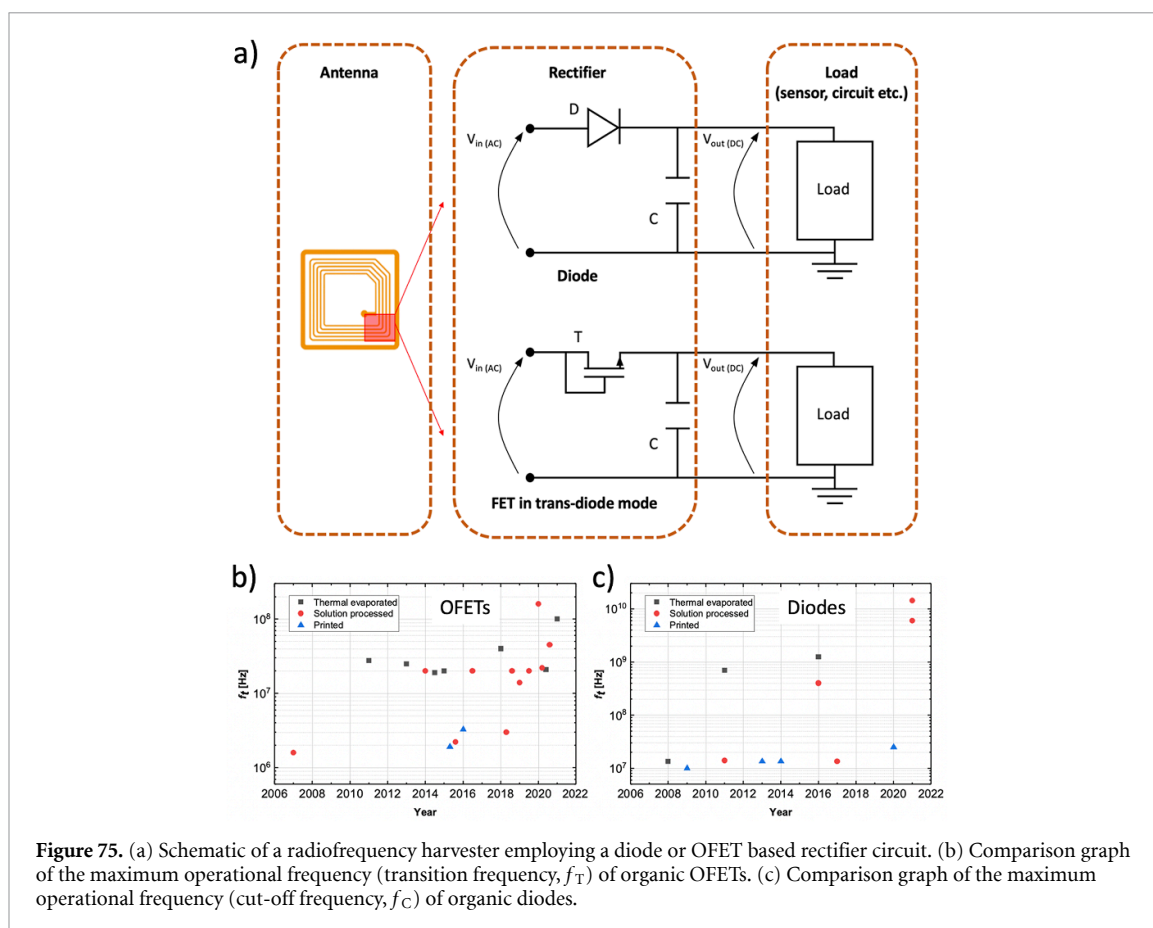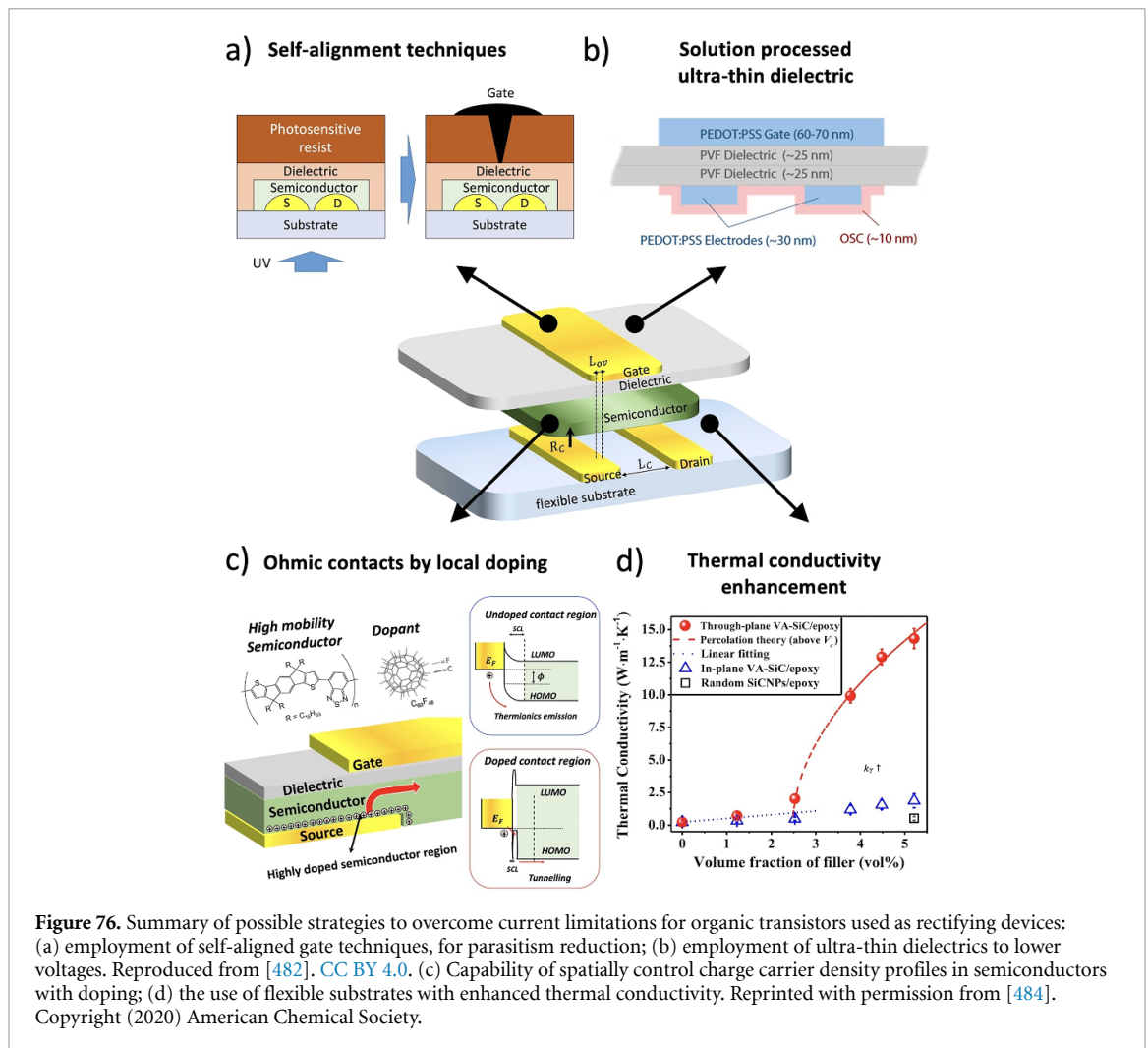
Figure 75. (a) Schematic of a radiofrequency harvester employing a diode or OFET based rectifier circuit. (b) Comparison graph of the maximum operational frequency (transition frequency, f_T) of organic OFETs. (c) Comparison graph of the maximum operational frequency (cut-off frequency, f_C) of organic diodes.

typical planar test-bed OFETs with micron-scale L_c, sustaining a current per unit width >1 mA mm^{-1} and voltages in the range of few tens of volts, need to dissipate efficiently a power density in the range of 10–100 W mm^{-2}. The *low thermal conductivity* of common flexible substrates and dielectrics does not allow it and irreversible thermal breakdowns take place. Reduction of driving voltages is by itself a challenge for f_T values at UHF, considering also that enhanced areal capacitances inevitably increase parasitism. Such thermal dissipation limit was evidenced also in vertical OFETs architectures, characterized by low voltages but much higher current densities, precluding continuous operation [478].

Advances in science and technology to meet challenges

As for UHF organic diodes, processes and architecture that can be exploited also for three-terminal transistors have the potential to enable monolithic integration of UHF circuitry. To this extent, recently proposed adhesion lithography nano-gaps [476], which were exploited to demonstrate coplanar organic diodes with f_C of 14 GHz, may offer an interesting platform also for nano-gap based organic transistors. At the same time, current developments in radiofrequency vertical organic transistors [479] should in principle offer excellent radiofrequency diodes. Yet, UHF operation has to be demonstrated in both cases, with necessary developments in charge injection and electrostatic control of nano-channels through a gate. Controlled multilayer methods, derived from vertical trench-based microfabrication techniques, have rarely been attempted with organics [480] and appear currently out of reach, yet might offer inspiration for future breakthroughs.

Concerning planar OFETs, charge injection issues are prevalent in limiting f_T, irrespectively of the technology adopted. The use of self-assembling monolayers (SAMs) on source and drain contacts, such as thiols, to reduce charge carrier injection barrier by energy levels matching and improved semiconductor morphology at the contacts, has been consistently adopted for more than 20 years [477]. Without doubt, this strategy sustained so far the improvement of AC characteristics of OFETs based on the adoption of more performing semiconductors in terms of mobility (e.g. dif-TES-ADT and DPh-DNTT for vacuum while IDT-BT, P(NDI2OD-T2) and DPPT-TT for solution based approaches). Yet, to benefit from even higher mobility materials (e.g. C$_9$-DNBDT, C$_8$-BTBT and organic blends between small molecules and insulating/semiconducting polymers such PS, PMMA and IDT-BT), alternative schemes are necessary to definitely overcome contact limitations. To this end, stable and controlled electronic doping strategies, to

Figure 76. Summary of possible strategies to overcome current limitations for organic transistors used as rectifying devices: (a) employment of self-aligned gate techniques, for parasitism reduction; (b) employment of ultra-thin dielectrics to lower voltages. Reproduced from [482]. CC BY 4.0. (c) Capability of spatially control charge carrier density profiles in semiconductors with doping; (d) the use of flexible substrates with enhanced thermal conductivity. Reprinted with permission from [484]. Copyright (2020) American Chemical Society.

allow engineering of *charge carrier density profiles* in organic semiconductors, are still largely missing. It is therefore important to further develop doping strategies, and in particular to achieve spatially controlled p- and n-type doping, so that charge carrier density can be controlled locally, e.g. at source and drain electrodes only, in order to achieve ohmic contacts while preserving current on-off ratio (figure 76c). The latter is particularly challenging owing to dopants diffusivity, which may change over time the doping profile.

Since contact resistance strongly depends on the local electric field at the electrode, in absence of local doping it is possible to mitigate its effect by exploiting high capacitance dielectrics [481]. High capacitances are also needed to reduce operating voltages, necessary for low power consumption. To this end, since low frequency relaxations make high-*k* organic dielectrics not viable, one efficient strategy may be represented by *pinhole-free ultra-thin dielectric layers*, robust enough against leakage currents and low voltage breakdowns [482] (figure 76b). The increased channel capacitance inherently produces a corresponding increase in capacitive parasitism, with an overall net decrease of f_T if more efficient device architectures for parasitism management are not adopted, compatibly scalable manufacturing. Self-alignment techniques are therefore highly desired. For instance, *self-aligned gate techniques*, whose compatibility with printing methods has been already demonstrated in the past [483], combined with local doping at contacts, appears to be a required advancement (figure 76a).

For what concerns the self-heating effect of OFETs, a further solution, along with reduce voltage operation, is the development of *flexible substrates with enhanced thermal conductivity* (κ), such as plastic composites, or the introduction of heat dissipation layers [484] (figure 76d).

Concluding remarks

Organic semiconductors are undoubtedly one of the most promising candidates for the development of radiofrequency rectifiers for IoT applications. They are particularly indicated when large area, high-throughput manufacturing, and easiness of integration with everyday objects are required. Moreover, they can offer many advantages (such as flexibility, energy efficient solution processability, low-cost,

bio-compatibility, recyclability), including the possibility of realizing complementary devices, with accessible schemes to monolithic circuit integration, distinguishing traits with respect to other emerging technologies. Yet, prospective downscaled manufacturing schemes should face real scenarios, with available fabrication facilities largely offering lithographic processes, and high-resolution mass scale printing facilities not yet deployed. Therefore, further scientific and technological advancements, required to tackle present drawbacks, should be contextualized in plausible manufacturing approaches to make this technology ready for commercialization towards a plethora of applications such as remote healthcare, distributed sensing, among others.

6.3. Metal-oxide semiconductors for radiofrequency rectifying devices

Dimitra G Georgiadou
Electronics and Computer Science, University of Southampton, Highfield Campus, Southampton SO17 1BJ, United Kingdom

Status

Metal oxide semiconductors are excellent candidates to replace Si and III–V compound semiconductors, such as gallium arsenide (GaAs), in wireless energy harvesting applications. They are characterized by good electrical properties, high optical transparency and compatibility with conventional semiconductor processes, e.g. photolithography. Metal oxide thin films can be deposited either via vacuum-based processes, such as sputtering, thermal evaporation, pulsed laser deposition (PLD) and atomic layer deposition (ALD) or solution-based methods (e.g. spin-coating, spray-coating, blade-coating, screen and inkjet printing), rendering processing on large-area flexible substrates possible. The potential to tune their optoelectronic properties through structural modification during deposition and their non-toxic nature render them ideal candidates to harvest wireless energy and power the IoT ecosystem or be implemented in novel wearable devices.

In their simpler binary form, they comprise a metal cation (i.e. Zn, In, Cu) and an oxide anion, while ternary, such as Indium Zinc Oxide (IZO), and quaternary metal oxides, such as Indium Gallium Zinc Oxide (IGZO), may also be formed. The latter oxides constitute amorphous semiconductors and are beneficial to the binary, usually polycrystalline ones, as they can be processed at lower temperatures and achieve greater film uniformity and higher device performance due to the lack of grain boundaries. Ultra-high mobilities over 100 cm^2 V^{-1} s^{-1} have been obtained with amorphous oxide-based thin-film transistors (TFT) [485].

From all metal oxides, IGZO is probably the most technologically mature material due to its wide implementation in the display industry. The Hosono group demonstrated in 2004 that high mobility IGZO films could be deposited with PLD at room temperature on flexible substrates [486]. Almost a decade later Schottky diodes based on radiofrequency-sputtered IGZO with rectification ratios $>10^8$, barrier heights of 0.85 eV and ideality factors close to unity were implemented by Chasin *et al* in a single-stage rectifier reaching 1.1 GHz frequencies [487]. The diodes were then integrated in energy harvesters comprising antenna, optimized impedance matching network and double half-wave rectifier with cut-off frequency of 3 GHz that could output >1 V_{dc} when placed 2 m away from the transmitter antenna [488]. Recently, record intrinsic cutoff frequencies >100 GHz and extrinsic cutoff frequencies of 42 GHz were demonstrated with Schottky diodes based on solution-processed ZnO [469] and IGZO [489], respectively, using a coplanar 10 nm gap asymmetric electrode structure.
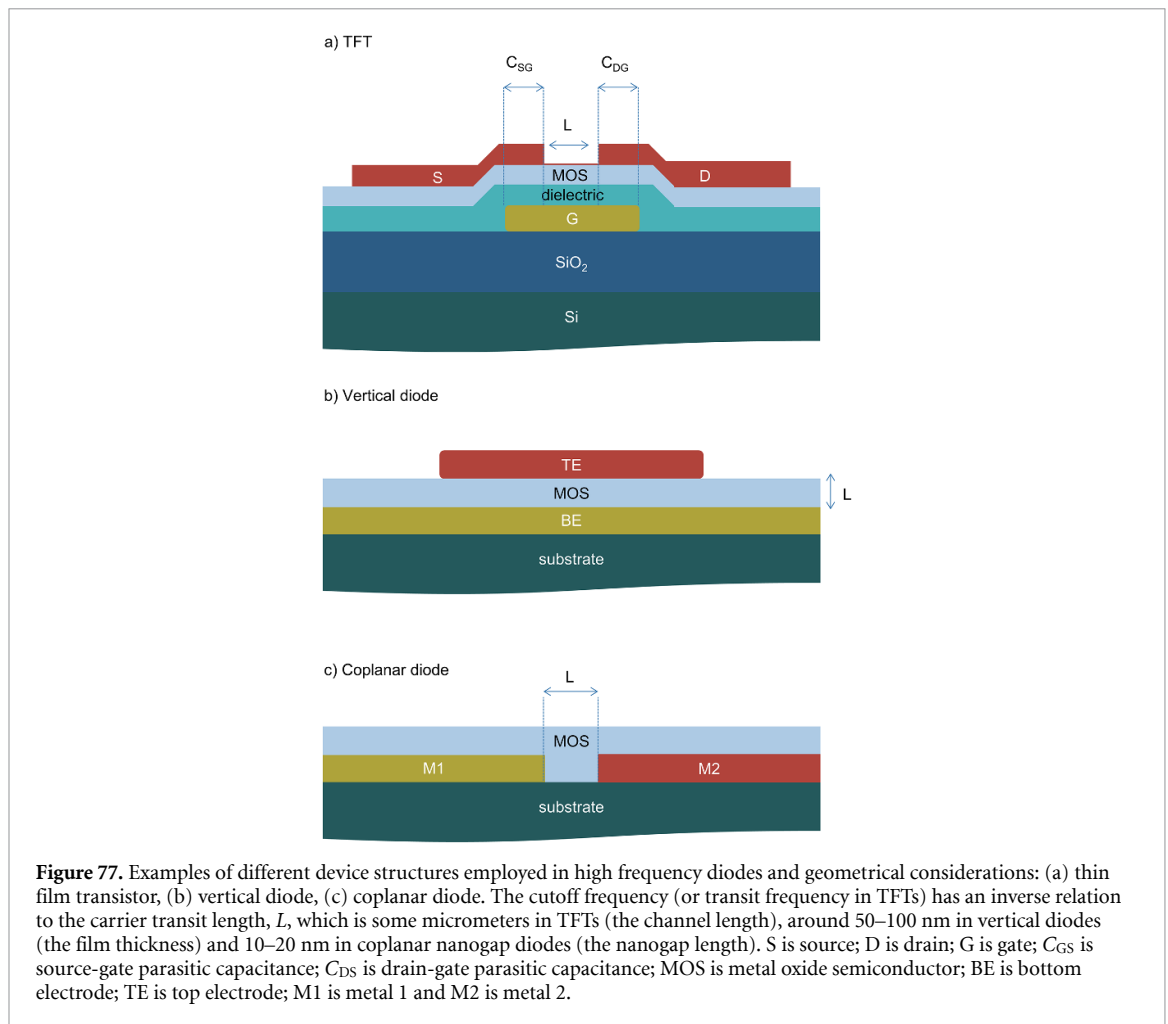
Current and future challenges

To increase the radiofrequency performance of Schottky diodes, junction resistance (R_j) and capacitance (C_j) need to be minimized at the same time. Increasing the mobility of metal oxide semiconductors is one way to reduce R_j and boost forward current. A thin layer of the oxide contributes also to resistance drop, although at the expense of lower rectification ratio and increased capacitance, limiting thus the frequency response.

Another issue with most metal oxides is the defects present in their structure, such as oxygen vacancies (V_O) formed during deposition or exposure to ambient air. The donor levels associated with V_O can lower the diode breakdown voltage and increase the leakage current.

The selection of suitable metal contacts and engineering the metal/semiconductor interface, both play a decisive role in the formation of ohmic or Schottky contacts. For instance, a polycrystalline top metal, exposing different facets to the semiconductor, may create inhomogeneities in the Schottky barrier height, whereas deposition of thin-film oxide semiconductors via sputtering often produces local variations in the oxide's electron affinity and the density of interface states [490]. On the other hand, certain metals can induce electrical doping of the oxide film. As an example, when Mo was used as bottom electrode in vertical diodes, where a zinc tin oxide film was produced from precursor inks, a low-doped Zn-Sn–Mo–O intermediate layer was formed. This has been found to form a rectifying junction, resulting in high voltage output $V_{out} \approx 5$ V when brought close to a Radio Frequency Identification (RFID) reader, while V_{out}/V_{in} exceeding 80% at <40 mm of distance was obtained [491].

The contact resistance challenge has been traditionally addressed by applying thermal annealing, oxygen plasma and UV-ozone to treat the Pt or Pd Schottky contacts with IGZO, as it ensures better stoichiometry at the interface. Lately, applying a hydrogen plasma treatment to the surface of an IGZO-based varactor to reach cutoff frequencies of 30 GHz was also demonstrated [492]. It was proposed that hydrogen passivates native defects in amorphous IGZO and increases the electron density, resulting in an ultra-low contact
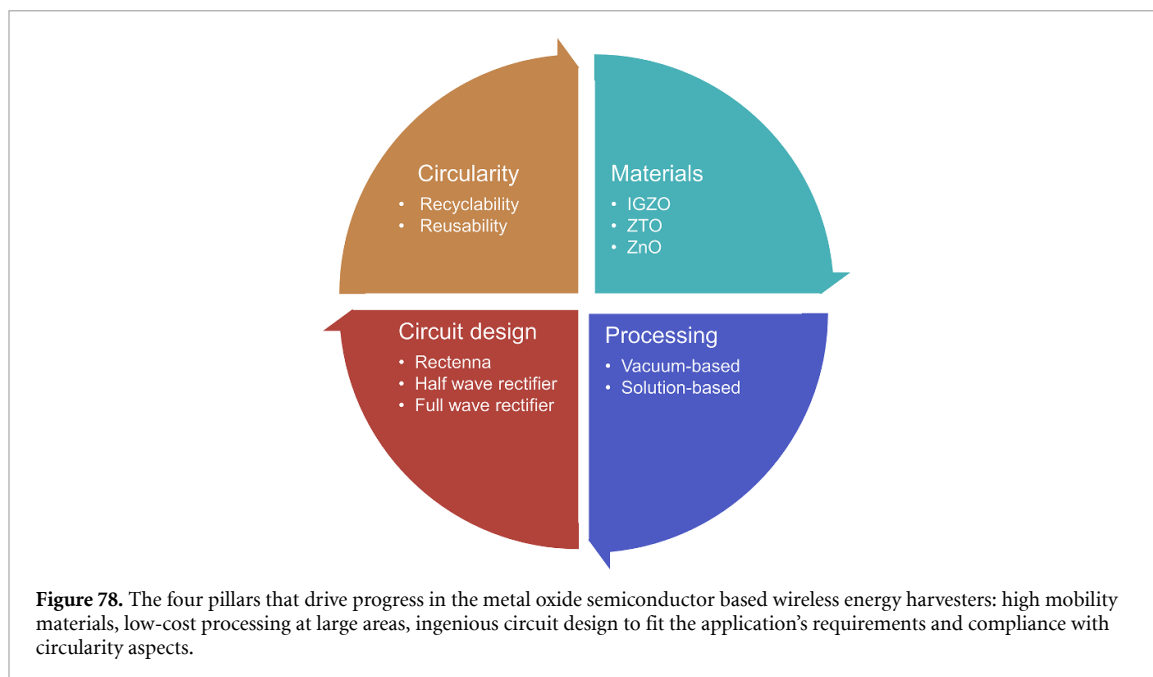
Figure 77. Examples of different device structures employed in high frequency diodes and geometrical considerations: (a) thin film transistor, (b) vertical diode, (c) coplanar diode. The cutoff frequency (or transit frequency in TFTs) has an inverse relation to the carrier transit length, *L*, which is some micrometers in TFTs (the channel length), around 50–100 nm in vertical diodes (the film thickness) and 10–20 nm in coplanar nanogap diodes (the nanogap length). S is source; D is drain; G is gate; C_{GS} is source-gate parasitic capacitance; C_{DS} is drain-gate parasitic capacitance; MOS is metal oxide semiconductor; BE is bottom electrode; TE is top electrode; M1 is metal 1 and M2 is metal 2.

resistance of 1.33×10^{-6} Ω cm^2 when Mo was used as the top metal. These concepts, however, have to be verified also for other metals and/or metal oxides.

Finally, from a purely material perspective, the future scarcity of some of the elements comprising the metal oxides should be taken into account, as the supply of Indium, Gallium and Zinc is uncertain in the longer term, while Tin is considered to be a conflict mineral.

Advances in science and technology to meet challenges

Despite recent advances, there is still a lot of room for improvement to overcome the current challenges of metal oxide radiofrequency energy harvesting devices and enable operation at 5G and 6G frequencies.

The quest to increase the rectifier performance in terms of operational frequency and power output demands ingenious geometry optimization in both TFTs and diodes structures. In TFTs, one approach is to minimize as much as possible the parasitic capacitance at the overlapping area between gate and source/drain by self-aligning the gate (figure 77(a)). First attempts towards this direction have resulted in maximum transit frequency (f_T) and oscillation frequency (f_{max}) beyond 1.1 and 3.1 GHz, respectively - the current record performance for IGZO-based TFTs [493]. In Schottky diodes, coplanar nanogap separated asymmetric electrodes (figure 77(c)), fabricated with a large area, high throughput nanopatterning technique, named adhesion lithography, constitute a promising recent development. Indeed, energy-harvesting circuits based on solution-processed ZnO and Al-doped ZnO films deposited on such 10 nm gap Al-Au coplanar electrodes showed intrinsic cutoff frequencies above 100 GHz and delivered output voltages of 600 mV and 260 mV at 2.45 GHz and 10 GHz for 8 dBm input, respectively [469]. However, the efficiency of these radiofrequency energy harvesters is still quite low, and their breakdown voltage is limiting the applications, thus more elaborate design of the electrodes is needed to minimize the transmission losses. It is noteworthy that, although there are several reports in the literature for such vertical nanotrench fabrication methods, there is no demonstration of those nanostructures in rectifier circuits, as they are significant challenges in creating asymmetric electrode structures, which are needed to obtain rectification in diodes. For this reason, they have been traditionally applied in biosensing applications [494]

Figure 78. The four pillars that drive progress in the metal oxide semiconductor based wireless energy harvesters: high mobility materials, low-cost processing at large areas, ingenious circuit design to fit the application's requirements and compliance with circularity aspects.

or in photonics [495]. There is, thus, ample room for further investigations in the field of nanotechnology, specifically targeting radiofrequency energy harvesting.

Moreover, from a manufacturing standpoint, it is important to increase the fabrication yield on flexible (e.g. plastic) substrates, as well as the monolithic patterning of the antenna and the rectifier on the same substrate, something which will be paramount in the field of flexible radiofrequency electronics. In this regard, substituting the annealing step of the metal oxide film by xenon flash lamp photonic sintering to protect the temperature sensitive substrates from prolonged exposure to high thermal budget processes has proven to be instrumental in obtaining solution-processed IGZO rectifiers operating at 47 GHz and can be applied more broadly in the fabrication of metal oxide films on flexible substrates [489].

Finally, the electronic devices still show insufficient durability to extreme physical deformation. To employ them in fully flexible applications, it is imperative to develop devices that can endure further mechanical stress.

Concluding remarks

Significant strides have been already made to develop efficient low-cost wireless energy harvesting systems to be deployed in the ever-growing IoT, especially in urban and industrial environments (figure 78). The development of ultra-high mobility metal oxide semiconductors, motivated by the next generation display industry, was achieved by controlling their chemical composition and applying diligent doping strategies. Although vacuum-based processes are well-established in complementary metal-oxide-semiconductor manufacturing and enable high-quality uniform films, solution-processing is a low-cost alternative, compatible with flexible and printable devices. The interplay between high frequency and maximum efficiency imposes meticulous design of the ensuing rectifier topology to tune the performance according to the requirements of the targeted applications. Finally, the potential to recycle or reuse the metals and metal oxides of the energy harvesting system will be critical in the following years, as we move towards a circular economy fostering more sustainable electronic technologies [496].

Acknowledgments

6.4. Carbon nanotubes for radiofrequency rectifying devices

Li Ding and Lian-Mao Peng
Key Laboratory for the Physics and Chemistry of Nanodevices and Center for Carbon-based Electronics,
School of Electronics, Peking University, Beijing 100871, People's Republic of China

Status

Carbon nanotubes can be derived from graphene by rolling up along a chiral vector C_h (n, m) which decides electrical properties such as excellent carrier mobility, saturation velocity and quasi-one-dimensional structure with small diameter leading to large current driving capability and high-speed performance for radiofrequency energy harvesting. Early rectifying devices built using carbon-nanotube-based diodes were fabricated on single carbon nanotubes by asymmetric contacts between Al or Ti (Schottky) and Au or Pt (Ohmic) [497–499] with cut-off frequency up to 6–18 GHz which were typically characterized with rectified signal (with frequency range from 7 to 18 GHz, a radiated power input of −8 to 9 dBm, and a 0.25 V bias) of 3.5–100 nA. But these approaches were limited severely by the use of individual semiconducting carbon nanotubes in the device channel, and more importantly the use of non-perfect contacts which inevitably leads to the formation of Schottky barrier which reduces the injection efficiency of electrons into the conducting carbon-nanotube channel and thus results in large series resistance of over several hundreds of $k\Omega$ to more than 1 $M\Omega$. Some other types of carbon-nanotube-based diodes were also reported, for example those based on half chemically doped channel [500] and heterojunction built with other nanomaterials [501]. However, the performance of these diodes is typically poor and these diodes are thus not suitable for radiofrequency rectifying devices.

The first high-performance carbon-nanotube-based rectifying barrier-free bipolar diode using individual semiconducting single-walled carbon nanotubes in the channel was reported in 2008 [502], where barrier-free and thus highly efficient carrier injection was realized by using Sc contact for n-region and Pd contact for p-region. Recent progress on aligned high-purity and high-density carbon-nanotube arrays by Peking University [503, 504] further remarkably improved carbon-nanotube-based radiofrequency rectifying devices, achieving a cut-off frequency of over 500 GHz, series resistance of down to 32 Ω and a large DC output of over 350 mV by rectifying 50 GHz signals. Figure 79 summarises progress on carbon-nanotube materials and device fabrication. It is worth noting, however, that the results achieved to date are still far from theoretical prediction, and it is expected that with further advances on carbon-nanotube materials and process, faster and more efficient carbon-nanotube-based rectifying devices will be soon developed.

Current and future challenges

Radiofrequency energy harvesting technologies demand excellent performance on conversion efficiency, insertion loss (series resistance R_s) and bandwidth (high-speed). Carbon nanotubes possess excellent electrical properties such as ultrathin bodies that resulting in excellent electrostatic properties and leading to high conversion efficiency, high current-carrying capability (low series resistance) derived from the ballistic nature of transport and high carrier mobility and saturation velocity with ultrasmall intrinsic capacitance for high-speed and have been regarded as promising materials for radiofrequency energy harvesting. However, based on reported results in figure 79, there remains large space for further performance improvement, and numerous challenges need to be solved to realize the complete potential of carbon-nanotube-based radiofrequency harvesting technology. These include: (1) Material challenges. Wafer-scale high-quality aligned semiconducting carbon-nanotube arrays are required for radiofrequency energy harvesting with a density of 200–300 carbon nanotubes per μm (over 300 carbon nanotubes per μm would suffer severe tube-tube shielding and crosstalk inducing performance degradation), a carrier mobility of more than 2500 cm^2 V^{-1} s^{-1} and a saturation velocity of up to 3.5×10^7 cm s^{-1}. An additional material challenge is to develop methods for decoupling polymer residues from solution-processed carbon-nanotube arrays while not introducing additional damages to the otherwise perfect carbon-nanotube structure. (2) Device structure and process. For improving current carrying capability and lowering series resistance, the rectifying device channel length should be scaled down to less than one micron or even 100 nm to maximize quantum efficiency. In principle metal parasitic resistance could be reduced by adopting specially designed device structures, such as T-shape contact. The fabrication of extremely scaled carbon-nanotube-based diodes with T-shape contact remains challenging for the commonly used planar fabrication approach, and more innovative approaches/architectures should be developed/adopted. (3) Circuits consideration. Energy
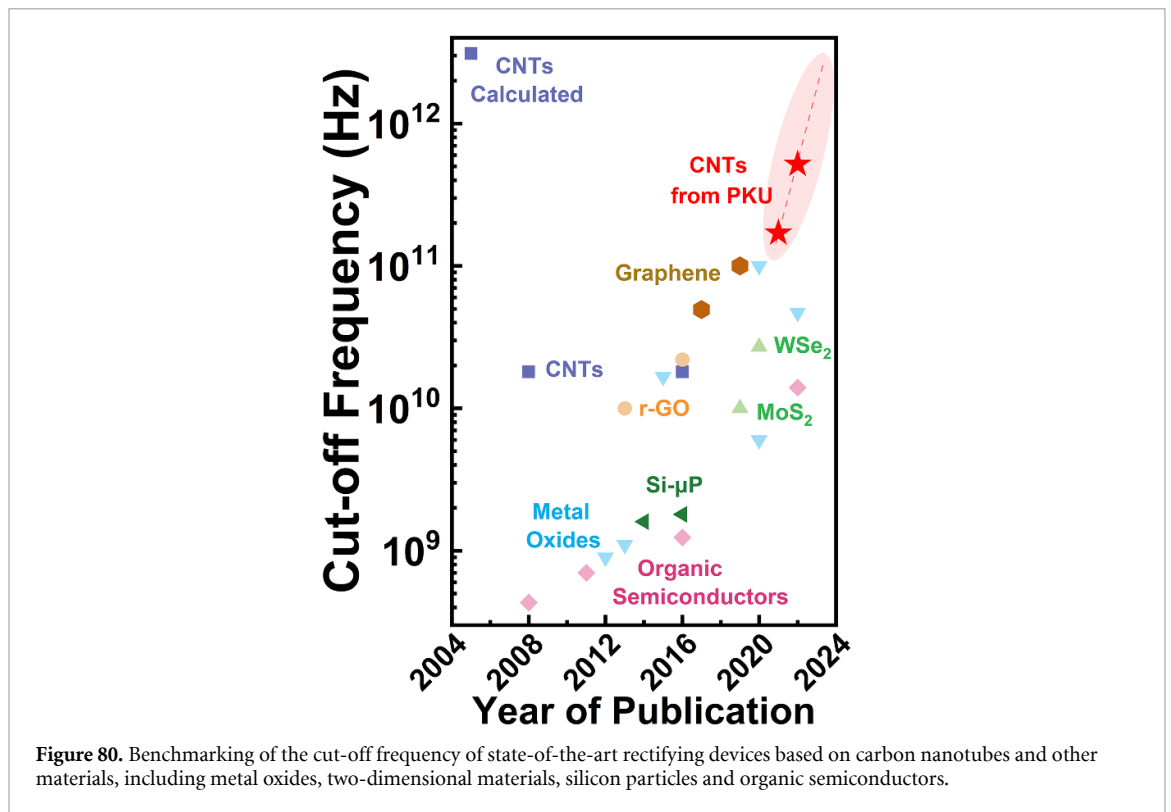
	Material	f_c (GHz)	$R_s (\Omega)$	C_j(F)	Rectified signal (V or A)	Rectification ratio	Year	Ref
1	Single-CNT	3100 (540) with 100 (4) CNTs, calculated	160K	N/A	N/A	~10^3	2005	[1]
2	CVD grown CNTs	> 18 GHz, extrapolated ~ 400 GHz, calculated	420K	~10^{-18}F	100 nA @ 7 GHz & 0.25 V (P_{in} = 9 dBm); 3.5 nA @ 18 GHz & 0.25 V (P_{in} = -8 dBm)	~10^2	2008	[2]
3	CVD grown single-CNT on Quartz	~ 6 GHz, extrapolated ~ 200 GHz, calculated	1.38 M	~ 100 aF	23 nA/mW @10 GHz& 1.5 V	~10^3	2011	[3]
4	Random oriented CNTs	N/A	N/A	N/A	1.8 V@10 MHz &3 V	>10^3	2011	[4]
5	Single-CNT	N/A	N/A	N/A	N/A	24	2021	[5]
6	Random oriented/ aligned CNTs	from 170 to over 500 GHz	<32Ω	C_{total}<100fF	350mV@50GHz & 1.5 V (P_{in} = -2 dBm)	N/A	2022	Unpublished

Figure 79. Representative works on carbon-nanotube-based radiofrequency rectifying devices, with such key performance parameters as cut-off frequency, series resistance and junction capacitance.

harvesting applications require more than just rectifying devices (diodes). In addition to the regular half/full wave bridge rectifier, voltage multiplier for boosting output and filtering circuits are also required. However, these important circuits have not been demonstrated for carbon-nanotube-based radiofrequency harvesting technology. Additional challenges include improvements on the uniformity of the tube-to-tube pitch, direction, and diameter of carbon nanotubes on a larger scale (such as on an 8-inch wafer).

Advances in science and technology to meet challenges

For material challenges, it is very important to design/select proper polymer molecules warping around carbon nanotubes for sorting and alignment procedure. Selection of polymer with fewer alkyl chains and decreased dispersion cycles would reduce scattering along the carbon nanotubes in the channel and improve carbon nanotube quality, leading to better mobility and saturation velocity. Degradable polymer would help for decoupling polymer from carbonnanotube arrays with dedicated post-treatment approaches. The density of carbon-nanotube arrays could be improved by selecting a pair of solution and polymer with stronger bonding force during the self-alignment procedure. Further, cheaper and larger scale processes are needed for preparing better carbon-nanotube materials for energy harvesting devices, i.e. monolayers or multilayers of high-purity and high-density semiconducting carbon nanotubes with narrower diameter distribution, lower defect density and better-quality interfaces with both metallic contacts and high-*k* dielectric for better control and utilization of wasted radiofrequency power in air. For device structure and fabrication, parasitic effects derived from channel length scaling and the adoption of T-shape contact should be further reduced by, e.g. adopting innovative three-dimensional integrated architecture [505]. For example, the two thick metal contacts of a diode could be fabricated separately into two adjacent layers to lower the parasitic effect of the conventional planar devices. Also, inkjet printing may be utilized for low-cost fabrication of carbon-nanotube-based devices. For circuits, due to the low power nature of harvested radiofrequency energy, extremely low-power processing and communication devices are required. To this end, carbon-nanotube Dirac source devices technology [506], which demonstrated almost half of power consumption compared with that of 14-nm-node silicon devices, could be utilized for carbon-nanotube-based radiofrequency rectifying devices. In principle, carbon nanotubes also have the advantage of being able to provide digital, radiofrequency and transducer components so that carbon-nanotube-based energy harvesting modules could be integrated into more powerful systems by system-on-chip-compatible processes with planar or even three-dimensional architecture. It is worth noting that relevant advances on radiofrequency rectifying technologies are of multidisciplinary nature and could

Figure 80. Benchmarking of the cut-off frequency of state-of-the-art rectifying devices based on carbon nanotubes and other materials, including metal oxides, two-dimensional materials, silicon particles and organic semiconductors.

also be utilized in a range of important emerging applications, including wireless sensor networks, IoT, machine-to-machine communications, smart skins/cities, medical monitoring and wearable electronics.

Concluding remarks

While early work has demonstrated that carbon-nanotube-based rectifying devices are promising in providing necessary modules for constructing highly efficient energy harvesting systems, numerous challenges need to be solved before the technology could be deployed into commercial products. It is expected that milestone performance progress on carbon-nanotube-based rectifying devices with low-cost and cut-off frequency surpassing 1 THz as shown in figure 80, will be accomplished in the near future with advances in science and technology including cheaper and larger scale material preparation processes and utilization of innovative three-dimensional integrated architectures with Dirac source devices technology for carbon-nanotube-based radiofrequency energy harvesting. Furthermore, the integration of carbon-nanotube-based radiofrequency rectifying devices, high-performance digital complementary-metal-oxide-semiconductor integrated circuits and ultrasensitive sensors in three-dimensional system-on-chip architectures will not only provide energy harvesting function, but also more active and powerful chips for a range of important emerging applications, including 5G/6G, IoT and smart skins/cities.

Acknowledgments

6.5. Two-dimensional materials for radiofrequency energy harvesting

Zhenxing Wang[1], Muh-Dey Wei[2], Renato Negra[2] and Max C Lemme[1,3]
[1] AMO GmbH, Otto-Blumenthal-Str. 25, 52074 Aachen, Germany
[2] Chair of High Frequency Electronics, RWTH Aachen University, Kopernikusstr. 16, 52074 Aachen, Germany
[3] Chair of Electronic Devices, RWTH Aachen University, Otto-Blumenthal-Str. 2, 52074 Aachen, Germany

Status

Two-dimensional materials, such as graphene and transition metal dichalcogenides (TMDCs), are considered for semiconductor technology applications due to their extraordinary electrical, optical, thermal and mechanical properties [507]. Specifically for the application in energy harvesting there are different approaches such as photovoltaic cells, thermoelectric energy harvesting, piezoelectric energy harvesting, rectifying antenna (rectenna-)based radiofrequency energy harvesting [146]. Here, we will focus on the rectenna-based approach, since the rest have been discussed in detail in [146].

A rectenna is typically composed of a nonlinear device like a diode and an antenna to harvest energy from electromagnetic radiation. The antenna receives an electromagnetic wave in free space, which is then converted to a DC voltage by the nonlinear device. There are many advantages in using two-dimensional materials such as graphene or TMDCs for such energy harvesting systems. Firstly, the high mobility of graphene is crucial to enable operation at THz frequencies or even optical frequency [508]. Secondly, graphene can be used to realize antennas with smaller dimensions compared to metals, which is relevant for the high-density integration of such systems [509]. In addition, the Fermi energy in graphene can be controlled by an electric field, which enables the tunability of the antenna oscillation frequency [509]. Last but not least, the high mechanical strength and flexibility of two-dimensional materials, combined with a thin-film technology that allows processing them on arbitrary substrates, largely expands the application field of graphene diodes and antennas for wearable electronics compared to canonical semiconductor devices.

For example, a flexible rectenna system has been realized for Wi-Fi band wireless energy harvesting based on MoS_2 material, as shown in figure 81(a). The core of this device is a Schottky diode based on a MoS_2 phase heterojunction, which operates up to 12 GHz, covering most of the unlicensed industrial, scientific and medical radio bands, including the bands for Wi-Fi [510]. At higher frequencies, graphene has been utilized for energy harvesting at frequencies up to 170 GHz, employing metal–insulator-graphene (MIG) diodes, as shown in figure 81(b) [511], and up to 28 THz based on geometrical graphene diodes, as shown in figure 81(c) and (d) [512].

Current and future challenges

Firstly, the operation frequency of the rectenna system is limited by the *RC* time constant, where *R* is the series resistance of the rectenna, and *C* is the parasitic capacitance. The sheet resistance of two-dimensional materials is typically much higher compared to bulk materials [513]. In addition, the electric contacts to two-dimensional materials also contribute considerably to the total resistance due to the van-der-Waals bonds between the metals and the two-dimensional materials [513]. These two components of *R* limit the operation frequency of the system. When it comes to the parasitic capacitance, *C*, two-dimensional materials have a clear advantage over other materials. For example, in the MIG diode configuration shown in figure 81(b), the parasitic capacitance can be largely reduced due to the 1-dimensional junction. In a geometrical diode like shown in figure 81(c), the parasitic capacitance is largely reduced since there is no dielectric involved in the operation of such diodes, although the resistance is a limiting factor due to the small dimension of the junction. These aspects must be considered when designing a rectenna for high frequency operation.

Secondly, the efficiency of the energy harvesting is limited by several factors. These include, but are not limited to, the absorption efficiency of the antenna, the impedance matching between the antenna and the diode and the power consumption of the electronic circuits that manage the power between the energy harvesting unit and the functional unit, e.g. the communication circuits.

Thirdly, the two-dimensional-material growth needs to be scaled up and become manufacturable, i.e. the quality, repeatability and reliability of the process technology must meet semiconductor industry standards. This is a prerequisite for two-dimensional-materials-based energy harvesting systems to achieve the desired functionality, because semiconductor technology provides a mature platform, especially in terms of
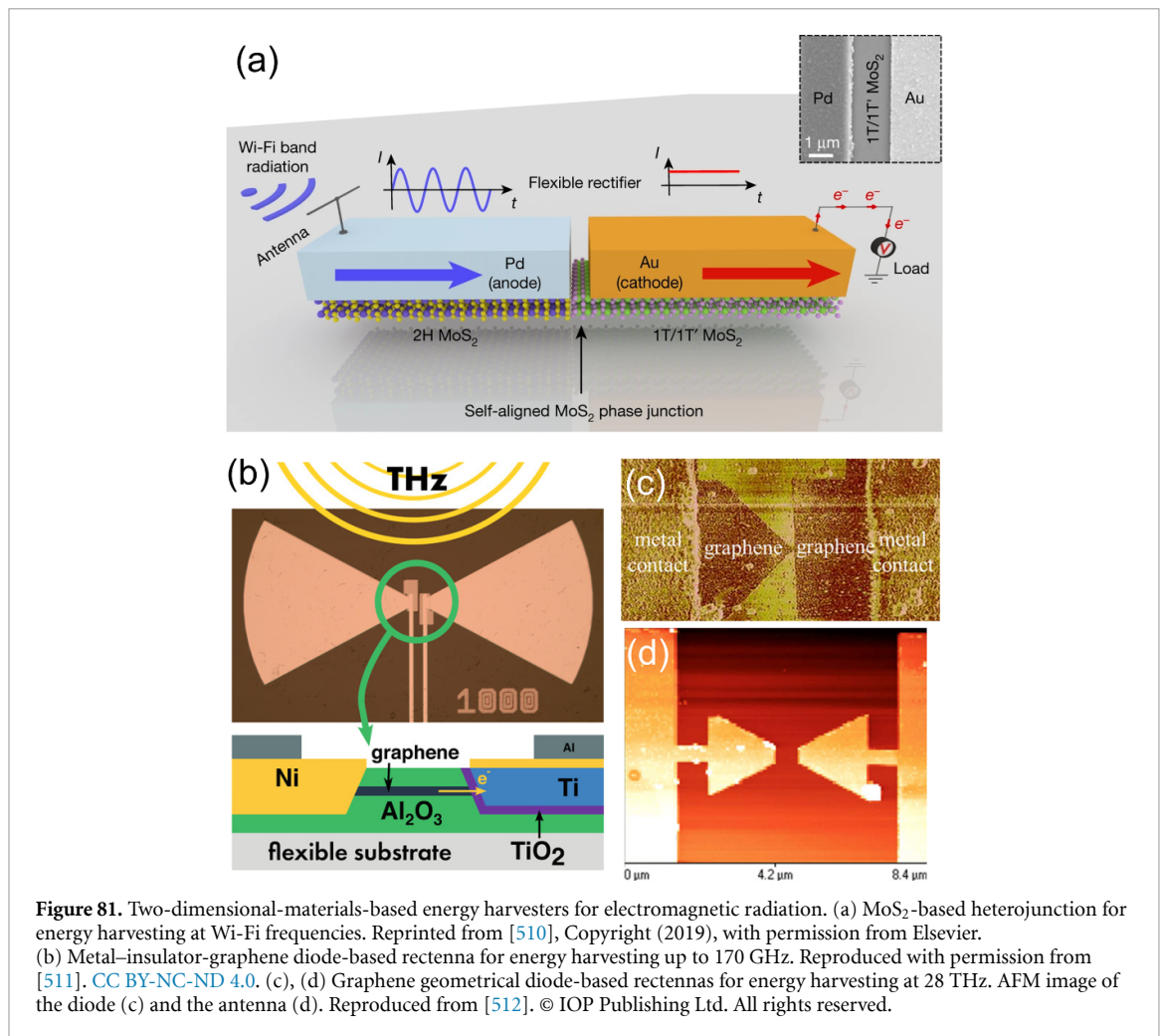
Figure 81. Two-dimensional-materials-based energy harvesters for electromagnetic radiation. (a) MoS$_2$-based heterojunction for energy harvesting at Wi-Fi frequencies. Reprinted from [510], Copyright (2019), with permission from Elsevier.
(b) Metal–insulator-graphene diode-based rectenna for energy harvesting up to 170 GHz. Reproduced with permission from [511]. CC BY-NC-ND 4.0. (c), (d) Graphene geometrical diode-based rectennas for energy harvesting at 28 THz. AFM image of the diode (c) and the antenna (d). Reproduced from [512]. © IOP Publishing Ltd. All rights reserved.

electronics [513]. Although this aspect can be considered an engineering issue, it is still rather challenging and will require substantial resources.

Advances in science and technology to meet challenges

Firstly, the quality of the two-dimensional materials grown by scalable methods such as chemical vapour deposition or epitaxy needs to be further improved to realize the lowest possible sheet resistance. Here, the availability of large-scale material is a significant point to address high-volume production. The material should be ideally single-crystalline material over entire wafers to enable ballistic transport at room temperature, which is especially relevant for the geometrical graphene diodes shown in figures 81(c) and (d). MIG diodes may have lower quality requirements and may tolerate uniform polycrystalline material with relatively high room temperature mobility. Similarly, a scalable approach is needed to provide low contact resistances between the metals and the two-dimensional materials, a challenge that has recently seen promising progress [514]. These efforts will lead to increasing the operation frequency of two-dimensional-materials-based rectennas.

Secondly, to design and optimize the input matching networks as well as the output load networks for rectifiers, a precise large-signal radiofrequency/microwave model is necessary [514] (as shown in figure 82(a)). A fully integrated rectifier with a suitable load impedance (C_L and R_L) is as critical as the input matching network (as shown in figure 82(b)). Such a model can then be used to optimize the load versus efficiency (as shown in figure 82(c)). This example indicates that an accurate large-signal model is essential to obtain high efficiency. Once, such a value chain is implemented, full integration is needed to realize rectifier arrays to boost output energy.

Lastly, device and circuit fabrication have to be scaled up to enable the integration into existing semiconductor platforms. Currently, the 2D Experimental Pilot Line (2D-EPL), a project funded by the
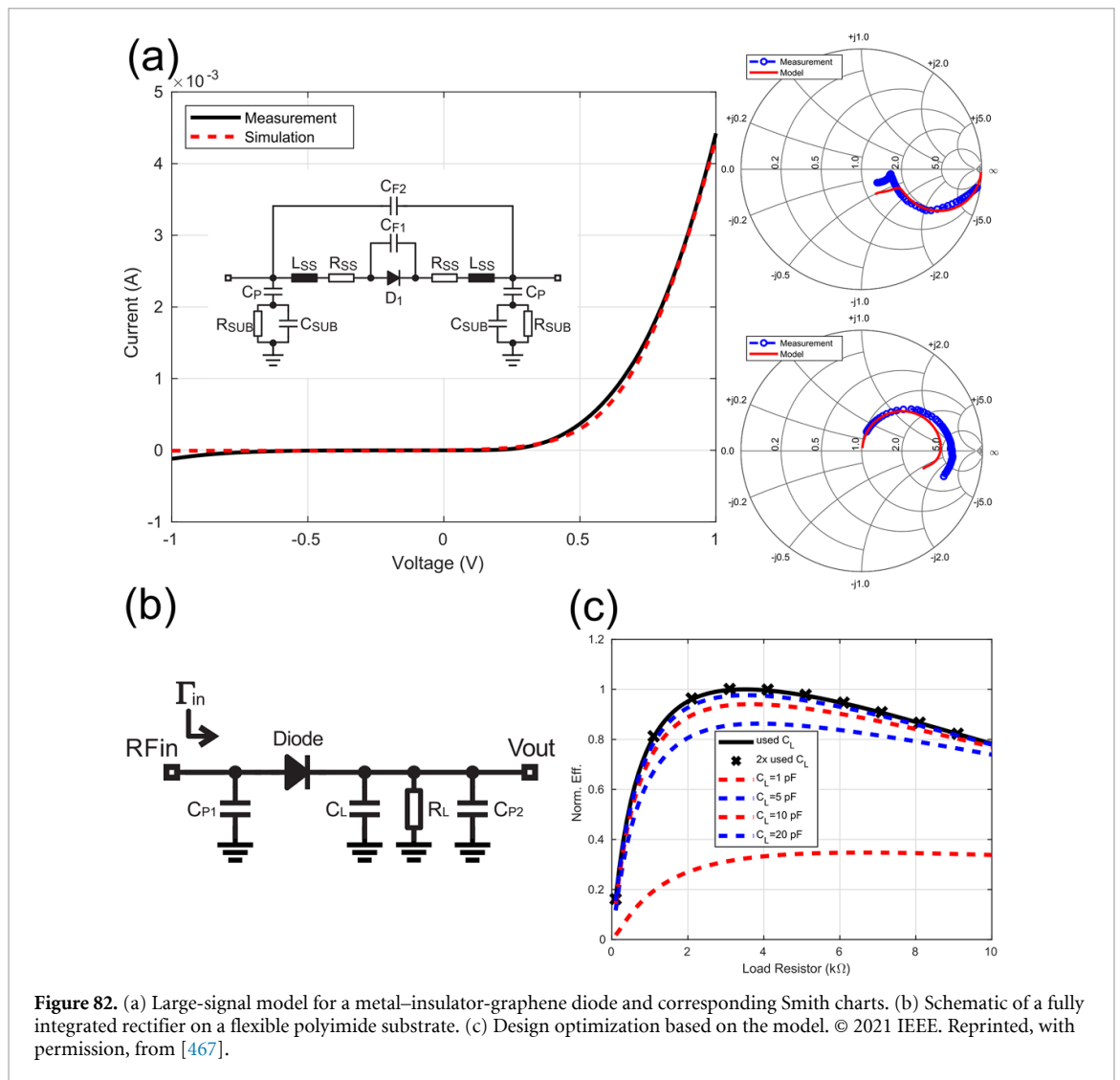
Figure 82. (a) Large-signal model for a metal–insulator-graphene diode and corresponding Smith charts. (b) Schematic of a fully integrated rectifier on a flexible polyimide substrate. (c) Design optimization based on the model. © 2021 IEEE. Reprinted, with permission, from [467].

European Commission, focusses efforts on solving issues with relevant process steps, such as two-dimensional layer growth and transfer, electrical contacts, active area patterning, passivation and process chemistry. If successful, this endeavour can pave the way towards reliable semiconductor manufacturing of two-dimensional materials and circuits.

Concluding remarks

Two-dimensional materials are promising candidates for energy harvesting devices, especially for wearable systems due to their mechanical flexibility. In this section we focused on rectennas for electromagnetic radiation harvesting. Graphene-based devices, in particular, have been shown to rectify signals up to THz frequencies. However, minimizing parasitic *RC* components will be required to maximize the efficiency of the energy harvesting systems. Wafer-scale fabrication in existing semiconductor platforms is a serious engineering problem but probably not a basic scientific roadblock. There are ample examples in literature that indicate that a technology based on two-dimensional materials can play a unique role for future (wearable) electronic systems.

Acknowledgments

6.6. Materials for rectennas and radiofrequency energy harvesters

Mahmoud Wagih[1,2] *and Steve Beeby*[2]
[1] James Watt School of Engineering, University of Glasgow, Glasgow G12 8QQ, United Kingdom
[2] School of Electronics and Computer Science, University of Southampton, Southampton SO17 1BJ, United Kingdom

Status

Rectennas were first conceived in the 1960s for powering unmanned aerial vehicles (UAVs), with over 100 W being received by a UAV rectenna array over five metres indicating that microwave power beaming can enable battery-less systems. Given the importance of mass in UAVs and in applications in microwave solar power beaming envisaged later, the first material challenge was realizing lightweight rectenna arrays that minimized the vehicle's payload [515]. The research then moved to mmWave frequencies to enable antenna miniaturization in both terrestrial and space, given the shorter wavelength which enables more directional antennas [516].

Nowadays, there is renewed interest in rectennas following the rise of energy harvesting as a method of powering the growing IoT. Rectennas can recycle ambient radiofrequency emissions from cellular networks [517], as well as receive microwatt-level power 'packets' in radiofrequency-powered networks. Rectennas are distinguishable from energy harvesters requiring smart materials such as piezoelectric and thermoelectric harvesters; rectennas only rely on conductors, for the antenna, and semiconductors, for the rectifiers; both are found in most electronic systems. With advances in 'large-area electronics' including flexible, printed, and textile-based conductors, rectennas can be utilized in new application domains, where other energy harvesters might be impractical or inappropriate. From a radiofrequency design perspective, this imposes new challenges, where cost and size are the major constraints, implying a potential trade-off between optimal radiofrequency performance and material choice.

Current and future challenges

For rectennas to replace, or augment, batteries, their power harvesting (converting radiation to guided waves) and power conversion (from radiofrequency to DC) efficiencies need to be improved. This has been the main research challenge in the context of radiofrequency energy harvesting [517] and is often limited by conductive and dielectric material losses. Therefore, passive radiofrequency components, such as a rectenna's matching network and antennas, are often implemented on low-loss materials. Additional challenges arise from the electromagnetic medium surrounding the rectennas, where rectennas cannot be considered in isolation of the materials in their environment. Antennas are affected, for example, by operating near high-permittivity or lossy (low-resistivity) materials including biological tissue [518], moisture absorbing materials, or reflective surroundings.

The traditional route of implementing rectennas on low-loss materials can compromise other requirements. The key electrical and mechanical requirements, which represent ongoing research challenges can be summarized as:

1. Rectenna conductors maintaining a low sheet resistance, at radiofrequency, to reduce conductive losses in the antenna and any rectifier impedance matching network.
2. The rectenna being limited to geometrical features which can be resolved using low-cost and scalable fabrication processes such as additive manufacturing.
3. Fabrication processes enabling the integration of packaged or unpackaged devices, e.g. Schottky diodes or monolithic complementary-metal-oxide-semiconductor integrated circuits, for different rectifier topologies.
4. The conductors, and any encapsulating dielectrics, exhibiting suitable mechanical properties for applications such as flexible, wearable, implantable, or spaceborne rectennas.
5. Ultimately, the rectennas must be able to maintain their radiofrequency performance in their deployment environment, for example without the antennas detuning or suffering from absorption.

Advances in science and technology to meet challenges

Rectennas have been successfully demonstrated across the breadth of IoT applications utilizing flexible conductors, textiles, Laser-induced Graphene (LiG), biodegradable metals (Mg), and ultra-thin liquid metals, as shown in figure 83. Transitioning to such materials, which often have sub-optimal radiofrequency properties, cannot be simply achieved by copying existing rectenna designs.

Material-induced losses can be minimized through effective rectenna design. For example, by designing the antennas to directly match a rectifier or the input impedance of an integrated circuit, a separate matching
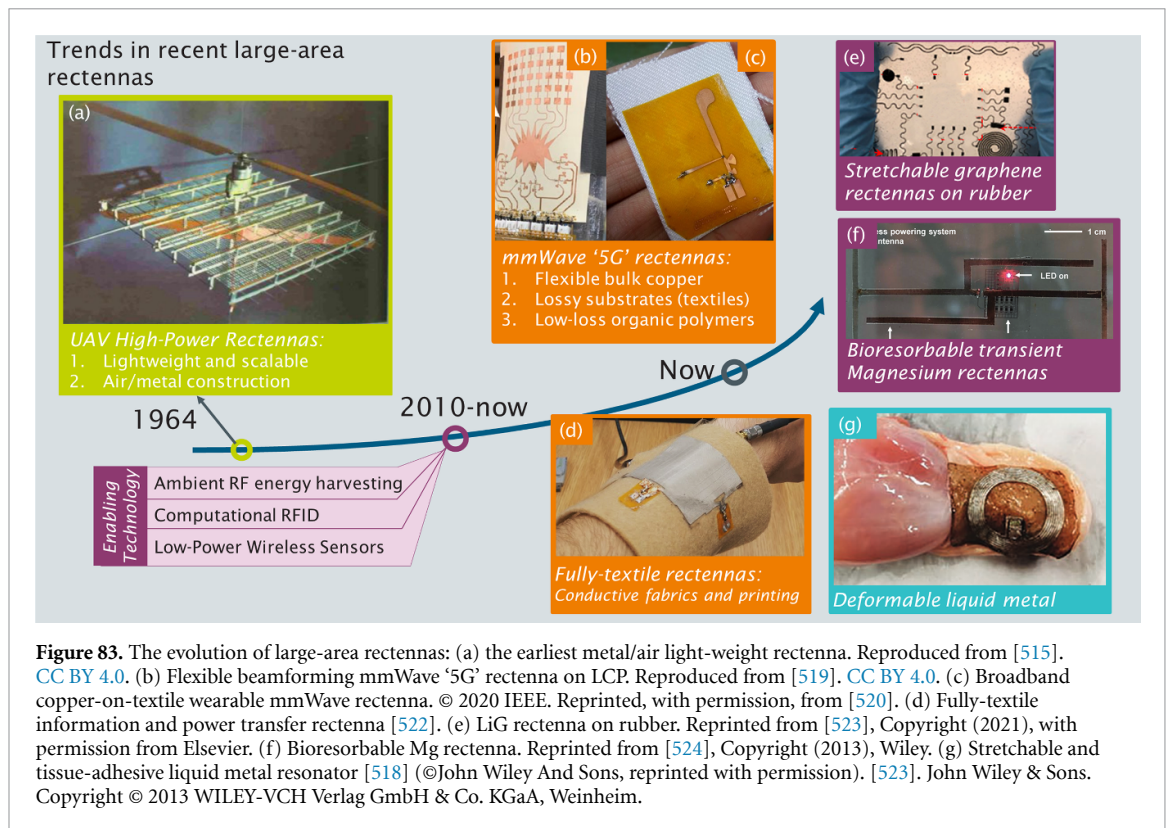
Figure 83. The evolution of large-area rectennas: (a) the earliest metal/air light-weight rectenna. Reproduced from [515]. CC BY 4.0. (b) Flexible beamforming mmWave '5G' rectenna on LCP. Reproduced from [519]. CC BY 4.0. (c) Broadband copper-on-textile wearable mmWave rectenna. © 2020 IEEE. Reprinted, with permission, from [520]. (d) Fully-textile information and power transfer rectenna [522]. (e) LiG rectenna on rubber. Reprinted from [523], Copyright (2021), with permission from Elsevier. (f) Bioresorbable Mg rectenna. Reprinted from [524], Copyright (2013), Wiley. (g) Stretchable and tissue-adhesive liquid metal resonator [518] (©John Wiley And Sons, reprinted with permission). [523]. John Wiley & Sons. Copyright © 2013 WILEY-VCH Verlag GmbH & Co. KGaA, Weinheim.

network stage can be eliminated reducing the additional insertion losses in planar transmission lines or lumped components [521, 524]. This antenna-circuit co-design approach has enabled a pervasive technology such as RFID; RFID tags are a rectenna with the rectifier monolithically integrated within an integrated circuit. Recently, rectennas were integrated within the aperture of communication antennas, enabling miniaturized systems that can simultaneously receive power and information without compromising the radiofrequency performance of either the communication or energy harvesting [521]. Effective radiofrequency and mechanical co-design has also be used to improve the resilience of rectennas. For example, a meandered structure can negate the effects of strain on the performance of a LiG-on-rubber rectenna [523]. The use of liquid metals and other highly deformable ultra-thin materials could enable rectennas to be utilized in implants and other challenging environments [518].

As low-cost IoT rectennas move towards the mmWave 'beyond 5G' spectrum (>24 GHz), new designs have evolved to overcome material and channel losses [516]. For instance, beamforming rectenna arrays can be used to achieve wide angular coverage and high gain [519], whereas broadband antennas miniaturized-radiator could be used to overcome dielectric losses on lossy or biodegradable substrates including textiles and paper [520]. Metamaterials and quasi-wireless transmission lines are expected to play a role in 'engineering' the environment surrounding rectennas, enabling higher efficiency than near-omnidirectional radiation [525].

Concluding remarks

Rectennas can be, and have been, realized using virtually any conductive material, making them a strong candidate for most power-autonomous systems. Future rectennas will be realized using hybrid integration of different platforms such as large-area passive circuits, monolithic integrated circuits, and novel semiconductors. Optimal rectenna design for overcoming material losses is expected to be an ongoing research challenge, as new biodegradable, flexible, and large-area electronic devices are developed.

Acknowledgments

7. Sustainability considerations on energy harvesting materials research

T Ibn-Mohammed[1], *K B Mustapha*[2] *and A P Joshi*[1]
[1] Warwick Manufacturing Group (WMG), The University of Warwick, Coventry CV4 7AL, United Kingdom
[2] Departments of Mechanical, Materials and Manufacturing Engineering, University of Nottingham (Malaysia Campus), Semenyih 43500, Selangor, Malaysia

The significance of sustainability in energy harvesting materials research
Remote wireless sensor networks, untethered devices associated with the IoT, self-powered wearable gadgets, and a host of other high-performance low-power microelectronics are central to the progress of connected cars, smart homes, smart factories, futuristic smart cities, large-scale embedded automation, and monitoring of critical infrastructure in dangerous/harsh/isolated environment. A crucial factor to consider for the operation of these devices is the power requirement. A cornerstone of the current source of power for most of these devices comprises various kinds of batteries, which may be in the form of either: (i) a primary battery, which is non-rechargeable and inherently beset by environmentally disastrous disposal problems; or (ii) a secondary battery which is rechargeable but plagued by cumbersome dismounting, recharging, and mounting routine.

No doubt, several notable revolutionary signs of progress have been reported about battery technology in recent years [526]. Despite this, as we inch closer to the possibility of a 'Trillion Sensor Universe' and the prediction of a spike in uptake of IoT-connected devices reaching tens of billions by 2023, valid concerns have been expressed about the cost and reliability of batteries. Besides, with the projected increase in sensors and IoT-connected devices, the cumulative public health and sustainability issues around the production, disposal, and recharging of zillions of batteries to power these devices have rightly ignited interest in scavenging low-profile, wasted energy through energy harvesting devices. Matured technologies in this regard include photovoltaic and wind energy harvester systems, both of which have received a preponderant of attention due to their higher power densities for macroscale power generations. However, waves of significant development in recent years have enabled the growth of low-amplitude power harvesting schemes [527]. Broadly, this includes: (i) harvesting of thermal gradients with thermoelectric generators; (ii) kinetic harvesting from mechanical movement through piezoelectric/triboelectric/magnetoelectric effects; and (iii) harvesting of ambient radio/electromagnetic wave/acoustic energy, among others.

Collectively, the above-mentioned energy harvesting systems have been recognized as essential to the achievement of the Sustainable Development Goal (Goal 7: 'Ensure access to affordable, reliable, sustainable and modern energy for all'). Fundamentally, the practical implementation of the energy harvesting scheme is tightly bound to rigorous materials research, regardless of the conversion technology category. Correspondingly, a huge volume of work has been dedicated to the investigation of the functional performance of the attendant materials [528], for instance, high-performance photovoltaic solar cells, thermoelectric materials with high electrical conductivity and Seebeck coefficient and low thermal conductivity, and kinetic energy harvesting materials. On the other hand, as these devices move from laboratory-based proof-of-concept to actual applications, the sustainability of materials, which has been much so far overlooked, must be pursued.

LCA case studies of energy harvesting materials technologies
In this section, four life cycle assessment (LCA) case studies that have identified environmental sustainability hotspots in energy harvesting materials technologies, including photovoltaics, piezoelectrics, triboelectrics, and thermoelectrics are discussed. LCA is a computational technique for assessing the potential environmental impacts associated with a product across its entire supply chain and it involves four main steps, including (i) goal and scope definition, (ii) inventory analysis, (iii) lifecycle impact assessment, and (iv) interpretation [529]. It is science-based, but not free from subjective judgement, covering a broad spectrum of environmental impacts to avoid burden shift from one aspect to another. Figure 84 provides a system boundary illustration for the comparative lifecycle analysis of non-oxide vs. oxide-based thermoelectric modules.

Several types of novel solar photovoltaic materials, including organic semiconductors, dye-sensitized oxides, colloidal quantum dots, and perovskites have emerged in recent years and have been touted to be economically and environmentally viable options to traditional silicon-based technology. To verify this assertion, several comparative LCA studies have been conducted. Gong *et al* presented the environmental impacts two types of perovskite solar cells across sixteen impact categories in comparison to other types of photovoltaic technologies, concluding that not only perovskite solar cells demonstrated environmental edge, but they also possess ultra-low energy payback period (EPBP) [530]. This reduced EPBP is attributed to a reduction in the energy-intensive processes required for the manufacturing of perovskite solar cells due to
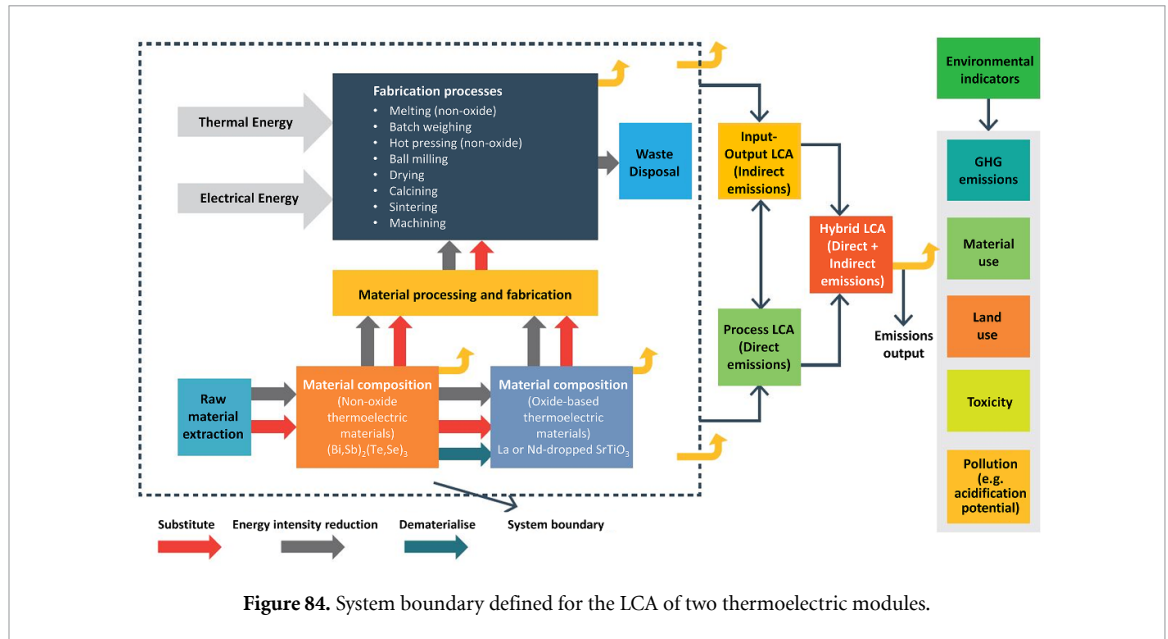
Figure 84. System boundary defined for the LCA of two thermoelectric modules.
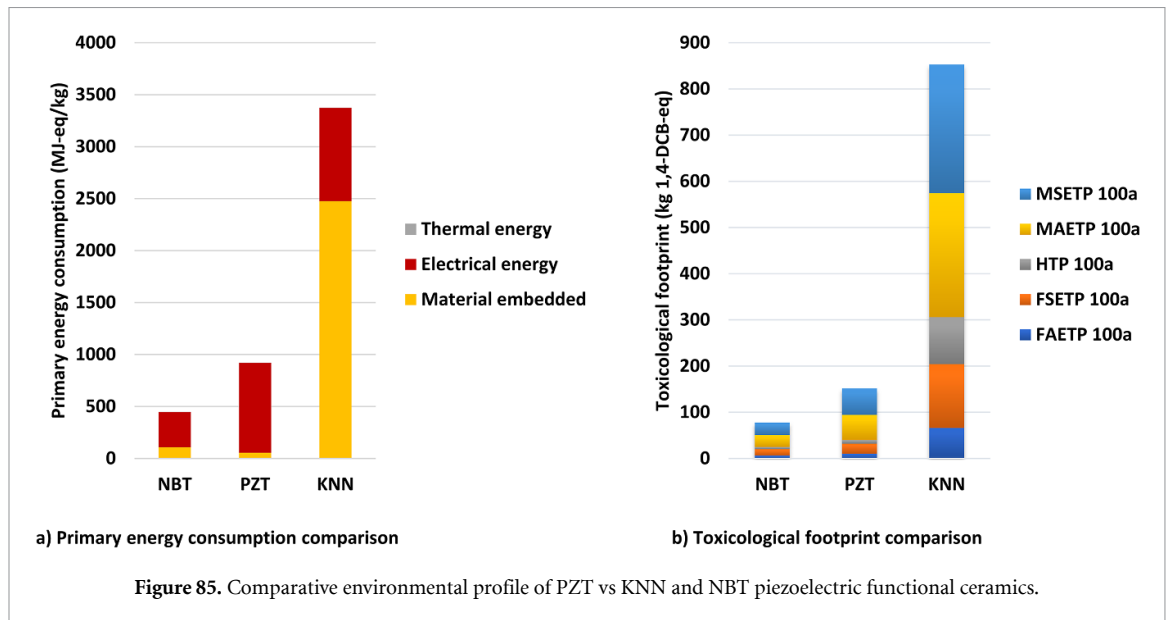

Figure 85. Comparative environmental profile of PZT vs KNN and NBT piezoelectric functional ceramics.

the elimination of silicon and rare earth element processing. Nonetheless, the use of gold in the material architecture of perovskite solar cells caused significant environmental impact due to the enormous energy required for its production from its ore. In the context of ambient energy harvesting for IoT applications, more LCA work is required.

Due to its toxicity, global policy initiatives and legislation, such as the Waste Electrical and Electronic Equipment and RoHS), have called for the prohibition of lead in piezoelectric materials. This has reinvigorated the race to develop lead-free alternatives based on potassium sodium niobate (KNN) and sodium bismuth titanate (NBT) for lead zirconate titanate (PZT). To ascertain the environmental benefits of lead-free alternatives over lead-based ones, Ibn-Mohammed *et al* adopted LCA to establish the fact that KNN is environmentally worse than PZT with respect to climate change and eco-toxicity due to the presence of the niobium pentoxide whose mining and milling, through hydro- and pyro-metallurgical processing, for refining niobium has substantial adverse impacts across numerous environmental indicators [531]. The same authors in another paper [532] highlighted that the lower energy consumed by NBT during synthesis yielded a lower overall environmental profile, based on primary energy consumption and toxicological impact, in comparison to PZT and KNN (see figure 85). Nonetheless, the authors noted that bismuth and its oxide constitute by-product of lead smelting, and when NBT is compared with PZT, it was shown that across several key indicators, bismuth oxide has a higher environmental impact compared to lead oxide, because of the additional processing and refining steps which pose extra challenges in metallurgical recovery.

Triboelectric nanogenerators offer the potential to generate energy in self-powered devices at low cost but their environmental impact was unknown until Ahmed *et al* conducted the LCA and techno-economic analysis of two triboelectric nanogenerator modules [533]. Module A, a thin-film-based micro-grating triboelectric nanogenerator, with its electrode arrays arranged linearly, generates enough energy to power standard electronics and Module B, which uses a planar structure based on electrodes generating periodically charged triboelectric potential, yielding energy from water and air flow and bodily movement. Their results reveal that, compared to Module B, Module A presents a better environmental profile, lower production costs, lower CO_2 emissions and a shorter EPBP. Module B's higher environmental impact is due to its higher content of acrylic in its structure and higher electrical energy requirements during fabrication. Acrylic can however be recycled or reused at the end-of-life stage releasing no toxic gases during combustion, thus improving its overall profile. Nonetheless, when compared with emerging solar photovoltaic technologies, triboelectric nanogenerator modules offer better environmental profile and a shorter EPBP, although Module B is marginally higher than that of a photovoltaic technology based on perovskite-structured methylammonium lead iodide. Future works on triboelectric nanogenerators pertain to lifetime and efficiency improvements rather than the identification of cheaper materials and manufacturing processes. Although EPBP was employed as a figure of merit in this analysis, this may not be the best for ambient energy harvesting applications. This is because the embodied energy (i.e. the emissions across the entire value chains) of ambient energy harvesters can be potentially high. As such, a better figure of merit would be the net environmental gain, which is a function of how the embodied energy compares with the operational energy saved over their lifetime as well as the energy that would otherwise be required if, for instance, batteries were employed as the power source. This aspect, however, has yet to be assessed in a systematic way, which demands further investigations across the various energy harvesting technologies.

Thermoelectric materials constitute the main element of thermoelectric generators, enabling the conversion of waste heat into electricity. Due to the presence of heavy metals and rare-earth elements in the constituent materials, attention has been paid to their toxicity, with less work focusing on their supply-chain environmental profile. However, Soleimani *et al* conducted a comparative lifecycle impacts of inorganic, organic and hybrid thermoelectric materials at their production stage, across multiple environmental indicators namely resource consumption, emission, waste, primary energy demand, and global warming potential [534]. The authors concluded that the inorganic type yielded significantly higher environmental impacts in comparison to the other two due to the energy-intensive nature of their manufacturing processes. Bi_2Te_3 was identified as the only inorganic exception whose environmental impact was the lowest compared to all the thermoelectric materials studied. For organic and hybrid types, issues pertaining to raw material supply risks were identified as the main sustainability issue.

Challenges and outlook in assessing the sustainability of energy harvesting materials

Charting the path toward sustainability of energy harvesting materials is not straightforward. One reason for this is due to the diversity of components such as transducers, power management and energy storage making up an entire energy harvesting device. To underscore this, in grappling with the challenge of sustainability of energy harvesting materials, a major challenge is the difficulty in synthesizing materials that are simultaneously efficient for maximum energy conversion and environmentally benign [535]. In cases where such materials are needed, the sustainability of the manufacturing route is not guaranteed. Nonetheless, concerns about the 'health' of our planet necessitate an evaluation of the environmental profile of energy harvesting materials and technologies at the design or pilot stage before expensive investments and resources are committed. Such evaluations, when conducted in a manner that anticipates foreseeable deleterious consequences whilst identifying opportunities for improvement and mitigation strategies, can aid the communication of key findings to materials developers and policymakers.

Data availability statement

No new data were created or analysed in this study.

ORCID iDs

Vincenzo Pecunia ⬤ https://orcid.org/0000-0003-3244-1620

S Ravi P Silva ⓘ https://orcid.org/0000-0002-0356-1319
Jamie D Phillips ⓘ https://orcid.org/0000-0003-2642-3717
Elisa Artegiani ⓘ https://orcid.org/0000-0001-8821-4545
Alessandro Romeo ⓘ https://orcid.org/0000-0001-5068-8788
Gregory C Welch ⓘ https://orcid.org/0000-0002-3768-937X
Audrey Laventure ⓘ https://orcid.org/0000-0002-0867-0231
Jie Xu ⓘ https://orcid.org/0000–0003-0416-5200
Thomas M Brown ⓘ https://orcid.org/0000–0003-2141-3587
Bo Hou ⓘ https://orcid.org/0000-0001-9918-8223
Da Bin Kim ⓘ https://orcid.org/0000-0002-1162-7429
Yong Soo Cho ⓘ https://orcid.org/0000-0002-1601-6395
Agnė Žukauskaitė ⓘ https://orcid.org/0000-0002-8125-3805
Stephan Barth ⓘ https://orcid.org/0000-0002-7933-2520
Jikui Luo ⓘ https://orcid.org/0000-0003-0310-2443
Bhaskar Dudem ⓘ https://orcid.org/0000-0003-1637-9927
Venkateswaran Vivekananthan ⓘ https://orcid.org/0000-0003-1756-6548
Luis Fonseca ⓘ https://orcid.org/0000-0002-1394-8074
Alex Morata ⓘ https://orcid.org/0000-0002-3300-4636
Marisol Martin-Gonzalez ⓘ https://orcid.org/0000-0002-5687-3674
Giovanni Pennelli ⓘ https://orcid.org/0000-0002-2774-3600
Robert J Quinn ⓘ https://orcid.org/0000-0003-3146-8848
Jan-Willem G Bos ⓘ https://orcid.org/0000-0003-3947-2024
Deepak Venkateshvaran ⓘ https://orcid.org/0000-0002-7099-7323
Bernd Kaestner ⓘ https://orcid.org/0000-0002-6575-6621
Oliver Fenwick ⓘ https://orcid.org/0000-0001-7499-5117
Dimitra G Georgiadou ⓘ https://orcid.org/0000-0002-2620-3346
Mahmoud Wagih ⓘ https://orcid.org/0000-0002-7806-4333
Steve Beeby ⓘ https://orcid.org/0000-0002-0800-1759

References

[1] Kong L B, Li T, Hng H H, Boey F, Zhang T and Li S 2014 Introduction *Waste Energy Harvesting* (Heidelberg: Springer) pp 1–18
[2] Portilla L *et al* 2022 Wirelessly powered large-area electronics for the internet of things *Nat. Electron.* **6** 10–17
[3] Pecunia V, Fattori M, Abdinia S, Sirringhaus H and Cantatore E 2018 *Organic and Amorphous-Metal-Oxide Flexible Analogue Electronics* (Cambridge: Cambridge University Press) (https://doi.org/10.1017/9781108559034)
[4] Hassan Q (ed) 2018 *Internet of Things A to Z* (Hoboken, NJ: Wiley) (https://doi.org/10.1002/9781119456735)
[5] Bryzek J 2013 Roadmap for the trillion sensor universe *iNEMI Spring Member Meeting and Webinar* (*Berkeley, CA*)
[6] Harrop P 2018 *Battery Elimination in Electronics and Electrical Engineering 2018–2028* (Cambridge) (available at: https://www.idtechex.com/en/research-report/battery-elimination-in-electronics-and-electrical-engineering-2018-2028/550)
[7] Pecunia V, Occhipinti L G and Hoye R L Z 2021 Emerging indoor photovoltaic technologies for sustainable internet of things *Adv. Energy Mater.* **11** 2100698
[8] Wang G, Hou C and Wang H (ed) 2020 *Flexible and Wearable Electronics for Smart Clothing* (Weinheim: Wiley) (https://doi.org/10.1002/9783527818556)
[9] Bose S, Shen B and Johnston M L 2020 A batteryless motion-adaptive heartbeat detection system-on-chip powered by human body heat *IEEE J. Solid-State Circuits* **55** 2902–13
[10] Song Y, Min J, Yu Y, Wang H, Yang Y, Zhang H and Gao W 2020 Wireless battery-free wearable sweat sensor powered by human motion *Sci. Adv.* **6** eaay9842
[11] Bandodkar A J *et al* 2019 Battery-free, skin-interfaced microfluidic/electronic systems for simultaneous electrochemical, colorimetric, and volumetric analysis of sweat *Sci. Adv.* **5** eaav3294
[12] Mathews I, Kantareddy S N, Buonassisi T and Peters I M 2019 Technology and market perspective for indoor photovoltaic cells *Joule* **3** 1415–26
[13] Nandy S, Fortunato E and Martins R 2022 Green economy and waste management: an inevitable plan for materials science *Prog. Nat. Sci.: Mater. Int.* **32** 1–9
[14] Silva S R P 2021 EDITORIAL: now is the time for energy materials research to save the planet *Energy Environ. Mater.* **4** 497–9
[15] BCC Research 2018 Global markets, technologies and devices for energy harvesting: EGY097C (Wellesley, MA) (available at: www.bccresearch.com/market-research/energy-and-resources/global-markets-technologies-and-devices-for-energy-harvesting.html) (Accessed 19 June 2022)
[16] Freunek M, Freunek M and Reindl L M 2013 Maximum efficiencies of indoor photovoltaic devices *IEEE J. Photovolt.* **3** 59–64
[17] Hou B *et al* 2020 Multiphoton absorption stimulated metal chalcogenide quantum dot solar cells under ambient and concentrated irradiance *Adv. Funct. Mater.* **30** 2004563
[18] Cao J-J, Lou Y-H, Yang W-F, Wang K-L, Su Z-H, Chen J, Chen C-H, Dong C, Gao X-Y and Wang Z-K 2022 Multifunctional potassium thiocyanate interlayer for eco-friendly tin perovskite indoor and outdoor photovoltaics *Chem. Eng. J.* **433** 133832
[19] Ma L-K *et al* 2020 High-efficiency indoor organic photovoltaics with a band-aligned interlayer *Joule* **4** 1486–500
[20] Dai Y, Kum H, Slocum M A, Nelson G T and Hubbard S M 2017 High efficiency single-junction InGaP photovoltaic devices under low intensity light illumination *2017 IEEE 44th Photovoltaic Specialist Conf. (PVSC)* (June) pp 222–5

[21] Mathews I, Kantareddy S N R, Liu Z, Munshi A, Barth K, Sampath W, Buonassisi T and Peters I M 2020 Analysis of CdTe photovoltaic cells for ambient light energy harvesting *J. Phys. D: Appl. Phys.* **53** 405501

[22] He X, Chen J, Ren X, Zhang L, Liu Y, Feng J, Fang J, Zhao K and Liu S 2021 40.1% record low-light solar-cell efficiency by holistic trap-passivation using micrometer-thick perovskite film *Adv. Mater.* **33** 2100770

[23] Michaels H, Rinderle M, Freitag R, Benesperi I, Edvinsson T, Socher R, Gagliardi A and Freitag M 2020 Dye-sensitized solar cells under ambient light powering machine learning: towards autonomous smart sensors for the internet of things *Chem. Sci.* **11** 2895–906

[24] Kim G, Lim J W, Kim J, Yun S J and Park M A 2020 Transparent thin-film silicon solar cells for indoor light harvesting with conversion efficiencies of 36% without photodegradation *ACS Appl. Mater. Interfaces* **12** 27122–30

[25] Teran S, Wong J, Lim W, Kim G, Lee Y, Blaauw D and Phillips J D 2015 AlGaAs photovoltaics for indoor energy harvesting in mm-scale wireless sensor nodes *IEEE Trans. Electron Devices* **62** 2170–5

[26] Phillips J, Moon E and Teran A 2020 Indoor photovoltaics based on AlGaAs *Indoor Photovoltaics: Materials, Modeling and Applications* (Hoboken, NJ: Wiley) ed M F Müller (https://doi.org/10.1002/9781119605768.ch9)

[27] Teran S, Moon E, Lim W, Kim G, Lee I, Blaauw D and Phillips J D 2016 Energy harvesting for GaAs photovoltaics under low-flux indoor lighting conditions *IEEE Trans. Electron Devices* **63** 2820–5

[28] Moon E, Barrow M, Lim J, Blaauw D and Phillips J D 2020 Dual-junction GaAs photovoltaics for low irradiance wireless power transfer in submillimeter-scale sensor nodes *IEEE J. Photovolt.* **10** 1721–6

[29] Lee K, Zimmerman J D, Hughes T W and Forrest S R 2014 Non-destructive wafer recycling for low-cost thin-film flexible optoelectronics *Adv. Funct. Mater.* **24** 4284–91

[30] Horowitz K A W, Remo T, Smith B and Ptak A 2018 A techno-economic analysis and cost reduction roadmap for III-V solar cell *National Renewable Energy Laboratory Technical Report NREL/TP-6A20-72103*

[31] Khatiwada D *et al* 2020 High-efficiency single-junction p-i-n GaAs solar cell on roll-to-roll epi-ready flexible metal foils for low-cost photovoltaics *Prog. Photovolt. Res. Appl.* **28** 1107–19

[32] Salavei A *et al* 2016 Comparison of high efficiency flexible CdTe solar cells on different substrates at low temperature deposition *Sol. Energy* **139** 13–18

[33] Fraunhofer Institute for Solar Energy Systems and PSE Projects GmbH 2022 Photovoltaics report —2022- Fraunhofer ISE (available at: www.ise.fraunhofer.de/conte%0Ant/dam/ise/d)

[34] Romeo A and Artegiani E 2021 Cdte-based thin film solar cells: past, present and future *Energies* **14** 1684

[35] Artegiani E *et al* 2019 Analysis of a novel CuCl₂ back contact process for improved stability in CdTe solar cells *Prog. Photovolt. Res. Appl.* **27** 706–15

[36] Bosio A, Romeo A, Menossi D, Mazzamuto S and Romeo N 2011 Review: the second-generation of CdTe and CuInGaSe₂ thin filmPV modules *Cryst. Res. Technol.* **46** 857–64

[37] Ojo A A and Dharmadasa I M 2016 15.3% efficient graded bandgap solar cells fabricated using electroplated CdS and CdTe thin films *Sol. Energy* **136** 10–14

[38] McCandless B E, A Buchanan W and Birkmire R W 2008 High throuput processing of CdTe/CdS solar cells *Conf. Record of the 33rd IEEE Photovoltaic Specialists Conf.* pp 1–6

[39] Bätzner D L, Romeo A, Zogg H and Tiwari A N 2002 CdTe/CdS solar cell performance under low irradiance *Proc. 17th European Photovoltaic Solar Energy Conf. and Exhibition* vol 1 pp 1180–3

[40] Salavei A, Rimmaudo I, Piccinelli F and Romeo A 2013 Influence of CdTe thickness on structural and electrical properties of CdTe/CdS solar cells *Thin Solid Films* **535** 257–60

[41] Park J *et al* 2021 Suppression of defects through cation substitution: a strategic approach to improve the performance of kesterite Cu₂ZnSn(S,Se)₄ solar cells under indoor light conditions *Sol. RRL* **5** 2100020

[42] Deng H, Sun Q, Yang Z, Li W, Yan Q, Zhang C, Zheng Q, Wang X, Lai Y and Cheng S 2021 Novel symmetrical bifacial flexible CZTSSe thin film solar cells for indoor photovoltaic applications *Nat. Commun.* **12** 3107

[43] Park J *et al* 2020 Investigation of low intensity light performances of kesterite CZTSe, CZTSSe, and CZTS thin film solar cells for indoor applications *J. Mater. Chem.* A **8** 14538–44

[44] Antunez P D, Bishop D M, Luo Y and Haight R 2017 Efficient kesterite solar cells with high open-circuit voltage for applications in powering distributed devices *Nat. Energy* **2** 884–90

[45] Cui X *et al* 2019 Cd-Free Cu₂ZnSnS₄ solar cell with an efficiency greater than 10% enabled by Al₂O₃ passivation layers *Energy Environ. Sci.* **12** 2751–64

[46] Zhang J, Tan H S, Guo X, Facchetti A and Yan H 2018 Material insights and challenges for non-fullerene organic solar cells based on small molecular acceptors *Nat. Energy* **3** 720–31

[47] Cheng P, Li G, Zhan X and Yang Y 2018 Next-generation organic photovoltaics based on non-fullerene acceptors *Nat. Photon.* **12** 131–42

[48] Hou J, Inganäs O, Friend R H and Gao F 2018 Organic solar cells based on non-fullerene acceptors *Nat. Mater.* **17** 119

[49] You Y-J, Song C E, Hoang Q V, Kang Y, Goo J S, Ko D-H, Lee -J-J, Shin W S and Shim J W 2019 Highly efficient indoor organic photovoltaics with spectrally matched fluorinated phenylene-alkoxybenzothiadiazole-based wide bandgap polymers *Adv. Funct. Mater.* **29** 1901171

[50] Shin S-C, Koh C W, Vincent P, Goo J S, Bae J-H, Lee J-J, Shin C, Kim H, Woo H Y and Shim J W 2019 Ultra-thick semi-crystalline photoactive donor polymer for efficient indoor organic photovoltaics *Nano Energy* **58** 466–75

[51] Cui Y *et al* 2019 Wide-gap non-fullerene acceptor enabling high-performance organic photovoltaic cells for indoor applications *Nat. Energy* **4** 1–8

[52] Dayneko S D, Pahlevani M and Welch G C 2019 Indoor photovoltaics: photoactive material selection, greener ink formulations, and slot-die coated active layers *ACS Appl. Mater. Interfaces* **11** 46017–25

[53] Tintori F, Laventure A, Koenig J B D and Welch G C 2020 High open-circuit voltage roll-to-roll compatible processed organic photovoltaics *J. Mater. Chem.* C **8** 13430–8

[54] Osterwald C R 1986 Translation of device performance measurements to reference conditions *Sol. Cells* **18** 269–79

[55] Freitag M *et al* 2017 Dye-sensitized solar cells for efficient power generation under ambient lighting *Nat. Photon.* **11** 372–8

[56] Li M, Igbari F, Wang Z K and Liao L-S 2020 Indoor thin-film photovoltaics: progress and challenges *Adv. Energy Mater.* **10** 1–25

[57] Zheng C, Wu Q, Guo S, Huang W, Xiao Q and Xiao W 2021 The correlation between limiting efficiency of indoor photovoltaics and spectral characteristics of multi-color white LED sources *J. Appl. Phys.* **54** 315503

[58] Li B, Hou B and Amaratunga G A J 2021 Indoor photovoltaics, the next big trend in solution-processed solar cells *InfoMat.* **3** 445–59

[59] Michaels H, Benesperi I and Freitag M 2021 Challenges and prospects of ambient hybrid solar cell applications *Chem. Sci.* **12** 5002–15

[60] Hittinger E and Jaramillo P 2019 Internet of things: energy boon or bane? *Science* **364** 326–8

[61] Chen C, Chang J, Chiang K, Lin H, Hsiao S and Lin H 2015 Perovskite photovoltaics for dim-light applications *Adv. Energy Mater.* **25** 7064–70

[62] Di Giacomo F, Zardetto V, Lucarelli G, Cinà L, Di Carlo A, Creatore M and Brown T M 2016 Mesoporous perovskite solar cells and the role of nanoscale compact layers for remarkable all-round high efficiency under both indoor and outdoor illumination *Nano Energy* **30** 460–9

[63] Lucarelli G, Giacomo F D, Zardetto V, Creatore M and Brown T M 2017 Efficient light harvesting from flexible perovskite solar cells under indoor white light-emitting diode illumination *Nano Res.* **10** 2130–45

[64] Dong C, Li X, Ma C, Yang W, Cao J, Igbari F, Wang Z and Liao L 2021 Lycopene-based bionic membrane for stable perovskite photovoltaics *Adv. Funct. Mater.* **31** 2011242

[65] Chen C *et al* 2022 Full-dimensional grain boundary stress release for flexible perovskite indoor photovoltaics *Adv. Mater.* **34** 2200320

[66] Castro-Hermosa S, Lucarelli G, Top M, Fahland M, Fahlteich J and Brown T M 2020 Perovskite photovoltaics on roll-to-roll coated ultra-thin glass as flexible high-efficiency indoor power generators *Cell Rep. Phys. Sci.* **1** 100045

[67] Lee M *et al* 2021 Enhanced hole-carrier selectivity in wide bandgap halide perovskite photovoltaic devices for indoor internet of things applications *Adv. Funct. Mater.* **31** 2008908

[68] Wu M, Kuo C, Jhuang L, Chen P, Lai Y and Chen F 2019 Bandgap engineering enhances the performance of mixed-cation perovskite materials for indoor photovoltaic applications *Adv. Energy Mater.* **9** 1901863

[69] Mathews I, Kantareddy S N R, Sun S, Layurova M, Thapa J, Correa-Baena J P, Bhattacharyya R, Buonassisi T, Sarma S and Peters I M 2019 Self-powered sensors enabled by wide-bandgap perovskite indoor photovoltaic cells *Adv. Funct. Mater.* **29** 1904072

[70] Cheng R, Chung C, Zhang H, Liu F, Wang W, Zhou Z, Wang S, B D A and Feng S 2019 Tailoring triple-anion perovskite material for indoor light harvesting with restrained halide segregation and record high efficiency beyond 36% *Adv. Energy Mater.* **9** 1901980

[71] Guo Z, Jena A K, Takei I, Ikegami M, Ishii A, Numata Y, NaoyukiShibayama S N and Miyasaka T 2021 Dopant-free polymer HTM-based CsPbI$_2$Br solar cells with efficiency over 17% in sunlight and 34% in indoor light *Adv. Funct. Mater.* **31** 2103614

[72] Ma S, Yuan G, Zhang Y, Yang N, Li Y and Chen Q 2022 Development of encapsulation strategies towards the commercialization of perovskite solar cells *Energy Environ. Sci.* **15** 13–55

[73] Muhammad B T, Kar S, Stephen M and Leong W L 2022 Halide perovskite-based indoor photovoltaics: recent development and challenges *Mater. Today Energy* **23** 100907

[74] Pecunia V, Occhipinti L G, Chakraborty A, Pan Y and Peng Y 2020 Lead-free halide perovskite photovoltaics: challenges, open questions, and opportunities *APL Mater.* **8** 100901

[75] Peng Y, Li F, Wang Y, Li Y, Hoye R L Z, Feng L, Xia K and Pecunia V 2020 Enhanced photoconversion efficiency in cesium-antimony-halide perovskite derivatives by tuning crystallographic dimensionality *Appl. Mater. Today* **19** 100637

[76] Mei J, Liu M, Vivo P and Pecunia V 2021 Two-dimensional antimony-based perovskite-inspired materials for high-performance self-powered photodetectors *Adv. Funct. Mater.* **31** 2106295

[77] Peng Y, Huq T N, Mei J, Portilla L, Jagt R A, Occhipinti L G, MacManus-Driscoll J L, Hoye R L Z and Pecunia V 2021 Lead-free perovskite-inspired absorbers for indoor photovoltaics *Adv. Energy Mater.* **11** 2002761

[78] Lamminen N *et al* 2023 Triple A-site cation mixing in 2D perovskite-inspired antimony halide absorbers for efficient indoor photovoltaics *Adv. Energy Mater.* **13** 2203175

[79] Chakraborty A, Pai N, Zhao J, Tuttle B R, Simonov A N and Pecunia V 2022 Rudorffites and beyond: perovskite-inspired silver/copper pnictohalides for next-generation environmentally friendly photovoltaics and optoelectronics *Adv. Funct. Mater.* **32** 2203300

[80] Li F, Wang Y, Xia K, Hoye R L Z and Pecunia V 2020 Microstructural and photoconversion efficiency enhancement of compact films of lead-free perovskite derivative Rb$_3$Sb$_2$I$_9$ *J. Mater. Chem.* A **8** 4396–406

[81] Turkevych, Kazaoui S, Shirakawa N, Fukuda N and Turkevych I 2021 Potential of AgBiI$_4$ rudorffites for indoor photovoltaic energy harvesters in autonomous environmental nanosensors *Jpn. J. Appl. Phys.* **60** SCCE06

[82] Grandhi G K *et al* 2022 Enhancing the microstructure of perovskite-inspired Cu-Ag-Bi-I absorber for efficient indoor photovoltaics *Small* **18** 2203768

[83] Grandhi G K, Toikkonen S, Al-Anesi B, Pecunia V and Vivo P 2023 Perovskite-inspired Cu$_2$AgBiI$_6$ for mesoscopic indoor photovoltaics under realistic low-light intensity conditions *Sustain. Energy Fuels* **7** 66–73

[84] Al-Anesi B *et al* 2023 Antimony-bismuth alloying: the key to a major boost in the efficiency of lead-free perovskite-inspired indoor photovoltaics *ChemRxiv* (https://doi.org/10.26434/chemrxiv-2023-nb5jj)

[85] Singh A, Lai P-T, Mohapatra A, Chen C-Y, Lin H-W, Lu Y-J and Chu C W 2021 Panchromatic heterojunction solar cells for Pb-free all-inorganic antimony based perovskite *Chem. Eng. J.* **419** 129424

[86] Ding Z, Zhao R, Yu Y and Liu J 2019 All-polymer indoor photovoltaics with high open-circuit voltage *J. Mater. Chem.* A **7** 26533–9

[87] Yang W-F, Cao J-J, Dong C, Li M, Tian Q-S, Wang Z-K and Liao L-S 2021 Suppressed oxidation of tin perovskite by Catechin for eco-friendly indoor photovoltaics *Appl. Phys. Lett.* **118** 023501

[88] Pecunia V *et al* 2021 Assessing the impact of defects on lead-free perovskite-inspired photovoltaics via photoinduced current transient spectroscopy *Adv. Energy Mater.* **11** 2003968

[89] Lee H K H, Li Z, Durrant J R and Tsoi W C 2016 Is organic photovoltaics promising for indoor applications? *Appl. Phys. Lett.* **108** 253301

[90] Semonin O E, Luther J M, Choi S, Chen H-Y, Gao J, Nozik A J and Beard M C 2011 Peak external photocurrent quantum efficiency exceeding 100% via MEG in a quantum dot solar cell *Science* **334** 1530–3

[91] Choi M-J *et al* 2020 Cascade surface modification of colloidal quantum dot inks enables efficient bulk homojunction photovoltaics *Nat. Commun.* **11** 103

[92] Song H, Lin Y, Zhang Z, Rao H, Wang W, Fang Y, Pan Z and Zhong X 2021 Improving the efficiency of quantum dot sensitized solar cells beyond 15% via secondary deposition *J. Am. Chem. Soc.* **143** 4790–800

[93] Kim T, Lim S, Yun S, Jeong S, Park T and Choi J 2020 Design strategy of quantum dot thin-film solar cells *Small* **16** 2002460

[94] Yan D J, Mwalukuku V M, Fauvel S, Riquelme A J, Anta J A, Maldivi P and Demadrille R 2022 Lead leaching of perovskite solar cells in aqueous environments: a quantitative investigation *Sol. RRL* **6** 2200332

[95] Randall F and Jacot J 2003 Is AM1.5 applicable in practice? Modelling eight photovoltaic materials with respect to light intensity and two spectra *Renew. Energy* **28** 1851–64

[96] Minnaert B and Veelaert P 2014 A proposal for typical artificial light sources for the characterization of indoor photovoltaic applications *Energies* **7** 1500–16

[97] Hamadani B H and Campanelli M B 2020 Photovoltaic characterization under artificial low irradiance conditions using reference solar cells *IEEE J. Photovolt.* **10** 1119–25

[98] IEC 60904-3 2008 *Photovoltaic devices – part 3: measurement principles for terrestrial photovoltaic (PV) solar devices with reference spectral irradiance data*

[99] 2018 *SEMI PV80-0218 - Specification of indoor lighting simulator requirements for emerging photovoltaic and perovskite solar cell (PSC)*

[100] Hamadani B H and Dougherty B 2016 Solar cell characterization *Semiconductor Materials for Solar Photovoltaic Cells* (Cham: Springer) ed M Paranthaman, W Wong-Ng and R Bhattacharya 229–45 Ch4

[101] Hamadani B, Long Y-S, Tsai M-A and Wu T-C 2021 Interlaboratory comparison of solar cell measurements under low indoor lighting conditions *IEEE J. Photovolt.* **11** 1430–5

[102] Hao J, Shen B, Zhai J, Liu C, XiaolongLi X and Gao X 2013 Switching of morphotropic phase boundary and large strain response in lead-free ternary $(Bi_{0.5}Na_{0.5})TiO_3-(K_{0.5}Bi_{0.5})TiO_3-(K_{0.5}Na_{0.5})NbO_3$ system *J. Appl. Phys.* **113** 114106

[103] Shrout T R, Eek Eagle Park S, Randall C A, Shepard J, Hackenberger L B, Pickrell D J and Hackenberger W S 1997 Recent advances in piezoelectric materials *Proc. SPIE* **3241**

[104] Godard N, Allirol L, Latour A, Glinsek S, Gerard M, Polesel J, Domingues Dos Santos F and Defay E 2020 1-mW vibration energy harvester based on a cantilever with printed polymer multilayers *Cell Rep. Phys. Sci.* **1** 100068

[105] Ricart T, Lassagne P-P, Boisseau S, Despesse G, Lefevre A, Billard C, Fanget S and Defay E 2011 Macro energy harvester based on aluminium nitride thin films *2011 IEEE Int. Ultrasonics Symp.* (IEEE) pp 1928–31

[106] Roundy S and Wright P K 2004 A piezoelectric vibration based generator for wireless electronics *Smart Mater. Struct.* **13** 1131–42

[107] Park S-E and Shrout T R 1997 Ultrahigh strain and piezoelectric behavior in relaxor based ferroelectric single crystals *J. Appl. Phys.* **82** 1804–11

[108] Yeo H G, Ma X, Rahn C and Trolier-mckinstry S 2016 Efficient piezoelectric energy harvesters utilizing (001) textured bimorph PZT films on flexible metal foils *Adv. Funct. Mater.* **26** 5940–6

[109] Coleman J W, Beechem T and Trolier-mckinstry S 2019 Effect of stresses on the dielectric and piezoelectric properties of $Pb(Zr_{0.52}Ti_{0.48})O_3$ thin films *J. Appl. Phys.* **126** 034101

[110] Ou-Yang J, Zhu B, Zhang Y, Chen S, Yang X and Wei W 2015 New KNN-based lead-free piezoelectric ceramic for high-frequency ultrasound transducer applications *Appl. Phys.* A **118** 1177–81

[111] Ma X, Wilson A, Rahn C D and Trolier-Mckinstry S 2016 Efficient energy harvesting using piezoelectric compliant mechanisms: theory and experiment *J. Vib. Acoust* **138** 021005

[112] Rödel J and Li J-F 2018 Lead-free piezoceramics: status and perspectives *MRS Bull.* **43** 576–80

[113] Zheng T, Wu J, Xiao D and Zhu J 2018 Recent development in lead-free perovskite piezoelectric bulk materials *Prog. Mater. Sci.* **98** 552–624

[114] Bai Y, Jantunen H and Juuti J 2018 Energy harvesting research: the road from single source to multisource' *Adv. Mater.* **30** 1707271

[115] Li F *et al* 2019 Giant piezoelectricity of Sm-doped $Pb(Mg1/3Nb2/3)O3-PbTiO_3$ single crystals *Science* **364** 264–8

[116] Li F *et al* 2018 Ultrahigh piezoelectricity in ferroelectric ceramics by design *Nat. Mater.* **17** 349–54

[117] Rödel W J K, Seifert T P, Anton E-M, Granzow T and Damjanovic D 2009 Perspective on the development of lead-free piezoelectrics *J. Am. Ceram. Soc.* **92** 1153–77

[118] Bai Y and Grinberg I 2022 ed *Ferroelectrics: Advances in Fundamental Studies and Emerging Applications* (Bristol: IOP Publishing)

[119] Bai Y 2015 Vibrational energy harvesting using piezoelectric ceramics and free-standing thick-film structures *PhD Thesis* University of Birmingham

[120] Bai Y Electro-ceramic material component, its manufacturing method and method of converting energy *Patents and patent application* PCT/FI2020/050810 (granted 2021), GB 2593105 (granted 2022), US 17/633,322 (filed 2022)

[121] Rödel J 2022 *Piezoelectric Materials and Applications Lecture notes* (University of Oulu)

[122] Cao X, Xiong Y, Sun J, Zhu X, Sun Q and Wang Z L 2021 Piezoelectric nanogenerators derived self-powered sensors for multifunctional applications and artificial intelligence *Adv. Funct. Mater.* **31** 2102983

[123] Mahapatra S D, Mohapatra P C, Aria A I, Christie G C, Mishra Y K, Hofmann S and Thakur V K 2021 Piezoelectric materials for energy harvesting and sensing applications: roadmap for future smart materials *Adv. Sci.* **8** 2100864

[124] Pandey R K, Dutta J, Brahma S, Rao B and Liu C 2021 Review on ZnO-based piezotronics and piezoelectric nanogenerators: aspects of piezopotential and screening effect *J. Phys. Mater.* **4** 044011

[125] Choi H J, Jung Y S, Han J and Cho Y S 2020 *In-situ* stretching strain-driven high piezoelectricity and enhanced electromechanical energy harvesting performance of a ZnO nanorod-array structure *Nano Energy* **72** 104735

[126] Kim D B, Kim S W, Kim Y E, Choi H J and Cho Y S 2022 Room-temperature processed $Ag/Pb(Zn_{1/3}Nb_{2/3})O3-Pb(Zr_{0.5}Ti_{0.5})O_3$-based composites for printable piezoelectric energy harvesters *Compos. Sci. Technol.* **218** 109151

[127] Chen H, Zhou L, Fang Z, Wang S, Yang T, Zhu L, Hou X, Wang H and Wang Z L 2021 Piezoelectric nanogenerator based on *in situ* growth all-inorganic $CsPbBr_3$ perovskite nanocrystals in PVDF fibers with long-term stability *Adv. Funct. Mater.* **31** 2011073

[128] Kim D B, Park K S, Park S J and Cho Y S 2022 Microampere-level piezoelectric energy generation in Pb-free inorganic halide thin-film multilayers with Cu interlayers *Nano Energy* **92** 106785

[129] Jung Y S, Choi H J, Park S H, Kim D, Park S and Cho Y S 2022 Nanoampere-level piezoelectric energy harvesting of lithography-free centimeter-scale MoS_2 monolayer film generators *Small* **18** 2200184

[130] Zhang C, Fan W, Wang S, Wang Q, Zhang Y and Dong K 2021 Recent progress of wearable piezoelectric nanogenerators *ACS Appl. Electron. Mater.* **3** 2449–67

[131] Han J, Kim D B, Kim J H, Kim S W, Ahn B U and Cho Y S 2022 Origin of high piezoelectricity in carbon nanotube/halide nanocrystal/P(VDF-TrFE) composite nanofibers designed for bending-energy harvesters and pressure sensors *Nano Energy* **99** 107421

[132] Akiyama M, Kamohara T, Kano K, Teshigahara A, Takeuchi Y and Kawahara N 2009 Enhancement of piezoelectric response in scandium aluminum nitride alloy thin films prepared by dual reactive cosputtering *Adv. Mater.* **21** 593–6

[133] Lu Y, Reusch M, Kurz N, Ding A, Christoph T, Prescher M, Kirste L, Ambacher O and Žukauskaitė A 2018 Elastic modulus and coefficient of thermal expansion of piezoelectric $Al_{1-x}Sc_xN$ (up to x = 0.41) thin films *APL Mater.* **6** 076105

[134] Barth S, Nizard H, Göller J, Spies P and Bartzsch H AlScN-dünnschichten auf Metallsubstraten für Energy Harvesting Anwendungen *Proc. 11 EASS Tagung Energieautonome Sensorsysteme* (*Erfurt, Germany, 05-06 July 2022*) pp 62–24

[135] Österlund E *et al* 2021 Stability and residual stresses of sputtered wurtzite AlScN thin films *Phys. Rev. Mater.* **5** 035001

[136] Höglund C, Birch J, Alling B, Bareno J, Czigány Z, Persson P O Å, Wingqvist G, Žukauskaitė A and Hultman L 2010 Wurtzite structure $Sc_{1-x}Al_xN$ solid solution films grown by reactive magnetron sputter epitaxy: structural characterization and first-principles calculations *J. Appl. Phys.* **107** 123515

[137] Sandu C, Parsapour F, Mertin S, Pashchenko V, Matloub R, LaGrange T, Heinz B and Muralt P 2019 Abnormal grain growth in AlScN thin films induced by complexion formation at crystallite interfaces *Phys. Status Solidi* a **216** 1800569

[138] Fichtner S, Wolff N, Lofink F, Kienle L and Wagner B 2019 AlScN: a III-V semiconductor based ferroelectric *J. Appl. Phys.* **125** 114103

[139] Manna S, Talley K, Gorai P, Mangum J, Zakutayev A, Brennecka G, Stevanovic V and Ciobanu C 2018 Enhanced piezoelectric response of AlN via CrN alloying *Phys. Rev. Appl.* **9** 034026

[140] Yokoyama T, Iwazaki Y, Onda Y, Sasajima Y, Nishihara T and Ueda M 2014 Highly piezoelectric co-doped AlN thin films for wideband FBAR applications *2014 IEEE Int. Ultrasonics Symp. (IUS)* (*September*) pp 281–8

[141] Schlögl M, Schneider M and Schmid U 2022 Piezoelectricity in $Y_{0.09}Al_{0.91}N$ thin films *Mater. Sci. Eng.* B **276** 115543

[142] Wu W *et al* 2014 Piezoelectricity of single-atomic-layer MoS_2 for energy conversion and piezotronics *Nature* **514** 470

[143] Wu W and Wang Z L 2016 Piezotronics and piezo-phototronics for adaptive electronics and optoelectronics *Nat. Rev. Mater.* **1** 16031

[144] Fei R, Li W, Li J and Yang L 2015 Giant piezoelectricity of monolayer group IV monochalcogenides: SnSe, SnS, GeSe, and GeS *Appl. Phys. Lett.* **107** 173104

[145] Kim S K, Bhatia R, Kim T-H, Seol D, Kim J H, Kim H, Seung W, Kim Y, Lee Y H and Kim S-W 2016 Directional dependent piezoelectric effect in CVD grown monolayer MoS_2 for flexible piezoelectric nanogenerators *Nano Energy* **22** 483–9

[146] Lee M H and Wu W 2022 2D Materials for Wearable Energy Harvesting *Adv. Mater. Technol.* **7** 2101623

[147] Duerloo K-A N, Ong M T and Reed E J 2012 Intrinsic Piezoelectricity in Two-Dimensional Materials *J. Phys. Chem. Lett.* **3** 2871–6

[148] Blonsky M N, Zhuang H L, Singh A K and Hennig R G 2015 *Ab Initio* Prediction of Piezoelectricity in Two-Dimensional Materials *ACS Nano* **9** 9885–91

[149] Cui C, Xue F, Hu W-J and Li L-J 2018 Two-dimensional materials with piezoelectric and ferroelectric functionalities *npj 2D Mater. Appl.* **2** 18

[150] Wang L, Liu S, Feng X, Zhang C, Zhu L, Zhai J, Qin Y and Wang Z L 2020 Flexoelectronics of centrosymmetric semiconductors *Nat. Nanotechnol.* **15** 661–7

[151] Wang Y, Qiu G, Wang Q, Liu Y, Du Y, Wang R, Kim M J, Ye P D and Wu W 2018 Field-effect transistors made from solution-grown two-dimensional tellurene *Nat. Electron.* **1** 228–36

[152] Sezer N and Koç M 2021 A comprehensive review on the state-of-the-art of piezoelectric energy harvesting *Nano Energy* **80** 105567

[153] Martins P, Lopes A C and Lanceros-Mendez S 2014 Electroactive phases of poly(vinylidene fluoride): determination, processing and applications *Prog. Polym. Sci.* **39** 683–706

[154] Maity K and Mandal D 2021 Piezoelectric polymers and composites for multifunctional materials *Advanced Lightweight Multifunctional Materials* ed P Costa, C M Costa and S Lanceros-Mendez (Cambridge: Woodhead Publishing) ch 7, pp 239–82

[155] Fukada E 2000 History and recent progress in piezoelectric polymers *IEEE Trans. Ultrason. Ferroelectr. Freq. Control* **47** 1277–90

[156] Guerin S, Tofail S A M and Thompson D 2019 Organic piezoelectric materials: milestones and potential *npj Asia Mater.* **11** 10

[157] Wan C and Bowen C R 2017 Multiscale-structuring of polyvinylidene fluoride for energy harvesting: the impact of molecular-, micro- and macro-structure *J. Mater. Chem.* A **5** 3091–128

[158] Mishra S, Unnikrishnan L, Nayak S K and Mohanty S 2019 Advances in piezoelectric polymer composites for energy harvesting applications: a systematic review *Macromol. Mater. Eng.* **304** 1800463

[159] Wu Y, Ma Y, Zheng H and Ramakrishna S 2021 Piezoelectric materials for flexible and wearable electronics: a review *Mater. Des.* **211** 110164

[160] Chen X *et al* 2022 Relaxor ferroelectric polymer exhibits ultrahigh electromechanical coupling at low electric field *Science* **375** 1418–22

[161] Mahmud M A P, Adhikary P, Zolfagharian A, Adams S, Kaynak A and Kouzani A Z 2022 Advanced design, fabrication, and applications of 3D-printable piezoelectric nanogenerators *Electron. Mater. Lett.* **18** 129–44

[162] Kholkin N A, Amdursky N, Bdikin I, Gazit E and Rosenman G 2010 Strong piezoelectricity in bioinspired peptide nanotubes *ACS Nano* **4** 610–4

[163] Guerin S, O'Donnell J, Haq E U, McKeown C, Silien C, Rhen F M, Soulimane T, Tofail S A and Thompson D 2019 Racemic amino acid piezoelectric transducer *Phys. Rev. Lett.* **122** 047701

[164] Maiti S, Karan S K, Kim J K and Khatua B B 2019 Nature driven bio-piezoelectric/triboelectric nanogenerator as next-generation green energy harvester for smart and pollution free society *Adv. Energy Mater.* **9** 1–41

[165] Li J, Long Y, Yang F and Wang X 2020 Degradable piezoelectric biomaterials for wearable and implantable bioelectronics *Curr. Opin. Solid State Mater. Sci* **24** 100806

[166] Denning D, Kilpatrick J I, Fukada E, Zhang N, Habelitz S, Fertala A, Gilchrist M D, Zhang Y, Tofail S A M and Rodriguez B J 2017 Piezoelectric tensor of collagen fibrils determined at the nanoscale *ACS Biomater. Sci. Eng.* **3** 929–35

[167] Zhang Y, Bowen C R, Ghosh S K, Mandal D, Khanbareh H, Arafa M and Wan C 2019 Ferroelectret materials and devices for energy harvesting applications *Nano Energy* **57** 118–40

[168] Ghosh S K and Mandal D 2016 Efficient natural piezoelectric nanogenerator: electricity generation from fish swim bladder *Nano Energy* **28** 356–65

[169] Ma J, Jia Y, Chen L, Zheng Y, Wu Z, Luo W, Jiang M, Cui X and Li Y 2020 Dye wastewater treatment driven by cyclically heating/cooling the poled (K0.5Na0.5)NbO3 pyroelectric crystal catalyst *J. Clean Prod.* **276** 124218

[170] Zheng Q, Zhang H, Mi H, Cai Z, Ma Z and Gong S 2016 High-performance flexible piezoelectric nanogenerators consisting of porous cellulose nanofibril (CNF)/poly(dimethylsiloxane) (PDMS) aerogel films *Nano Energy* **26** 504–12

[171] Zhang Y, Jeong C K, Yang T, Sun H, Chen L-Q, Zhang S, Chen W and Wang Q 2018 Bioinspired elastic piezoelectric composites for high-performance mechanical energy harvesting *J. Mater. Chem.* A **6** 14546–52

[172] Karan S K, Maiti S, Kwon O, Paria S, Maitra A, Si S K, Kim Y, Kim J K and Khatua B B 2018 Nature driven spider silk as high energy conversion efficient bio-piezoelectric nanogenerator *Nano Energy* **49** 655–66

[173] Alluri N R, Maria Joseph Raj N P, Khandelwal G, Vivekananthan V and Kim S-J 2020 Aloe vera: a tropical desert plant to harness the mechanical energy by triboelectric and piezoelectric approaches *Nano Energy* **73** 104767

[174] Heredia A *et al* 2012 Nanoscale ferroelectricity in crystalline γ-glycine *Adv. Funct. Mater.* **22** 2996–3003

[175] Seyedhosseini E *et al* 2017 Self-assembly of organic ferroelectrics by evaporative dewetting: a case of β-glycine *ACS Appl. Mater. Interfaces* **9** 20029–37

[176] Fan F R, Tian Z-Q and Wang Z L 2012 Flexible triboelectric generator *Nano Energy* **1** 328

[177] Wang Z L 2021 From conctact electrication to triboelectric nanogenerators *Rep. Prog. Phys.* **84** 096502

[178] Wang Z L, Lin L, Chen J, Niu S M and Zi Y L 2016 *Triboelectric Nanogenerators* (Switzerland: Springer)

[179] Hinchet R, Yoon H, Ryu H, Kim M, Choi E, Kim D and Kim S 2019 Transcutaneous ultrasound energy harvesting using capacitive triboelectric technology *Science* **365** 491

[180] Guo Y, Zhang X-S, Wang Q, Gong W H, Zhang Q, Wang H and Brugger J 2018 All-fiber hybrid piezoelectric-enhanced triboelectric nanogenerator for wearable gesture monitoring *Nano Energy* **48** 152

[181] Wang Z L 2017 New wave power *Nature* **542** 159

[182] Choi Y, Jing Q, Datta A, Boughey C and Kar-Narayan S 2017 A triboelectric generator based on self-poled Nylon-11 nanowires fabricated by gas-flow assisted template wetting *Energy Environ. Sci.* **10** 2180

[183] Xu W *et al* 2020 A droplet-based electricity generator with high instantaneous power density *Nature* **578** 392

[184] Wang Z L 2013 Triboelectric nanogenerators as new energy technology for self-powered systems and as active mechanical and chemical sensors *ACS Nano* **7** 9533

[185] Wang Z L, Chen J and Lin L 2015 Progress in triboelectric nanogenertors as new energy technology and self-powered sensors *Energy Environ. Sci.* **8** 2250

[186] Wang Z L 2017 *Mater. Today* **20** 74

[187] Wang Z L 2020 On the first principle theory of nanaogenerators from Maxwell's equations *Nano Energy* **68** 104272

[188] Wang Z L 2022 On the expanded Maxwell's equations for moving charged media system – general theory, mathematical solutions and applications in TENG *Mater. Today* **52** 348–63

[189] Wang Z L and Wang A C 2019 On the origin of contact electrification *Mater. Today* **30** 34–51

[190] Lin S, Chen X and Wang Z L 2022 Contact-electrification at liquid-solid interface *Chem. Rev.* **122** 5209–32

[191] Zheng Y, Cheng L, Yuan M, Wang Z, Zhang L, Qin Y and Jing T 2014 An electrospun nanowire-based triboelectric nanogenerator and its application in a fully self-powered UV detector *Nanoscale* **6** 7842–6

[192] Zhang L, Su C, Cheng L, Cui N, Gu L, Qin Y, Yang R and Zhou F 2019 Enhancing the performance of textile triboelectric nanogenerators with oblique microrod arrays for wearable energy harvesting *ACS Appl. Mater. Interfaces* **11** 26824–9

[193] Cui N, Liu J, Lei Y, Gu L, Xu Q, Liu S and Qin Y 2018 High-performance triboelectric nanogenerator with a rationally designed friction layer structure *ACS Appl. Energy Mater.* **1** 2891–7

[194] Xu L, Bu T Z, Yang X D, Zhang C and Wang Z L 2018 Ultrahigh charge density realized by charge pumping at ambient conditions for triboelectric nanogenerators *Nano Energy* **49** 625–33

[195] Cheng L, Xu Q, Zheng Y, Jia X and Qin Y 2018 A self-improving triboelectric nanogenerator with improved charge density and increased charge accumulation speed *Nat. Commun.* **9** 1–8

[196] Liu W, Wang Z, Wang G, Liu G, Chen J, Pu X, Xi Y, Wang X, Guo H and Hu C 2019 Integrated charge excitation triboelectric nanogenerator *Nat. Commun.* **10** 1–9

[197] Li S, Wang S, Zi Y, Wen Z, Lin L, Zhang G and Wang Z L 2015 Largely improving the robustness and lifetime of triboelectric nanogenerators through automatic transition between contact and noncontact working states *ACS Nano* **9** 7479–87

[198] Lin Z, Zhang B, Zou H, Wu Z, Guo H, Zhang Y, Yang J and Wang Z L 2020 Rationally designed rotation triboelectric nanogenerators with much extended lifetime and durability *Nano Energy* **68** 104378

[199] Lin Z, Zhang B, Guo H, Wu Z, Zou H, Yang J and Wang Z L 2019 Super-robust and frequency-multiplied triboelectric nanogenerator for efficient harvesting water and wind energy *Nano Energy* **64** 103908

[200] Jiang T, Pang H, An J, Lu P, Feng Y, Liang X, Zhong W and Wang Z L 2020 Robust swing-structured triboelectric nanogenerator for efficient blue energy harvesting *Adv. Energy Mater.* **10** 2000064

[201] Wu J, Xi Y and Shi Y 2020 Toward wear-resistive, highly durable and high performance triboelectric nanogenerator through interface liquid lubrication *Nano Energy* **72** 104659

[202] Meng J, Guo Z H, Pan C, Wang L, Chang C, Li L, Pu X and Wang Z L 2021 Flexible textile direct-current generator based on the tribovoltaic effect at dynamic metal-semiconducting polymer interfaces *ACS Energy Lett.* **6** 2442–50

[203] Xu C *et al* 2018 On the electron-transfer mechanism in the contact-electrification effect *Adv. Mater.* **30** 1706790

[204] Zi Y, Niu S, Wang J, Wen Z, Tang W and Wang Z L 2015 Standards and figure-of-merits for quantifying the performance of triboelectric nanogenerators *Nat. Commun.* **6** 8376

[205] Zou H *et al* 2019 Quantifying the triboelectric series *Nat. Commun.* **10** 1427

[206] Zhang X, Chen L, Jiang Y, Lim W and Soh S 2019 Rationalizing the triboelectric series of polymers *Chem. Mater.* **31** 1473–8

[207] Zhao Z, Zhou L, Li S, Liu D, Li Y, Gao Y, Liu Y, Dai Y, Wang J and Wang Z L 2021 Selection rules of triboelectric materials for direct-current triboelectric nanogenerator *Nat. Commun.* **12** 4686

[208] Pu X, Liu M, Chen X, Sun J, Du C, Zhang Y, Zhai J, Hu W and Wang Z L 2017 Ultrastretchable, transparent triboelectric nanogenerator as electronic skin for biomechanical energy harvesting and tactile sensing *Sci. Adv.* **3** e1700015

[209] Zhang R and Olin H 2020 Material choices for triboelectric nanogenerators: a critical review *EcoMat* **2** eom2.12062

[210] Soin N *et al* 2016 High performance triboelectric nanogenerators based on phase-inversion piezoelectric membranes of poly(vinylidene fluoride)-zinc stannate (PVDF-ZnSnO$_3$) and polyamide-6 (PA6) *Nano Energy* **30** 470–80

[211] Im J-S and Park I-K 2018 Mechanically robust magnetic Fe$_3$O$_4$ nanoparticle/polyvinylidene fluoride composite nanofiber and its application in a triboelectric nanogenerator *ACS Appl. Mater. Interfaces* **10** 25660–5

[212] Zheng Z, Yu D and Guo Y 2021 Dielectric modulated glass fiber fabric-based single electrode triboelectric nanogenerator for efficient biomechanical energy harvesting *Adv. Funct. Mater.* **31** 2102431

[213] Zhang R, Örtegren J, Hummelgård M, Olsen M, Andersson H and Olin H 2022 A review of the advances in composites/nanocomposites for triboelectric nanogenerators *Nanotechnology* **33** 212003

[214] Kang X, Pan C, Chen Y and Pu X 2020 Boosting performances of triboelectric nanogenerators by optimizing dielectric properties and thickness of electrification layer *RSC Adv.* **10** 17752–9

[215] Meunier M and Quirke N 2000 Molecular modeling of electron trapping in polymer insulators *J. Chem. Phys.* **113** 369–76

[216] Balke N, Maksymovych P, Jesse S, Kravchenko I I, Li Q and Kalinin S V 2014 Exploring local electrostatic effects with scanning probe microscopy: implications for piezoresponse force microscopy and triboelectricity *ACS Nano* **8** 10229–36

[217] Chen J 2016 Triboelectric nanogenerators *PhD Dissertation* Georgia Institute of Technology, Atlanta, GA (available at: https:// smartech.gatech.edu/handle/1853/54956) (Accessed 20 March 2022)

[218] Shin S-H, Bae Y E, Moon H K, Kim J, Choi S-H, Kim Y, Yoon H J, Lee M H and Nah J 2017 Formation of triboelectric series via atomic-level surface functionalization for triboelectric energy harvesting *ACS Nano* **11** 6131–8

[219] Ahmed A, Hassan I, Pourrahimi A M, Helal A S, El-Kady M F, Khassaf H and Kaner R B 2020 Toward high-performance triboelectric nanogenerators by engineering interfaces at the nanoscale: looking into the future research roadmap *Adv. Mater. Technol.* **5** 2000520

[220] Xu J, Zou Y, Nashalian A and Chen J 2020 Leverage surface chemistry for high-performance triboelectric nanogenerators *Front. Chem.* **8** 577327

[221] Zhou Y, Deng W, Xu J and Chen J 2020 Engineering materials at the nanoscale for triboelectric nanogenerators *Cell Rep. Phys. Sci.* **1** 100142

[222] Lin Z-H, Zhu G, Zhou Y S, Yang Y, Bai P, Chen J and Wang Z L 2013 A selfpowered triboelectric nanosensor for mercury ion detection *Angew. Chem., Int. Ed. Engl.* **52** 5065–9

[223] Li X, Jiang C, Ying Y and Ping J 2020 Biotriboelectric nanogenerators: materials, structures, and applications *Adv. Energy Mater.* **10** 2002001

[224] Zheng Q, Zou Y, Zhang Y, Liu Z, Shi B, Wang X, Jin Y, Ouyang H, Li Z and Wang Z L 2016 Biodegradable triboelectric nanogenerator as a life-time designed implantable power source *Sci. Adv.* **2** e1501478

[225] Cao L, Qiu X, Jiao Q, Zhao P, Li J and Wei Y 2021 Polysaccharides and proteins-based nanogenerator for energy harvesting and sensing: a review *Int. J. Biol. Macromol.* **173** 225–43

[226] Kim D W, Kim S-W and Jeong U 2018 Lipids: source of static electricity of regenerative natural substances and nondestructive energy harvesting *Adv. Mater.* **30** 1804949

[227] Graham S A, Chandrarathna S C, Patnam H, Manchi P, Lee J-W and Yu J S 2021 Harsh environment–tolerant and robust triboelectric nanogenerators for mechanical-energy harvesting, sensing, and energy storage in a smart home *Nano Energy* **80** 105547

[228] Zou H *et al* 2020 Quantifying and understanding the triboelectric series of inorganic non-metallic materials *Nat. Commun.* **11** 1–7

[229] Graham S A, Dudem B, Mule A R, Patnam H and Yu J S 2019 Engineering squandered cotton into eco-benign microarchitectured triboelectric films for sustainable and highly efficient mechanical energy harvesting *Nano Energy* **61** 505–16

[230] Dudem B, Dharmasena R D I G, Graham S A, Leem J W, Patnam H, Mule A R, Silva S R P and Yu J S 2020 Exploring the theoretical and experimental optimization of high-performance triboelectric nanogenerators using microarchitectured silk cocoon films *Nano Energy* **74** 104882

[231] Wang N, Zheng Y, Feng Y, Zhou F and Wang D 2020 Biofilm material based triboelectric nanogenerator with high output performance in 95% humidity environment *Nano Energy* **77** 105088

[232] Wang Y-M, Zeng Q, He L, Yin P, Sun Y, Hu W and Yang R 2021 Fabrication and application of biocompatible nanogenerators *Iscience* **24** 102274

[233] Jiang C, Wu C, Li X, Yao Y, Lan L, Zhao F, Ye Z, Ying Y and Ping J 2019 All-electrospun flexible triboelectric nanogenerator based on metallic MXene nanosheets *Nano Energy* **59** 268–276

[234] Dong Y C, Mallineni S S K, Maleski K, Behlow H, Mochalin V N, Rao A M, Gogotsi Y and Podila R 2018 Metallic MXenes: a new family of materials for flexible triboelectric nanogenerators *Nano Energy* **44** 103–10

[235] Bhatta T, Maharjan P, Cho H, Park C, Yoon S H, Sharma S, Salauddin M, Rahman M T, Rana S M and Park J Y 2021 High-performance triboelectric nanogenerator based on MXene functionalized polyvinylidene fluoride composite nanofibers *Nano Energy* **81** 105670

[236] Cao W-T, Ouyang H, Xin W, Chao S Y, Ma C, Li Z, Chen F and Ma M-G 2020 A stretchable highoutput triboelectric nanogenerator improved by MXene liquid electrode with high electronegativity *Adv. Funct. Mater.* **30** 2004181

[237] Luo X X, Zhu L P, Wang Y-C, Li J Y, Nie J J and Wang Z L 2021 A flexible multifunctional triboelectric nanogenerator based on MXene/PVA hydrogel *Adv. Funct. Mater.* **31** 2104928

[238] Salauddin M *et al* 2022 Fabric-assisted MXene/silicone nanocomposite-based triboelectric nanogenerators for self-powered sensors and wearable electronics *Adv. Funct. Mater.* **32** 2107143

[239] Cao Y L, Guo Y B, Chen Z X, Yang W F, Li K R, He X Y and Li J M 2022 Highly sensitive self-powered pressure and strain sensor based on crumpled mxene film for wireless human motion detection *Nano Energy* **92** 106689

[240] Wang D Y, Zhang D Z, Yang Y, Mi Q, Zhang J Z and Yu L D 2021 Multifunctional latex/polytetrafluoroethylene-based triboelectric nanogenerator for self-powered organ-like MXene/metal−organic framework-derived CuO nanohybrid ammonia sensor *ACS Nano* **15** 2911–9

[241] Li P D, Su N, Wang Z Y and Qiu J S 2021 A $Ti_3C_2T_x$ MXene-based energy-harvesting soft actuator with self-powered humidity sensing and real-time motion tracking capability *ACS Nano* **15** 16811–8

[242] Ding R, Wong M-C and Hao J 2020 Recent advances in hybrid perovskite nanogenerators *EcoMat* **2** 12057

[243] Jiang F, Zhou X, Lv J, Chen J, Chen J, Kongcharoen H, Zhang Y and Lee P S 2022 Stretchable, breathable, and stable lead-free perovskite/polymer nanofiber composite for hybrid triboelectric and piezoelectric energy harvesting *Adv. Mater.* **34** 2200042

[244] Wang Y, Duan J, Yang X, Liu L, Zhao L and Tang Q 2020 The unique dielectricity of inorganic perovskites toward high-performance triboelectric nanogenerators *Nano Energy* **69** 104418

[245] Yu X P, Wang Y, Zhang J, Duan J, Yang X, Liu L and Tang Q 2020 Halogen regulation of inorganic perovskites toward robust triboelectric nanogenerators and charging polarity series *J. Mater. Chem.* A **8** 14299

[246] Kojcinovic J *et al* 2022 Nanocrystalline triple perovskite compounds $A_3Fe_2BO_9$ (A = Sr,Ba;B = W,Te) with ferromagnetic and dielectric properties for triboelectric energy harvesting *Mater. Chem. Front.* **6** 1116

[247] Su L, Zhao Z X, Li H Y, Yuan J, Wang Z L, Cao G Z and Zhu G 2015 High-performance organolead halide perovskite-based self-powered triboelectric photodetector *ACS Nano* **9** 11310–6

[248] Yang X D *et al* 2019 Robust perovskite-based triboelectric nanogenerator enhanced by broadband light and interface engineering *J. Mater. Sci.* **54** 9004–16

[249] Huang S Y *et al* 2020 Controlling performance of organic–inorganic hybrid perovskite triboelectric nanogenerators via chemical composition modulation and electric field-induced ion migration *Adv. Energy Mater.* **10** 2002470

[250] Huang S Y *et al* 2021 Surface electrical properties modulation by multimode polarizations inside hybrid perovskite films investigated through contact electrification effect *Nano Energy* **89** 106318

[251] Wang H B *et al* 2022 Coexistence of contact electrification and dynamic p−n junction modulation effects in triboelectrification *ACS Appl. Mater. Interfaces* **14** 30410

[252] Libanori A, Chen G, Zhao X, Zhou Y and Chen J 2022 Smart textiles for personalized healthcare *Nat. Electron.* **5** 142–56

[253] Xiong J, Chen J and Lee P S 2021 Functional fibers and fabrics for soft robotics, wearables, and human–robot interface *Adv. Mater.* **33** 2002640

[254] Zhong J, Zhang Y, Zhong Q, Hu Q, Hu B, Wang Z L and Zhou J 2014 Fiber-based generator for wearable electronics and mobile medication *ACS Nano* **8** 6273–80

[255] Chen G, Li Y, Bick M and Chen J 2020 Smart textiles for electricity generation *Chem. Rev.* **120** 3668–720

[256] Lv J, Chen J and Lee P S 2021 Sustainable wearable energy storage devices self-charged by human-body bioenergy *SusMat* **1** 285–302

[257] Xiong J, Cui P, Chen X, Wang J, Parida K, Lin M-F and Lee P S 2018 Skin-touch-actuated textile-based triboelectric nanogenerator with black phosphorus for durable biomechanical energy harvesting *Nat. Commun.* **9** 4280

[258] Chen J, Huang Y, Zhang N, Zou H, Liu R, Tao C, Fan X and Wang Z L 2016 Micro-cable structured textile for simultaneously harvesting solar and mechanical energy *Nat. Energy* **1** 16138

[259] Wang J, Li S, Yi F, Zi Y, Lin J, Wang X, Xu Y and Wang Z L 2016 Sustainably powering wearable electronics solely by biomechanical energy *Nat. Commun.* **7** 12744

[260] Zhang M *et al* 2019 Printable smart pattern for multifunctional energy-management E-textile *Matter* **1** 168–79

[261] Niu S, Liu Y, Wang S, Lin L, Zhou Y S, Hu Y and Wang Z L 2013 Theory of sliding-mode triboelectric nanogenerators *Adv. Mater.* **25** 6184–93

[262] Dharmasena R D I G, Jayawardena K D G I, Mills C A, Deane J H B, Anguita J V, Dorey R A and Silva S R P 2017 Triboelectric nanogenerators: providing a fundamental framework *Energy Environ. Sci.* **10** 1801–11

[263] Niu S, Liu Y, Chen X, Wang S, Zhou Y S, Lin L, Xie Y and Wang Z L 2015 Theory of freestanding triboelectric-layer-based nanogenerators *Nano Energy* **12** 760–74

[264] Dudem B, Dharmasena R D I G, Riaz R, Vivekananthan V, Wijayantha K G U, Lugli P, Petti L and Silva S R P 2022 Wearable triboelectric nanogenerator from waste materials for autonomous information transmission via morse code *ACS Appl. Mater. Interfaces* **14** 5328–37

[265] Dudem B, Graham S A, Dharmasena R I, Silva S R and Yu J S 2021 Natural silk-composite enabled versatile robust triboelectric nanogenerators for smart applications *Nano Energy* **83** 105819

[266] Dharmasena R D I G, Deane J H B and Silva S R P 2018 Nature of power generation and output optimization criteria for triboelectric nanogenerators *Adv. Energy Mater.* **8** 1802190

[267] Xu G, Li X, Xia X, Fu J, Ding W and Zi Y 2019 On the force and energy conversion in triboelectric nanogenerators *Nano Energy* **59** 154–61

[268] Yan Q and Kanatzidis M G 2022 High-performance thermoelectrics and challenges for practical devices *Nat. Mater.* **21** 503–13

[269] He J and Tritt T M 2017 Advances in thermoelectric materials research: looking back and moving forward *Science* **357** 1090–5

[270] Tan G, Zhao L-D and Kanatzidis M G 2016 Rationally designing high-performance bulk thermoelectric materials *Chem. Rev.* **116** 12123–49

[271] Su X *et al* 2017 Multi-scale microstructural thermoelectric materials: transport behavior, non-equilibrium preparation, and applications *Adv. Mater.* **29** 1602013

[272] Snyder G J and Toberer E S 2008 Complex thermoelectric materials *Nat. Mater.* **7** 105–14

[273] Goldsmid H J 2016 *Introduction to Thermoelectricity* (Berlin: Springer) (https://doi.org/10.1007/978-3-662-49256-7)

[274] Zhao L-D, Lo S-H, Zhang Y, Sun H, Tan G, Uher C, Wolverton C, Dravid V P and Kanatzidis M G 2014 Ultralow thermal conductivity and high thermoelectric figure of merit in SnSe crystals *Nature* **508** 373–7

[275] Su L, Wang D, Wang S, Qin B, Wang Y, Qin Y, Jin Y, Chang C and Zhao L-D 2022 High thermoelectric performance realized through manipulating layered phonon-electron decoupling *Science* **375** 1385–9

[276] Biswas K, He J, Blum I D, Wu C-I, Hogan T P, Seidman D N, Dravid V P and Kanatzidis M G 2012 High-performance bulk thermoelectrics with all-scale hierarchical architectures *Nature* **489** 414–8

[277] Zheng Y, Slade T J, Hu L, Tan X Y, Luo Y, Luo Z-Z, Xu J, Yan Q and Kanatzidis M G 2021 Defect engineering in thermoelectric materials: what have we learned? *Chem. Soc. Rev.* **50** 9022–54

[278] Zheng G, Su X, Li X, Liang T, Xie H, She X, Yan Y, Uher C, Kanatzidis M G and Tang X 2016 Toward high-thermoelectric-performance large-size nanostructured BiSbTe alloys via optimization of sintering-temperature distribution *Adv. Energy Mater.* **6** 1600595

[279] Shi X-L, Zou J and Chen Z-G 2020 Advanced thermoelectric design: from materials and structures to devices *Chem. Rev.* **120** 7399–515

[280] Zhou C *et al* 2021 Polycrystalline SnSe with a thermoelectric figure of merit greater than the single *Cryst. Nat. Mater.* **20** 1378–84

[281] Bu Z, Zhang X, Shan B, Tang J, Liu H, Chen Z, Lin S, Li W and Pei Y 2021 Realizing a 14% single-leg thermoelectric efficiency in GeTe alloys *Sci. Adv.* **7** eabf2738

[282] Yang D *et al* 2020 Blocking ion migration stabilizes the high thermoelectric performance in Cu_2Se composites *Adv. Mater.* **32** 2003730

[283] Qiu P *et al* 2019 High-efficiency and stable thermoelectric module based on liquid-like materials *Joule* **3** 1538–48

[284] Jiang B *et al* 2021 High-entropy-stabilized chalcogenides with high thermoelectric performance *Science* **371** 830–4

[285] Pei Y, Shi X, LaLonde A, Wang H, Chen L and Snyder G J 2011 Convergence of electronic bands for high performance bulk thermoelectrics *Nature* **473** 66–69

[286] Yang J, Xi L, Qiu W, Wu L, Shi X, Chen L, Yang J, Zhang W, Uher C and Singh D J 2016 On the tuning of electrical and thermal transport in thermoelectrics: an integrated theory-experiment perspective *npj Comput. Mater.* **2** 15015

[287] Heusler F 1903 Über magnetische Manganlegierungen *Verh. Dtsch. Phys. Ges.* **12** 219 (in German)

[288] Tanja G, Felser C and Parkin S S P 2011 Simple rules for the understanding of Heusler compounds *Prog. Solid State Chem.* **39** 1–50

[289] Sakai A *et al* 2018 Giant anomalous Nernst effect and quantum-critical scaling in a ferromagnetic semimetal *Nat. Phys.* **14** 1119–24

[290] Nishino Y, Kato H, Kato M and Mizutani U 2001 Effect of off-stoichiometry on the transport properties of the Heusler-type Fe$_2$VAl compound *Phys. Rev.* B **63** 233303

[291] Garmroudi F, Parzer M, Riss A, Beyer S, Khmelevskyi S, Mori T, Reticcioli M and Bauer E 2022 Large thermoelectric power factors by opening the band gap in semimetallic Heusler alloys *Mater. Today Phys.* **27** 100742

[292] Parzer M, Garmroudi F, Riss A, Khmelevskyi S, Mori T and Bauer E 2022 High solubility of Al and enhanced thermoelectric performance due to resonant states in Fe$_2$VAl$_x$ *Appl. Phys. Lett.* **120** 071901

[293] Garmroudi F *et al* 2022 Anderson transition in stoichiometric Fe$_2$Val: high thermoelectric performance from impurity bands *Nat. Commun.* **13** 3599

[294] Hinterleitner B *et al* 2020 Stoichiometric and off-stoichiometric full Heusler Fe$_2$V$_{1-x}$W$_x$Al thermoelectric systems *Phys. Rev.* B **102** 075117

[295] Hinterleitner B *et al* 2019 Thermoelectric performance of a metastable thin-film Heusler alloy *Nature* **576** 85–90

[296] Fukuta K, Tsuchiya K, Miyazaki H and Nishino Y 2022 Improving thermoelectric performance of Fe$_2$VAl-based Heusler compounds via high-pressure torsion *Appl. Phys.* A **128** 1–8

[297] Bilc D I *et al* 2015 Low-dimensional transport and large thermoelectric power factors in bulk semiconductors by band engineering of highly directional electronic states *Phys. Rev. Lett.* **114** 136601

[298] Khandy S A, Islam I, Gupta D C, Bhat M A, Ahmad S, Dar T A, Rubab S, Dhiman S and Laref A 2018 A case study of Fe$_2$TaZ (Z= Al, Ga, In) Heusler alloys: hunt for half-metallic behavior and thermoelectricity *RSC Adv.* **8** 40996–1002

[299] He J, Amsler M, Xia Y, Naghavi S S, Hegde V I, Hao S, Goedecker S, Ozoliņš V and Wolverton C 2016 Ultralow thermal conductivity in full Heusler semiconductors *Phys. Rev. Lett.* **117** 046602

[300] Wang S-F, Zhang Z-G, Wang B-T, Zhang J-R and Wang F-W 2022 Intrinsic ultralow lattice thermal conductivity in the full-heusler compound Ba$_2$AgSb *Phys. Rev. Appl.* **17** 034023

[301] Tsuji N, Nishide A, Hayakawa J and Mori T 2019 Observation of enhanced thermopower due to spin fluctuation in weak itinerant ferromagnet *Sci. Adv.* **5** eaat5935

[302] Robinson R A 2021 Large violation of the Wiedemann–Franz law in Heusler, ferromagnetic, Weyl semimetal Co$_2$MnAl *J. Appl. Phys.* **54** 454001

[303] Quinn R J and Bos J-W G 2021 Advances in half-Heusler alloys for thermoelectric power generation *Mater. Adv.* **2** 6246–66

[304] Al Malki M, Shi X, Qiu P, Snyder G J and Dunand D C 2021 Creep behavior and post-creep thermoelectric performance of the N-type skutterudite alloy yb0.3co4sb12 *J. Materiomics* **7** 89–97

[305] Brod M K, Anand S and Snyder G J 2022 The importance of avoided crossings in understanding high valley degeneracy in half-heusler thermoelectric semiconductors *Adv. Electron. Mater.* **8** 2101367

[306] Zevalkink A *et al* 2018 A practical field guide to thermoelectrics: fundamentals, synthesis, and characterization *Appl. Phys. Rev.* **5** 021303

[307] Guo S, Anand S, Brod M K, Zhang Y and Snyder G J 2022 Conduction band engineering of half-heusler thermoelectrics using orbital chemistry *J. Mater. Chem.* A **10** 3051–7

[308] Dylla M T, Dunn A, Anand S, Jain A and Snyder G J 2020 Machine learning chemical guidelines for engineering electronic structures in half-heusler thermoelectric materials *Research* **2020** 1–8

[309] Gurunathan R, Sarker S, Borg C, Saal J, Ward L, Mehta A and Snyder G J 2022 Mapping thermoelectric transport in a multicomponent alloy space (arXiv:2205.01520)

[310] Xie H-H, Mi J-L, Hu L-P, Lock N, Chirstensen M, Fu C-G, Iversen B B, Zhao X-B and Zhu T-J 2012 Interrelation between atomic switching disorder and thermoelectric properties of ZRNISN half-heusler compounds *CrystEngComm* **14** 4467

[311] Luo T *et al* 2021 Dopant-segregation to grain boundaries controls electrical conductivity of N-Type NBCO(PT)SN half-heusler alloy mediating thermoelectric performance *Acta Mater.* **217** 117147

[312] Rogl G *et al* 2016 Mechanical properties of half-Heusler alloys *Acta Mater.* **107** 178–95

[313] Shevelkov A V 2016 Thermoelectric power generation by clathrates *Thermoelectrics for Power Generation - A Look at Trends in the Technology* ed S Skipidarov and M Nikitin (London: IntechOpen) (https://doi.org/10.5772/65600)

[314] Dolyniuk J, Owens-Baird B, Wang J, Zaikina J V and Kovnir K 2016 Clathrate thermoelectrics *Mater. Sci. Eng.* R **108** 1–46

[315] Kauzlarich S M, Sui F and Perez C J 2016 Earth abundant element type I clathrate phases *Materials* **9** 714

[316] Takabatake T, Suekuni K, Nakayama T and Kaneshita E 2014 Phonon-glass electron-crystal thermoelectric clathrates: experiments and theory *Rev. Mod. Phys.* **86** 669–716

[317] Wang J, Dolyniuk J-A J-A and Kovnir K 2018 Unconventional clathrates with transition metal-phosphorus frameworks *Acc. Chem. Res.* **51** 31–39

[318] Freer R *et al* 2022 Key properties of inorganic thermoelectric materials – tables (version 1) *J. Phys. Energy* **4** 022002

[319] Wang L-H and Chang L-S 2017 Thermoelectric properties of p-type Ba$_8$Ga$_{16}$Ge$_{30}$ type-I clathrate compounds prepared by the vertical bridgman method *J. Alloys Compd.* **722** 644–50

[320] Bhattacharya A, Carbogno C, Böhme B, Baitinger M, Grin Y and M S 2017 Formation of vacancies in Si- and Ge-based clathrates: role of electron localization and symmetry breaking *Phys. Rev. Lett.* **118** 236401

[321] Wang J *et al* 2020 Clathrate BaNi$_2$P$_4$: an interplay of heat and charge transport due to strong host-guest interactions *Chem. Mater.* **32** 7935–40

[322] Gunatilleke W D C B, Ojo O P, Poddig H and Nolas G S 2022 Synthesis and characterization of phase-pure clathrate-II Rb$_{12.9}$Si$_{136}$ *J. Solid State Chem.* **311** 123152

[323] Slack G A 1995 New materials and performance limits for thermoelectric cooling *CRC Handbook of Thermoelectrics* ed D M Rowe (Boca Raton, FL: CRC Press) p 407

[324] Uher C 2021 *Thermoelectric Skutterudites* (Boca Raton, FL: CRC Press, Taylor & Francis Group)

[325] Jeitschko W and Braun D J 1977 LaFe$_4$P$_{12}$ with filled CoAs$_3$-type structure and isotypic lanthanoid-transition metal polyphosphides *Acta Crystallogr.* **B33** 3401

[326] Shi X, Yang J, Salvador J R, Chi M F, Cho J Y, Wang H, Bai S Q, Yang J H, Zhang W Q and Chen L D 2011 Multiple-filled skutterudites: high thermoelectric figure of merit through separately optimizing electrical and thermal transports *J. Am. Chem. Soc.* **133** 7837

[327] Rogl G, Grytsiv A, Yubuta K, Puchagger S, Bauer E, Raja C, Mallik R C and Rogl P 2015 In-doped multifilled n-type skutterudites with ZT = 1.8 *Acta Mater.* **95** 201

[328] Rogl G, Grytsiv A, Rogl P, Peranio N, Bauer E, Zehetbauer M and Eibl O 2014 n-Type skutterudites (R,Ba,Yb)$_y$Co$_4$Sb$_{12}$ (R = Sr, La,Mm, DD, SrMm, SrDD) approaching ZT ≈ 2.0 *Acta Mater.* **63** 30

[329] Rogl G, Grytsiv A, Heinrich P, Bauer E, Kumar P, Peranio N, Eibl O, Horky J, Zehetbauer M and Rogl P 2015 New bulk p-type skutterudites $DD_{0.7}Fe_{2.7}Co_{1.3}Sb_{12-x}X_x$ (X = Ge, Sn) reaching ZT > 1.3 *Acta Mater.* **91** 227

[330] Hu C Z *et al* 2017 *Phys. Rev.* B **95** 165204

[331] Tang Y L, Gibbs Z M, Agapito L A, Li G, Kim H-S, Nardelli M B, Curtarolo S and Snyder G J 2015 *Nat. Mater.* **14** 1223

[332] Zhang Q H, Liao J C, Tang Y S, Gu M, Ming C, Qiu P F, Bai S Q, Shi X, Uher C and Chen L D 2017 *Energy Environ. Sci.* **10** 956

[333] Terasaki I, Sasago Y and Uchinokura K 1997 Large thermoelectric power in $NaCo_2O_4$ single crystals *Phys. Rev.* B **56** R12685–7

[334] Shikano M and Funahashi R 2003 Electrical and thermal properties of single-crystalline $(Ca_2CoO_3)_{0.7}CoO_2$ with a $Ca_3Co_4O_9$ structure *Appl. Phys. Lett.* **82** 1851–3

[335] Romo-De-La-Cruz C-O, Chen Y, Liang L, Williams M and Song X 2020 Thermoelectric oxide ceramics outperforming single crystals enabled by dopant segregations *Chem. Mater.* **32** 9730–9

[336] Lan J-L, Liu Y-C, Zhan B, Lin Y-H, Zhang B, Yuan X, Zhang W, Xu W and Nan C-W 2013 Enhanced thermoelectric properties of Pb-doped BiCuSeO ceramics *Adv. Mater.* **25** 5086–90

[337] Liu Y, Zhao L-D, Zhu Y, Liu Y, Li F, Yu M, Liu D-B, Xu W, Lin Y-H and Nan C-W 2016 Synergistically optimizing electrical and thermal transport properties of BiCuSeO via a dual-doping approach *Adv. Energy Mater.* **6** 1502423

[338] Tan X, Liu Y, Liu R, Zhou Z, Liu C, Lan J-L, Zhang Q, Lin Y-H and Nan C-W 2019 Synergistical enhancement of thermoelectric properties in n-type Bi_2O_2Se by carrier engineering and hierarchical microstructure *Adv. Energy Mater.* **9** 1900354

[339] Acharya M, Jana S S, Ranjan M and Maiti T 2021 High performance (ZT>1) n-type oxide thermoelectric composites from earth abundant materials *Nano Energy* **84** 105905

[340] Lin Y, Dylla M T, Kuo J J, Male J P, Kinloch I A, Freer R and Snyder G J 2020 Graphene/strontium titanate: approaching single crystal–like charge transport in polycrystalline oxide perovskite nanocomposites through grain boundary engineering *Adv. Funct. Mater.* **30** 1910079

[341] Matsubara I, Funahashi R, Takeuchi T, Sodeoka S, Shimizu T and Ueno K 2001 Fabrication of an all-oxide thermoelectric power generator *Appl. Phys. Lett.* **78** 3627–9

[342] Zhang R-Z, Wang C-L, Li J-C and Koumoto K 2010 Simulation of thermoelectric performance of bulk $SrTiO_3$ with two-dimensional electron gas grain boundaries *J. Am. Ceram. Soc.* **93** 1677–81

[343] Perez-Taborda J A, Muñoz Rojo M, Maiz J, Neophytou N and Martin-Gonzalez M 2016 Ultra-low thermal conductivities in large-area Si-Ge nanomeshes for thermoelectric applications *Sci. Rep.* **6** 32778

[344] Donmez-Noyan I *et al* 2019 SiGe nanowire arrays based thermoelectric microgenerator *Nano Energy* **57** 492–9

[345] Dimaggio E and Pennelli G 2016 Reliable fabrication of metal contacts on silicon nanowire forests *Nano Lett.* **16** 4348–54

[346] Morata A, Pacios M, Gadea G, Flox C, Cadavid D, Cabot A and Tarancón A 2018 Large-area and adaptable electrospun silicon-based thermoelectric nanomaterials with high energy conversion efficiencies *Nat. Commun.* **9** 4759

[347] Salleras M *et al* 2021 Managing heat transfer issues for thermoelectric microgenerators *Heat Transfer - Design, Experimentation and Applications* (IntechOpen) ch 18, p 23

[348] Dhawan R, Madusanka P and Lee M 2020 $Si_{0.97}Ge_{0.03}$ microelectronic thermoelectric generators with high power and voltage densities *Nat. Commun.* **11** 4362

[349] Hochbaum A I, Chen R, Delgado R D, Liang W, Garnett E C, Najarian M, Majumdar A and Yang P 2008 Enhanced thermoelectric performance of rough silicon nanowires *Nature* **451** 163–7

[350] Neophytou N, Zianni X, Kosina H, Frabboni S, Lorenzi B and Narducci D 2013 Simultaneous increase in electrical conductivity and Seebeck coefficient in highly boron-doped nanocrystalline Si *Nanotechnology* **24** 205402

[351] Cuffe J *et al* 2015 Reconstructing phonon mean free path contributions to thermal conductivity using nanoscale membranes *Phys. Rev.* B **91** 245423

[352] Donmez-Noyan I, Dolcet M, Salleras M, Stranz A, Calaza C, Gadea G, Pacios M, Morata A, Tarancon A and Fonseca L 2019 All-silicon thermoelectric micro/nanogenerator including a heat exchanger for harvesting applications *J. Power Sources* **413** 125–33

[353] De Boor J, Dasgupta T, Saparamadu U, Müller E and Ren Z F 2017 Recent progress in p-type thermoelectric magnesium silicide based solid solutions *Mater. Today Energy* **4** 105–21

[354] Khan A U, Vlachos N and Kyratsi T 2013 High thermoelectric figure of merit of $Mg_2Si_{0.55}Sn_{0.4}Ge_{0.05}$ materials doped with Bi and Sb *Scr. Mater.* **69** 606–9

[355] Skomedal G *et al* 2016 Design, assembly and characterization of silicide-based thermoelectric modules *Energy Convers. Manage.* **110** 13–21

[356] Miyazaki Y, Saito Y, Hayashi K, Yubuta K and Kajitani T 2011 Preparation and thermoelectric properties of a chimney-ladder $(Mn_{1-x}Fe_x)Si_\gamma$ ($\gamma\sim1.7$) solid solution *Jpn. J. Appl. Phys.* **50** 035804

[357] Nemoto T, Iida T, Sato J, Sakamoto T, Hirayama N, Nakajima T and Takanashi Y 2013 Development of an Mg_2Si unileg thermoelectric module using durable Sb-doped Mg_2Si legs *J. Electron. Mater.* **42** 2192–7

[358] Nieroda P, Mars K, Nieroda J, Leszczyński J, Król M, Drożdż E, Jeleń P, Sitarz M and Koleżyński A 2019 New high temperature amorphous protective coatings for Mg_2Si thermoelectric material *Ceram. Int.* **45** 10230–5

[359] Nandihalli N, Gregory D and Mori T 2022 Energy-saving pathways for thermoelectric nanomaterial synthesis: hydrothermal/solvothermal, microwave-assisted, solution-based, and powder processing *Adv. Sci.* **9** 2106052

[360] Petsagkourakis I, Petsagkourakis I, Tybrandt K, Crispin X, Ohkubo I, Satoh N and Mori T 2018 Thermoelectric materials and applications for energy harvesting power generation *Sci. Technol. Adv. Mater.* **19** 836–62

[361] Lima M S L, Aizawa T, Ohkubo I, Baba T, Sakurai T and Mori T 2021 High power factor in epitaxial Mg_2Sn thin films via Ga doping *Appl. Phys. Lett.* **119** 254101

[362] Ohkubo I *et al* 2022 Miniaturized in-plane p-type thermoelectric device composed of a II–IV semiconductor thin film prepared by microfabrication *Mater. Today Energy* **28** 101075

[363] Bos J-W G 2022 Intermetallic thermoelectrics – design and preparation of half-Heuslers, skutterudites and Zintl-type materials *Inorganic Thermoelectric Materials* (London: Royal Society of Chemistry) ch 5 (https://doi.org/10.1039/9781788019590-00216)

[364] Kauzlarich S M, Zevalkink A, Toberer E and Jeff Snyder G 2016 Zintl phases: recent developments in thermoelectrics and future outlook *Thermoelectric Materials and Devices* ch 1 (https://doi.org/10.1039/9781782624042-00001)

[365] Quinn R J, Stevens C, LongLeong H, Huxley A D and Bos J-W G 2022 New sustainable ternary copper phosphide thermoelectrics *Chem. Commun.* **58** 11811

[366] Mao J, Zhu H, Ding Z, Liu Z, Gamage G A, Chen G and Ren Z 2019 High thermoelectric cooling performance of n-type Mg_3Bi_2-based materials *Science* **365** 495–8

[367] Zhang J, Song L, Pedersen S, Yin H, Hung L T and Iversen B B 2017 Discovery of high-performance low-cost n-type Mg$_3$Sb$_2$-based thermoelectric materials with multi-valley conduction bands *Nat. Commun.* **8** 13901

[368] Zou T, Qin X, Zhang Y, Li X, Zeng Z, Li D, Zhang J, Xin H, Xie W and Weidenkaff A 2015 Enhanced thermoelectric performance of β-Zn$_4$Sb$_3$ based nanocomposites through combined effects of density of states resonance and carrier energy filtering *Sci. Rep.* **5** 17803

[369] Zhang J, Song L, Madsen G, Fischer K F F, Zhang W, Shi X and Iversen B B 2016 Designing high-performance layered thermoelectric materials through orbital engineering *Nat. Commun.* **7** 10892

[370] Toberer E S , Cox C A , Brown S R , Ikeda T , May A F , Kauzlarich S M and Snyder G J 2008 Traversing the metal-insulator transition in a Zintl phase: rational enhancement of thermoelectric efficiency in Yb$_{14}$Mn$_{1-x}$Al$_x$Sb$_{11}$ *Adv. Funct. Mater.* **18** 2795

[371] Tamaki H, Sato H K and Kanno T 2016 Isotropic conduction network and defect chemistry in Mg$_{3+\delta}$Sb$_2$-based layered Zintl compounds with high thermoelectric performance *Adv. Mater.* **28** 10182

[372] Narducci D 2011 Do we really need high thermoelectric figures of merit? A critical appraisal to the power conversion efficiency of thermoelectric materials *Appl. Phys. Lett.* **99** 102104

[373] Ohno S, Aydemir U, Amsler M, Pöhls J-H, Chanakian S, Zevalkink A, Anne White M, Bux S K and Chris Wolverton G J S 2017 Achieving zT > 1 in inexpensive Zintl phase Ca$_9$Zn$_{4+x}$Sb$_9$ by phase boundary mapping *Adv. Mater.* **27** 1606361

[374] Wood M, Kuo J J, Imasato K and Snyder G J 2019 Improvement of low-temperature zT in a Mg$_3$Sb$_2$–Mg$_3$Bi$_2$ solid solution via Mg-vapor annealing *Adv. Mater.* **31** 1902337

[375] Brown S R, Kauzlarich S M, Gascoin F and Snyder G J 2006 Yb$_{14}$MnSb$_{11}$: new high efficiency thermoelectric material for power generation *Chem. Mater.* **18** 1873–7

[376] May A F, Fleurial J-P and Snyder G J 2008 Thermoelectric performance of lanthanum telluride produced via mechanical alloying *Phys. Rev.* B **78** 125205-1–12

[377] Cheikh D, Hogan B E, Vo T, Von Allmen P, Lee K, Smiadak D M, Zevalkink A, Dunn B S, Fleurial J-P and Bux S K 2018 Praseodymium telluride: a high-temperature, high-ZT thermoelectric material *Joule* **2** 698–709

[378] Vinning C B and Fleurial J-P Silicon-Germanium: An Overview of Recent Development 1993 *10th Symp. on Space Nuclear Power and Propulsion* (*Albuquerque, New Mexico, 10-14 January 1993*) pp 87–120

[379] Zhou T, Lenoir B, Colin M, Dauscher A, Al Rahal Al Orabi R, Gougeon P, Potel M and Guilmeau E 2011 Promising thermoelectric properties in Ag$_x$Mo$_9$Se$_{11}$ compounds (3.4 ≤ x ≤ 3.9) *Appl. Phys. Lett.* **98** 162106-1–3

[380] Al Rahal Al Orabi R *et al* 2014 X-ray characterization, electronic band structure, and thermoelectric properties of the cluster compound Ag$_2$Tl$_2$Mo$_9$Se$_{11}$ *Inorg. Chem.* **53** 11699–709

[381] Gougeon P, Gall P, Merdrignac-Conanec O, Aranda L, Dauscher A, Candolfi C and Lenoir B 2017 Synthesis, crystal structure, and transport properties of the hexagonal Mo$_9$ cluster compound Ag$_3$RbMo$_9$Se$_{11}$ *Inorg. Chem.* **56** 9684–92

[382] Gougeon P *et al* 2012 Synthesis, crystal and electronic structures, and thermoelectric properties of the novel cluster compound Ag$_3$In$_2$Mo$_{15}$Se$_{19}$ *Chem. Mater.* **24** 2899–908

[383] Caillat T, Fleurial J-P and Snyder G J 1999 Potential of chevrel phases to thermoelectric applications *Solid State Sci.* **1** 535–44

[384] Gougeon P *et al* 2021 Tl$_{0.6}$Mo$_3$S$_5$, an original large tunnel-like molybdenum sulfide with Mo zigzag chains and disordered Tl cations *Mater. Adv.* **2** 6020–30

[385] Liu J *et al* 2020 N-type organic thermoelectrics: demonstration of ZT> 0.3 *Nat. Commun.* **11** 5694

[386] Abutaha A, Kumar P, Yildirim E, Shi W, Yang S-W, Wu G and Hippalgaonkar K 2020 Correlating charge and thermoelectric transport to paracrystallinity in conducting polymers *Nat. Commun.* **11** 1737

[387] Broch K *et al* 2017 Measurements of ambipolar seebeck coefficients in high-mobility diketopyrrolopyrrole donor–acceptor copolymers *Adv. Electron. Mater* **3** 1700225

[388] Lindorf M, Mazzio K A, Pflaum J, Nielsch K, Brütting W and Albrecht M 2020 Organic-based thermoelectrics *J. Mater. Chem.* A **8** 7495

[389] Russ B, Glaudell A, Urban J J, Chabinyc M L and Segalman R A 2016 Organic thermoelectric materials for energy harvesting and temperature control *Nat. Rev. Mater.* **1** 16050

[390] Campoy-Quiles M 2019 Will organic thermoelectrics get hot? *Phil. Trans. R. Soc.* A **377** 20180352

[391] Zapata-Arteaga O, Perevedentsev A, Marina S, Martin J, Reparaz J S and Campoy-Quiles M 2020 Reduction of the lattice thermal conductivity of polymer semiconductors by molecular doping *ACS Energy Lett.* **5** 2972–8

[392] Finn P A, Asker C, Wan K, Bilotti E, Fenwick O and Nielsen C B 2021 Thermoelectric materials: current status and future challenges *Front. Electron. Mater.* **1** 677845

[393] Ulrich G *et al* 2020 Thermoelectric nanospectroscopy for the imaging of molecular fingerprints *Nanophotonics* **9** 4347–54

[394] Janda T *et al* 2020 Magneto-Seebeck microscopy of domain switching in collinear antiferromagnet CuMnAs *Phys. Rev. Mater.* **4** 094413

[395] Hicks L and Dresselhaus M S 1993 Effect of quantum-well structures on the thermoelectric figure of merit *Phys. Rev.* B **47** 12727

[396] Zhao Y, Cai Y, Zhang L, Li B, Zhang G and Thong J T L 2020 Thermal transport in 2D semiconductors—considerations for device applications *Adv. Funct. Mater.* **30** 1903929

[397] Wu J, Chen Y, Wu J and Hippalgaonkar K 2018 Perspectives on thermoelectricity in layered and 2D materials *Adv. Electron. Mater.* **4** 1800248

[398] Wan C *et al* 2015 Flexible n-type thermoelectric materials by organic intercalation of layered transition metal dichalcogenide TiS$_2$ *Nat. Mater.* **14** 622–7

[399] Li G, Yao K and Gao G 2017 Strain-induced enhancement of thermoelectric performance of TiS$_2$ monolayer based on first-principles phonon and electron band structures *Nanotechnology* **29** 015204

[400] Ouyang Y, Zhang Z and Li D 2019 Emerging theory, materials, and screening methods: new opportunities for promoting thermoelectric performance *Ann. Phys.* **531** 1800437

[401] Zhao Y, Yu P, Zhang G, Sun M, Chi D, Hippalgaonkar K, Thong J T L and Wu J 2020 Low-symmetry PdSe$_2$ for high performance thermoelectric applications *Adv. Funct. Mater.* **30** 2004896

[402] Suh J *et al* 2015 Simultaneous enhancement of electrical conductivity and thermopower of Bi$_2$Te$_3$ by multifunctionality of native defects *Adv. Mater.* **27** 3681–6

[403] Chen S and Ren Z 2013 Recent progress of half-Heusler for moderate temperature thermoelectric applications *Mater. Today* **16** 387–95

[404] Wang T, Zhang C, Snoussi H and Zhang G 2020 Machine learning approaches for thermoelectric materials research *Adv. Funct. Mater.* **30** 1906041

[405] Blackburn J L, Ferguson A J, Cho C and Grunlan J C 2018 Carbon-nanotube-based thermoelectric materials and devices *Adv. Mater.* **30** 1704386

[406] Ichinose Y *et al* 2019 Solving the thermoelectric trade-off problem with metallic carbon nanotubes *Nano Lett.* **19** 7370–6

[407] Nonoguchi Y, Ohashi K, Kanazawa R, Ashiba K, Hata K, Nakagawa T, Adachi C, Tanase T and Kawai T 2013 Systematic conversion of single walled carbon nanotubes into n-type thermoelectric materials by molecular dopants *Sci. Rep.* **3** 3344

[408] Nakai Y, Honda K, Yanagi K, Kataura H, Kato T, Yamamoto T and Maniwa Y 2014 Giant Seebeck coefficient in semiconducting single-wall carbon nanotube film *Appl. Phys. Express* **7** 025103

[409] Macleod B A *et al* 2017 Large n- and p-type thermoelectric power factors from doped semiconducting single-walled carbon nanotube thin films *Energy Environ. Sci.* **10** 2168–79

[410] Choi J, Jung Y, Yang S J, Oh J Y, Oh J, Jo K, Son J G, Moon S E, Park C R and Kim H 2017 Flexible and robust thermoelectric generators based on all-carbon nanotube yarn without metal electrodes *ACS Nano* **11** 7608–14

[411] Nakashima Y, Nakashima N and Fujigaya T 2017 Development of air-stable n-type single-walled carbon nanotubes by doping with 2-(2-methoxyphenyl)-1,3-dimethyl-2,3-dihydro-1H-benzo[d]imidazole and their thermoelectric properties *Synth. Met.* **225** 76–80

[412] Nonoguchi Y, Nakano M, Murayama T, Hagino H, Hama S, Miyazaki K, Matsubara R, Nakamura M and Kawai T 2016 Simple salt-coordinated n-type nanocarbon materials stable in air *Adv. Funct. Mater.* **26** 3021–8

[413] Yamamoto T and Fukuyama H 2018 Possible high thermoelectric power in semiconducting carbon nanotubes ∼A case study of doped one-dimensional semiconductors *J. Phys. Soc. Japan* **87** 024707

[414] Soleimani Z, Zoras S, Ceranic B, Cui Y and Shahzad S 2021 A comprehensive review on the output voltage/power of wearable thermoelectric generators concerning their geometry and thermoelectric materials *Nano Energy* **89** 106325

[415] Dresselhaus M S, Chen G, Tang M, Yang R, Lee H, Wang D, Ren Z, Fleurial J-P and Gogna P 2007 New directions for low-dimensional thermoelectric materials *Adv. Mater.* **19** 1043–53

[416] Zhang Y, Zhang Q and Chen G 2020 Carbon and carbon composites for thermoelectric applications *Carbon Energy* **2** 408–36

[417] Meng C, Liu C and Fan S 2010 A promising approach to enhanced thermoelectric properties using carbon nanotube networks *Adv. Mater.* **22** 535–9

[418] Li Z, Deng L, Lv H, Liang L, Deng W, Zhang Y and Chen G 2021 Mechanically robust and flexible films of ionic liquid-modulated polymer thermoelectric composites *Adv. Funct. Mater.* **31** 2104836

[419] Hung N T, Nugraha A R T, Hasdeo E H, Dresselhaus M S and Saito R 2015 Diameter dependence of thermoelectric power of semiconducting carbon nanotubes *Phys. Rev.* B **92** 165426, 10/21/

[420] Mai C-K, Liu J, Evans C M, Segalman R A, Chabinyc M L, Cahill D G and Bazan G C 2016 Anisotropic thermal transport in thermoelectric composites of conjugated polyelectrolytes/single-walled carbon nanotubes *Macromolecules* **49** 4957–63

[421] Wang Q, Yao Q, Chang J and Chen L 2012 Enhanced thermoelectric properties of CNT/PANI composite nanofibers by highly orienting the arrangement of polymer chains *J. Mater. Chem.* **22** 17612–8

[422] Abol-Fotouh D, Dörling B, Zapata-Arteaga O, Rodríguez-Martínez X, Gómez A, Reparaz J S, Laromaine A, Roig A and Campoy-Quiles M 2019 Farming thermoelectric paper *Energy Environ. Sci.* **12** 716–26

[423] Wan K, Liu Z, Schroeder B C, Chen G, Santagiuliana G, Papageorgiou D G, Zhang H and Bilotti E 2021 Highly stretchable and sensitive self-powered sensors based on the N-Type thermoelectric effect of polyurethane/Nax(Ni-ett)n/graphene oxide composites *Compos. Commun.* **28** 100952

[424] Cho C, Stevens B, Hsu J-H, Bureau R, Hagen D A, Regev O, Yu C and Grunlan J C 2015 Completely organic multilayer thin film with thermoelectric power factor rivaling inorganic tellurides *Adv. Mater.* **27** 2996–3001

[425] Sun T, Peavey J L, David Shelby M, Ferguson S and O'Connor B T 2015 Heat shrink formation of a corrugated thin film thermoelectric generator *Energy Convers. Manage.* **103** 674–80

[426] Urban J J, Menon A K, Tian Z, Jain A and Hippalgaonkar K 2019 New horizons in thermoelectric materials: correlated electrons, organic transport, machine learning, and more *J. Appl. Phys.* **125** 180902

[427] Yang L, Gordon M P, Menon A K, Bruefach A, Haas K, Scott M C, Prasher R S and Urban J J 2021 Decoupling electron and phonon transport in single-nanowire hybrid materials for high-performance thermoelectrics *Sci. Adv.* **7** eabe6000

[428] Zaia E W, Gordon M P, Yuan P and Urban J J 2019 Progress and perspective: soft thermoelectric materials for wearable and internet-of-things applications *Adv. Electron. Mater.* **5** 1800823

[429] Yee S K, LeBlanc S, Goodson K E and Dames C 2013 \ per W metrics for thermoelectric power generation: beyond ZT *Energy Environ. Sci.* **6** 2561–71

[430] Lee H, Jang Y, Choe J K, Lee S, Song H, Lee J P, Lone N and Kim J 2020 3D-printed programmable tensegrity for soft robotics *Sci. Robot.* **5** eaay9024

[431] Sajadi Seyed M *et al* 2021 Damage-tolerant 3D-printed ceramics via conformal coating *Sci. Adv.* **7** eabc5028

[432] Choi J, Dun C, Forsythe C, Gordon M P and Urban J J 2021 Lightweight wearable thermoelectric cooler with rationally designed flexible heatsink consisting of phase-change material/graphite/silicone elastomer *J. Mater. Chem.* A **9** 15696–703

[433] Elmoughni H M, Menon A K, Wolfe R M W and Yee S K 2019 A textile-integrated polymer thermoelectric generator for body heat harvesting *Adv. Mater. Technol.* **4** 1800708

[434] Kang S D and Snyder G J 2017 Charge-transport model for conducting polymers *Nat. Mater.* **16** 252–7

[435] Gregory S A, Hanus R, Atassi A, Rinehart J M, Wooding J P, Menon A K, Losego M D, Snyder G J and Yee S K 2021 Quantifying charge carrier localization in chemically doped semiconducting polymers *Nat. Mater.* **20** 1414–21

[436] He Y and Galli G 2014 Perovskites for solar thermoelectric applications: a first principle study of $CH_3NH_3AI_3$ (A = Pb and Sn) *Chem. Mater.* **26** 5394–400

[437] Yan L, Wang M, Zhai C, Zhao L and Lin S 2020 Symmetry breaking induced anisotropic carrier transport and remarkable thermoelectric performance in mixed halide perovskites $CsPb(I_{1-x}Br_x)_3$ *ACS Appl. Mater. Interfaces* **12** 40453–64

[438] Jung Y-K, Han I T, Kim Y C and Walsh A 2021 Prediction of high thermoelectric performance in the low-dimensional metal halide $Cs_3Cu_2I_5$ *npj Comput. Mater.* **7** 51

[439] Herz L M 2017 Charge-carrier mobilities in metal halide perovskites: fundamental mechanisms and limits *ACS Energy Lett.* **2** 1539–48

[440] Lee W *et al* 2017 Ultralow thermal conductivity in all-inorganic halide perovskites *Proc. Natl Acad. Sci.* **114** 8693

[441] Liu T, Zhao X, Li J, Liu Z, Liscio F, Milita S, Schroeder B C and Fenwick O 2019 Enhanced control of self-doping in halide perovskites for improved thermoelectric performance *Nat. Commun.* **10** 5750

[442] Zheng L, Zhu T, Li Y, Wu H, Yi C, Zhu J and Gong X 2020 Enhanced thermoelectric performance of F4-TCNQ doped $FASnI_3$ thin films *J. Mater. Chem.* A **8** 25431–42

[443] Tang W *et al* 2020 Substitutional doping of hybrid organic–inorganic perovskite crystals for thermoelectrics *J. Mater. Chem.* A **8** 13594–9

[444] Stassen I, Burtch N C, Talin A A, Falcaro P, Allendorf M D and Ameloot R 2017 An updated roadmap for the integration of metal-organic frameworks with electronic devices and chemical sensors *Chem. Soc. Rev.* **46** 3185–241

[445] Talin A A, Jones R E and Hopkins P E 2016 Metal-organic frameworks for thermoelectric energy-conversion applications *MRS Bull.* **41** 877–82

[446] Sun L *et al* 2017 A microporous and naturally nanostructured thermoelectric metal-organic framework with ultralow thermal conductivity *Joule* **1** 168–77

[447] Xue Y F, Zhang Z, Zhang Y, Wang X, Li L, Wang H and Chen G 2020 Boosting thermoelectric performance by *in situ* growth of metal organic framework on carbon nanotube and subsequent annealing *Carbon* **157** 324–9

[448] Erickson K J, Léonard F, Stavila V, Foster M E, Spataru C D, Jones R E, Foley B M, Hopkins P E, Allendorf M D and Talin A A 2015 Thin film thermoelectric metal-organic framework with high seebeck coefficient and low thermal conductivity *Adv. Mater.* **27** 3453–9

[449] Tsuchikawa R, Lotfizadeh N, Lahiri N, Liu S, Lach M, Slam C, Louie J and Deshpande V V 2020 Unique thermoelectric properties induced by intrinsic nanostructuring in a polycrystalline thin-film two-dimensional metal–organic framework, copper benzenehexathiol *Phys. Status Solidi* a **217** 2000437

[450] Kim G-H, Shao L, Zhang K and Pipe K P 2013 Engineered doping of organic semiconductors for enhanced thermoelectric efficiency *Nat. Mater.* **12** 719–23

[451] Wu G D, Huang J H, Zang Y, He J and Xu G 2017 Porous field-effect transistors based on a semiconductive metal-organic framework *J. Am. Chem. Soc.* **139** 1360–3

[452] Dong R *et al* 2018 High-mobility band-like charge transport in a semiconducting two-dimensional metal–organic framework *Nat. Mater.* **17** 1027–32

[453] Chen T, Dou J-H, Yang L, Sun C, Libretto N J, Skorupskii G, Miller J T and Dincă M 2020 Continuous electrical conductivity variation in M₃(Hexaiminotriphenylene)₂ (M = Co, Ni, Cu) MOF alloys *J. Am. Chem. Soc.* **142** 12367–73

[454] IoT Analytics Research 2022 Global IoT market forecast (available at: https://iot-analytics.com/number-connected-iot-devices/)

[455] Tiseo I Global E-Waste - Statistics & Facts 2023 (available at: www.statista.com/topics/3409/electronic-waste-worldwide/#dossierKeyfigures)

[456] Semple J, Georgiadou D G, Wyatt-Moon G, Gelinck G and Anthopoulos T D 2017 *Semicond. Sci. Technol.* **32** 123002

[457] Hemour S and Wu K 2014 Radio-frequency rectifier for electromagnetic energy harvesting: development path and future outlook *Proc. IEEE* **102** 1667–91

[458] Yi J, Ki W and Tsui C 2007 Analysis and design strategy of UHF micro-power CMOS rectifiers for micro-sensor and RFID applications *IEEE Trans. Circuits Syst.* I **54** 153–66

[459] Tripathi A K *et al* 2011 *Appl. Phys. Lett.* **98** 162102

[460] Cantatore E, Geuns T C T, Gelinck G H, van Veenendaal E, Gruijthuijsen A F A, Schrijnemakers L, Drews S and de Leeuw D M 2007 A 13.56-MHz RFID system based on organic transponders *IEEE J. Solid-State Circuits* **42** 84–92

[461] Rotzoll R, Mohapatra S, Olariu V, Wenz R, Grigas M, Dimmler K, Shchekin O and Dodabalapur A 2006 *Appl. Phys. Lett.* **88** 123502

[462] Myny K *et al* 2010 Organic RFID transponder chip with data rate compatible with electronic product coding *Org. Electron.* **11** 1176–9

[463] Franklin A D 2015 Nanomaterials in transistors: from high-performance to thin-film applications *Science* **2750** 6249

[464] Dai H, Lu Y, Law M-K, Sin S-W, Seng-Pan U and Martins R P 2015 A review and design of the on-chip rectifiers for RF energy harvesting (*Shenzhen, China*) *2015 IEEE Int. Wireless Symp. (IWS 2015)* pp 1–4

[465] Chen Z N, Nakano H, Qing X and Zwick T (eds) *Handbook of Antenna Technologies* (Singapore: Springer) (https://doi.org/10.1007/978-981-4560-44-3_56)

[466] Hemmetter A*et al* 2021 Terahertz rectennas on flexible substrates based on one-dimensional metal-insulator-graphene diodes *ACS Appl. Electron. Mater.* **3** 3747–53

[467] Fan C-Y, Wei M-D, Uzlu B, Wang Z, Neumaier D and Negra R 2021 Fully integrated 2.4-GHz flexible rectifier using chemical-vapor-deposition graphene MMIC process *IEEE Trans. Electron Devices* **68** 1326–33

[468] Zhang X, Grajal J, López-Vallejo M, McVay E and Palacios T 2020 Opportunities and challenges of ambient radio-frequency energy harvesting *Joule* **4** 1148–52

[469] Georgiadou D G *et al* 2020 100 GHz zinc oxide Schottky diodes processed from solution on a wafer scale *Nat. Electron.* **3** 718–25

[470] Kang C-M *et al* Organic electronics: 1 GHz pentacene diode rectifiers enabled by controlled film deposition on SAM-treated Au anodes (Adv. Electron. Mater. 2/2016)

[471] Kwan J C and Fapojuwo A O 2016 Measurement and analysis of available ambient radio frequency energy for wireless energy harvesting *2016 IEEE 84th Vehicular Technology Conf. (Vtc-fall)* pp 1–6

[472] Chu Y, Qian C, Chahal P and Cao C 2019 Printed diodes: materials processing, fabrication, and applications *Adv. Sci.* **6** 1801653

[473] Viola F A, Brigante B, Colpani P, Dell'Erba G, Mattoli V, Natali D and Caironi M 2020 A 13.56 MHz rectifier based on fully inkjet printed organic diodes *Adv. Mater.* **32** 1–7

[474] Yamamura A, Sakon T, Takahira K, Wakimoto T, Sasaki M, Okamoto T, Watanabe S and Takeya J 2020 High-speed organic single-crystal transistor responding to very high frequency band *Adv. Funct. Mater.* **30** 1909501

[475] Perinot A, Giorgio M, Mattoli V, Natali D and Caironi M 2021 Organic electronics picks up the pace: mask-less, solution processed organic transistors operating at 160 MHz *Adv. Sci.* **8** 1–6

[476] Loganathan K *et al* 2022 14 GHz schottky diodes using a p-doped organic polymer *Adv. Mater.* **34** 2108524

[477] Borchert J W, Weitz R T, Ludwigs S and Klauk H 2022 A critical outlook for the pursuit of lower contact resistance in organic transistors *Adv. Mater.* **34** 2104075

[478] Klinger M P, Fischer A, Kleemann H and Leo K 2018 Non-linear self-heating in organic transistors reaching high power densities *Sci. Rep.* **8** 1–9

[479] Kheradmand-Boroujeni B, Klinger M P, Fischer A, Kleemann H, Leo K and Ellinger F 2018 A pulse-biasing small-signal measurement technique enabling 40 MHz operation of vertical organic transistors *Sci. Rep.* **8** 1–9

[480] Ghosh J, Salvan G and Reuter D 2020 Study of laterally stacked nanostructures using an organic semiconducting channel fabricated by trench isolation technique *IEEE Trans. Nanotechnol.* **19** 410–4

[481] Borchert J W, Peng B, Letzkus F, Burghartz J N, Chan P K L, Zojer K, Ludwigs S and Klauk H 2019 Small contact resistance and high-frequency operation of flexible low-voltage inverted coplanar organic transistors *Nat. Commun.* **10** 1–11

[482] Viola F A, Barsotti J, Melloni F, Lanzani G, Kim Y-H, Mattoli V and Caironi M 2021 A sub-150-nanometre-thick and ultraconformable solution-processed all-organic transistor *Nat. Commun.* **12** 5842

[483] Noh Y-Y, Zhao N, Caironi M and Sirringhaus H 2007 Downscaling of self-aligned, all-printed polymer thin-film transistors *Nat. Nanotechnol.* **2** 784–9

[484] Vu M C, Choi W-K, Lee S G, Park P J, Kim D H, Islam M A and Kim S-R 2020 High thermal conductivity enhancement of polymer composites with vertically aligned silicon carbide sheet scaffolds *ACS Appl. Mater. Interfaces* **12** 23388–98

[485] Choi J Y and Lee S Y 2017 Comprehensive review on the development of high mobility in oxide thin film transistors *J. Korean Phys. Soc.* **71** 516–27

[486] Nomura K, Ohta H, Takagi A, Kamiya T, Hirano M and Hosono H 2004 Room-temperature fabrication of transparent flexible thin-film transistors using amorphous oxide semiconductors *Nature* **432** 488–92

[487] Chasin A, Nag M, Bhoolokam A, Myny K, Steudel S, Schols S, Genoe J, Gielen G and Heremans P 2013 Gigahertz operation of a-IGZO schottky diodes *IEEE Trans. Electron Devices* **60** 3407–12

[488] Chasin A, Volskiy V, Libois M, Myny K, Nag M, Rockele M, Vandenbosch G A E, Genoe J, Gielen G and Heremans P 2014 An integrated a-IGZO UHF energy harvester for passive RFID tags *IEEE Trans. Electron Devices* **61** 3289–95

[489] Loganathan K *et al* 2022 Rapid and up-scalable manufacturing of gigahertz nanogap diodes *Nat. Commun.* **13** 3260

[490] Wilson J, Zhang J, Li Y, Wang Y, Xin Q and Song A 2017 Influence of interface inhomogeneities in thin-film Schottky diodes *Appl. Phys. Lett.* **111** 213503

[491] Son Y and Peterson R L 2019 Exploiting *in situ* redox and diffusion of molybdenum to enable thin-film circuitry for low-cost wireless energy harvesting *Adv. Funct. Mater.* **29** 1806002

[492] Park H, Yun J, Park S, Ahn I-S, Shin G, Seong S, Song H-J and Chung Y 2022 Enhancing the contact between a-IGZO and metal by hydrogen plasma treatment for a high-speed varactor (>30 GHz) *ACS Appl. Electron. Mater.* **4** 1769–75

[493] Tückmantel C, Kalita U, Haeger T, Theisen M, Pfeiffer U and Riedl T 2020 Amorphous indium-gallium-zinc-oxide TFTs patterned by self-aligned photolithography overcoming the GHz threshold *IEEE Electron. Device Lett.* **41** 1786–9

[494] He Q and Tang L 2022 Sub-5 nm nanogap electrodes towards single-molecular biosensing *Biosens. Bioelectron.* **213** 114486

[495] Im H, Bantz K C, Lindquist N C, Haynes C L and Oh S H 2010 Vertically oriented sub-10-nm plasmonic nanogap arrays *Nano Lett.* **10** 2231–6

[496] Li S, Liu Y, Che Y, Song J, Shu Y, He J, Xu B and Yang B 2020 Recycling of spent indium–gallium–zinc oxide based on molten salt electrolysis *ACS Sustain. Chem. Eng.* **8** 16296–303

[497] Manohara H M, Wong E W, Schlecht E, Hunt B D and Siegel P H 2005 Carbon nanotube Schottky diodes using Ti—Schottky and Pt—ohmic contacts for high frequency applications *Nano Lett.* **5** 1469–74

[498] Cobas E and Fuhrer M S 2008 Microwave rectification by a carbon nanotube Schottky diode *Appl. Phys. Lett.* **93** 043120

[499] Cobas E D, Anlage S M and Fuhrer M S 2011 Single carbon nanotube Schottky diode microwave rectifiers *IEEE Trans. Microw. Theory Tech.* **59** 2726–32

[500] Biswas C, Lee S Y, Ly T H, Ghosh A, Dang Q N and Lee Y H 2011 Chemically doped random network carbon nanotube p–n junction diode for rectifier *ACS Nano* **5** 9817–23

[501] Feng Y, Li H, Inoue T, Chiashi S, Rotkin S V, Xiang R and Maruyama S 2021 One-dimensional van der Waals heterojunction diode *ACS Nano* **15** 5600–9

[502] Wang S, Zhang Z, Ding L, Liang X, Shen J, Xu H, Chen Q, Cui R, Li Y and Peng L-M 2008 A doping-free carbon nanotube CMOS inverter-based bipolar diode and ambipolar transistor *Adv. Mater.* **20** 3258–62

[503] Liu L *et al* 2020 Aligned, high-density semiconducting carbon nanotube arrays for high-performance electronics *Science* **368** 850–6

[504] Shi H *et al* 2021 Radiofrequency transistors based on aligned carbon nanotube arrays *Nat. Electron.* **4** 405–15

[505] Shulaker M M, Hills G, Park R S, Howe R T, Saraswat K, Wong H-S P and Mitra S 2017 Three-dimensional integration of nanotechnologies for computing and data storage on a single chip *Nature* **547** 74–78

[506] Qiu C *et al* 2018 Dirac-source field-effect transistors as energy-efficient, high-performance electronic switches *Science* **361** 387–92

[507] Lemme M C, Akinwande D, Huyghebaert C and Stampfer C 2022 2D materials for future heterogeneous electronics *Nat. Commun.* **13** 1392

[508] Wang Z, Hemmetter A, Uzlu B, Saeed M, Hamed A, Kataria S, Negra R, Neumaier D and Lemme M C 2021 Graphene in 2D/3D heterostructure diodes for high performance electronics and optoelectronics *Adv. Electron. Mater* **7** 2001210

[509] Abadal S *et al* Graphene-based wireless agile interconnects for massive heterogeneous multi-chip processors (arXiv:2011.04107)

[510] Zhang X *et al* 2019 Two-dimensional MoS$_2$-enabled flexible rectenna for Wi-Fi-band wireless energy harvesting *Nature* **566** 368

[511] Hemmetter A *et al* 2021 Terahertz rectennas on flexible substrates based on one-dimensional metal-insulator-graphene diodes *ACS Appl. Electron. Mater.* **3** 3747

[512] Zhu Z, Joshi S, Grover S and Moddel G 2013 Graphene geometric diodes for terahertz rectennas *J. Phys. D: Appl. Phys* **46** 185101

[513] Neumaier D, Pindl S and M C L 2019 Integrating graphene into semiconductor fabrication lines *Nat. Mater.* **18** 525

[514] Shen P-C *et al* 2021 Ultralow contact resistance between semimetal and monolayer semiconductors *Nature* **593** 7858

[515] Rodenbeck C T, Jaffe P I, Strassner B H II, Hausgen P E, McSpadden J O, Kazemi H, Shinohara N, Tierney B B, DePuma C B and Self A P 2021 Microwave and millimeter wave power beaming *IEEE J. Microw.* **1** 229–59

[516] Wagih M, Weddell A S and Beeby S 2020 Millimeter-wave power harvesting: a review *IEEE Open J. Antennas Propag.* **1** 560–78

[517] Gu X, Hemour S and Wu K 2022 Far-field wireless power harvesting: nonlinear modeling, rectenna design, and emerging applications *Proc. IEEE* **110** 56–73

[518] Yamagishi K, Zhou W, Ching T, Huang S Y and Hashimoto M 2021 Ultra-deformable and tissue-adhesive liquid metal antennas with high wireless powering efficiency *Adv. Mater.* **33** 2008062

[519] Eid A, Hester J G D and Tentzeris M M 2021 5G as a wireless power grid *Sci. Rep.* **11** 636

[520] Wagih M, Hilton G S, Weddell A S and Beeby S 2020 Broadband millimeter-wave textile-based flexible rectenna for wearable energy harvesting *IEEE Trans. Microw. Theory Tech.* **68** 4960–72

[521] Wagih M, Weddell A S and Beeby S 2020 Rectennas for radio-frequency energy harvesting and wireless power transfer: a review of antenna design [antenna applications corner] *IEEE Antennas Propag. Mag.* **62** 95–107

[522] Wagih M, Hilton G S, Weddell A S and Beeby S 2021 Dual-polarized wearable antenna/rectenna for full-duplex and MIMO simultaneous wireless information and power transfer (SWIPT) *IEEE Open J. Antennas Propag.* **2** 844–57

[523] Zhu J *et al* 2021 Stretchable wideband dipole antennas and rectennas for RF energy harvesting *Mater. Today Phys.* **18** 100377

[524] Hwang S-W *et al* 2013 Materials for bioresorbable radio frequency electronics *Adv. Mater.* **25** 3526–31

[525] Tian X, Lee P M, Tan Y J, Wu T L Y, Yao H, Zhang M, Li Z, Ng K A, Tee B C K and Ho J S 2019 Wireless body sensor networks based on metamaterial textiles *Nat. Electron.* **2** 243–51

[526] Titirici M 2021 Sustainable batteries—quo vadis? *Adv. Energy Mater.* **11** 2003700

[527] Akinaga H 2020 Recent advances and future prospects in energy harvesting technologies *Jpn. J. Appl. Phys.* **59** 110201

[528] Calautit K, Nasir D S N M and Hughes B R 2021 Low power energy harvesting systems: state of the art and future challenges *Renew. Sustain. Energy Rev.* **147** 111230

[529] Hellweg S and Milà I Canals L 2014 Emerging approaches, challenges and opportunities in life cycle assessment *Science* **344** 1109–13

[530] Gong J, Darling S B and You F 2015 Perovskite photovoltaics: life-cycle assessment of energy and environmental impacts *Energy Environ. Sci.* **8** 1953–68

[531] Ibn-Mohammed T, Koh S C L, Reaney I M, Acquaye A, Wang D, Taylor S and Genovese A 2016 Integrated hybrid life cycle assessment and supply chain environmental profile evaluations of lead-based (lead zirconate titanate) versus lead-free (potassium sodium niobate) piezoelectric ceramics *Energy Environ. Sci.* **9** 3495–520

[532] Ibn-Mohammed T, Reaney I M, Koh S C L, Acquaye A, Sinclair D C, Randall C A, Abubakar F H, Smith L, Schileo G and Ozawa-Meida L 2018 Life cycle assessment and environmental profile evaluation of lead-free piezoelectrics in comparison with lead zirconate titanate *J. Eur. Ceram. Soc.* **38** 4922–38

[533] Ahmed A, Hassan I, Ibn-Mohammed T, Mostafa H, Reaney I M, Koh L S C, Zu J and Wang Z L 2017 Environmental life cycle assessment and techno-economic analysis of triboelectric nanogenerators *Energy Environ. Sci.* **10** 653–71

[534] Soleimani Z, Zoras S, Ceranic B, Shahzad S and Cui Y 2021 The cradle to gate life-cycle assessment of thermoelectric materials: a comparison of inorganic, organic and hybrid types *Sustain. Energy Technol. Assess.* **44** 101073

[535] Mori T and Priya S 2018 Materials for energy harvesting: at the forefront of a new wave *MRS Bull.* **43** 176–80